CONFERENCE SERIES

Jürgen Stohner, Chahan Yeretzian (Eds.)

XXth Symposium on Atomic, Cluster and Surface Physics 2016 (SASP 2016)

February 7 – 12, 2016

Davos, Switzerland

Contributions

innsbruck university press

CONFERENCE SERIES

innsbruck university press

Universität Innsbruck
1st edition

www.uibk.ac.at/iup
ISBN 978-3-903122-04-8

Jürgen Stohner, Chahan Yeretzian (Eds.)

XXth Symposium on Atomic, Cluster and Surface Physics 2016 (SASP 2016)

February 7 – 12, 2016

Davos, Switzerland

Contributions

XXth Symposium on Atomic, Cluster and Surface Physics 2016 (SASP 2016)

February 7 - 12, 2016
Davos, Switzerland

International Scientific Committee:

Davide Bassi (Universitá degli Studi di Trento)
Tilmann D. Märk (Universität Innsbruck)
Nigel Mason (Open University, UK)
Martin Quack (Eidgenössische Technische Hochschule Zürich)
Tom Rizzo (EPFL Lausanne)
Paul Scheier (Universität Innsbruck)

Organizing Committee:

Institut für Chemie und Biotechnologie (IBT), Zürcher Hochschule für Angewandte Wissenschaften (ZHAW)

Chahan Yeretzian and Jürgen Stohner (chairpersons)
Marianne Schenker, Vanessa Galati, Manuel Mazenauer, Manuela Meister, Mathias Schilling, Manov Stole

SASP 2016 was sponsored by

BRUKER HIDEN ANALYTICAL Radiant Dyes Laser

Preface

The international Symposium on Atomic, cluster and Surface Physics, SASP, is a continuing biennial series of conferences, founded in 1978 by members of the Institute of Atomphysik, now Institute of Ionphysics and Applied Physics of the University of Innsbruck, Austria. SASP symposia aim to promote the growth of scientific knowledge and effective exchange of information among scientists in the field of atomic, molecular, cluster and surface physics, stressing both fundamental concepts and applications across these areas of interdisciplinary science. A major focus of SASP 2016 is on ion-molecule reactions, intermolecular interactions, gas and surface dynamics, cold molecules/ions and chirality. Since the beginning, the SASP format has been similar to that of a Gordon Conference, with invited lectures, hot topic oral presentations, posters and ample time for discussions. The attendance to the symposium has been kept to about 100 participants to favor interdisciplinary and multidisciplinary discussions.

SASP usually takes place in Austria, but every second time, it may be held in another alpine country. So far, the SASP conferences were held in the following locations:

1978 Zirog, Italy
1980 Maria Alm, Austria
1982 Maria Alm, Austria
1984 Maria Alm, Austria
1986 Obertraun, Austria
1988 La Plagne, France
1990 Obertraun, Austria
1992 Pampeago, Italy
1994 Maria Alm, Austria
1996 Engelberg, Switzerland
1998 Going, Austria
2000 Folgaria, Italy
2002 Going, Austria
2004 La Thuile, Italy
2006 Obergurgl, Austria
2008 Les Diablerets, Switzerland
2010 Obergurgl, Austria
2012 Alpe d´Huez, France
2014 Obergurgl, Austria
2016 Davos, Switzerland

SASP Erwin Schrödinger Gold Medal 2016

The „SASP Award for Outstanding Scientific Achievements" was initiated in 1992 by the SASP International Scientific Committee. This award is granted during the bienniel SASP meeting to one or two scientists, chosen among those who have strong connections to the activities of SASP.
The recipients of the SASP award 2016 – in the form of the "Erwin Schrödinger Gold Medal" designed by Zdenek Herman – will be

Roberto Marquardt
Université de Strasburg, France

Paul Scheier
Universität Innsbruck, Austria

Roberto Marquardt will receive this award for his outstanding theoretical contributions to molecular quantum dynamics, including in particular the construction of analytical multidimensional potential hypersurfaces and the time dependent quantum dynamics of isolated molecules and of species adsorbed at surfaces.

Paul Scheier will receive this award for his outstanding experimental contributions to ion and cluster physics including in particular a wide range of systems at the nanometer scale, systems at surfaces and ion surface collisions as well as molecular systems of biological importance.

At previous SASP meetings the Schrödinger Gold Medal was awarded to:

1992 David Smith, Birmingham, UK
1994 Zdenek Herman, Praha, Czech Republic
1996 Werner Lindinger and Tilmann Märk, Innsbruck, Austria
1998 Eldon Ferguson, Boulder, USA and Chava Lifshitz, Jerusalem, Israel
2000 Jean H. Futrell, Richland, USA
2002 Eugen Illenberger, Berlin, Germany
2004 Anna Giardini-Guidoni, Roma, Italy
2006 Davide Bassi, Trento, Italy and Martin Quack, Zürich, Switzerland
2008 Helmut Schwarz, Berlin, Germany
2010 Kurt Becker, New York, USA
2012 Dieter Gerlich, Chemnitz, Germany and John Maier, Basel, Switzerland
2014 Stephen D. Price, London, United Kingdom

	Sunday	Monday	Tuesday	Wednesday	Thursday	Friday
	February 7	February 8	February 9	February 10	February 11	February 12
7h00		Breakfast	Breakfast	Breakfast	Breakfast	Breakfast
8h30		Welcome				
		Chair: Yeretzian	Chair: Maier	Chair: Merkt	Chair: Leutwyler	Chair: Scheier
9h00		**Ernst W**	**Becker**	**Wodtke**	**Berger**	**Merkt**
9h30		**Tschurl**	**Wörner**	**Mayhew**	**Schnell**	**Boyarkin**
10h00		**Cederquist**	**Field**	**Müller-Dethlefs**	**Niedner-Schatteburg**	*Marquardt*
10h30		Coffee & Tea break	Coffee & Tea break	Coffee & Tea break	Coffee & Tea break	Coffee & Tea break
11h00		*Lindinger*	*Jusko*	*Govers*	*Kunitski*	Departure
11h30		*Seyfang*	*Albert*	*Roucka*	*Kitsopoulos*	
11h50		*Dörfler*	*Beyer*	*Kranabetter*	*Kuhn*	
		Discussions	Discussions	Discussions	Discussions	
16h00	Registration	Coffee & Tea break	Coffee & Tea break	Coffee & Tea break	Coffee & Tea break	**Invited Talks bold: 30 min. including discussion** *Hot Topic Talks slanted: 20 min. including discussion*
		Chair: Marquardt	Chair: Quack	Chair: Berger	Chair: Ernst KH	
16h30		**Maier**	**Sauer**	**Chen**	**Leutwyler**	
17h00		**Asmis**	**Price**	**Rizzo**	**Beck**	
17h30		**Willitsch**	**Ernst KH**	**Schöffler**	**Wester**	
18h00		*van Reijzen*	**Monti**	*Bersenkowitsch*	**Troe**	
18h20		*Trunec*		*Kaiser*		
18h40						
19h00		Dinner	Dinner	Dinner	Schrödinger Award Chair: Quack	
19h15						
20h15	**Quack** Chair: Stohner				Conference Dinner	
20h30			Chair: Monti			
21h00		Poster Session	**Zimmermann**	Poster Session		
21h30	Reception		**Rühl**			

Content
Invited Papers

Hot Topic Papers

Contributed Papers
Posters

Invited Papers

Molecules and Clusters in Motion: Looking Back and Looking Forward, SASP and Beyond

Martin Quack,
Physical Chemistry, ETH Zurich, CH-8093 Zurich, Switzerland,
Martin@Quack.CH; www.IR.ETHz.CH

1. Introduction

Having been asked to briefly review also some aspects of the SASP meetings [1], we shall start out with a few words about this superb series of highly interdisciplinary conferences covering topics ranging from fundamental physics, applied and surface physics, atomic, molecular, ion and cluster physics, photonics and electron collision physics, and reaction dynamics towards physical and theoretical chemistry and biophysics as well as biophysical chemistry and physics and chemistry on the nanometer scale and analytical chemistry with emphasis on mass spectrometry.

SASP was founded in 1978 as a biennial winter conference by members of the Institute for Atom Physics, then the Institute for Ion Physics and since 2006 the Institute for Ion Physics and Applied Physics of the Leopold Franzens University and organized for a long time under the crucial influence of Werner Lindinger and Tilmann Märk. Initially it was almost a local Austrian enterprise, but then was extended to become a European and highly international conference being located in various Alpine countries, moving 1988 from Austria to France (La Plagne), and 1992 to Pampeago (Italy). Nevertheless the Austrian base has remained a "constant of the motion" for this meeting, returning every second time to Austria. Every other time is has been organized in another Alpine country, 1996 for the first time in Switzerland. A novelty at this Engelberg meeting was to introduce a conference book publication with an ISBN number and publisher (VdF [2]), providing a citeable record of the papers at the meeting, usually intended to be four pages, reporting results of high novelty and quality. The foresight of Tilmann Märk has resulted in the foundation of Innsbruck University Press, where this book series has been printed from the year 2006 onwards [3]. This conference volume had been distinguished by a beautiful artistic cover prepared by

Zdenek Herman. It is fitting that after another decade SASP returns to Switzerland, being organized in Davos for the first time. We shall briefly comment on some highlights of the SASP conferences including reference also to some exceptional papers by some particularly original authors, who seem to have chosen SASP as their playground for some time [4-6].

2. Symmetries and Intramolecular Primary Processes between Yoctoseconds and Days as Derived from High Resolution Spectroscopy and Theory

The study of the primary processes of molecular motion provides the basis for chemical reaction dynamics and kinetics. We introduce the two major experimental approaches towards intramolecular quantum dynamics and kinetics from spectra: (i) time resolved ("pump-probe") spectroscopy, which has a long history of many decades, and (ii) deriving time dependent quantum dynamics from highly frequency resolved molecular spectra developed largely in the Zürich group over the last three decades [7-13]. We shall then discuss the role of the successive breaking of approximate symmetries in providing an understanding of the very different time scales found for molecular primary processes [11]. The general principles will be illustrated with results on femtosecond to nanosecond intramolecular energy flow [8-13] picosecond to nanosecond tunneling reactions [14-17], nuclear spin symmetry conservation and violation [18-20] and finally time dependent evolution of parity in chiral molecules on the timescale of milliseconds to days due to electroweak parity violation, [11, 18, 21-27]. We shall address some recent fundamental open problems in molecular quantum dynamics including the evolution of biomolecular homochirality in the early evolution of life [25, 28].

If time permits, we shall also address the interesting process of vibrational preionization after infrared multiphoton excitation first observed in for C_{60} in the framework of a collaboration initiated at the SASP meetings [29] and for which some interesting developments and considerations have arisen in more recent years.

Acknowledgement: Our work is supported by ETH Zurich, Schweizerischer Nationalfonds (SNF) and the European Research

Council (ERC) by an Advanced Grant 290925 and the COST action MOLIM. I am particularly indebted to my coworkers as cited in the list of references and more completely in [30] and also represented by further papers at this meeting.

1. M. Quack, *Molecules and Clusters in Motion, Lecture at SASP 2016, Davos*, Innsbruck University Press 2016, Innsbruck, **2016**.
2. J. P. Maier, M. Quack (Eds.), *Proceedings of the 10th International Symposium on Atomic, Molecular, Cluster, Ion, and Surface Physics, Engelberg, Switzerland, 21 - 26 January 1996*. VdF publishers, Zürich, **1996**, ISBN 3 7281 23293.
3. V. Grill, T. D. Märk (Eds.), *Proceedings 15th Symposium on Atomic and Surface Physics and Related Topics, Obergurgl, Österreich, 4. - 9.2.2006*. Innsbruck University Press, Innsbruck, **2006**, ISBN 3-901249-82-6.
4. W. S. Overcome, *Contributed Paper,* in *Proceedings SASP 86, 9.-15. February 1986, Obertraun, Austria,* p. 169, **1986**.
5. W. S. Overcome, *Contributed Paper,* in *Proceedings SASP 94, 20. - 26. March 1994, Maria Alm,* p. 442, **1994**.
6. A. M. Q. Zack, *Recent Advances in the Physics of Skiing on Surfaces (SOS): Yoctosecond Spectroscopy of Skiing on the Real and Imaginary Time Axes and in the Complex Plane,* in *Proceedings of the 10th International Symposium on Atomic, Molecular, Cluster, Ion, and Surface Physics, Engelberg, Switzerland 21 to 26 January 1996,* pp. 305-309 (Eds.: J. P. Maier, M. Quack), VdF Hochschulverlag, Zürich, **1996**, ISBN 3 7281 2329 3.
7. M. Quack, *Molecular Physics Lecture, Molecules in Motion: Symmetries and Intramolecular Primary Processes Between Yoctoseconds and Days as Derived from High Resolution Spectroscopy and Theory* in *Proc. 24th Coll. High Resolution Mol. Spectr., Dijon, August 2015,* pp. 37-38 (Ed.: V. Boudon), Univ. de Bourgogne-Dicolor groupe (Dépot legal de l'imprimeur 15-07-1857), Dijon, **2015**.
8. M. Quack, *Spectra and dynamics of coupled vibrations in polyatomic molecules, Annu. Rev. Phys. Chem.*, **1990**, *41*, 839-874.
9. M. Quack, *Molecular femtosecond quantum dynamics between less than yoctoseconds and more than days: Experiment and*

theory, in *Femtosecond Chemistry,* Chapt. 27*,* pp. 781-818 (Eds.: J. Manz, L. Woeste), Verlag Chemie, Weinheim, **1995**.

10. M. Quack, *Molecules in Motion, Chimia*, **2001**, *55*, 753-758, see also: M. Quack, *Molecular spectra, reaction dynamics, symmetries and life*, *Chimia*, **2003**, 57, 147-160.
11. M. Quack, *Fundamental Symmetries and Symmetry Violations from High Resolution Spectroscopy,* in *Handbook of High Resolution Spectroscopy, Vol. 1*, Chapt. 18*,* pp. 659-722 (Eds.: M. Quack, F. Merkt), Wiley, Chichester, New York, **2011**, ISBN 978-0-470-06653-9.
12. F. Merkt, M. Quack, *Molecular Quantum Mechanics and Molecular Spectra, Molecular Symmetry, and Interaction of Matter with Radiation,* in *Handbook of High-Resolution Spectroscopy, Vol. 1*, Chapt. 1*,* pp. 1-55, **2011** (see 11).
13. S. Albert, K. Keppler Albert, H. Hollenstein, C. Manca Tanner, M. Quack, *Fundamentals of Rotation-Vibration Spectra,* in *Handbook of High-Resolution Spectroscopy, Vol. 1*, Chapt. 3*,* pp. 117-173, **2011** (see 11).
14. B. Fehrensen, D. Luckhaus, M. Quack, *Stereomutation dynamics in hydrogen peroxide, Chem. Phys.*, **2007**, *338*, 90-105.
15. M. Hippler, E. Miloglyadov, M. Quack, G. Seyfang, *Mass and Isotope Selective Infrared Spectroscopy,* in *Handbook of High Resolution Spectroscopy, Vol. 2*, Chapt. 28*,* pp. 1069-1118, **2011** (see 11).
16. R. Marquardt, M. Quack, *Global Analytical Potential Energy Surfaces for High Resolution Molecular Spectroscopy and Reaction Dynamics,* in *Handbook of High-Resolution Spectroscopy, Vol. 1*, Chapt. 12*,* pp. 511-549, **2011** (see 11).
17. S. Albert, P. Lerch, R. Prentner, M. Quack, *Tunneling and Tunneling Switching Dynamics in Phenol and Its Isotopomers from High-Resolution FTIR Spectroscopy with Synchrotron Radiation, Angew. Chem. Int. Ed.*, **2013**, *52*, 346-349.
18. M. Quack, *Detailed symmetry selection-rules for reactive collisions, Mol. Phys.*, **1977**, *34*, 477-504.
19. C. Manca Tanner, M. Quack, D. Schmidiger, *Nuclear spin symmetry conservation and relaxation in water ($^{1}H_2{}^{16}O$) studied by Cavity Ring-Down (CRD) spectroscopy of supersonic jets J. Phys. Chem. A*, **2013**, *117*, 10105-10118.
20. M. Snels, V. Horká-Zelenková, H. Hollenstein, M. Quack, *High Resolution FTIR and Diode Laser Spectroscopy of Supersonic*

Jets, in *Handbook of High Resolution Spectroscopy, Vol. 2*, Chapt. 27*,* pp. 1021-1067, **2011** (see 11).

21. M. Quack, *On the measurement of the parity violating energy difference between enantiomers, Chem. Phys. Lett.*, **1986**, *132*, 147-153.
22. M. Quack, J. Stohner, M. Willeke, *High-resolution spectroscopic studies and theory of parity violation in chiral molecules, Annu. Rev. Phys. Chem.*, **2008**, *59*, 741-769.
23. Ľ. Horný, M. Quack, *Computation of molecular parity violation using the coupled-cluster linear response approach, Mol. Phys.*, **2015**, *113*, 1768-1779.
24. P. Dietiker, E. Miloglyadov, M. Quack, A. Schneider, G. Seyfang, *Infrared Laser Induced Population Transfer and Parity Selection in $^{14}NH_3$: A Proof of Principle Experiment Towards Detecting Parity Violation in Chiral Molecules, J. Chem. Phys.*, **2015**, *143* , 244305-1-23.
25. M. Quack, *Frontiers in Spectroscopy,* in *Faraday Discussions, Vol. 150,* pp. 533-565, **2011**.
26. C. Fábri, Ľ. Horný, M. Quack, *Tunneling and Parity Violation in Trisulfane (HSSSH): An Almost Ideal Molecule for Detecting Parity Violation in Chiral Molecules, ChemPhysChem*, **2015**, *16,* 3584-3589. DOI: 10.1002/cphc.201500801.
27. R. Prentner, M. Quack, J. Stohner, M. Willeke, *Wavepacket Dynamics of the Axially Chiral Molecule Cl-O-O-Cl under Coherent Radiative Excitation and Including Electroweak Parity Violation, J. Phys. Chem. A*, **2015**, *119* , 12805-12822. doi: 10.1021/acs.jpca.5b08958.
28. M. Quack, *On Biomolecular Homochirality as a Quasi-Fossil of the Evolution of Life, Adv. Chem. Phys.*, **2014**, *157*, 249-290.
29. M. Hippler, M. Quack, R. Schwarz, G. Seyfang, S. Matt, T. Märk, *Infrared multiphoton excitation, dissociation and ionization of C_{60}, Chem. Phys. Lett.*, **1997**, *278*, 111-120.
30. R. R. Ernst, T. Carrington Jr, G. Seyfang, F. Merkt, *Mol. Phys.*, **2013**, *111*, 1939-1963.

Formation of Metal Clusters and Nanowires in Superfluid Helium Droplets and their Surface Deposition

Wolfgang E. Ernst
Institute of Experimental Physics, Graz University of Technology, Petersgasse 16, A-8010 Graz, Austria

1. Introduction

The unique experimental conditions provided by superfluid helium nanodroplets (He_N) are not only utilized in spectroscopy [1] but are also interesting for the purpose of cluster synthesis. Superfluid droplets of 10^4 to 10^7 helium atoms (He_N) are doped with one or several atoms or molecules that move freely in or on the droplets and may form complexes in this cold environment.

2. Helium barrier

For a while, it was believed that all species that are collected inside a droplet, will immediately coagulate and form a stable aggregate in the cold environment. Unfortunately, things are not so simple. Depending on the dopant-helium interaction, a helium barrier may keep the atoms or molecules separated [2, 3].

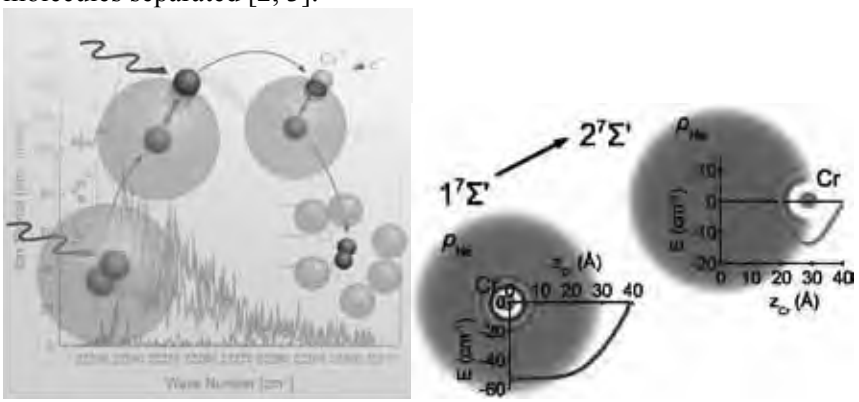

Fig. 1, left: a Cr dimer dissociates after photoexcitation with one atom remaining in the droplet center and one finding a stable location at the surface; recombination is observed after photoionization (from ref. 3); **right:** depending on the electronic state, Cr atoms can reside in the center or at the surface of the droplet (from ref. 2).

In the case of aggregation, we recently derived collision times for the coinage metal atoms Cu, Ag and Au in He-droplets [4] by applying helium density functional theory and molecular dynamics simulations.

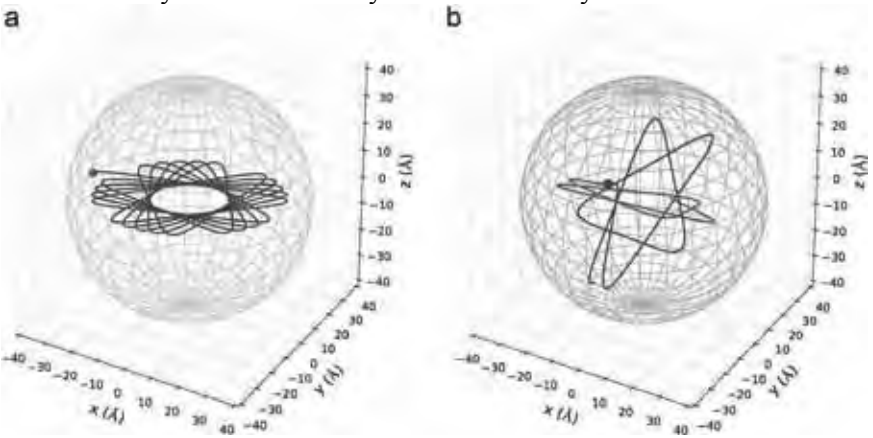

Fig. 2: Typical trajectories for a single (left) or for two atoms (right), given the example of Cu dopants in He_{5000}. Note the conservation of the angular momentum in the case of a single atom deposition, which leads to a rosetta-like, planar trajectory. In the right picture, where the two atoms attract each other, only the total angular momentum is conserved. Both particles move independently in their planes until the internuclear distance is accidentally small enough for the attractive interaction to force them on a collision course.

3. Cluster aggregation and soft landing

In our lab, cold Cu; Ag, Au, and Ni aggregates of different size and morphology have been generated in helium droplets [5, 6] and their landing on a solid substrate was modelled in a molecular dynamics simulation [7].

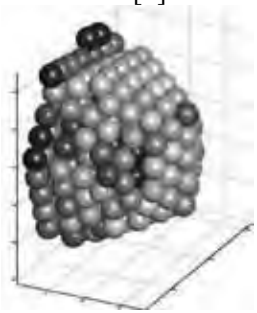

Fig. 3:
Simulated final morphology of an initial n = 309 icosahedral. The colors represent the local order. Here, yellow corresponds to fcc local order, light blue corresponds to hcp local order, and dark blue corresponds to fivefold axes, the other colors are
for intermediate states or not classified surface states. For details and assumptions see ref. 7.

4. Core shell clusters and nanowires

Fig. 4: Experimental scheme.

Nanowires and core-shell clusters with one metal surrounding a core of different kind were observed, deposited on solid substrates [8, 9], and analyzed by high resolution electron microscopy and tomography [10]. As it turns out, the temperature of the substrate [9] and the doping rate [11] have an important influence on the final cluster or wire structure. As will be shown in this talk, the systematic studies will help to provide recipes for the creation of tailored nanoparticles.

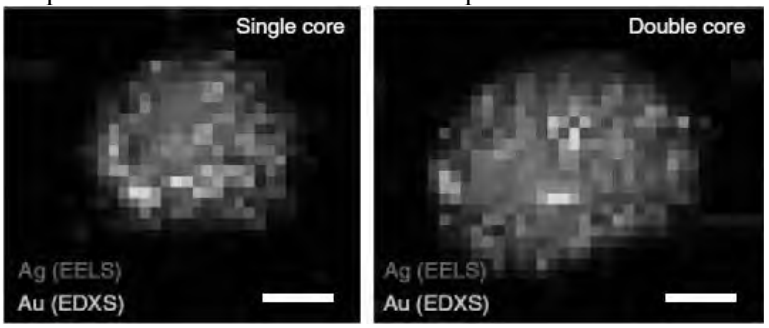

Fig. 5, left: single core cluster; **right:** double core cluster (Ag red, Au green), scale bars 2 nm, for details see ref. 10.

1. C. Callegari and W. E. Ernst, Handbook of High Resolution Spectroscopy, Eds. F. Merkt and M. Quack, 1st Edition, Vol. 3, 1551-1594 (2011).
2. M. Ratschek, J. V. Pototschnig, A. W. Hauser, and W. E. Ernst, Solvation and Spectral Line Shifts of Chromium Atoms in Helium Droplets based on a Density Functional Theory Approach, J. Phys. Chem. A **118** (33), 6622-6631 (2014) (Festschrift in honor of Franco Gianturco), http://pubs.acs.org/doi/abs/10.1021/jp5034036.
3. A. Kautsch, M. Koch, and W. E. Ernst, Photoinduced Molecular Dissociation and Photoinduced Recombination Mediated by

Superfluid Helium Nanodroplets, PCCP **17**, 12310-12316 (2015), http://dx.doi.org/10.1039/c5cp01009h .

4. A. W. Hauser, A. Volk, P. Thaler and W. E. Ernst, Atomic collisions in superfluid helium-nanodroplets: Timescales for metal-cluster formation derived from He-density functional theory, PCCP **17**, 10805-10812 (2015), http://dx.doi.org/10.1039/c5cp01110h.
5. A. Volk, P. Thaler, M. Koch, E. Fisslthaler, W. Grogger, and W. E. Ernst, High resolution electron microscopy of Ag-clusters in crystalline and non-crystalline morphologies grown inside superfluid helium nanodroplets, J. Chem. Phys. **138**, 214312-1-7 (2013), http://dx.doi.org/10.1063/1.4807843.
6. P. Thaler, A. Volk, D. Knez, F. Lackner, J. Steurer, M. Schnedlitz, and W. E. Ernst, Synthesis of Nanoparticles in Helium Droplets - a Characterization Comparing Mass-Spectra and Electron Microscopy Data, J. Chem. Phys. **143**, 134201-1-10 (2015), http://dx.doi.org/10.1063/1.4932182 .
7. P. Thaler, A. Volk, M. Ratschek, M. Koch, and W. E. Ernst, Molecular dynamics simulation of the deposition process of cold Ag-clusters under different landing conditions, J. Chem. Phys. **140**, 044326-1-9 (2014), http://dx.doi.org/10.1063/1.4862917 .
8. P. Thaler, A. Volk, F. Lackner, J. Steurer, D. Knez, W. Grogger, F. Hofer, and W. E. Ernst, Formation of core-shell nanowires along vortices in superfluid He nanodroplets, Phys. Rev. B **90**, 155442-1-5 (2014) http://link.aps.org/doi/10.1103/PhysRevB.90.155442.
9. A. Volk, D. Knez, P. Thaler, A. W. Hauser, W. Grogger, F. Hofer and W. E. Ernst, Thermal instabilities and Rayleigh breakup of ultrathin silver nanowires grown in helium nanodroplets, PCCP **17**, 24570-24575 (2015), http://dx.doi.org/10.1039/C5CP04696C.
10. G. Haberfehlner, P. Thaler, D. Knez, A. Volk, F. Hofer, W. E. Ernst, G. Kothleitner, Formation of bimetallic clusters in superfluid helium nanodroplets analyzed by atomic resolution electron tomography, Nature Communications 6, 8779-1-6 (2015), http://www.nature.com/ncomms/2015/151028/ncomms9779/full/ncomms9779.html .
11. A. Volk, P. Thaler, D. Knez, A. W. Hauser, J. Steurer, W. Grogger, F. Hofer, and W. E. Ernst, The impact of doping rates on the morphologies of silver and gold nanowires grown in helium nanodroplets, PCCP advance article (2015), http://dx.doi.org/10.1039/C5CP06248A .

The Oxidation of Ta Cluster Cations in the Gas Phase

Martin Tschurl

Lehrstuhl für Physikalische Chemie, Chemistry Department & Catalysis Research Center, Technische Universität München, Lichtenbergstraße 4, 85748 Garching bei München, Germany

There is a manifold of approaches for the study of ion/molecule reactions of metal clusters in the gas phase (see e.g. [1]). Most commonly applied techniques as FT-ICR MS or crossed beam experiments work under single-collision conditions. Experiments under multi-collision conditions are usually conducted by the guidance of the clusters through a fixed and defined reaction region (e.g. with guided beam experiments or flow tube reactors). Another approach exploits the storage of charged clusters in ion traps, which are filled with a buffer gas at pressures of up to some Pa [2]. Similar to a flow tube reactor, reactions are carried out in a multi-collisional regime, where the clusters are thermalized to achieve isothermal conditions. Furthermore and in contrast to methods with a fixed reaction region, the precise variation of the reaction time over a considerable long time frame can also be achieved.

In our approach we have combined a ring-electrode ion trap (RET) [3] with a laser evaporation source. The development of a new electronic device for the operation of the trap enables the storage of charged molecules in a mass range from about 200 to 20'000 amu with a subsequent controlled extraction of the ions. Besides other advantages, this extraction enables the efficient and simultaneous detection of several masses in a Re-TOF MS with good mass resolution [4].

With such a setup the elucidation of complex reaction schemes becomes possible. Based on the oxidation of Ta cluster cations the possibility to obtain new physical insights in the cluster properties is demonstrated by the deliberate change of different reaction parameters; i.e. the reaction time, the concentration of the reactant and the temperature of the molecules in the trap.

For example, a size-dependent behaviour is found for the oxidation of cationic Ta clusters. Smaller clusters undergo several oxidative fragmentation steps and the resulting intermediates (the tantalum oxides) are subsequently oxidized further. The high oxygen content of the final reaction product of clusters in this size regime is close to the composition of (bulk) Ta(V) oxide. This indicates a complete change of the clusters'

structure upon the reaction with oxygen. Larger clusters, on the other hand, stay intact and the product composition as well as the reaction progression suggest that oxidation only occurs at the clusters' surface. In the intermediate regime (Ta_9^+ to Ta_{12}^+) the reaction pathways are even more complex. Both reaction pathways are accessible and the product composition is not scalable.

The origin of the three different regimes is interpreted to arise from the clusters' heat capacity. If the cluster comprises a certain number of atoms its internal degrees of freedom enable an efficient redistribution of the released heat, which is caused by the dissociation of molecular oxygen. In this case dissociation can be avoided, which is the not possible for the reaction of smaller tantalum clusters.

The oxidation of tantalum clusters is chosen as model reaction, because this material and its oxides are widely used in several applications, as for example in optical coatings [5], in coatings of sensors [6] and in electrochemistry as materials for the oxygen evolution reaction [7]. Furthermore, tantalum oxides are active in many oxidation reactions, for example for several hydrocarbons including methane [8], which make such materials promising for catalytic applications as well.

References:

[1] H. Schwarz, How and Why Do Cluster Size, Charge State, and Ligands Affect the Course of Metal-Mediated Gas-Phase Activation of Methane?, Isr J Chem, 54 (2014) 1413-1431.

[2] S.M. Lang, T.M. Bernhardt, Gas phase metal cluster model systems for heterogeneous catalysis, Phys Chem Chem Phys, 14 (2012) 9255-9269.

[3] N. Heine, K.R. Asmis, Cryogenic ion trap vibrational spectroscopy of hydrogen-bonded clusters relevant to atmospheric chemistry, International Reviews in Physical Chemistry, 34 (2015) 1-34.

[4] D. Neuwirth, J.F. Eckhard, K. Lange, B. Visser, M. Wiedemann, R. Schröter, M. Tschurl, U. Heiz, Using controlled ion extraction to combine a ring electrode trap with a reflectron time-of-flight mass spectrometer, Int J Mass Spectrom, 387 (2015) 8-15.

[5] G. Harry, T.P. Bodiya, R. DeSalvo, Optical Coatings and Thermal Noise in Precision Measurements, Cambridge University Press, 2012.

[6] C. Christensen, R. de Reus, S. Bouwstra, Tantalum oxide thin films as protective coatings for sensors, J Micromech Microeng, 9 (1999) 113-118.

[7] F. Cardarelli, P. Taxil, A. Savall, C. Comninellis, G. Manoli, O. Leclerc, Preparation of oxygen evolving electrodes with long service life under extreme conditions, J Appl Electrochem, 28 (1998) 245-250.

[8] S.H. Taylor, J.S.J. Hargreaves, G.J. Hutchings, R.W. Joyner, An Initial Strategy for the Design of Improved Catalysts for Methane Partial Oxidation, Appl Catal a-Gen, 126 (1995) 287-296.

Fragmentation and molecular growth: PAHs and fullerenes

M. Gatchell, L. Giacomozzi, N de Ruette, M. Wolf, H.T. Schmidt, H. Zettergren, and H Cederquist
Stockholm University, AlbaNova University Center, S 106 91, Stockholm, Sweden

M.H. Stockett
University of Aarhus, Dept. Phys. & Astron., DK-8000, Aarhus C, Denmark

R. Delaunay, P. Rousseau, A. Domaracka, and B. Huber
CIMAP UMR6252 CEA CNRS Ensicaen Unicaen, F-140 70, Caen 5, France

Y Wang, M. Alcami, and F. Martin
Univ. Autonoma Madrid, Dept. Quim, Modulo 13, E-280 49 Madrid, Spain

In this presentation, we will discuss recent results on the fragmentation of Polycyclic Aromatic Hydrocarbon (PAH) molecules in collisions with atoms or ions. We have identified a new fragmentation channel, which becomes important at rather low collision energies and where the PAH-molecule only looses one of its carbon atoms [1]. We have in particular studied collisions with He

$$C_nH_m^+ + He \rightarrow C_{n-1}H_{m-x}^+ + CH_x + He. \quad (1)$$

Here, the loss of a single C-atom is often accompanied by the loss of one or several H-atoms. This behaviour (single-carbon loss) is very different from that of PAHs excited by photons [2], electrons [3] or heavier particles with high kinetic energies [4]. In these latter cases, CH_x-loss does not occur and C_2H_2-loss is the dominant carbon-backbone fragmentation channel

$$C_nH_m^+ + \text{photon/e}^-\text{/ion/atom} \rightarrow C_{n-2}H_{m-2}^+ + C_2H_2. \quad (2)$$

Different mechanisms on different timescales are responsible for processes (1) and (2). The loss of a C_2H_2-unit is, together with H-loss, the lowest-energy dissociation channel for many PAH molecules [5], while single-carbon loss is associated with high reaction barriers [1]. C_2H_2-loss is thus often a dominating decay channel when the excitation energy has time to distribute (statistically) over all vibrational degrees of freedom. This occurs on picosecond timescales and may be referred to as *statistical* fragmentation. In the case of process (1), however, the fragmentation (single carbon loss) is caused by prompt Rutherford-like carbon-knockout by the He atom. This only takes of the order of femtoseconds and is in the following referred to as *non-statistical* fragmentation. Here, there is no time for the excitation energy to distribute evenly before the fragmentation occurs. For both processes ((1) and (2)), additional fragmentation steps may occur due to remaining internal excitations in the fragments [1]. We would like to stress that "statistical" and "non-statistical" refers to the fragmentation step only. The distributions of impact parameters in heavy-particle collisions are statistical in both cases.

The PAHs are typically composed of three or more merged benzene-like rings and are in many cases planar. This makes direct observations of the prompt single-carbon knockout process (1) relatively simple through the identification of $C_{n-1}H_{m-x}^+$ - fragments [1]. In non-planar molecules like the fullerenes and most biomolecules, however, this becomes much more difficult. For the close to spherical fullerenes, there is the possibility that a heavy projectile knocks out more than one of the carbon atoms. In addition, a carbon atom that is knocked out may itself knock out other carbon atoms on its way out from a damaged fullerene [1,6,7]. Both these effects are much less important for two-dimensional structures for simple geometrical reasons. For the more irregular biomolecules single-atom knockout is also more difficult to study since these molecules typically have many different fragmentation channels with similarly low dissociation energies. For the PAHs there are usually just two low-energy dissociation channels C_2H_2-loss, and H-loss, which are well separated in energy from other dissociation channels. This makes the PAHs ideal systems for studies of knockout although these effects should be important for molecules in general [1]. Prompt knockout, or non-statistical fragmentation, are highly interesting phenomena as they may

give rise to efficient and unique molecular growth processes when the molecules are parts of larger aggregates of matter [6-8].

We will now discuss secondary reactions due to ion-cluster collisions. For clusters of fullerenes we have, for example, observed efficient formation of C_{119}-molecules. They are produced in a series of events where one C-atom is knocked out from one C_{60} molecule in the cluster. This so formed C_{59}-fragment is highly reactive [7] and combines very rapidly with an intact C_{60} molecule in the cluster to form a C_{119} dumbbell molecule [6,7]. This all happens well before [7] the cluster has fragmented which typically takes a few picoseconds [6]. The efficiencies of molecular growth processes depend on the balance between impact fragmentation and electronic excitation processes in the individual molecules. This has been shown explicitly for ions of different mass colliding with clusters of fullerenes [9,10], clusters of PAH molecules [8], and mixed PAH-fullerene clusters [11]. As discussed above, ion-collisions at low energies and photo-absorption processes lead to partly different PAH-fragmentation behaviours. This is true also for the fullerenes, which explains why secondary reactions in clusters of these molecules are qualitatively different for interactions with ions [10] and photons [12]. In the presentation we will show experimental results on ion-induced molecular growth in PAH- and fullerene-clusters and results from classical Molecular Dynamics simulations. The agreement between the experimental results and the simulations are excellent [8].

So far we have discussed fragmentation of *native* PAH molecules and secondary reactions of their fragments in clusters. However, there is currently also considerable interest in (super-) hydrogenated PAHs. There are several reasons for this. It has been suggested that hydrogenation may act as a protection for the PAH carbon backbone when PAH molecules are excited – for example in harsh conditions in the interstellar medium [13]. Further, hydrogenated PAHs are of interest as they possibly could offer formation pathways for molecular hydrogen, H_2, in astrophysical environments [14]. The idea here is that the additional hydrogen atoms are more loosely bound than the native ones and may boil off when the molecule is heated. This could protect the carbon backbone. At the same time, migration of the extra H-atoms may facilitate H_2-formation on the PAH surface or rim [15]. Reitsma *et al*. [13], have recently performed a pioneering photo-absorption experiment on hydrogenated PAHs from which they concluded that the net effect of hydrogenation was protection

of the carbon backbone. On the other hand, Gatchell *et al* collided hydrogenated PAH cations with He atoms at low center-of-mass energies [16] and arrived at the opposite conclusion. They showed that the weakening of the carbon-carbon bonds in the PAH backbone is a more important effect than the boil-off of the additional, loosely bound, H-atoms. Thus, hydrogenation does not seem to protect the PAH in this case. Here, we have two experiments with seemingly contradicting conclusions. It remains to be discussed - and investigated – to what extent differences in PAH-size (coronene in [13] and pyrene in [16]), differences in the degrees of hydrogenation, and in excitation methods may play a role here. Very recently, Stockett *et al*. [17] and Wolf *et al.* [18] investigated the fragmentation behaviours of native [17] and hydrogenated [18] pyrene as functions of collision energy. Wolf *et al.* [18] found that hydrogenation had a strongly weakening effect on the carbon backbone and that statistical CH_x-loss is a very important fragmentation channel at least for hydrogenated pyrene [16,17,18]. This tends to support the idea that hydrogenation makes PAH carbon backbones more [16] – rather than less [13] – sensitive to radiation.

References

[1] M.H. Stockett *et al.*, Phys Rev A **89**, 032701 (2014); M.H. Stockett *et al.*, Phys Chem Chem Phys **16**, 21980 (2014).
[2] M. Kjellberg *et al*., J Chem Phys **133**, 074308 (2010).
[3] S. Denifl *et al.*, Int J Mass Spectrom **249**, 343 (2006).
[4] A.I.S. Holm *et al.*, Phys Rev Lett **105**, 213401 (2010); A. Lawicki *et al.*, Phys Rev A **83**, 022704 (2011).
[5] A.I.S. Holm *et al.*, J Chem Phys **134**, 044301 (2011).
[6] H. Zettergren *et al*., Phys Rev Lett **110**, 185501 (2013).
[7] Y. Wang *et al.*, Phys Rev A **89** 062708 (2014).
[8] R. Delaunay *et al.*, J Phys Chem Lett **6**, 1536 (2015).
[9] F. Seitz *et al.*, J Chem Phys **139**, 034309 (2013).
[10] H. Zettergren *et al.*, J Chem Phys **133**, 104301 (2010).
[11] M. Gatchell *et al.*, Phys Rev A **90**, 022713 (2014).
[12] M. Heden *et al.*, Phys Rev A **71**, 055201 (2005).
[13] G. Reitsma *et al.*, Phys Rev Lett **113**, 053002 (2014).
[14] A.L. Skov, J.D. Thrower, and L. Hornekaer, Faraday Discuss **168**, 223 (2014).
[15] T. Chen *et al.*, J Chem Phys **142**, 144305 (2015).
[16] M. Gatchell *et al.*, Phys Rev A, Rap Comm **92**, 050702 (2015).
[17] M.H. Stockett *et al.*, J Phys Chem Lett **6**, 4504 (2015).
[18] M. Wolf *et al*., European Journal of Physics D, *submitted* December 2015.

Electronic Spectrum of $C60^+$: Diffuse Interstellar Bands Becoming Unravelled

John P. Maier
Department of Chemistry, University of Basel, Klingelbergstrasse 80, CH-4046 Basel, Switzerland
j.p.maier@unibas.ch

Shortly after the discovery of C60 (1), the question of its relevance to the diffuse interstellar bands was raised. In 1987 H.W.Kroto wrote: ”The present observations indicate that C60 might survive in the general interstellar medium (probably as the ion $C60^+$) “ (2).
In 1994 two diffuse interstellar bands (DIBs) at 9632 and 9577 Å were detected and proposed to be the absorption features of $C60^+$ (3). This was based on the proximity of these wavelengths to the two prominent absorption bands of $C60^+$ measured in a neon matrix by us in 1993 (4). Confirmation of the assignment required the gas phase spectrum of $C60^+$ and has taken 20 years.
The approach which succeeded to obtain these data confines $C60^+$ ions in a radiofrequency trap (22- or 4- pole), cools them by collisions with high density helium allowing in situ synthesis of the weakly bound $C60^+$− He complexes below 10 K. The photofragmentation spectrum of this mass-selected complex is then recorded using a cw laser. In order to infer the position of the absorption features of the bare $C60^+$ ion, measurements on $C60^+$− He2 were also made. The spectra show that the presence of a helium atom shifts the absorptions by less than 0.2 Å, much less than the accuracy of the astronomical measurements. The two absorption features in the laboratory have band maxima at 9632.7(1) and 9577.5(1) Å, exactly the DIB wavelengths, and the widths and relative intensities agree. This leads to the first definite identification of now four bands among the several hundred DIBs features known and proves the presence of gaseous $C60^+$ in the interstellar medium (5), (6). The electronic spectrum of cold C70+ has also been obtained by this approach and the implications for the relevance of fullerene cations in general in the interstellar medium can be discussed.

(1) H.W.Kroto, J.R.Heath, S.C.O’Brian, R.E.Curl and R.E.Smalley, Nature, 318, 162 1985.

(2) H.W.Kroto in “Polycyclic aromatic hydrocarbons and astrophysics”, eds. A.Leger, L.B. d’ Hendecourt and N.Boccara, Reidel, Dordrecht, 1987, p.197.
(3) B.H.Foing & P.Ehrenfreund, Nature, 369, L296, 1994.
(4) J.Fulara, M.Jakobi and J.P.Maier, Chem.Phys.Lett., 211, 227, 1993.
(5) E.K.Campbell, M.Holz, D.Gerlich and J.P.Maier, Nature, 523, 323, 2015.
(6) G.A.H. Walker, D.A. Bohlender, J.P. Maier and E. Campbell, Astrophys.J.Lett., 812, L8, 2015

Ion Microsolvation Probed by Cryogenic Ion Trap Vibrational Spectroscopy

Knut R. Asmis
Wilhelm-Ostwald-Institut für Physikalische und Theoretische Chemie
Univeristät Leipzig, Linnéstr. 2, 04109 Leipzig, Germany
knut.asmis@uni-leipzig.de

How ions are solvated in solution has intrigued physical chemists since the development of the theory of electrolytic dissociation at the end of the nineteenth century. A molecular-level understanding of ion solvation is not only important for understanding chemical processes in solution, but also plays an important role in understanding the surface speciation and reactivity of aerosols. Infrared photodissociation (IRPD) spectroscopy of mass-selected ions, thermalized to cryogenic temperatures, allows for a detailed characterization of the influence of the stepwise solvation of an ion on its properties, one solvent molecule at a time. Recent advances in the vibrational spectroscopy of microhydrated anions and ionic salt complexes are highlighted, with particular emphasis on the spectral fingerprint of large amplitude motion resulting from dynamic and entropic effects.

Cold and Controlled Ion Chemistry

Stefan Willitsch
Department of Chemistry, University of Basel, Klingelbergstrasse 80, 4056 Basel, Switzerland

Recent advances in the preparation and manipulation of neutral molecules and ions at temperatures below 1 K have opened up new possibilities for the study and control of chemical reactions. Samples of cold and spatially localized ions in traps, often referred to as Coulomb crystals [1], are attractive systems in this context because they enable the study of reactive processes on the level of single particles. In the talk, we will give an overview of recent experiments performed in our laboratory which rely on Coulomb-crystallized ions for precise studies of chemical dynamics.

First, we will focus on investigations of chemical reactions at temperatures just slightly above the absolute zero point of the temperature scale. We will discuss reactive collisions of ultracold neutral atoms with cold atomic ions in the millikelvin regime using a “hybrid” trap, i.e., a trap for the simultaneous confinement of both species. We will illustrate the exotic chemical processes and features of the dynamics which occur in ion-neutral systems under these conditions [2]. We will present results from a recently developed “dynamic” hybrid-trapping experiment which enables the study of cold ion-neutral reactions with a greatly improved energy resolution so that collisional quantum features such as resonances should be resolvable. Moreover, we will discuss the extension of hybrid trapping technology to molecular systems which is achieved by combining methods for the trapping of cold molecules and cold molecular ions.

Second, we will review recent work on reactive collisions between Coulomb-crystallized ions and larger neutral molecules which have been conformationally selected using an electrostatic deflector thus introducing a new method to study and control conformational effects in bimolecular reactions of complex molecules [3]. We will explore the potential of this approach for the precise study of reaction mechanisms relevant for synthetic chemistry.

Third, we will highlight recent advances in ion trapping technology which focus on the miniaturization of ion experiments on the surface of an ion trap chip. We will review recent results on a prototype surface-electrode trap for cold molecular ions [4] and discuss our ongoing development of a miniaturized guided-ion-beam machine on a chip.

[1] S. Willitsch, *Int. Rev. Phys. Chem.* **2012,** *31,* 175
[2] F.H.J. Hall et al., *Phys. Rev. Lett.* **2011**, *107,* 243202; *Phys. Rev. Lett.* **2012**, 109, 233202; *Mol. Phys.,* **2013,** *111,* 2020*; Mol. Phys.* **2013,** 111, 1683
[3] Y.-P. Chang et al., *Science* **2013**, *342*, 98; D. Rösch et al., *J. Chem. Phys*. **2014**, *140*, 124202
[4] A. Mokhberi and S. Willitsch, Phys. Rev. A **2014**, *90*, 023402; New J. Phys. **2015**, *17*, 045008

20 Years of Microplasma Research

Kurt Becker [1] and Karl H. Schoenbach [2]

[1] *Dept. of Mechanical and Aerospace Engineering and Dept. of Applied Physics, New York University Tandon School of Engineering, Brooklyn, NY 11201* (kurt.becker@nyu.edu)

[2] *Frank Reidy Research Center for Bioelectrics, Old Dominion University, Norfolk, VA 23508* (kschoenb@odu.edu)

Abstract: The field of microplasmas gained recognition as a well-defined area of research and application within the larger field of plasma science and technology about 20 years ago. Since then, the activity in microplasma research and applications has continuously increased. A survey of peer reviewed papers focusedon microplasmas published annually shows a steady increase from fewer than 20 papers in 1995 to about 75 in 2005 and more than150 in 2014. This count excludes papers that deal exclusively with technological applications where the microplasma is used solely as a tool. This presentation aims to provide a snap shot of the current state of microplasma research and applications. Given the rapid proliferation of microplasma applications, this presentation will focus primarily on the status of microplasma science and our understanding of the physics principles that enable microplasma operation.

Microplasmas, defined as plasmas where at least one dimensions is in the submillimeter range, include microarcs and microsparks, which are generated by electrical breakdown in gases and in liquids. They are generated either by applying an overvoltage to electrodes or by focusing high power laser radiation into the discharge medium. These plasmas are generally thermal plasmas, where the gas temperature is far above the room temperature and is approaching the electron temperature. Another group of microplasmas, which is based on glow discharges, however, is nonthermal, with gas temperatures much below the electron temperatures. Research in this area has undergone an enormous growth in the past two decades. The attraction of microplasmas is based on the fact that they can be operated stably at high gas pressures, in rare gases as well as in molecular gases, in a direct current (dc) mode as well as in pulsed dc and alternate current (ac) modes.

The first topical reviews [1-3] provided summaries of research into the

basic properties of microplasmas and results from some of the applications of microplasmas that occurred in the first 10 years, since research on this topic lifted off. Other review papers on microplasmas followed in 2008 and 2011 [4,5]. The most recent topical review paper, which covers microplasmas, but expands the view to include transient, filamentary plasmas, was published in 2013 [6]. Other review papers include reviews on UV light sources [7], microdischarge-based sensors [8], photonic devices [9], guided ionization waves in plasma jets [10,11], and microwave-sustained microplasmas [12]. Another area of application, which has gained strongly in interest by the scientific community, is plasma medicine. Reviews on this topic, but covering generally only parts of this expanding research area, have been published as early as 2005 [13-16] and continue to appear regularly in the literature. Modeling and improved diagnostics have allowed us in the past decade to gain more insight into the physics of nonthermal microdischarges. At the same time, the range of applications has been expanding at a rapid speed. This presentation covers the basic science of microplasmas and shows how the increasing scientific knowledge has led to the development of new plasma technologies. It does not cover micro-arc discharges and micro-sparks in gases, and provides limited information on filamentary dielectric barrier discharges, which can be found in other reviews [6,16].

For glow discharges, high pressure and small size are mutually consistent, based on similarity laws, which were shown to hold not only for the breakdown voltage (Paschen's law), but can be extended to sustained glow discharges. The minimum size of a glow discharge between two parallel-plane electrodes is given approximately by the cathode fall length of a normal glow discharge. Shorter lengths are possible, but at a drastically increased voltage. According to the similarity laws, the cathode fall length is inversely dependent on the pressure, p. Minimizing the axial dimension of a normal glow discharge thus requires maximizing the pressure. The product of cathode fall thickness and pressure depends on cathode material and type of gas. It varies between 0.23 Torr cm for an air discharge between copper electrodes to 1.45 Torr cm for He discharges between magnesium electrodes [17]. Assuming an average value of 1 Torr cm, reducing the thickness of the discharge plasma to 100 μm requires increasing the pressure to about 100 Torr, for 10 μm to more than atmospheric pressure. However, the similarity laws, on which this estimate is based, rely on the assumption that the electron generation at the cathode is due to ion impact. Experimental studies on microgaps [18,19] showed that for gaps

in the micrometer range, the breakdown voltage actually decreases with decreasing electrode spacing, d, instead of increasing, as expected from the Paschen's law. This deviation from the Paschen curve for very small gaps (>2μm) is likely caused by pure field emission (Fowler-Nordheim field emission) and, in the transition region (up to about 10μm), through ion-enhanced field emission caused by the presence of positive ions near the cathode surface [20]. The smallest gaps for which the breakdown voltage in atmospheric pressure gas (air and N_2) was measured were approximately half a micrometer [23,24]. Since the electrical breakdown voltage in such small gaps is strongly affected by the surface roughness of the electrodes [25], reproducible electric field breakdown results for these extremely small gaps could only be obtained by polishing the electrodes to a very high finish [23,24].

Whereas the minimum axial dimension of a glow discharge is likely determined by the surface roughness of the electrodes, the limitations in the transverse direction is determined by the transition from a normal glow discharge into a subnormal glow discharge. Reducing the current in a normal glow discharge causes a reduction in the diameter of the cathode fall area. When the diameter reaches values on the order of the cathode fall length (dark space at the cathode), the discharge voltage rises [26]. This increase is due to the increased radial losses of charged particles. Based on these considerations, and assuming that the thickness of the cathode fall region is determined by values of pD in the range of 0.5 to 1 Torr cm, the minimum size of an atmospheric pressure glow discharge in the lateral direction is about 10 μm.

Minimum size atmospheric pressure glow discharge plasmas generated between plane parallel electrodes are disk shaped with radial dimensions on the order of 10 μm. Their axial dimensions are dependent on the surface roughness of the electrodes, and consequently even for highly polished electrodes are not much below 1 μm. Theoretically, the smallest dimension of a microdischarge is determined by the Debye length, D_b. With measured electron densities of high pressure mico-glow discharges greater than 10^{14} cm^{-3} and average electron energies of approximately 1 eV, typical Debye lengths are less than 0.35 μm, which is less than the minimum axial dimension of a microdischarge determined by the electrode surface roughness.

References

1. R. Foest, M. Schmidt, K. Becker, Int. J. Mass Spectrom. **248**, 87 (2005)
2. K.H. Becker, K.H. Schoenbach, and J.G. Eden, J. Phys. D: Appl. Phys. **39**,

R55 (2006)
3. K. Tachibana, IEEJ Trans., **1**, 145-155 (2006)
4. F. Iza, G.J. Kim, S.M. Lee et al., Plasma Proc. Polymers **5**, 322 (2008)
5. A.P.Papadakis, S. Rossides, A.C. Metaxas, The Open Appl. Physics Journal **4**, 45 (2011)
6. P. Bruggenman, R. Brandenburg, J. Phys. D: Appl. Phys., **46**, 464001 (2013)
7. K.H. Schoenbach, W. Zhu, IEEE J. Quantum Electr., **48(6)**, 768-782 (2012)
8. C.K. Eun, Y. Gianchandani, IEEE J. Quantum Electronics, **48(6)**, 814-826 (2012)
9. J.G. Eden, S.-J. Park, J. H. Cho et al., IEEE Trans. Plasma Science **41**, 661 (2013).
10. X. Lu, M. Laroussi, V. Puech, Plasma Sources Sci. Techn., **21**, 034005 (2012)
11. X. Lu, G.V. Neidis, M. Laroussi, K. Ostrikov, Physics Reports **540**, 123-166 (2014)
12. J. Hopwood, A. Hoskinson, J. Gregorio, Plas. Sources Sci. Technol. **23**, 064002 (2014).
13. K. Becker, A. Koutsospyros, S.-M. Yin, C. Christodoulatos, N. Abramzon, J.C. Joaquin, and G. Brelles-Mariño, Plasma Phys. Controlled Fusion **47**, B513-23 (2005)
14. M.G. Kong, G. Kroesen, G., Morfill, T., Nosenko, T. Shimizu, J., van Dijk, J.L. Zimmer, New Journal of Physics, **11**, 115012 (2009)
15. M. Laroussi, IEEE Trans. Plasma Science **43**, 703712(2015).
16. U. Kogelschatz, Plasma Chemistry and Plasma Processing, **23(1)**, 1-46 (2003)
17. J.D. Cobine, *Gaseous Conductors, Theory and Engineering Applications.* Dover Publications, Inc, New York 1958, table 8.3. [20]
18. T. Ono, D.Y. Sim, M. Esachi, J. Micromech. Microeng., **10**, 445-45 (2000).
19. G.P. Slade, E.D. Taylor, IEEE Trans. Compon. Packag. Technol., **25**, 390-396 92002)
20. D.B. Go, A.D. Pohlman, J. Appl. Phys., **107**, 103303 (2010)
21. W. Zhang, T.S. Fisher, S.V. Garimella, J. Appl. Phys., **96,** 6066-6072 (2004)
22. G. Tirumala, D.B. Go, Appl. Phys. Lett., **97**, 151502 (2010)
23. E. Hourdakis, B. Simonds, N.M. Zimmerman, Rev. Sci. Instrum., **77**, 034702 1-4 (2006)
24. R.S. Dhariwal, J.-M. Torres, M.P.Y. Desmulliez, IEEE Proc.-Sci. Meas. Technol., **147**, 261-265 (2000)
25. J.-M. Torres, R.S. Dhariwal, Nanotechnology, **10**, 102-107 (1999)
26. A. von Engel, *Ionized Gases*, American Vacuum Society Classics, American Institute of Physics, reprint by arrangement with Oxford University Press, 1965

Attosecond dynamics of photoionization: from atoms to the liquid phase

Martin Huppert, Inga Jordan and Hans Jakob Wörner
Laboratorium für physikalische Chemie, ETH Zürich

Photoionization is one of the most fundamental consequences of short-wavelength light-matter interaction. Within scattering theory, the process of photoemission can be characterized by a species-, initial state- and partial-wave-specific scattering phase shift. The derivative of the scattering phase with respect to energy has the dimension of time and corresponds to a photoionization delay or Wigner delay [1]. Typical photoionization delays amount to tens of attoseconds (1 as = 10^{-18} s) and have recently become accessible in the time domain. In this lecture, experimental results on attosecond time-resolved photoionization [2] of atoms, molecules and liquid water will be discussed and interpreted.

The photoionization delays between photoelectrons associated with the $^2P_{3/2}$ and $^2P_{1/2}$ states of Xe^+ and Kr^+ display small (-20 to +10 as), energy-dependent relative delays that provide the first experimental access to scattering phase shifts between non-degenerate continua. Combined with classical photoelectron measurements, these results enable the first complete quantum-mechanical description of the photoionization process of a p^6 shell.

The extension of photoionization-delay measurements to molecules will then be described, including the solution of technical challenges caused by spectral overlap of photoelectron spectra generated by attosecond pulses. The measured photoionization delays between the X^+ and A^+ states of H_2O^+ are found to lie very close to zero for all investigated photon energies, consistent with the unstructured photoionization continua associated with these two electronic states. In contrast, the photoionization delays between the X^+ and A^+ states of N_2O^+ are found to be much larger, reflecting the presence of two shape resonances in the photoionization continuum of the A^+ state.

Finally, the extension of attosecond-time-resolved spectroscopy to the liquid phase is reported. Coupling a liquid microjet to a photoelectron spectrometer [3] enabled us to collect photoelectron spectra from liquid- and gas-phase water simultaneously. The binding energies of $H_2O(l)$ and $H_2O(g)$ are sufficiently different to allow for a complete separation of the electrons associated with the X^+ state of both species. We measure a delay of ~50 as between the electrons from the two phases. Since our measurements on solvated water molecules are referenced to isolated molecules, the measured delays reflect the effects of (i) electron propagation through the aqueous environment and (ii) solvation of the parent molecule. Comparison of the experiments with theory shows that the measured delays are much smaller than the time scales of both electron transport and inelastic scattering, but comparable to the expected elastic scattering times. These results are expected to provide unprecedented insights into the nature of photoionization and electron transport in liquid water. More generally, they demonstrate the feasibility of attosecond time-resolved measurements in the liquid phase.

[1] E. P. Wigner, *Phys. Rev.* 98, 145 (1955)
[2] M. Huppert, I. Jordan, H. J. Wörner *Rev. Sci. Instrum.* 86, 123106 (2015)
[3] I. Jordan, M. Huppert, M. A. Brown, J. A. van Bokhoven, H. J. Wörner, *Rev. Sci. Instrum.* 86, 123905 (2015)

Spontaneously electrical solids: spontelectrics

David Field[*], Andrew Cassidy[*], Martin McCoustra[**], Alexander Rosu-Finsen[**], Jérôme Lasne[***].

[*]Dept. of Physics and Astronomy, Aarhus University, Denmark; [**]Institute of Chemical Sciences, Heriot-Watt University, Scotland; [***]Laboratoire Interuniversitaire des Systèmes Atmosphériques, Université Paris-Est Créteil, Université Paris Diderot, France.

We describe the discovery of a spontaneously electrical form of the solid state, which has been given the name 'spontelectric'.[1,2,3,4,5,6,7,8,9,10,11] Below we outline some of the properties of spontelectrics. These properties reveal new and intriguing physics, which sets the spontelectric effect apart from the ferroelectric effect, which might otherwise be thought of as comparable. Spontelectrics are also quite distinct from such special cases as certain polyimide films[1] or porous amorphous solid water.[12]

This short review is divided into (i) the discovery of spontelectrics in electron beam experiments, (ii) the properties uncovered, including those of heterolayer structures, (iii) a model for the spontelectric effect, (iv) the independent identification of the spontelectric effect using reflection absorption infrared spectroscopy (RAIRS) in collaboration with the group of Martin McCoustra at Heriot-Watt University and (v) spontelectrics in regions of star formation.

(i) the discovery of spontelectrics in electron beam experiments.
When gases are condensed at sufficiently low temperature onto a solid surface, they form films which may spontaneously exhibit electric fields in excess of 10^8 V/m. These spontelectric films may be composed of a number of quite mundane dipolar materials which include such diverse species as propane, nitrous oxide or methyl formate. This phenomenon was discovered by serendipity in an instrument designed to study the interaction of very low energy electrons with solid material.

Electrons, formed by synchrotron photoionization of Ar at a well-defined potential[13], were allowed to impinge on solid material in the form of film prepared by low temperature deposition from the gas phase. A current may pass into the sample when the sample is held at a potential more positive than that at which the

electrons were formed, as found for water ice[14]. However similar films, formed not of water ice but of nitrous oxide (N_2O), were found to *attract* electrons. A negative bias, which could be of many volts, had to be applied to the metallic substrate on which the N_2O film was formed in order to null the observed current. Evidently the N_2O surface was spontaneously biased electrically positive, as set out in [2], the original paper in which the effect was described.

(ii) Salient properties of spontelectric solids

We find:

a). The measured surface potential may be either positive or negative, for example for toluene or isopentane, respectively.

b). The voltage is linearly proportional to the thickness of the film. The highest voltage measured was 38V on a ~1100 ML film of nitrous oxide.

c). The spontelectric field depends on the temperature at which the film is deposited. It is in general less for higher temperatures.

d). For methyl formate films, the spontelectric field at first falls but then *increases* with temperature beyond a critical temperature of deposition.

e). Warming of a spontelectric film in general causes at first little change in the spontaneous potential on the surface of the film. A critical temperature is reached at which the spontelectric effect decays abruptly. By analogy with ferromagnetism, this is referred to as the Curie point. Subsequent cooling to below the Curie point has not been observed to reintroduce a surface potential.

f). The spontelectric potential is in general stable with time, at least over a period of many hours.

g). The nature of the surface upon which spontelectric films are deposited has essentially no bearing on the values of surface potential.

h). Spontelectric films can be laid down one on the other and behave approximately independently, making feasible the creation of any desired structure of electric fields on the nanoscale.

(iii) a model for the spontelectric effect

A phenomenological model has been developed which assumes that oriented dipoles give rise to the surface potential. This potential may now be seen as a polarization potential. Given some degree of orientation, we introduce the concept that constituent molecules in the film experience (i) a local symmetric field,

$<E_{sym}>((1+ \zeta(<\mu_z>/\mu)^2)$, where $<E_{sym}>$ and ζ are derived from fitting to experimental data. Here $<\mu_z>/\mu$, is the temperature dependent degree of dipole orientation, defined as the ratio of the average z-component of the dipole moment and the total dipole moment of the molecular species in the solid state. (ii) An asymmetrical field, the spontelectric field, E_S, given by $4\pi(<\mu_z>/\mu)\ \mu/\Omega$, where Ω, related to the molecular volume, may be treated as a parameter of the model. Mean field theory gives an implicit expression for $<\mu_z>/\mu$, yielding the familiar Langevin function for orientational interactions.[15]

This model can be used to describe the deposition temperature dependence of the spontelectric field in a convincing manner[1], giving credence to the notion that the spontelectric effect is due to spontaneous dipole orientation. Remarkably, the model also reproduces the experimental data in which the spontelectric field in methyl formate drops as the deposition temperature is increased to 80K, but then rises rapidly at higher deposition temperatures. This behaviour, quite unawaited in what appears to be an order-disorder system and otherwise unknown in the solid state, underlines the non-local, non-linear nature of the spontelectric effect.

(iv) identification of the spontelectric effect using RAIRS

In pursuit of a new phenomenon, it is well to have a completely independent experimental method of its identification. The spontelectric field should create a vibrational Stark shift in RAIRS spectra of spontelectric solids. This could indeed be observed and the extent of the Stark shift could be shown to correspond to the spontelectric fields known from experimental determinations for N_2O, based on the electron beam technique. The crux of the technique is that a measureable temperature dependence of spectral features in RAIRS, reflecting the known temperature dependence of the spontelectric field, is diagnostic of the spontelectric nature of the film of material concerned.

A valuable spin-off of RAIRS was that we were able to demonstrate that solid CO displayed the spontelectric effect and to determine the field in thin films of CO. This has interesting implications in the interstellar medium.

(v) spontelectrics in regions of star formation.

Radio observations show that in the earliest period of star formation, there can be strong depletion[16] of gas phase CO, the otherwise most prevalent molecule after H_2. IR observations find that CO is condensed onto 10K dust grains and our experiments demonstrate that dust grains will therefore acquire a positive potential of ~80 mV. This attracts electrons and ions from the interstellar plasma, where they recombine on the surface of the grains. This mechanism reduces the degree of gas phase ionization of the medium by a factor between 5 and 10.

The effect of this reduction is to allow the magnetic field to slip out of the medium on a time scale of a few hundred thousand years. Since the so-called 'magnetic pressure' is instrumental in holding up gravitational collapse to form protostars, the presence of spontelectric grains can speed up the rate of this earliest stage of star formation by a corresponding factor of 5 to 10.

---

[1] D. Field, O. Plekan, A. Cassidy, R. Balog, N. C. Jones, and J. Dunger, *Int. Rev. Phys. Chem.*, 2013, **32**, 345–392
[2] R. Balog, P. Cicman, N. Jones, and D. Field, *Phys. Rev. Lett.*, 2009, **102**, 2–5
[3] D. Field, O. Plekan, A. Cassidy, R. Balog, and N. Jones, *Europhys. News*, 2011, **42**, 32–35.
[4] O. Plekan, A. Cassidy, R. Balog, N. C. Jones, and D. Field, *Phys. Chem. Chem. Phys.*, 2011, **13**, 21035–44.
[5] O. Plekan, A. Cassidy, R. Balog, N. C. Jones, and D. Field, *Phys. Chem. Chem. Phys.*, 2012, **14**, 9972–6.
[6] A. Cassidy, O. Plekan, R. Balog, N. C. Jones, and D. Field, *Phys. Chem. Chem. Phys.*, 2012, **15**, 108–113.
[7] A. Cassidy, O. Plekan, , J.Dunger, R. Balog, N. C. Jones, J. Lasne, A.Rosu-Finsen, M.R.S.McCoustra and D. Field *Phys. Chem. Chem. Phys.*, 2014, **16**, 23843
[8] J. Lasne, A.Rosu-Finsen, A.Cassidy, M.R.S.McCoustra, D. Field, *Phys. Chem. Chem. Phys.*, 2015, **17**, 20971
[9] A.Rosu-Finsen, J. Lasne, A.Cassidy, M.R.S.McCoustra, D. Field, *Phys. Chem. Chem. Phys.*, 2015, **17**, 30177
[10] A.Cassidy, O. Plekan, R.Balog, J.Dunger, D. Field, *J.Phys.Chem.* 2014, **118**, 6615
[11] J. Lasne, A.Rosu-Finsen, A.Cassidy, M.R.S.McCoustra, D. Field, *Phys. Chem. Chem. Phys.*, 2015, DOI: 10.1039/c5cp07049j.
[12] C. Bu, J. Shi, U. Raut, E. H. Mitchell, R. A. Baragiola, *J. Chem. Phys.,* 2015, **142**, 134702
[13] S.V. Hoffmann, S.L. Lunt, N.C. Jones, D. Field, J.-P. Ziesel, *Rev. Sci. Instrum.* 2002, **73**, 4157.
[14] R. Balog, P. Cicman, D. Field, L. Feketeova, K. Hoydalsvik, *J.Phys.Chem*., 2011, **115**, 6820
[15] C. Kittel, *Introduction to Solid State Physics*, Wiley, 3rd edn., 2005
[16] Lada C. J., Bergin E. A., Alves J. F., Huard T. L.,2003, Astrophys.J, **586**, 286

Ab initio free energy calculations with chemical accuracy for molecule - surface interactions

Joachim Sauer
Institut für Chemie, Humboldt-Universität, Unter den Linden 6, 10000 Berlin, Germany
js@chemie.hu-berlin.de

A hybrid method that combines MP2 on cluster models with DFT+dispersion on periodic models and adds CCSD(T) corrections is presented. The method yields binding energies for molecules on metal oxide surfaces and in nanoporos materials with chemical accuracy (within ± 4 kJ/mol) or better. Examples are the binding of CH_4, N_2, CO and CO_2 on the internal surfaces of metal organic frameworks (MOF),[1] as well as the adsorption of hydrocarbons in zeolites.[2,3] Entropies of adsorption can also be calculated with chemical accuracy from vibrational partition functions calculated by DFT+dispersion, when anharmonicities are included.[2] This is shown for the adsorption equilibrium of small alkenes in a zeolite with Brønsted sites (H chabazite).[3] The accurate calculations of energy barriers[4] and pre-exponentials allows the *ab initio* calculation for rate-constants with chemical accuracy for systems with several hundred atoms as shown for the methylation of alkenes in H-ZSM-5.[5]

1 K. Sillar and J. Sauer, *J. Am. Chem. Soc.*, 2012, **134**, 18354.
2 G. Piccini and J. Sauer, *J. Chem. Theory Comput.*, 2014, **10**, 2479.
3 G. Piccini, M. Alessio, J. Sauer, Y. Zhi, Y. Liu, R. Kolvenbach, A. Jentys and J. A. Lercher, *J. Phys. Chem. C*, 2015, **119**, 6128.
4 S. Svelle, C. Tuma, X. Rozanska, T. Kerber and J. Sauer, *J. Am. Chem. Soc.*, 2009, **131**, 816.
5 G. Piccini, M. Alessio and J. Sauer, *publication in preparation*, 2016.

The reactions of atoms with molecules on the surfaces of cold molecular ices

Helen Kimber and Stephen D. Price
Chemistry Department, University College London, 20 Gordon Street, London WC1H 0AJ, UK.
s.d.price@ucl.ac.uk

In the 1960's the critical role of heterogeneous (gas-surface) chemistry in the tenuous and cold environment of the interstellar medium was predicted.[1] Specifically, modelling revealed that the formation of the most ubiquitous of interstellar molecules, molecular hydrogen, must occur efficiently on the surfaces of the cold dust grains that were present in interstellar clouds. Laboratory experiments required until early this century to satisfactorily characterize this low-temperature reactivity of H-atoms to form dihydrogen.[2-7] Since this early work on the self-reaction of H-atoms, laboratory investigations have diversified to study the reactions of H, O and N atoms with prototypical examples of the molecules that are expected to be found frozen to the surface of interstellar dust grains in cold interstellar clouds.[8] To this end, early experiments investigated, for example, the reaction of H atoms with CO to form methanol.[9] Indeed, methanol is an interstellar molecule where the shortfall in the predicted yield from gas-phase chemistry readily highlighted the crucial role of heterogeneous chemistry in interstellar synthesis.[9]

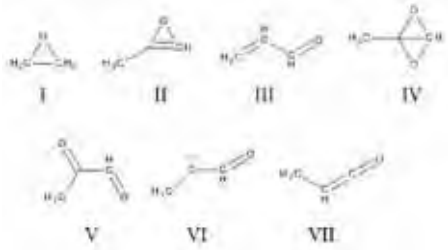

Organic structures relevant to the discussion of the reaction of O atoms with propyne.

Reactions in and on molecular ices, under pseudo-interstellar conditions, can be classified broadly as *thermal* or *non-thermal*. Non-thermal reactivity occurs where one of the reagents, commonly an atom or radical, is generated *in-situ*, in the ice, by an energetic particle (e.g. a cosmic ray) or a photon. This energized species then reacts with another component of the ice to generate products. The "non-thermal" label for this class of reactivity arises because the atom or radical is not necessarily

thermalized with the ice and can possess a significant internal energy. This internal energy can allow non-thermal reactants to overcome energy barriers in potential reactive pathways. A significant number of experimental investigations of non-thermal reactivity pertinent to the interstellar medium have been performed, generating the reactive species by, for example, high-energy proton or electron impact.[10,11]

This paper reports the recent results from an experimental apparatus designed to investigate thermal (or pseudo-thermal) reactivity relevant to the interstellar medium, where the reactant species (atoms in our case) are generated away from the surface, are thermalized (to a greater or lesser extent), and then react with molecules bound to the cold dust grain.[12,13] We will report on investigations of the reactions of O and H atoms with small organic molecules such a propyne (CH_3-CCH).[14] These investigations show, perhaps surprisingly at these low temperatures, that both O and H atoms are readily reactive with small unsaturated organic molecules at surface temperatures from 15 K to 70 K. Similar reactivity is observed by other groups studying these low temperature phenomena.[8,15,16] Since many of the reactive pathways observed have significant activation barriers in the gas-phase, it is clear that a chemist would consider the surface is acting as a catalyst by providing lower energy reactive pathways to facilitate these potentially important interstellar reactions.

We will also report on the results of our collaboration with modellers and observational astronomers. These collaborations involve successful attempts to incorporate the surface reactions we characterize experimentally into current models of interstellar chemistry. These modelling efforts indicate that it is not just for the case of methanol where heterogeneous chemistry can influence molecular abundances observed in the interstellar medium.[17-19]

The current experimental arrangement at UCL, in brief, involves dosing the output from a microwave discharge in O_2 or H_2, to form O or H atoms respectively, onto a molecular ice formed on a cooled graphite surface. Following this dosing. the surface is warmed and the desorbed products identified by time-of-flight mass spectrometry. This experimental arrangement, although productive, possesses some fundamental limitations which will be discussed. Progress on a new experimental initiatives to overcome these shortcomings will be presented.

References

1 R. J. Gould and E. E. Salpeter, Astrophys. J. **138,** 393, (1963).
2 L. Hornekaer, A. Baurichter, V. V. Petrunin, A. C. Luntz, B. D. Kay, and A. Al-Halabi, J. Chem. Phys. **122**, (2005).
3 L. Hornekaer, E. Rauls, W. Xu, Z. Sljivancanin, R. Otero, I. Stensgaard, E. Laegsgaard, B. Hammer, and F. Besenbacher, Phys. Rev. Lett. **97**, (2006).
4 L. Gavilan, J. L. Lemaire, G. Vidali, T. Sabri, and C. Jaeger, Astrophys. J. **781**, (2014).
5 G. Vidali, Chemical Reviews **113,** 8762, (2013).
6 F. Islam, E. R. Latimer, and S. D. Price, J. Chem. Phys. **127**, (2007).
7 E. R. Latimer, F. Islam, and S. D. Price, Chem. Phys. Lett. **455,** 174, (2008).
8 H. Linnartz, S. Ioppolo, and G. Fedoseev, International Reviews in Physical Chemistry **34,** 205, (2015).
9 H. Hidaka, M. Watanabe, A. Kouchi, and N. Watanabe, Astrophys. J. **702,** 291, (2009).
10 S. Maity and R. I. Kaiser, Astrophysical Journal **773**, (2013).
11 T. Sabri, G. A. Baratta, C. Jager, M. E. Palumbo, T. Henning, G. Strazzulla, and E. Wendler, Astronomy & Astrophysics **575,** 11, (2015).
12 M. D. Ward, I. A. Hogg, and S. D. Price, Monthly Notices of the Royal Astronomical Society **425,** 1264, (2012).
13 M. D. Ward and S. D. Price, Astrophysical Journal **741**, (2011).
14 H. J. Kimber, C. P. Ennis, and S. D. Price, Faraday Discussions **168,** 167, (2014).
15 E. Congiu, M. Minissale, S. Baouche, H. Chaabouni, A. Moudens, S. Cazaux, G. Manico, V. Pirronello, and F. Dulieu, Faraday Discussions **168,** 151, (2014).
16 M. Minissale, J. C. Loison, S. Baouche, H. Chaabouni, E. Congiu, and F. Dulieu, Astronomy & Astrophysics **577**, (2015).
17 A. Occhiogrosso, A. Vasyunin, E. Herbst, S. Viti, M. D. Ward, S. D. Price, and W. A. Brown, Astronomy & Astrophysics **564**, (2014).
18 A. Occhiogrosso, S. Viti, M. D. Ward, and S. D. Price, Monthly Notices of the Royal Astronomical Society **427,** 2450, (2012).
19 P. M. Woods, A. Occhiogrosso, S. Viti, Z. Kanuchova, M. E. Palumbo, and S. D. Price, Monthly Notices of the Royal Astronomical Society **450,** 1256, (2015).

Modification of surfaces with non-planar hydrocarbons

Quirin Stöckl, Johannes Seibel, Anais Mairena, Manfred Parschau, Karl-Heinz Ernst
Empa, Swiss Federal Laboratories for Materials Science and Technology

Ya-Chu Hsieh, Yao-Ting Wu
Department of Chemistry, National Cheng Kung University, Taiwan

Alix F. Tröster, Konstantin Grenader, Andreas Terfort
Institut für Anorganische und Analytische Chemie, Goethe-Universität Frankfurt, Frankfurt, Germany

Susanne Baumann, Christopher P. Lutz, Andreas J. Heinrich
IBM Almaden Research Center, San Jose, USA

Oliver Allemann, Laura Zoppi
Department of Chemistry, University of Zurich, Zürich, Switzerland

Jay S. Siegel,
School of Pharmaceutical Science and Technology, Tianjin University, PR China

1. Introduction

Modification of surfaces with aromatic organic molecules is the key approach to new materials for organic photovoltaics (OPV), organic light emitting devices (OLEDs), and molecular electronics such as organic field effect transistors (OFETs). The interfaces between active layers and electrodes influence the electronic and optical properties as well as the device performance. Furthermore, because the spatial extent of the molecular wavefunctions is rarely isotropic, the relative orientation of the molecules in the film, and thereby the degree of overlap of the frontier orbitals, will play an important role in determining film properties. Bowl- and helically shaped polynuclear hydrocarbons offer a special opportunity in this arena owing to their substantial dipole moment, large conjugated network and shape complementarity.

2. Buckybowls

We have studied a large variety of different bowl-shaped molecules on single crystalline copper surfaces (Fig. 1). All compounds were deposited by sublimation *in vacuo* onto the single-crystalline metal surfaces. Their two-dimensional crystallization during cooling has been studied by scanning tunnelling microscopy (STM).

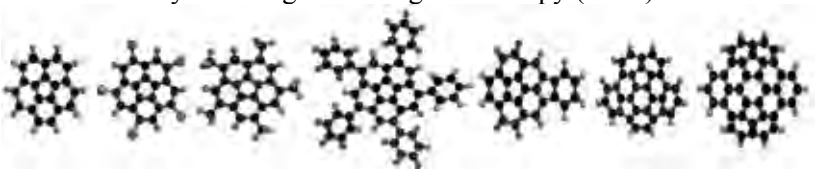

Fig. 1: Buckybowls (from left to right): corannulene $C_{20}H_{10}$, pentachloro corannulene, pentamethyl corannulene, pentaphenyl corannulene, indeno corannulene, tribenzo corannulene, the C_{70}-fragment bowl $C_{38}H_{14}$

In particular stereochemical issues like tiling the plane with chiral fivefold-symmetric molecules has been addressed in our studies, with focus on the pentagonally shaped pentamethyl corannulene (Me_5cor) and the five-star-shaped pentaphenyl corannulene (Ph_5cor, see Fig. 2).[1]

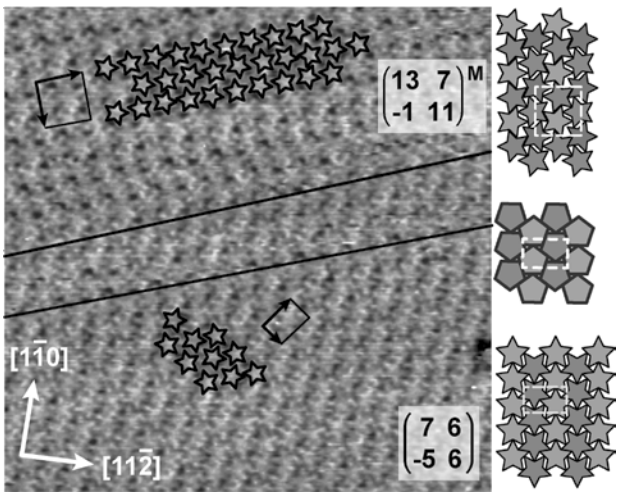

Fig. 2. Two coexisting phases of star-shaped Ph_5cor on Cu(111). The plane groups are p2gg (top) and p2mg (bottom). The latter is assumed to provide the densest packing for hard pentagons and has been observed for Me_5cor as well.[2]

3. Helicenes

Molecular helicity, the ability of molecules to form left- and right-handed helical structures, is a manifestation of chirality and has important implications in molecular biology, in molecular spin filters, and photonic devices using organic materials. However, the way helical molecules interact with each other and assemble into macroscopic structures is still an open question. We focus on stereochemical recognition among 'carbohelicenes', which are *ortho*-annulated, π-conjugated aromatic hydrocarbons. The two-dimensional self-assembly and crystallization of the 5- and 7-ring carbohelicene analogues, penta- and heptahelicene, has been investigated (Fig. 3).

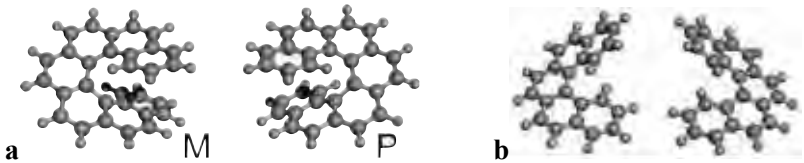

Fig. 3. Ball-and-stick models of enantiomers of hepta- (left) and pentahelicene (right).

Nevertheless, little is known about intermolecular interactions in the simplest case, a dimer of molecules. We report the differences in homochiral and heterochiral recognition among the molecules in dimers by means of submolecular resolved STM as well as STM manipulation of the entities (Fig. 4), and discuss the role of the stereochemical recognition between the molecular footprint and the surface symmetry, as well as the role of viable nuclei for further growth.[3]

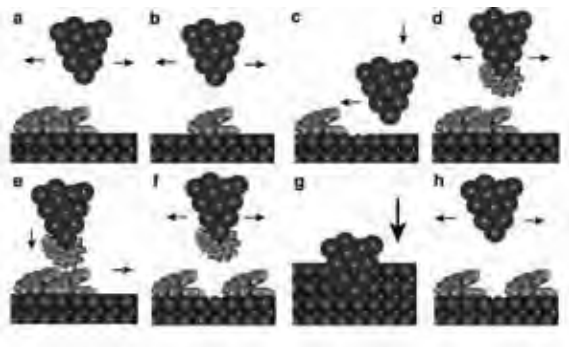

Fig. 4. Scheme of the manual separation procedure of helicene dimers.

Finally, cooperative chiral effects induced by using enantiomeric excess or unbalanced diasteriomeric mixtures of different helicene species, will be discussed.[4]

References

(1) Q. Stöckl, D. Bandera, C. S. Kaplan, K.-H. Ernst, J. S. Siegel, *J. Am. Chem. Soc.* **2014**, *136*, 606–609.
(2) a) T. Bauert, L. Merz, D. Bandera, M. Parschau, J. S. Siegel, K.-H. Ernst, *J. Am. Chem. Soc.* **2009**, *131*, 3460–3461;
b) L. Zoppi, T. Bauert, J. S. Siegel, K. K. Baldridge, K. H. Ernst, *Phys Chem Chem Phys* **2012**, *14*, 13365–13369.
(3) a) K.-H. Ernst, S. Baumann, C. P. Lutz, J. Seibel, L. Zoppi, A. J. Heinrich, *Nano Lett.* **2015**, *15*, 5388–5392.
b) J. Seibel, M. Parschau, K.-H. Ernst, *J. Phys. Chem. C* **2014**, *118*, 29135–29141.
c) J. Seibel, M. Parschau, K.-H. Ernst, *J. Am. Chem. Soc.* **2015**, *137*, 7970–7973.
d) J. Seibel, L. Zoppi, K.-H. Ernst, *Chem. Commun.* **2014**, *50*, 8751–8753.
(4) a) M. Parschau, K.-H. Ernst, *Angew. Chem. Int. Ed.* **2015**, *54*, 14422–14426;
b) R. Fasel, M. Parschau, K.-H. Ernst, *Nature* **2006**, *439*, 449–452.
c) J. Seibel, O. Allemann, J. S. Siegel, K.-H. Ernst, *J. Am. Chem. Soc.* **2013**, *135*, 7434–7437.

Ultrafast Carrier Dynamics at Hybrid Organic / Inorganic Interfaces

O.L.A. Monti
The University of Arizona, Tucson, AZ 85721, USA

Hybrid organic / inorganic interfaces play a central role in organic optoelectronics as charge harvesting layers or charge-recombination layers. The properties that determine electronic structure, dynamics and charge collection efficiencies are however at present poorly understood. I will discuss recent results for the paradigmatic interface of organic semiconductors with highly conductive ZnO films and a quasi-2D metal dichalcogenide. Using a wide range of steady-state and time-resolved spectroscopic approaches, I will show how defect-driven strong electronic interactions determine interfacial energy-level alignment, carrier dynamics on the sub-fs time-scale and device function. These interactions can be controlled by judicious preparation of the interface, with immediate consequences for carrier-harvesting efficiencies.

[1] Hybridization-Induced Carrier Localization at the C60 / ZnO Interface, L.L. Kelly, D.A. Racke, H. Kim, P. Ndione, A.K. Sigdel, J.J. Berry, S. Graham, D. Nordlund, and O.L.A. Monti, Adv. Mater., http://dx.doi.org/10.1002/adma.201503694 (2015)
[2] Disrupted Attosecond Charge Carrier Delocalization at a Hybrid Organic/Inorganic Semiconductor Interface, D.A. Racke, L.L. Kelly, H. Kim, P. Schulz, A. Sigdel, J.J. Berry, S. Graham, D. Nordlund, and O.L.A. Monti, J. Phys. Chem. Lett. 6, 1935-1941 (2015).
[3] Integer Charge Transfer and Hybridization at an Organic Semiconductor / Conductive Oxide Interface, M. Gruenewald, L.K. Schirra, P. Winget, M. Kozlik, P.F. Ndione, A.K. Sigdel, J.J. Berry, R. Forker, J.-L. Bredas, T. Fritz, and O.L.A. Monti, J. Phys. Chem. C 119, 4865-4873 (2015).
[4] Tailoring Electron-Transfer Barriers at Zinc Oxide / C60 Fullerene Interfaces, P. Schulz, L.L. Kelly, P.D. Winget, H. Li, H. Kim, P.F. Ndione, A.K. Sigdel, J.J. Berry, S. Graham, J.-L. Bredas, A. Kahn and O.L.A. Monti, Adv. Func. Mater., 24, 7381-7389 (2014).
[5] Defect-Driven Interfacial Electronic Structure at an Organic / Inorganic Semiconductor Heterojunction, P.D. Winget, L.K. Schirra, D. Cornil, H. Li, V. Coropceanu, P.F. Ndione, A.K. Sigdel, D.S. Ginley, J.J. Berry, J. Shim, H. Kim, B. Kippelen, J.-L. Bredas and O.L.A. Monti, Adv. Materials 26, 4711-4716 (2014).

New analytical and statistical tools to study the flavor formation during the roasting process of coffee beans, cacao beans and nuts

R. Zimmermann[1*], S. Ehlert[1,2], H. Czech[1], C. Schepler[1], M. Fishcer[1], S.Wohlfahrt[1], R. Hertz-Schünemann[1], T.Denner[3], J.Howell[4], C. Yeretzian[5], A. Walte[2], T. Streibel[1]

[1] *Joint Mass Spectrometry Centre of University of Rostock (Chair of Analytical Chemistry) and Helmholtz Zentrum Munich (CMA), Rostock and Munich, Germany,*
[2] *Photonion GmbH, Schwerin, Germany*
[3] *Netzsch-Gerätebau GmbH, Selb, Germany*
[4] *Smuckers Inc., Orrville, OH, USA*
[5] *ZHAW-University of Applied Sciences, Wädenswil, Switzerland*
* send correspondence to: ralf.zimmermann@uni-rostock.de

The mild roasting of plant seeds such as green coffee beans, cocoa beans or nuts generate a multitude of different flavour compounds. Thus roasting represents a very important value-generating process for the food industry, inducing a lot of fundamental and applied research in this food chemical field. However, in order to foster understanding of the flavour generation processes, modern on-line analytical approaches need to be applied to follow the processes in real-time. Furthermore advanced statistical are required to analyse the obtained data.

One possibility to monitor the effluents of flavours and other volatile roasting processes is photo ionisation (PI) mass spectrometry. By using different PI approaches, trace compounds can be ionized selectively or a universal but soft ionisation is obtained. So PIMS has been applied successfully to investigate evolved roasting gases from the interior of individual single coffee beans [1] as well as from industrial roasters with a capacity of more than one metric ton per hour [2]. A well suited tool for laboratory investigation of food roasting processes in a thermal analysis device (e.g. thermogravimetry) coupled to a PIMS system. In order to further increase the selectivity a newly developed optically heating fast-cycling gas chromatograph (fast OHGC) can be placed between the TA-oven and the PIMS-system. With this system e.g. the

evolution of pyrazines, furan derivatives, phenols and carbonylic compounds from the mild roasting of different nuts (e.g. peanuts) or coffee can be followed. However, in order to utilize the fundamental information of the flavour formation for an industrial roasting control, a statistical analysis of a large number of roasting experiments is required, using advanced multivariate methods such as non-negative matrix factorisation (NMF) followed by e.g. PCA analysis of obtained factors. Finally a roasting model needs to developed, that is allowing a fast real time control of the roasting process also under industrial conditions.
In the lecture the analytical and statistical approaches as well as different PIMS applications from in-bean monitoring and single bean TA-simulation via laboratory roaster analyses to industrial scale monitoring will be discussed.

[1] Hertz-Schünemann, R., Streibel, T., Ehlert, S., Zimmermann, R. Anal. Bioanal. Chem. 405, 7083-7096 (2013)
[2] Hertz-Schünemann, R., Dorfner, R., Yeretzian, C., Streibel, T., Zimmermann R., J. Mass Spectrom. 48, 1253–1265 (2013)

Clusters and Nanoparticles in Fundamental and Applied Research

Eckart Rühl
Physical Chemistry, Freie Universität Berlin
Takustr. 3, 14195 Berlin, Germany

Clusters and nanoparticles have gained recently substantial interest, since size effects of matter are not only of fundamental interest, but they have also the potential to be exploited for numerous applications. Size effects of matter rely on the one hand on the variable surface-to-bulk ratio of the constituents and on the other hand there are changes in electronic and geometric structure as well as dynamical properties. Firstly, selected examples of atomic and molecular clusters are discussed, which have been investigated in the regime of inner-shell and inner-valence shell excitation [1]. Specifically, results on clusters prepared in jet expansions as well as size-selected clusters are reported. Rydberg- and valence-transitions as well as ionization energies allow us to derive distinct information on local changes in electronic structure as a function of cluster size.

As a complement to gas phase work on clusters we report on recent results on cluster formation in aqueous solution [2]. Single levitated microdroplets are trapped either by electrodynamic or optical levitation. These provide a suitable way to prepare supersaturated or supercooled solution droplets. Cluster formation precedes the spontaneous nucleation process in these liquids leading to the formation of solid particles. Results from detailed studies on supersaturated aqueous microdroplets are presented, where the crucial parameters for cluster formation in solution are summarized. Experimental results from inner-shell excitation and model calculations indicate that structural motifs of pre-nucleation clusters can be derived as a function of solute concentration.

Nanoparticles are most suitably prepared under well defined conditions by colloidal chemistry, so that their size and surface properties are fully controlled [3]. The surface of nanoparticles is of crucial importance for their interactions with the environment. This concerns aggregation

between nanoparticles as well as their adsorption to surfaces and interfaces.

Often, size-dependent properties of nanoparticles are either investigated in solution or the particles are dried on suitable substrates. However, these approaches often suffer from difficulties to separate the intrinsic properties of nanoparticles from their interactions with the surroundings. Furthermore, charging and radiation damage may occur, if ionizing radiation is used to investigate these samples. An alternative is offered by preparing isolated and size-selected nanoparticles in an aerodynamically focused beam [4]. The size regime of nanoparticles that can be prepared in this way reaches from large clusters to microparticles, so that size effects of nanoscopic matter can be studied in a wide range. This particle preparation scheme also allows for structural and dynamical investigations on single nanoparticles, if intense radiation sources, such as free electron lasers, are used.

Experiments on free nanoparticles using either synchrotron radiation or short pulse lasers require, however, that one has to average over a larger quantity of nanoparticles, which implies to prepare the particles in narrow size distributions by colloidal chemistry. Recent results on photoemission studies are discussed, where the dynamics of electron emission from free nanoparticles was experimentally studied and these results were compared to model calculations [5]. Special emphasis is put on size effects of matter that are related to ultra-fast dynamical processes reaching from picosecond dynamics into the attosecond time regime [6].

Finally, an outlook is made towards the use of nanoscopic matter in life sciences. Nanoparticles are attempted to be used for diagnostics and therapy offering a wide range of possible applications. Specifically, the role of nanoparticles for drug delivery in the context of inflammatory skin diseases is discussed. Label free-approaches, such as X-ray microscopy and stimulated Raman scattering, are used. Especially, X-ray microscopy allows us to follow quantitatively the penetration of drugs into cells and tissue [7]. The role of nanoparticles as drug carriers and optimized dermal drug delivery vehicles for continuous and triggered drug release is presented.

References

1 V. Senz et al., Phys. Rev. Lett. **102**, 138303 (2009); J. Bahn et al., New J. Phys. **14**, 075008 (2012); R. Flesch et al., Phys. Chem. Chem. Phys. **14**, 9397 (2012); R. Flesch et al., Z. Phys. Chem. **228**, 387 (2014).
2 Y. Zhang, J. Chem. Phys. **139**, 134506 (2013).
3 C. Graf et al., Langmuir **22**, 5604 (2006); C. Graf et al., Adv. Functional Mat. **19**, 2501 (2009); C. Graf et al., Langmuir **18**, 7598 (2012); D. Nordmeyer et al., Nanoscale **6**, 9646 (2014).
4 E. Antonsson et al., Chem. Phys. Lett., Frontiers Article **559**, 1 (2013).
5 E. Antonsson et al., J. Electron Spectrosc. **200**, 216 (2015).
6 S. Zherebtsov et al., Nat. Phys. **7**, 656 (2011); F. Süßmann et al., Nat. Commun **6**, 7944 (2015).
8 K. Yamamoto et al., Anal. Chem. **61**, 6173 (2015).

The dynamics of molecular interactions and chemical reactions at metal surfaces: Testing the foundations of theory

Oliver Bünermann, Hongyan Jiang, Yvonne Dorenkamp, Alexander Kandratsenka, Svenja M. Janke, Daniel J. Auerbach, Alec M. Wodtke

Institute for Physical Chemistry, Georg-August University of Göttingen, Tammannstrasse 6, 37077 Göttingen, Germany.

Department of Dynamics at Surfaces, Max Planck Institute for Biophysical Chemistry, Am Faßberg 11, 37077 Göttingen, Germany.

In 1929, Nobel Laureate Paul Dirac made comments to the effect that Chemistry had been solved. With the advent of quantum mechanics "*The underlying physical laws necessary for the mathematical theory of… …the whole of chemistry are… …completely known*…. However, on a practical level computational chemistry is still in an early stage of development. Dirac went on: "*the difficulty is only that the exact application of these laws leads to equations much too complicated to be soluble.*" Despite electrifying advances in computational power since that time, Dirac is still right. The theory of chemistry requires approximations before theoretical descriptions and predictions of chemical reactions can be made.

The advent of the Born-Oppenheimer Approximation led to the development of the *standard model of chemical reactivity* where the electronically adiabatic potential energy surface for nuclear motion is derived and quantum motion of the nuclei on that surface can be calculated. For simple gas phase reactions, this approach has become an extraordinarily useful and reliable tool. For surface chemistry, additional approximations are commonly made: 1) classical mechanics for describing nuclear motion, 2) density functional theory (usually at the generalized gradient level) for calculating electronic states, 3) reduced dimensionality approximations and as

before 4) the Born-Oppenheimer approximation to separate electronic and nuclear degrees of freedom. I call this collection of approximations the *provisional model for surface chemistry* as we in the field are still testing and improving it.

In this talk, I will describe how a fruitful interplay between experiment and theory can lead to accurate atomic-scale simulations of simple reactions at metal surfaces. I will describe the very significant challenges surface chemistry presents including the problems of high dimensionality and the common failure of the Born Oppenheimer approximation. As a concrete example, I will present results of a full dimensional theoretical approach to hydrogen atom adsorption at a metal surface that includes the effects of Born-Oppenheimer failure. This leads to an atomic scale view of H-atom adsorption at a noble metal.

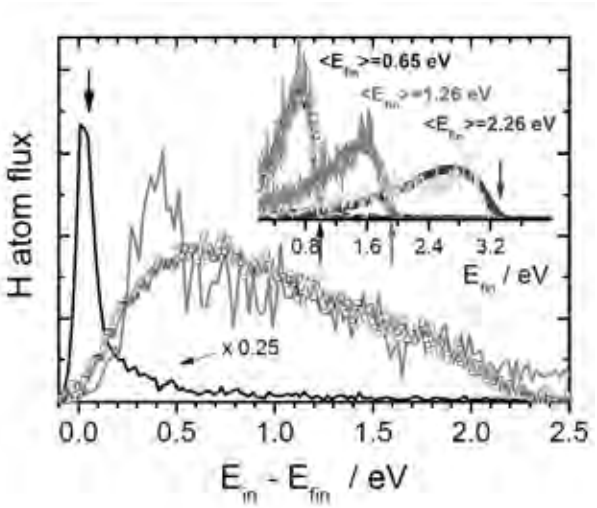

H-atom inelastic scattering from Au(111) - Comparison of the experimentally obtained kinetic energy loss spectrum to theoretical simulations. Theoretical energy loss found when neglecting (solid black line) and including (solid gray line) electronic excitation. Experimental energy loss for E_{in} = 2.76 eV are shown as open squares. The vertical arrow marks the expected energy loss for a binary collision between an H and an Au atom. The inset shows the incidence energy dependence, E_{in}, of the experimentally derived translational inelasticity (open squares) and comparison to theory (solid lines): E_{in} = 3.33 eV (blue), 1.92 eV (red), and 0.99 eV (black). Colored arrows mark the three incidence energies. Also shown are the average final translational energies, $<E_{fin}>$. The scattering angles are ϑi = 45°, ϑs = 45°. In all cases, the scattered H atoms remain unthermalized with the solid, emerging with a substantial fraction of their incidence translational energy.

ENHANCING SELECTIVITY AND SENSITIVITY OF CHEMICAL COMPOUNDS USING AN ION FUNNEL PROTON TRANSFER REACTION - MASS SPECTROMETER

Ramón González-Méndez, Peter Watts, and Chris A. Mayhew
School of Physics and Astronomy, University of Birmingham, Edgbaston, B15 2TT, UK
D. Fraser Reich, Stephen J. Mullock, and Clive A. Corlett
KORE Technology Ltd, Cambridgeshire Business Park, Ely, Cambridgeshire CB7 4EA, UK

1. Introduction

Ion funnels (IF) have been used since the late 90s in conjunction with several ionisation and mass spectrometric techniques with the purpose of increasing the analytical detection sensitivity through an increase in the ion transmission efficiency.[1] Recently, this approach has been taken into proton transfer reaction mass spectrometery by equipping a PTR-MS drift tube (DT) with an ion funnel (IF).[2] Reported increases in sensitivity have been shown to be dependent on the *m*/*z* of the product ions e.g. an increase of 45 for protonated acetaldehyde and 200 for protonated acetone at a reduced electric field of 120 Td.[2] In addition to increasing sensitivity, recent investigations within a collaborative project involving KORE Technology Ltd. and the University of Birmingham have shown that an IF can be used to change the nature of the soft chemical ionisation processes occuring within the DT of a PTR-MS to alter the product ion distribution in a selective way. This change results from increasing the collisional energies of the ions with the neutral gases caused by the applied RF field. We will present initial results obtained from this new IF-PTR-MS instrument for various chemicals of importance to Homeland Security.

2. Methods

A KORE Technology Ltd. IF Proton Transfer Reaction - Time of Flight - Mass Spectrometer (PTR-ToF-MS) was used.[3] The ion funnel consists of 29 stainless steel plates of 0.2 mm thickness, mounted on precision-machined ceramic rods at an even spacing of 3.2 mm per plate. The orifice diameters of the plates through the first half of the stack is 40 mm, as used in the standard drift tube reactor. In the second half of the drift

tube the orifice diameter steadily decreases to 6 mm at the final plate before the exit orifice. To this second part a fixed RF field is applied applied of frequency of 800 kHz and amplitude of 170 V which is superimposed on the dc voltage gradient.

3. Illustrative Instrumental Results

In this abstract we illustrate the analytical power of the IF-PTR-ToF-MS by showing changes in the ion-molecule chemistry occuring in the instrument for the detection of 2,4,6-trinitrotoluene (TNT). Using a standard PTR-ToF-MS system we have previously shown that there is an unusual dependence of the intensity of protonated TNT on the reduced electric field (the ratio of the electric field, *E*, and the buffer gas number density, *N*). Nearly all compounds investigated to date using a PTR-MS show a decrease in sensitivity of detection with increasing *E*/*N*. The major causes for this are reduced reaction times, fragmentation to non-specific product ions, and reduction in ion transmission. In comparison to this, the intensity of protonated TNT initially rises with increasing *E*/*N*, reaches a maximum and then shows the normal decrease. The explanation of this unusual intensity dependence has been described in detail.[4] In brief it is a result of an unusual secondary reaction of $TNTH^+.H_2O$ with H_2O leading to a terminal ion which does not contain TNT, namely $H_3O^+.H_2O$. For all *E*/*N* values investigated only one product ion was observed, namely the protonated TNT at *m*/*z* 228. However, when the ion funnel is turned on, another fragment ion is observed at *m*/*z* 210, the intensity of which increases with decreasing *E*/*N*, down to reduced electric field values under which normal PTR-MS stops operating. The results of measurements are shown in figure 1.

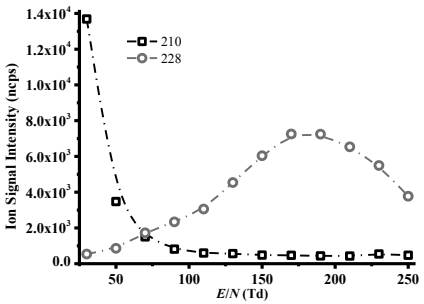

Figure 1. Product ions observed as a function of *E*/*N* with IF operating. The data have been taken using 100 ng of TNT. The ion signals have been normalised to 10^6 H_3O^+ reagent ions and drift times.

The ion at *m*/*z* 210 results from an elimination of H_2O from the protonated TNT via enhanced collisional induced dissociation caused by the RF field:

$$H_3O^+ + TNT \Vdash (TNTH^+)^* + H_2O$$
$$(TNTH^+)^* + M \Vdash (TNT\text{-}H_2O)H^+ + H_2O + M$$

4. Computational Details

Protonation of TNT can occur on the nitro groups at the 2 and 4 positions, both having similar proton affinities, although as elimination of water from $TNTH^+$ will presumably involve the methyl group only protonation of the nitro group in the 2- position is of relevance. However, protonation on the 4 nitro will occur (the PA and GB are slightly greater than the 2 nitro) and this will reduce the amount of $TNTH^+$ available to lose water. Two configurations are possible for protonation in the 2 position:

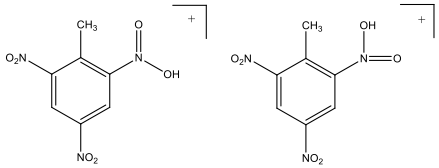

anti syn

with the anti being slightly more stable by ca. 8 kJ mol^{-1}. The transition state energetics for interconversion are $\Delta H^{\ddagger}_{298}$ +46 kJ mol^{-1} and $\Delta G^{\ddagger}_{298}$ +51 kJ mol^{-1} above the anti conformation, but whichever is formed there is sufficient energy in the initial protonation to allow rapid interconversion (Table1).

Products	ΔH_{298} kJ mol^{-1}	ΔG_{298} kJ mol^{-1}
$TNTH^+(2NO_2syn) + H_2O$	-46	-47
$TNTH^+(2NO_2anti) + H_2O$	-55	-55
$TNTH^+(4NO_2) + H_2O$	-68	-60
TS syn/anti + H_2O	-9	-5

Table1. Energetics for the proton transfer from H_3O^+ to TNT calculated using the B3LYP functional and the 6-31+G(d,p) basis set.

There are three stable structures for the ion remaining after loss of water from $TNTH^+$. These are

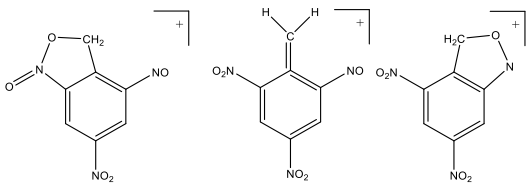

$TNTH^+$- H_2O (a) $TNTH^+$- H_2O (b) $TNTH^+$- H_2O (c)

A fourth structure, similar to $TNTH^+$ - H_2O (b) with the hydrogens of the methylene group orthogonal to the ring, proved to be unstable and

rearranged to $TNTH^+$ - H_2O (a) . The energetics for the transformation of $TNTH^+$ to $TNTH^+$ - H_2O (a-c) + H_2O are given in Table2.

Products	ΔH_{298} kJ mol^{-1}	ΔG_{298} kJ mol^{-1}
$TNTH^+$ - H_2O (a) + $2H_2O$	-104	-145
$TNTH^+$ - H_2O (b) + $2H_2O$	+47	-7
$TNTH^+$ - H_2O (c) + $2H_2O$	-128	-168

Table 2. Energetics for the loss of water from TNT following proton transfer from H_3O^+.

Various attempts using the QST3 approach were made to find transition states for these possible reactions but all lead to $TNTH^+$- H_2O (c), though interestingly the transition state had a close resemblance to $TNTH^+$- H_2O (b). The transition state was characterised by one imaginary frequency and the IRC leading to $TNTH^+$- H_2O (c) in the forward direction and $TNTH^+$ with the proton on the 2-nitro group in the syn conformation in the reverse direction. The activation energies relative to TNT + H_3O^+ $\Delta H^{\ddagger}_{298}$ +158 kJ mol^{-1} and $\Delta G^{\ddagger}_{298}$ +162 kJ mol^{-1}.

5. Conclusions

A novel PTR-ToF-MS equipped with an ion funnel, originally designed to improve sensitivity, has been used in an unusual way to induce fragmentation of product ions through changes in collisional induced dissociation. We have illustrated in this abstract the instruments capabilities for the determination of TNT. Two reaction mechanisms have been described for the reaction of H_3O^+ with TNT:

(i) No IF: $TNT + H_3O^+ \rightarrow (TNTH)^+ + H_2O$

(ii) With IF: $TNT + H_3O^+ \rightarrow (TNT\text{-}H_2O)H^+ + 2H_2O$ (E/N < 70 Td)

$TNT + H_3O^+ \rightarrow (TNTH)^+ + H_2O$ (E/N > 70 Td).

This study highlights the application of an ion funnel system for not only improved chemical compound sensitivity but also selectivity using PTR-ToF-MS.

6. References

1. Kelly, R. T., et al., *Mass Spectrometry Reviews* **2010,** *29* (2), 294.
2. Barber, S., et al., *Analytical Chemistry* **2012,** *84* (12), 5387.
3. González-Méndez R., et al., Int. J. Mass Spectrom. **2015**, *385*, 13.
4. Sulzer, P., et al., *Anal. Chem.* **2012,** *84*, 4161.

7. Acknowledgements

This project was supported by the PIMMS ITN which in turn is supported by the European Commission's 7th Framework Programme under Grant Agreement Number 287382.

Observation of solitons in a quantum degenerate plasma

Francois Michels and Klaus Müller-Dethlefs

The Photon Science Institute and School of Chemistry
University of Manchester
Alan Turing Building
Manchester M13 9PL
k.muller-dethlefs@manchester.ac.uk

1. Introduction

A long life-time (>0.3 ms) quantum degenerate molecular Rydberg plasma is generated in the high-density region of a pulsed supersonic jet expansion by two-colour resonant excitation of nitric oxide (10%) in neon (5bar) into the high-*n* Rydberg threshold region close to the ionization limit. Under those conditions, *i.e* for an ion density of 10^{13} to 10^{16} cm^{-3} and excitation of *ca.* 4 cm^{-1} below the ionization threshold of NO, the electron Rydberg orbit radius of 1.4 μm (for a single Rydberg state, $n \approx 165$) is much bigger than the average distance of a few hundred nm between the cations. Since this ensemble of cations and electrons is produced collectively during excitation into the Rydberg region the electrons instantaneously loose the memory of their parent cation, resulting in the *direct* formation of a plasma. The plasma produced shows little expansion. The molecular Rydberg plasma is observed over a broad range of excitation energies, from threshold down to Rydberg states as low as $n = 12$.

Considering the well-known properties of pulsed supersonic jet expansions and textbook plasma physics the ultra-cold plasma produced here is already close to electron degeneracy (Landau-Lifshitz, Statistical Physic Part 1 and 2). This makes it necessary to consider the Fermi energy $E_F = (3\pi^2)^{2/3} n_e^{2/3} h^2/8\pi^2 m_e$ and the plasma degeneracy parameter $\theta^1 = E_F/kT$. For the plasma densities of $< 10^{16}$ cm^{-3} reached in our

experiments the electrons should become *quantum degenerate*, *i.e.* the electron *de Broglie* wavelength becomes larger than the Wigner-Seitz radius *a* relevant to describe the mean distance between the particles. The degeneracy condition for the electrons in an ultra-cold ion-electron plasma should be fulfilled for an initial electron temperature of $0.1K$ (defined by the laser bandwidth of 0.06 cm^{-1}) and a density above 10^{13} cm^{-3}.

2. Observation of solitons

We are reporting a surprising result: the observation by time-of-flight measurements of self-sustained solitons in a quantum degenerate plasma.

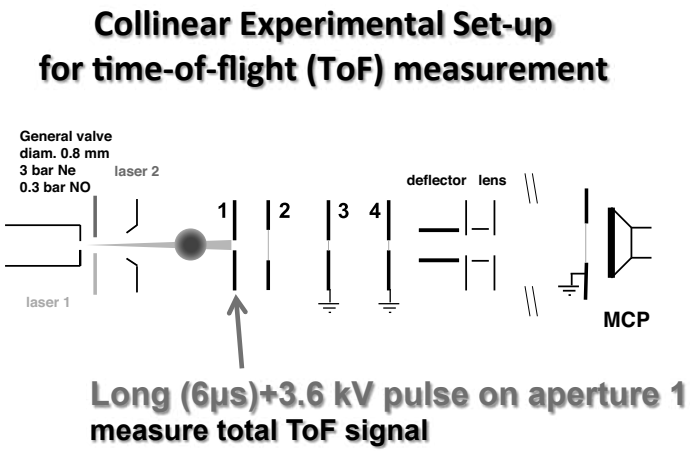

When the plasma cloud approaches the metal plate (1), which has an aperture, a high-voltage pulse 1 of 3.6 kV is applied and the plasma is separated into a negatively and positively charged cloud. After passing through aperture (1) a second high voltage pulse 2 then generates, for a specific voltage of 1200V, very narrow (<2ns) peaks in the time-of-flight (tof) spectrum (red). Detuning the voltage of the second pulse (green: 1140V, blue: 1260V) broadens the tof peaks significantly.

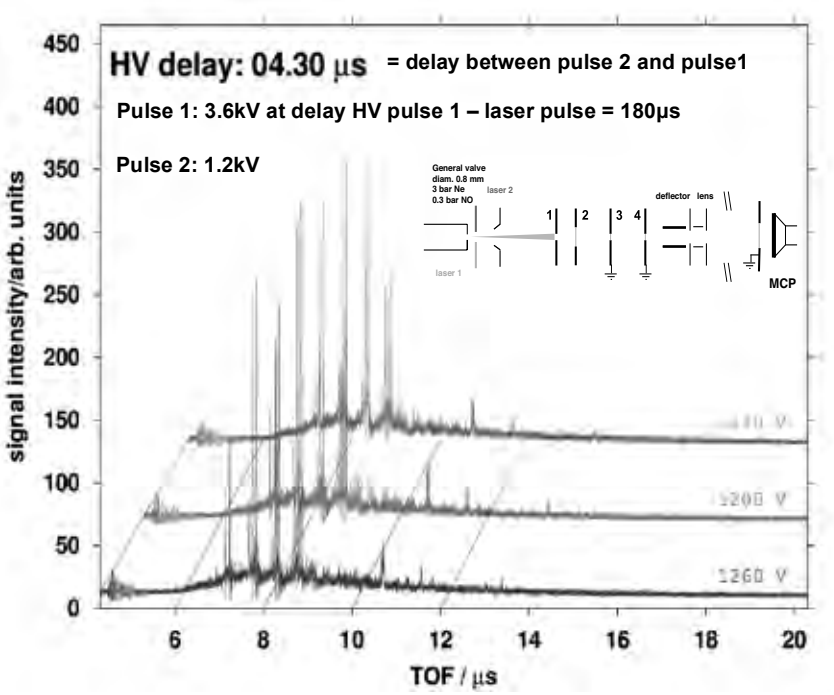

In a further refinement of the experiment, we applied a double high-voltage pulse to the first plate, as outlined in the scheme:

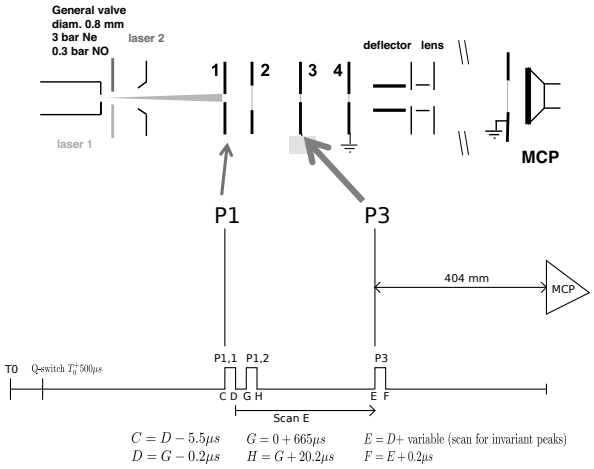

With a gap of 200ns in the pulse applied to aperture 1 (D to G in the preceding figure), very clear peaks appear in the tof spectrum as seen in the figure.

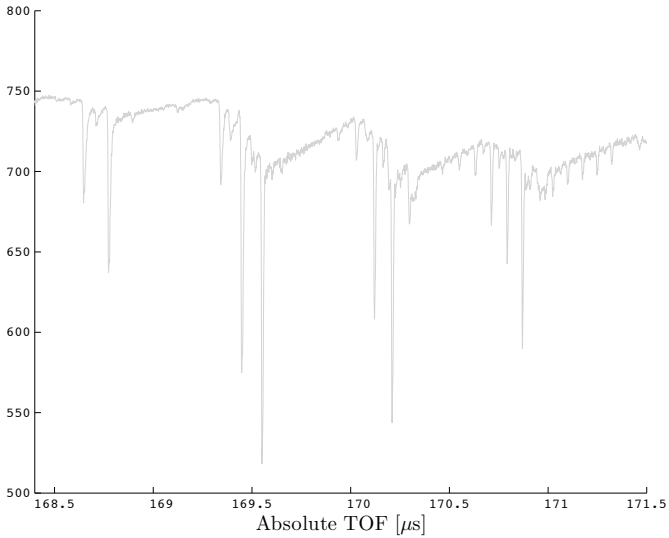

These sharp resonances in the tof spectrum can be interpreted as solitons (= ”standing waves”) of counter-propagating surface plasmons, which are excited by the combination of pulsed fields.

The lecture will outline an interpretation for these observations.

Steric Effects in the Gas Phase and in Solution

Prof. Dr. Peter Chen
Laboratorium für Organische Chemie
ETH Zürich

Abstract

The picture of steric effects commonly taught in elementary organic chemistry is challenged with a combination of gas-phase and solution measurements of bond dissociation energies. In the gas phase, proton-bound dimers of substituted pyridines display bond dissociation energies, measured by energy-resolved collision-induced dissociation cross-section experiments, which change little as substituents are made larger. The results are confirmed by both dispersion-corrected DFT calculations, as well as CCSD(T) taken to the CBS limit. The same systems, measured in solution by variable temperature NMR, show binding enthalpies which are only weakly dependent on substitution, i.e. steric bulk. The entire, apparent steric repulsion appears in the entropic contribution, which appears to be largely related to solvation.

Combining cryogenic ion spectroscopy and ion mobility for structural studies of biomolecular ions

Michael Z. Kamrath, Antoine Masson, and Thomas R. Rizzo
Laboratoire de Chimie Physique Moléculaire, École Polytechnique Fédérale de Lausanne, EPFL SB ISIC LCPM, Station 6, CH-1015 Lausanne, Switzerland

Over the last number of years we have used cryogenic ion spectroscopy to investigate the structures of biomolecular ions in the gas phase.[1, 2] After producing them by electrospray, we cool them to ~10 K in an RF ion trap through collisions with cold helium and then use IR-UV double resonance photofragment spectroscopy to measure conformation-specific vibrational spectra. We use these spectra to determine the structure by comparing them with theoretical spectra calculated by DFT. Once validated by experiment, the calculations provide the structure of the molecule.

From the experimental side, as one applies this approach to biomolecular ions of increasing complexity, it becomes more difficult to resolve individual conformers in the UV spectrum, and this inhibits our ability to measure conformation-specific vibrational spectra and hence to determine structure. From the theoretical side, the conformational search space for larger molecules becomes difficult to sample exhaustively, inhibiting our ability to find the lowest energy structures.

To be able to further simplify complex spectra and to help the conformational search process, we have combined our cryogenic ion spectroscopy technique with ion mobility. This combined approach allows us to sort conformations of molecules by their drift time and inject only one or a subset of them into the ion trap. Moreover, the orientationally averaged cross-section that we obtain from the drift time helps narrow the conformational search space by adding additional constraints on the calculated structures.

This talk will describe our recently constructed hybrid instrument in which we combine drift-tube in mobility with a newly designed, cryogenic planar ion trap, which is in turn coupled to a time-of-flight

mass spectrometer.[3] We show a series of experiments on small peptides that demonstrate our ability to selectively inject ions into our ion trap that have been first separated by their drift time. We also demonstrate how we can intentionally isomerize molecules by collisionally activating them in the drift tube, which helps determine which conformations may be "kinetically trapped" from solution. Finally, we demonstrate how this combined approach can provide information on the preferred conformations of molecules in solution before electrospray.

References

[1] T. R. Rizzo, J. A. Stearns, and O. V. Boyarkin, Int. Rev. Phys. Chem. **28**, 481 (2009).

[2] T. Rizzo and O. Boyarkin, in *Gas-Phase IR Spectroscopy and Structure of Biological Molecules*, edited by A. M. Rijs, and J. Oomens (Springer International Publishing, 2015), pp. 43-97.

[3] A. Masson, M. Z. Kamrath, M. A. S. Perez, M. S. Glover, U. Rothlisberger, D. E. Clemmer, and T. R. Rizzo, J. Am. Soc. Mass Spectrom. **26**, 1444 (2015).

Chiral Molecules under the Reaction Microscope

M. Pitzer, G. Kastirke, H. K. Gill, M. Tia, T. Bauer, J. Becht, H. Gassert, Ch. Goihl, A. Hartung, K. Henrichs, T. Jahnke, H.-K. Kim, A. Kuhlins, M. Kunitski, J. Rist, H. Sann, L. Ph. H. Schmidt, C. Schober, J. Siebert, F. Sturm, D. Trabert, F. Trinter, M. Waitz, R. Wallauer, N. Wechselberger, F. Wiegandt, H. Schmidt-Böcking, R. Dörner and M. S. Schöffler
Institut für Kernphysik, J. W. Goethe-Universität Frankfurt, Germany

A. S. Johnson
University of Ottawa, ON K1N 6N5, Canada

H. Fukuzawa, K. Ueda
Institute of Multidisciplinary Research for Advanced Materials, Tohoku University, Sendai 980-8577, Japan

Ph. Demekhin
Institut für Physik, Universität Kassel, 34132 Kassel, Germany

J. B. Williams
Department of Physics,University of Nevada, Reno, Nevada 89557, USA

M. Mazenauer, B. Spenger and J. Stohner
Institute of Chemistry and Biological Chemistry, Zurich, 8820 Wädenswil, Switzerland

J. Kiedrowski, M. Reggelin, S. Marquardt, S. Marquardt, A. Schiesser and R. Berger
Clemens-Schöpf Institute, Technische Universität Darmstadt, Germany

Abstract:

While an atom is a fully symmetric system, diatomic molecules are rotationally symmetric around the molecular axis. By adding more atoms the complexity increases, while symmetries are being lost. One very special class of this "complex" molecules are so-called chiral, with a lower limit of at least 4 atoms. They exist, similar to our hands, in a left and a right version. These enantiomers have the same physical properties (melting point, density, ionization energy etc.), distinguishing left and right poses a major challenge for scientists. A wide variety of techniques has been developed during the last 50 years. Except Bijovet's method, which employs anomalous diffraction of X-rays, all of the other methods (as for example optical rotation, circular dichroism, NMR spectroscopy) are indirect. This means that the derived signal cannot be assigned directly to right or left; quantum chemical calculations or empirical rules are necessary to assign the absolute configuration.

Today's multi particle coincidence techniques as the COLTRIMS (cold target recoil ion momentum spectroscopy) reaction microscope [1] open a new window to investigate molecular chirality. A famous approach is to investigate circular dichroism: Right and left circular polarized light is differently absorbed by one enantiomer. This usually very tiny effect (10^{-4}) can be increased if the photoelectron angular distribution is investigated [2]. This PECD can reach up to a few % even in randomly oriented molecules. The signal strength can be increased further, if the photoelectron is measured in coincidence with the fragmenting ions; first by selecting a certain break-up channel and second by fixing them in

space. Therefore we core ionized methyl oxirane (C_3H_6O). We will give an intuitive picture how the rotation of the electric field is converted into a forward-backward asymmetry, which is being observed in the PECD and compare our findings with calculations.

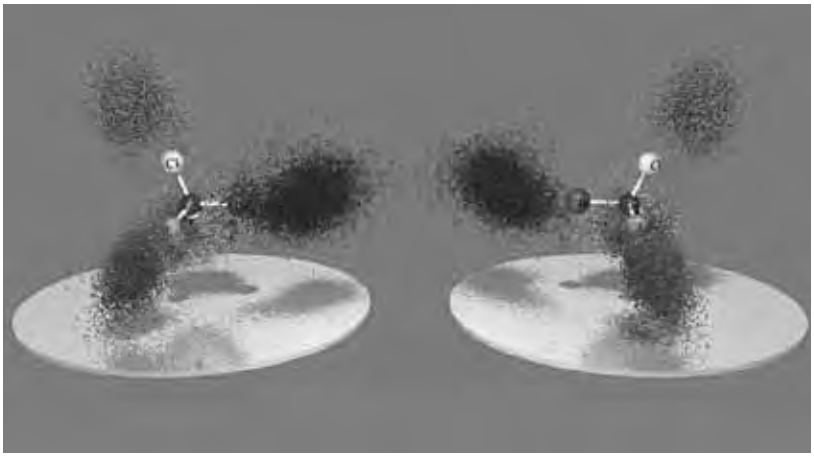

Fig. 1: Measured linear momenta of the various atomic ions in 5-fold ionic fragmentation of S-CHBrClF (left) and R-CHBrClF (right).

A more sophisticated approach to directly determine a molecule's handedness is Coulomb Explosion Imaging [3,4]. When enough electrons are removed from the molecule the Coulomb repulsion separates the ions very quickly. Thus by measuring the momentum vectors of all fragments, the geometry and thereby the initial handedness of a single molecule can be reconstructed. For the show case example of racemic CHBrClF we will discuss the fragmentation dynamics, initiated by a femtosecond laser pulse or a high energetic photon (E_γ = 500 – 710 eV) and how to determine the handedness. In Figure 1 the linear momenta for the

reconstructed S- (left) and R- (right) enantiomer of CHBrClF are shown after single photon absorption.

Furthermore we will give a broader outlook on future perspectives employing this technique, especially in terms of boundary conditions, time scale, nuclear dynamics and efficiency.

References:

[1] R. Dörner et al., *"Cold target recoil ion momentum spectroscopy: a 'momentum micrscope' to view atomic collision dynamics"*, Physics Reports, **330**, 95, (2000)

[2] G. A. Garcia et al., *"Circular dichroism in the photoelectron angular distribution from randomly oriented enantiomers of camphor",* J. Chem. Phys., **119**, 8781, (2003)

[3] Z. Vager et al., *"Coulomb explosion imaging of small molecules",* Science, **244,** 426, (1989)

[4] M. Pitzer et al., *"Direct determination of absolute configuration in the gas phase"*, Science, **341**, 1096, (2013)

Theory for lasercoolable molecules

Robert Berger
Fachbereich Chemie, Philipps-Universität Marburg, Hans-Meerwein-Str. 4, 35032 Marburg, Germany

Timur Isaev
Petersburg Nuclear Physics Institute, 188300, Orlova Roscha 1, Russia

Doppler cooling of atoms with slightly off-resonantly tuned lasers is a well-established technique to yield cold samples of atoms. One of the major obstacles for transferring this powerful approach to the molecular regime is the existence of unfavourable Franck-Condon factors that are accompanied with unacceptable losses in the cooling cycles.

We have analysed in Ref. 1 the situation of diatomic molecules, identified classes of molecules and pointed to the possibility of a nearly diagonal Franck-Condon matrix in the diatomic molecule radium monofluoride (RaF), which is also of considerable interest for studying fundamental interactions [2,3].

Recently, we have used simple theoretical concepts to point to the possibility that also polyatomic molecules with nearly diagonal Franck-Condon matrices may exist [4]. In this talk, these concepts will be outlined, molecular candidate systems will be presented and the unique opportunities arising from cold polyatomic molecules will be discussed in the framework of fundamental symmetries and interactions.

[1] T. A. Isaev, S. Hoekstra, R. Berger, Phys. Rev. A, 114 (2010) 052521.
[2] T. A. Isaev, R. Berger, arXiv:1310.1511.
[3] A. D. Kudashov, A. N. Petrov, L. V. Skripnikov, N. S. Mosyagin, T. A. Isaev, R. Berger, A. V. Titov, Phys. Rev. A, 90 (2014) 052513.
[4] T. A. Isaev, R. Berger, Phys. Rev. Lett. (accepted for publication); T.A. Isaev, R. Berger, arXiv:1504.08326.

Enantiomer differentiation using broadband rotational spectroscopy

Melanie Schnell
Max-Planck-Institut für Struktur und Dynamik der Materie and The Hamburg Centre for Ultrafast Imaging, Hamburg

Most molecules of biochemical relevance are chiral. Even though the physical properties of two enantiomers are nearly identical, they can exhibit completely different biochemical effects, such as different odors. In nature and as products of chemical syntheses, chiral molecules often exist in mixtures with other chiral molecules. The analysis of these complex mixtures to identify the molecular components, to determine which enantiomers are present, and to measure the enantiomeric excesses (ee) remains a challenging task for analytical chemistry.

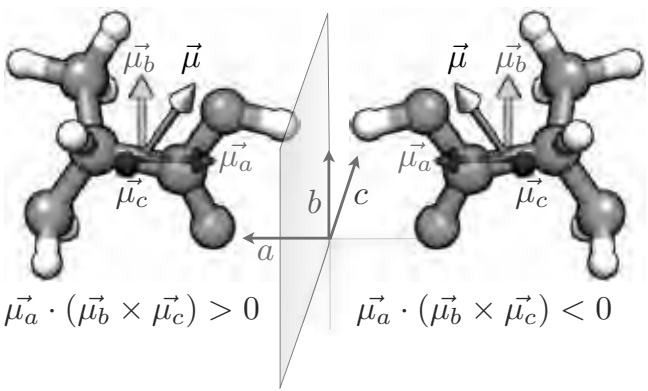

Figure 1: The two enantiomers are mirror images of each other as are their dipole moments. This property leads to opposite signs for the scalar triple products of the transition dipole moment components for a fixed coordinate system, since the sign of the scalar triple product depends on the order of the vectors. It changes upon mirror reflection and is even under time-reversal symmetry, which makes this quantity a measure of chirality.

We recently experimentally demonstrated a new method of differentiating enantiomeric pairs of chiral molecules in the gas phase (*Nature* 497 (2013) 475, *Angew. Chem. Int. Ed*. 52 (2014) 1152). It is based on broadband rotational spectroscopy and is a three-wave mixing process that involves a closed cycle of three rotational transitions. It relies on the fact that the enantiomers are mirror images of each other and so are their dipole moments (Figure 1). This property leads to opposite signs for the scalar triple products of the transition dipole moment components for a fixed coordinate system.

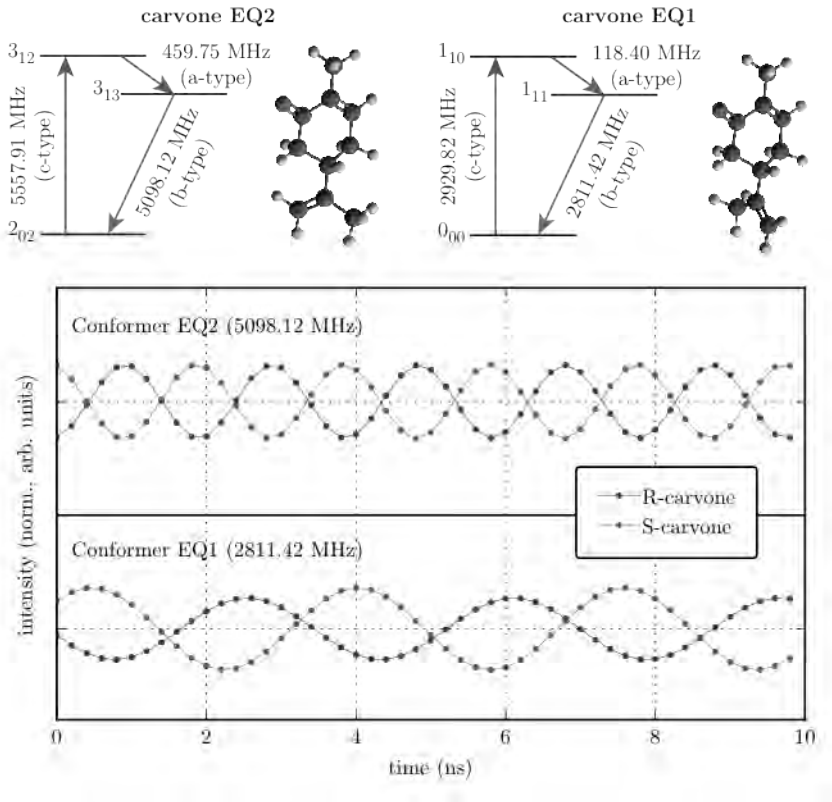

Figure 2: Chirality-sensitive microwave three-wave mixing to distinguish the enantiomers for two conformers (EQ2 and EQ1) of carvone. In the upper part, the molecular structures and the applied microwave three-wave mixing schemes are shown. In the lower part, magnifications of the free-induction decays are displayed. For both conformers, the clear phase difference of about 180° (π radians) between the R and the S enantiomer can be seen.

As a result, we observe a characteristic phase difference by 180° in the free-induction decay of the microwave three-wave mixing process. The phase of the acquired signal bares the signature of the enantiomer, as it depends upon the product of the transition dipole moments, and the signal amplitude is proportional to the ee. Two examples for such microwave three-wave mixing cycles and the resulting phase difference in the free-induction decay of the probe transition are shown in Figure 2 for the example of two conformers of the terpene carvone.

With known transition dipole matrix elements, the absolute configuration of enantiomers can in principle be determined from a single measurement. A unique advantage of our technique is that it can also be applied to mixtures of chiral molecules, even when the molecules are very similar. The resonant character and the high resolution and sensitivity of the technique make it highly mixture-compatible, which can be particularly relevant for natural and pharmaceutical samples.

In my lecture, I will introduce the technique and give an update on the recent developments as well as on future directions, such as extending the technique to chemical analysis. Experiments aiming at manipulating and finally controlling the composition of a chiral sample using well-defined microwave pulses can open up a fascinating new area of molecular physics experiments.

Surfaces of Clusters: Adsorption, Kinetics and Spectroscopy

Jennifer Mohrbach*, Sebastian Dillinger*,
and Gereon Niedner-Schatteburg
Fachbereich Chemie und Forschungszentrum OPTIMAS,
Technische Universität Kaiserslautern, 67663 Kaiserslautern, Germany

1. Motivation

It is short of hundred years ago that surface science reached maturity at the molecular level [1]. Knowledge driven surface science elucidates well defined surfaces, e.g. of single crystals and at high perfection. Application driven research in catalysis aims at high figures of merit, e.g. turn over numbers (TON), product yields and specificity [2]. Both disciplines often ran in parallel with seeming risk to miss each other. Cross fertilization did occur [3], and sometimes it was omitted.

The cluster surface analogy has been recognized long time ago [4]. We have studied the C-H bond activation of various organic molecules by naked transition metal clusters before [5]. It showed, that cluster size dependent variations of reaction rates were in part beyond comprehension, and they withstood quantum chemical interpretation by and large. It became mandatory to invoke (a) temperature control and (b) dedicated means of spectroscopy – and to switch to simpler systems.

2. Methodology

We have taken time to setup a tandem cryo ion trap instrument that allows for the study of adsorption and reaction kinetics of clusters under single collision conditions in conjunction with temperature control to as low as 11 Kelvin. In the present cases it proved advantageous to utilize a doped Helium buffer gas at 26 Kelvin.

Spectroscopy comes into play through application of Infrared Multiple Photon Dissociation (IR-MPD) by optical parametric oscillator/amplifier (OPO/OPA) photon sources. One and two colour investigations of metal organic complexes by such technique were subject of presentation at SASP 2014, and according results are published elsewhere [6].

3. Findings in short

We have started a systematic study of N_2 and H_2 cryo adsorption on Fe, Co, and Ni clusters and alike, very first results being published [7]. The kinetics of adsorption reveal manifold features. In most cases, there are clearly discernible mono layer like adsorbate shells which manifest in recorded intensities at first sight, and in kinetic modelling unambiguously. In some cases, the found stoichiometry reveal trends and unexpected exceptions superposing (cf. Fig. 1).

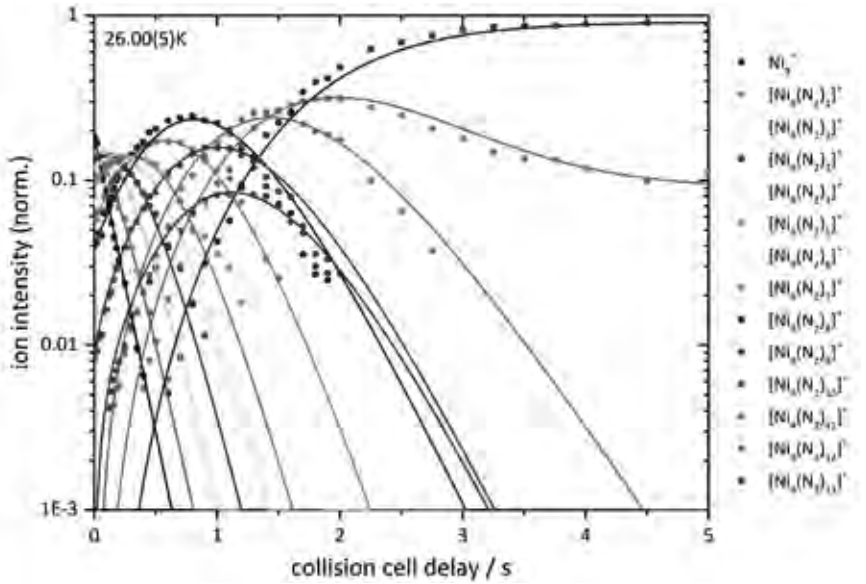

Figure 1: At 26 Kelvin the adsorption of single N_2 molecules onto isolated Ni_9^+ clusters proceeds with close to collision rate and in a reaction chain of up to 13 consecutive steps until it seizes to proceed. This and similar results elucidate cluster size dependent adsorption kinetics much beyond swift comprehension.

Beyond such mere kinetics – though interesting in themselves – we recorded IR-MPD spectra of dinitrogen stretching vibrations within such $[M_n(N_2)_m]^+$ cluster surface – adsorbate layer complexes by variation of their stoichiometry, *n* and of *m* alike. Complicated patterns of known and unknown features arise (cf. Fig. 2), and these shall be subject of

presentation and discussion. Electronic structure modelling (by DFT) is work in progress and to report.

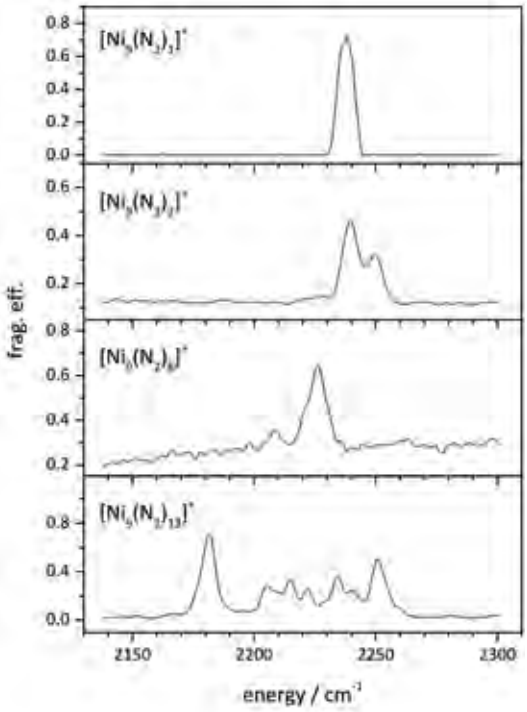

Figure 2: Infrared Multiple Photon Dissociation (IR-MPD) spectra of Nickel cluster Ni_9^+ Nitrogen adsorbate complexes. Red shifts of the N-N stretching vibration depend on the cluster size and on the surface coverage by adsorbate molecules. Be-yond a first monolayer at n = 8, there is further adsorption up to n = 13, which leads to a complicated vibrational pattern. A conceivable interpretation arises through structural reorganization of the adsorbate layer, to discuss.

We have conducted synchrotron X-ray based studies of spin and orbital contributions to the toal magnetic moments of isolated iron, cobalt and nickel clusters, presented at SASP 2012 and published subsequently [7]. The found magnetic magnitudes do not clearly correlate with the findings of our current studies in kinetics and spectroscopy.

4. Summary and outlook

This invited presentation shall elucidate the current state of cluster adsorbate studies under cryo conditions and in isolation. It aims to put into perspective the findings from adsorption kinetics, IR spectroscopy, DFT modelling and magnetic spectroscopy. It concludes with an outlook onto the road ahead.

5. Acknowledgements

This work was supported by the Deutsche Forschungsgemeinschaft in the framework of the transregional collaborative research center SFB/TRR 88 **3MET.de**. These co-authors (*) contributed equally.

6. References

[1] I. Langmuir, J. Am. Chem. Soc. **1918**, *40*, 1361-1403.

[2] G. Somorjay and Y. Li: *Introduction to Surface Chemistry and Catalysis*, 2nd edition, Wiley Hoboken **2010**; *Catalysis from A to Z – A concise Encyclopedia* (B. Cornils, W. A. Hermann, R. Schlögl, C.-H. Wong eds.), Wiley-VCH, Weinheim **2000**.

[3] G. Ertl, *Angew. Chem. Int. Ed.*, **2008**, *47*, 3524 – 3535.

[4] E. L. Muetterties, T. N. Rhodin, E. Band, C. F. Brucker, W. R. Pretzer, *Chem. Rev.*, **1979**, *79*, 91-137.

[5] B. Pfeffer, S. Jaberg, and G. Niedner-Schatteburg, *J. Chem. Phys.* **2009**, *131*, 194305; L. Barzen, M. Tombers, C. Merkert, J. Hewer, and G. Niedner-Schatteburg, *Int. J. Mass Spectrom.* **2012**, *330–332*, 271–276; M. Tombers, L. Barzen, and G. Niedner-Schatteburg, *J. Phys. Chem. A* **2013**, *117*, 1197-1203.

[6] Y. Nosenko, F. Menges, C. Riehn, G. Niedner-Schatteburg *Phys. Chem. Chem. Phys.* **2013**, *15*, 8171; J. Lang, M. Gaffga, F. Menges, and G. Niedner-Schatteburg, *Phys. Chem. Chem. Phys.* **2014**, *16*, 17417 – 17421.

[7] S. Dillinger, J. Mohrbach, J. Hewer, M. Gaffga, and G. Niedner-Schatteburg, *Phys. Chem. Chem. Phys.* **2015**, *17*, 10358.

[8] S. Peredkov, M. Neeb, W. Eberhardt, J. Meyer, M. Tombers, H. Kampschulte, G. Niedner-Schatteburg, *Phys. Rev. Lett.* **2011**, *107*, 233401; J. Meyer, M. Tombers, C. van Wüllen, G. Niedner-Schatteburg, S. Peredkov, W. Eberhardt, M. Neeb, S. Palutke, M. Martins, and W. Wurth, *J. Chem. Phys.* **2015**, *143*, 104302.

Jet-Cooled Cytosines have Nanosecond Lifetimes

M. A. Trachsel, S. Blaser, T. Wiedmer, H.-M. Frey, S. Leutwyler
Dept. für Chemie und Biochemie, Universität Bern, CH-3012 Bern

Abstract

UV radiative damage to DNA is believed to be inefficient because of the ultrafast $S_1 \rightarrow S_0$ internal conversion of its constituent nucleobase chromophores. In room temperature aqueous solution the S_1 state lifetimes of the canonical nucleobases are in the τ=0.5-1.5 ps range.

We measured the $S_1(^1\pi\pi^*)$ state lifetimes of supersonic jet-cooled keto-amino cytosine (Cyt) and its N_1-derivatives 1-methyl-, 1-ethyl-, 1-isopropyl- and 1-(2-tetrahydrofuranyl)-Cyt using the ps pump/delayed ionization technique [1].

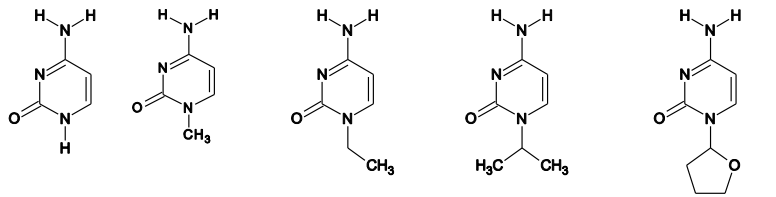

Astonishingly, the S_1 vibrationless (v'=0) lifetime of Cyt is found to be τ=700 ps [2], which is 15 times longer than the lower limit of τ=45 ps derived from rotational contour fits assuming Lorentzian linewidths [3]. Furthermore, the v'=0 lifetime is ~500-700 times longer than those measured by fs pump/probe ionization at vibrational excess energies of E_{exc}=1500-4000 cm^{-1} above the v'=0 level [3].

The intersystem crossing (ISC) quantum yields of the low-lying S_1 vibronic levels of cytosine are Q_{ISC}=0.03-0.05 [4], giving $k_{ISC}=4\text{-}7\cdot10^7\ s^{-1}$, and the calculated S_1 radiative rate is $k_{rad}=8\cdot10^7\ s^{-1}$, so the nonradiative relaxation of cytosine is dominated by internal conversion to the S_0 state ($k_{IC}=1.2\cdot10^9\ s^{-1}$) [2].

The S_1 (v'=0) lifetimes of the four N_1-derivatives lie between τ=100 ps and 1.5 ns, varying irregularly with the length and complexity of the N_1-substituent. This reveals that the S_1 state nonradiative dynamics of cytosine is highly sensitive to the N_1-substituent and cannot just be explained

in terms of the amino-pyrimidinone chromophore [2], as has been previously attempted in theoretical work.
Our correlated excited-state calculations predict that the energy gap between the S_1 ($^1\pi\pi^*$) and S_2 ($^1n\pi^*$) states varies strongly [2] as a function of the substituent length, substituent structure and internal-rotation angle ϕ around the N_1-C bond. For some substituents and for certain ranges of ϕ, strong $^1\pi\pi^*/^1n\pi^*$ coupling and even state inversion occurs. This is expected to strongly influence the S_1 state lifetimes.

References

[1] S. Blaser, H.-M. Frey, C.G Heid. S. Leutwyler, CHIMIA **68** (2014) 260.
[2] S. Blaser, M. A. Trachsel S. Lobsiger, T. Wiedmer, H.-M. Frey, S. Leutwyler, J. Phys. Chem. Lett, submitted.
[3] K. Kosma, C. Schröter, E. Samoylova, I. V. Hertel, T. Schultz, J. Am. Chem. Soc. **131** (2009) 16939; J. W. Ho, H.C. Yen, W.K. Chou, C.N. Weng, L.H. Cheng, H.Q. Shi, S.H. Lai, P.Y. Cheng, J. Phys. Chem. A 115 (2011) 8406.
[4] S. Lobsiger, M. A. Trachsel, H.-M. Frey, S. Leutwyler. J. Phys. Chem. B **117** (2013) 6106.
[5] S. Lobsiger, M. Etinski, S. Blaser, H.-M. Frey C. Marian, S. Leutwyler, J. Chem. Phys. **143** (2015) 234301.

Exploring Gas/Surface Reaction Dynamics via Quantum State Resolved Molecular Beam Experiments

Maarten van Reijzen, Jörn Werdecker, Helen Chadwick, Ana Gutiérrez and Rainer D. Beck
Ecole Polytechnique Fédérale de Lausanne (EPFL), 1015 Lausanne, Switzerland

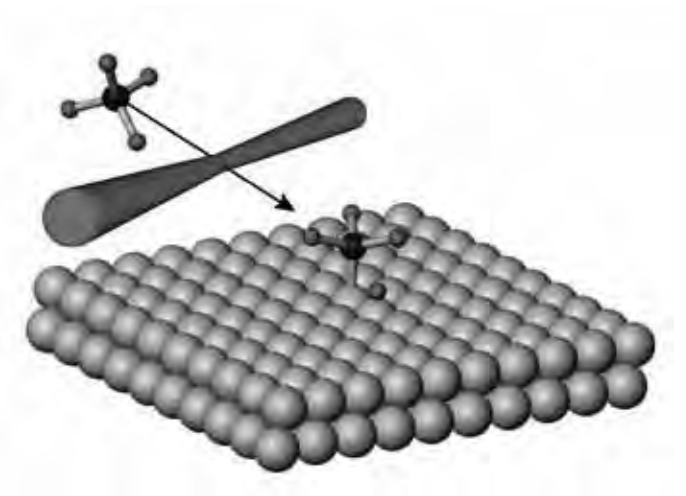

We present recent results from our laboratory on quantum state resolved reactivity measurements for the dissociative chemisorption of methane and water and their deuterated isotopologues on Ni and Pt surfaces[1-7]. Both dissociation reactions play an important role in the steam reforming process used to convert methane and water into a mixture of hydrogen and carbon monoxide by heterogeneous catalysis. Using state-selective reactant preparation by rapid adiabatic passage in a molecular beam, we prepare the surface incident methane and water molecules in specific ro-vibrational quantum states and measure the state-resolved reactivity on a single crystal surface using surface analytical techniques such Auger electron spectroscopy, King & Wells beam reflectivity, and reflection absorption infrared spectroscopy (RAIRS). We also probe the quantum state distribution of the nonreactive scattered molecules by combining infrared laser tagging with bolometric detection. The results of our measurements provide evidence for mode- and bond-

specificity as well as steric effects in chemisorption reactions and show that the dissociation of both methane and water cannot be described by statistical rate theory but require dynamical treatments including all internal vibrational and rotational degrees of freedom of the dissociating molecule. The detailed reactivity data obtained in our measurements serves as stringent test for the development of a predictive understanding of these industrially important gas/surface using first principles theory.

References

[1] L. Chen, H. Ueta and R.D. Beck, J. Phys. Chem. C, **119**, 11199 (2015).
[2] H.J. Chadwick and R.D. Beck, Chem. Soc. Rev. 2015, avail. online **DOI:** 10.1039/C5CS00476D
[3] P.M. Hundt, B. Jiang, M.E. Van Reijzen, H. Guo, and R.D. Beck, *Science*, **344**, 504 (2014).
[4] P.M. Hundt, M.E. Van Reijzen, H. Ueta, and R.D. Beck, *J. Phys. Chem. Lett.*, **5**, 1963 (2014).
[5] H. J. Chadwick, P.M. Hundt, M.E. Van Reijzen, B. Yoder and R.D. Beck, *J. Chem Phys*, **140**, 34321 (2014).
[6] F. Nattino et al, *J. Phys. Chem. Lett.*, **5**, 1294 (2014).
[7] H. Ueta, L. Chen, R.D. Beck, I. Colon-Diaz, and B. Jackson, *Phys. Chem. Chem. Phys.*, 15, 20526 (2013).

Ion-molecule reaction dynamics: from substitution to elimination

Roland Wester
Institute for Ion Physics and Applied Physics, University of Innsbruck, Austria
roland.wester@uibk.ac.at

In this talk I will present recent studies of the dynamics of nucleophilic substitution and elimination reactions, which we have performed using crossed-beam velocity map ion imaging [1]. By analysing the differential scattering cross sections, we have identified several distinct reaction mechanisms for the nucleophilic substitution reactions of Cl^-, F^- and OH^- anions with CH_3I and a good agreement has been obtained with direct dynamics simulations [2-6]. The different mechanisms depend differently on the relative collision energy. Recently, we studied the influence of the leaving group on an S_N2-reaction by comparing the reactants CH_3I and CH_3Cl and observed a profound difference for the two - in good agreement with dynamics simulations. This is explained by subtle differences in the interaction in the entrance channel [7].

In order to clarify the influence of spectator vibrational modes on the reaction dynamics we studied the reaction of F^- with CH_3I for CH-stretch excited reactant molecules. Both the S_N2-product and the proton transfer product were observed. For the latter a strong effect of the infrared excitation was manifest, whereas the former is only marginally affected by the vibrational excitation, which indicates spectator-like dynamics [8].

In crossed-beam experiments with larger alkyl halides we recently found evidence for the bimolecular elimination reaction (E2), which competes with the S_N2 reaction when more than one carbon atom is present [9].

References

[1] R. Wester, Phys. Chem. Chem. Phys. 16, 396 (2014)
[2] J. Mikosch, S. Trippel, C. Eichhorn, R. Otto, U. Lourderaj, J. X. Zhang, W. L. Hase, M. Weidemüller, R. Wester, Science 319, 183 (2008)
[3] J. Zhang, J. Mikosch, S. Trippel, R. Otto, M. Weidemüller, R. Wester, W. L. Hase, J. Phys. Chem. Lett. 1, 2747 (2010)

[4] J. Mikosch, J. Zhang, S. Trippel, C. Eichhorn, R. Otto, R. Sun, W. DeJong, M. Weidemüller, W. L. Hase, R. Wester, J. Am. Chem. Soc. 135, 4250 (2013)
[5] R. Otto, J. Brox, S. Trippel, M. Stei, T. Best, R. Wester, Nature Chem. 4, 534 (2012)
[6] J. Xie, R. Otto., J. Mikosch, J. Zhang, R. Wester, W. L. Hase, Acct. Chem. Res. 47, 2960 (2014)
[7] M. Stei, E. Carrascosa, M. A. Kainz, A. H. Kelkar, J. Meyer, I. Szabó, G. Czakó, R. Wester, Nature Chemistry (in press)
[8] M. Stei et al., in preparation
[9] E. Carrascosa et al., in preparation

Simplified Analysis of Complex-Forming Bimolecular Ion-Molecule Reactions

Jürgen Troe
Institut für Physikalische Chemie, Universität Göttingen

Bimolecular gas phase reactions of the type A + B → C + D often proceed by intermediate formation of complexes AB* which can have a rich intrinsic dynamics, either be stabilized in collisions (or by radiation) or rearrange in a sequence of processes finally leading to products like C + D. Because of attractive forces between A and B, ion-molecule reactions particularly frequently show this behaviour, often resulting in specific temperature (and energy) as well as pressure dependences. The analysis of such processes involves a series of generally not well known intra- and intermolecular quantities. In addition, the treatment of the dynamics is not simple. This talk discusses possibilities to arrive at a simplified but nevertheless realistic representation of this type of processes. Intramolecular processes are treated by unimolecular rate theory, while master equations account for collisional energy transfer.

Examples to be discussed are the reaction $FeO^+ + H_2 \rightarrow Fe^+ + H_2O$ with a short-lived intermediate such that a collisional stabilization of the FeO^+H_2 adduct would require large bath gas pressures and the reaction experimentally was observed [1] in the low-pressure limit of the reaction. In contrast, the reaction $Fe^+ + CH_3OCH_3 \rightarrow Fe^+CH_2O + CH_4$ showed some pressure dependence [2] at bath gas pressures in the Torr-range, indicating a transition between the low- and high pressure ranges of the reaction with dominant collisional stabilization of the adduct at high pressures. These reactions in addition have the possibility of single or multiple spin inversion. The proposed simplified analysis of such complex-forming bimolecular reactions [3] well accounts for the experimental observations and allows for a meaningful simplified interpretation of the observables.

[1] S. G. Ard, J. J. Melko, O. Martinez jr, V. G. Ushakov, A. Li, R. S. Johnson, N. S. Shuman, H. Guo, J. Troe, A. A. Viggiano J. Phys. Chem. A **118**, 6789 (2014).

[2] S. G. Ard, R. S. Johnson, O. Martinez jr, N. S. Shuman, H. Guo, J. Troe, A. A. Viggiano (in preparation).

[3] J. Troe J. Phys. Chem DOI:10.1021/acsjpca.5b6019.

On the use of Rydberg states of hydrogen to study the quasi-bound states of H_2^+ and the $H_2^+ + H_2 = H_3^+ + H$ reaction at low temperature

M. Beyer, P. Allmendinger, J. Deiglmayr, O. Schullian, K. Höveler and F. Merkt
Physical Chemistry Laboratory, ETH Zurich, Switzerland

In Rydberg states of high principal quantum number ($n > 30$), the Rydberg electron moves at large distances from its ion core. The classical radius of a Rydberg-electron orbit ($a_0 n^2$) is about 50 nm at n=30 and about 500 nm at n=100. At high n values, the Rydberg electron hardly interacts with the ion core and can be regarded as a passive spectator of the core motion. This concept has been successfully used in several scientific applications devoted to the studies of molecular cations, for instance in studies by zero-kinetic-energy photoelectron spectroscopy (1). In this contribution, we present the results of two experiments in which we have used high Rydberg states of H_2 to study primary processes in simple positively charged chemical systems.

In the first experiment, we use high Rydberg states to measure the properties of H_2^+ and HD^+ in the vicinity of their dissociation limits $H^+ + H$, $H^+ + D$ and $H + D^+$, with particular emphasis on the quasi-bound rotational levels of the $X^+\ ^2\Sigma_g^+$ ground state, i.e., rovibrational states located close to the top of the centrifugal barriers and which decay by quantum-mechanical tunneling. Although the existence of these quasi-bound levels has been predicted a long time ago, they have never been observed. Their positions and widths have not been calculated either. Given the role that such states play in the three-body and radiative recombination of H(1s) and H^+ to form H_2^+, this lack of data may be regarded as one of the largest unknown aspects of this otherwise accurately known fundamental molecular cation. We present measurement of the positions and widths of the lowest-lying quasi-bound rotational levels of H_2^+ and compare the experimental results with the positions and widths we calculate for these levels using a potential model for the X^+ state of H_2^+ which includes adiabatic, non-adiabatic, relativistic and radiative corrections to the Born-Oppenheimer potential energies.

In the second experiment, we use high Rydberg states of H_2 in a merged-beam experiment to study the ion-molecule reaction $H_2^+ + H_2 = H_3^+ + H$ at low collision energies. The reaction takes place within the Rydberg-electron orbit and is not influenced by the Rydberg electron, the sole function of which being to shield the ions from stray electric fields. Such fields influence the kinetic energy of the ions, which reduces the energy resolution in other experiments and prevent measurements at very low collision energies. The $H_2^+ + H_2 = H_3^+ + H$ reaction is a key reaction in interstellar clouds and is at the origin of most gas-phase astrochemical reaction cycles. So far, the reaction has only been studied at collision energies above 8 meV (E/k = 100 K) (2). By carefully controlling the direction and velocity of a supersonic beam of H_2 Rydberg molecules and merging it with a supersonic beam of ground state H_2 molecules, we have been able to measure the relative reaction cross section as a function of the collision energy from 8 meV down to 8 μeV (E/k = 100 mK). The results of these measurements will be compared to the results of Ref. (2), to Langevin capture cross sections and discussed in the context of theoretical predictions of the cross sections at very low temperatures (3).

(1) K. Müller-Dethlefs and E. W. Schlag, Chemical applications of zero kinetic energy (ZEKE) photoelectron spectroscopy, Angew. Chem. Int. Ed. **37**, 1346 (1998)
(2) T. Glenewinkel-Meyer and D. Gerlich, Single and merged beam studies of the reaction $H_2^+(v=0,1;J=0\text{-}4)+H_2 = H_3^+ + H$, Isr. J. Chem. **37**, 343-352 (1997)
(3) E. I. Dashevskaya, I. Livtin, E. E. Nikitin and J. Troe, Rates of complex formation in collisions or rotationally-excited homonuclear diatoms with ions at very low temperatures. Application to hydrogen isotopes and hydrogen-containing ions, J. Chem. Phys. **120**, 9989 (2004)

2D UV-MS cold ion spectroscopy of biomolecules

Oleg Boyarkin and Vladimir Kopysov
Laboratoire de Chimie Physique Moléculaire, École Polytechnique Fédérale de Lausanne, CH-1015 Lausanne, Switzerland
Alexander Makarov
Thermo Fisher Scientific, Hanna-Kunath Str. 11, 28199 Bremen, Germany

We integrate UV photofragmentation spectroscopy of cold ions with high-resolution Orbitrap mass spectrometry (MS) and use mathematical analysis of the recorded 2D data arrays for structural identification of biomolecules. The synergy of the two orthogonal techniques makes these arrays unique fingerprints of molecular ions, enabling their reliable identifications. Cryogenic cooling enables vibrational resolution in UV spectra, while the use of a broadband Orbitrap mass-analyzer enables detection of all charged fragments at each UV wavenumber with high mass-resolution. Using preliminary created libraries of fingerprints, the UV-MS approach was successfully applied for quantitative identification of exact isobaric molecules in their mixtures, which is one of the challenging cases for mass spectrometry. We also demonstrate how, in certain cases, the number of unknown chemical components of a mixture and their UV absorption and fragmentation mass spectra can be recovered from its fingerprint using mathematical methods of matrix analysis.[1]

Such "blind" analysis is equally applicable for distinguishing conformers of gas-phase aromatic biomolecules. It is based on the fact that UV electronic excitation of peptides may produce some specific fragments, which do not appear in thermal dissociation. High sensitivity of electronic states to the local environment of UV chromophores makes

the abundance of such fragments, to a certain extend, dependent on the ion geometry. This dependence may allow for distinguishing the conformers, in which the chromophore environments are sufficiently different. A recorded a two-dimensional data array (ion abundance *vs* m/z and UV wavenumber) is analyzed to identify the distinguishable conformers pf ions using matrix factorization analysis. The number of essential conformers $\boldsymbol{k}$ contributing to the data array is evaluated using the bi-cross-validation (BCV) approach by minimizing the BCV error. The data array is then approximated by a product of two non-negative matrices of appropriate dimensions, and the matrices are varied to minimize the residue of the factorization. The first matrix of the optimized product contains $\boldsymbol{k}$ UV absorption spectra of the conformers, while the second one collects $\boldsymbol{\kappa}$ conformer-specific UV fragmentation mass spectra of parent ions. It is fundamental to the approach that only the conformers, which differ both in absorption and in fragmentation, can be revealed mathematically. We, first, validated the UV-MS analysis of conformers with a benchmark protonated dipeptide YA-H^+ and then use this aapproach to derive some structural constraints for a larger ion, doubly protonated decapeptide gramicinin s, and for a small non-peptides drug molecule homatropine.

We also use the 2D UV-MS of cold ions for conformer-selective detection of resonance energy transfer (FRET) between the aromatic rings of Tyr and Phe residues in pain relief drugs enkephalins. The distance between these aromatic rings is one key structural parameter that governs the pharmacological activity of these opioid peptides. In contrast to the known condensed-phase structures, these distances, evaluated by FRET for isolated ions, appear to differ substantially in enkephalins with

different pharmacological efficiencies, suggesting that gas-phase structures might be a better pharmacophoric metric for ligand peptides.[2]

References

1. Kopysov, V.; Makarov, A.; Boyarkin, O. V., Colors for Molecular Masses: Fusion of Spectroscopy and Mass Spectrometry for Identification of Biomolecules. *Anal. Chem.* **2015,** *87* (9), 4607-4611.

2. Kopysov, V.; Boyarkin, O. V., Resonance Energy Transfer Relates the Gas-Phase Structure and Pharmacological Activity of Opioid Peptides. *Angew. Chem. Int. Ed.* **2016,** *55* (2), 689-692.

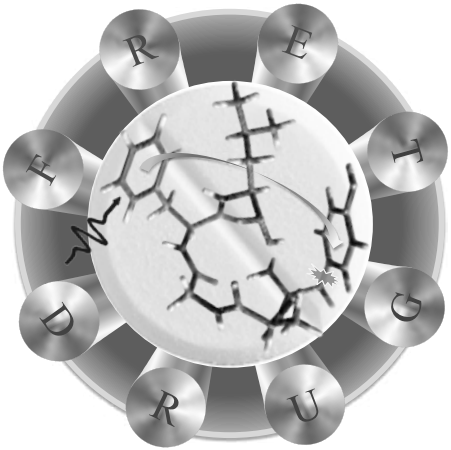

Hot Topic Papers

Selective multiphoton excitation of molecules in solution and on helium droplets by shaped laser pulses

Albrecht Lindinger
Institut für Experimentalphysik, Freie Universität Berlin, Arnimallee 14, D-14195 Berlin, Germany

Pulse shaping is reported for selective multiphoton processes of molecules in solution and on superfluid helium droplets. Particularly phase-tailored pulses are employed for three-photon excited fluorescence of different terphenyl dyes in a liquid and a good agreement between experiment and simulation is obtained. A considerable change of the fluorescence contrast between two dyes is achieved which is relevant for imaging applications. Furthermore, the dynamics of alkali dimer ionization on helium droplets is controlled with shaped pulses by activating or inhibiting different ionization paths due to wavepacket interference.

1. Introduction

In recent years, various processes like ionization, dissociation, and isotope and isomer selection were controlled by using tailored laser pulses. An important issue in this regard is the information coded in the optimized laser pulse shape which supplies insight about the underlying processes [1]. Recently, pulse shaping methods were used to investigate biologically relevant systems. There, pulse shaping is applied to multiphoton excited fluorescence where interference effects are utilized [2]. It enables imaging by multiphoton microscopy, e.g. for conducting cancer diagnosis [3].

This contribution reports on new pulse shaping methods for coherent control of multiphoton processes. The tailored laser pulses enable selective multiphoton induced fluorescence of dye mixtures. Special antisymmetric phase functions are employed for scans of the multiphoton excitation [4]. Selective three-photon excitations of the two UV dyes p-Terphenyl (PTP) and BM-Terphenyl (BMT) are reported. The main advantages of three photonic microscopy is the achievement of higher spatial resolution and lager imaging depth than in two photonic microscopy. Three-photon excitation enables to directly excite amino acids. This is relevant for photo-inducing the fluorescence of peptides which do not absorb the second but the third harmonic of a Ti:Sa-laser.

Furthermore, the dynamics of the ionization of K_2 on superfluid helium droplets is controlled. Phase differences between subpulses are employed to activate or inhibit different ionization paths by wavepacket interference.

2. Experimental

The experimental setup consists of a femtosecond laser system (RegA amplifier with Mira oscillator, Coherent Inc.) which delivers 60 fs pulses at 805 nm central wavelength with a repetition rate of 286 kHz. Pulse shaping is performed by a spatial light modulator (SLM640, CRi) placed in the Fourier plane of a 4f-setup for the dye experiments. The center pixels of the pulse modulator are aligned to the central wavelength of 805 nm. The fluorescence signal of the dyes is collected by two lenses and focused into a photomultiplier tube (R943-02, Hamamatsu). Two colored glass filters (BG 39 and UG 11) are placed in front of the photomultiplier to absorb scattered light in the visible as well as in the IR range. PTP and BMT are solved in ethanol. Both dyes are aromatic hydrocarbons consisting of a linear chain of three benzene rings. BMT and PTP were chosen because they absorb around 268.3 nm which is the third harmonic of the spectral pulse maximum. The concentration of dyes in the solutions was 3.5 mM for PTP and 5 mM for BMT, respectively.

For the generation of helium droplets, ultrapure helium 6.0 is used which is cooled down before passing through the nozzle. The nozzle orifice diameter is 5 μm. The helium is prepared at 30 bar and the system is cooled down to 13.5 K by a liquid helium cryostat, CTI-Cryogenics model 8300. A Lakehore 331 temperature controller and a silicon diode glued to the cylinder ensure thermal stabilization. This allows for generation of droplets with 10^4 atoms at a temperature of 0.37 K. After a skimmer, the helium droplet beam transfers the pick-up chamber and picks up potassium atoms. The temperature of the oven is set to predominantly attach two potassium atoms. Then the droplets arrive in the detection chamber where the laser enters the chamber and crosses the helium beam right below the detection device. The quadrupole mass analyzer (BALZERS QMA 400) detects the ions created by the action of the laser pulses on the potassium dimers.

3. Results

Selective three-photon excitation of terphenyl dyes

Molecule selective excitation can be achieved by coherent control of the three-photon excitation with shaped pulses. The effective field driving a multiphoton transition is due to interference between spectral components of the pulse field. For three-photon excitations in absence of intermediate resonances the effective field of an ultrashort pulse is given by

$$E^{(3)}(\Delta) \propto \int_{-\infty}^{\infty}\int_{-\infty}^{\infty} \left|E(\Omega_1)\right\|E(\Omega_2)\right\|E(\Delta-\Omega_1-\Omega_2)\left|e^{i\left[\varphi(\Omega_1)+\varphi(\Omega_2)+\varphi(\Delta-\Omega_1-\Omega_2)\right]}d\Omega_1 d\Omega_2 \qquad (1)$$

where each photon is spectrally detuned by Ω_1, Ω_2 or $(-\Omega_1-\Omega_2)$, and Δ is the detuning from the third-order multiple of the carrier frequency of the pulse (ω-3ω_0) [2]. It is therefore possible to change the ratio of the intensities of two dyes by manipulating the phase $\varphi(\omega)$ to get constructive interference at low and destructive interference at high frequencies and vice versa. That is if one dye has a higher absorbance for low frequencies and the other for high frequencies. Examples for effective three-photon spectra of shaped pulses with maxima at $\lambda_0/3$ are shown in Fig. 1(a).

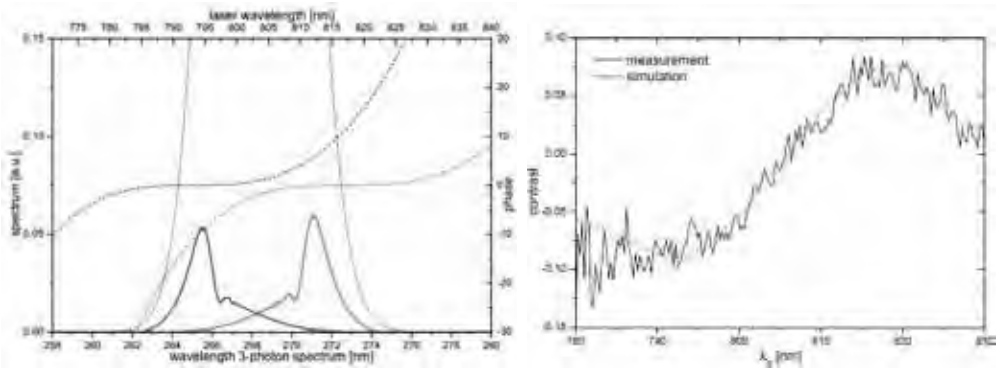

Fig. 1: (a) Effective three-photon spectra (solid lines) and phases (dashed lines) of pulses with a cubic phase function with a scaling factor of $2 \cdot 10^5$ fs^3, λ_0 = 793nm (black), and λ_0 = 817nm (red). The maximum of the transform-limited pulse spectrum (blue doted) is normalized to 1. (b) Contrast measurement (solid line) and simulation (dashed line) of the PTP and BMT fluorescence signal for third-order spectral phases with λ_0 shifted from 780 nm to 830 nm.

Third-order phase functions are written on the modulator for different wavelengths λ_0. At each λ_0 the contrast was calculated by $(I_{PTP} - I_{BMT})/ (I_{PTP} + I_{BMT})$. Here, I_{PTP} and I_{BMT} are the fluorescence signals of PTP and BMT measured with the photomultiplier and normalized by the fluorescence signal of a transform-limited pulse. Their result is displayed in fig. 1(b). The measured curve is in very good agreement with the simulation and a difference of Δc=0.15 between highest and lowest contrast is achieved.

Selection of ionization paths of K_2 on helium droplets

Pump-probe scans of the ionization of potassium dimers on helium droplets were conducted by using a pulse shaper. Interesting results were obtained by changing the phase difference between the two sub pulses from zero to π (see fig. 2). A significantly modified ion signal was observed by only varying the phase difference. This is attributed to a notably differing ionization path. For a zero phase difference the well-known wave packet oscillation in the first excited state $A^1\Sigma_u^+$ is utilized (500 fs oscillation period)

with the initial excitation at the inner turning point and the further excitation and ionization also at the inner turning point [5]. The wave packets interfere thereby constructively due to the zero phase difference. In contrary to that, for the phase difference of π one gets a destructive interference in the first excited state which means less signal whereas presumably the second excited state $2^1\Pi_g$ is utilized. Here, the initial excitation occurs at the inner turning point and the further excitation and ionization at the outer turning point. This can be observed in the pump-probe signal since the characteristic oscillation has a phase of π (meaning a minimum at time zero). A longer oscillation period is obtained in this case which is consistent with oscillation in the $2^1\Pi_g$ state. Hence, a phase shift between different subpulses results in a remarkably different ionization path via different excited states. This can be regarded as wave function interference control by phase-locked pump-probe performed by Scherer et al. [6], but now for molecules on helium droplets and with a drastic change of the excitation path.

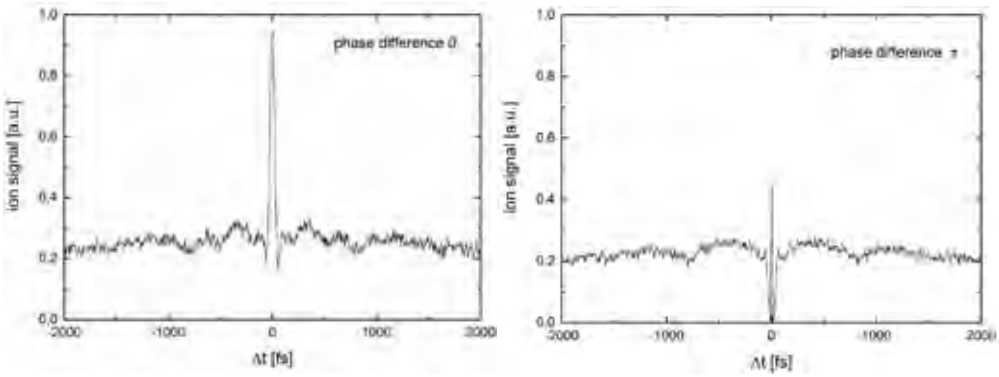

(a) (b)

Fig. 2: Pump-probe scans of the ionization of potassium dimers on helium droplets by using a pulse shaper. The $^{78}K_2^+$ signal is recorded. (a) The phase difference between the two subpulses is zero. (b) The phase difference between the pulses amounts to π. A significant change is observed by only altering the phase difference which is attributed to a remarkably differing wave packet dynamics.

References

[1] B. Schäfer-Bung et al., J. Phys. Chem. A **108**, 4175 (2004).
[2] V.V. Lozovoy, I. Pastirk, K.A. Walowicz, and M. Dantus, JCP **118**, 3187 (2002).
[3] S. Perry, R. Burke, and E. Brown, Ann. Biomed. Eng. **40**, 277 (2012).
[4] A. Patas, G. Achazi, C. Winta, and A. Lindinger, JOSA B **31**, 2208 (2014).
[5] P. Claas et al., J. Phys. B: At. Mol. Opt. Phys. **39**, S1151 (2006).
[6] N. F. Scherer et al., JCP **95**, 1487 (1991).

Intramolecular Vibrational Energy Redistribution in Cyano-Acetylene (HCCCN)

A. Kushnarenko, E. Miloglyadov, M.Quack, G. Seyfang

Physical Chemistry, ETH Zurich
CH-8093Zürich, Switzerland

1. Introduction

Intramolecular vibrational energy redistribution (IVR) is the primary process in almost all thermal reactions and its understanding can be considered as a stringent test on the validity and applicability of statistical theories [1-6]. It may even open routes to new types of chemistry. Investigating the details of IVR we have to answer the following questions: Is the energy flow mode specific, what are the time scales of the energy flow and does it lead ultimately to a statistical relaxation and finally to a microcanonical equilibrium ?
Like other time dependent molecular processes IVR can be studied directly as well in the time domain as in the frequency domain. In the latter approach from the analysis of highly resolved infrared molecular spectra an effective and a real Hamiltonian is constructed and the time evolution of the wave packet dynamics is then obtained from the integration of the time dependent Schrödinger equation. This method has been applied very successfully in the past to investigate the IVR processes after overtone excitation of the CH-chromophore in different molecules and different chemical environments [2-5]. The results from the high resolution spectroscopic analysis can be compared to results from time resolved femtosecond pump-probe experiments [7-10]. Due to different advantages and disadvantages of these two concepts the final results have to be considered as complementary rather than competitive in many cases.
We have selected cyano-acetylene as a prototypical molecule because of its comparably simple spectra [11-14] and the well separated acetylenic CH-stretching chromophore. Also, with just 5 atoms it is amenable to full dimensional quantum mechanical calculations [15-17]. Thus it may become a prototypical system for IVR, both in high resolution spectroscopic and time dependent perspectives [18, 19]
.

2. Experimental

The experiments are performed with a fairly standard pump-probe set-up providing a time resolution of about 150 fs [9, 10]. A Ti:Sapphire laser pumps two identical near-IR optical parametric generators. One of them is used directly to excite the molecules to the first overtone of the CH-stretching vibration. The two outputs from the second generator are sent to a difference frequency unit to obtain the probe pulse around 3 micron. To measure a spectrally resolved IVR dynamics, the probe signal behind the sample cell is sent to monochromator and is then detected either on a single detector or a detector array allowing for a spectral resolution of 2 to 4 cm^{-1}. To improve the signal-to-noise ratio the simple sample cell with focused geometry is replaced by a capillary with an inner diameter of 250 micron and a length of 50 cm [9, 10].

3 Results:

Cyano-acetylene is a linear molecule with 4 stretching and 3 degenerate bending modes, summarized in table 1. To our knowledge, it is the first example for which the IVR dynamics has been obtained for the same process from both methods, time resolved and frequency resolved. The spectroscopy of the low lying states up to 1000 cm^{-1} is quite well understood, whereas for some of the higher lying states only a partial analysis is available which does not take into account any rovibrational coupling [11-14]. In our experiments the molecules are excited to the region of the first overtone of the CH-stretching vibration $2\nu_1$ which can be coupled to one or more background states. The IVR dynamics is probed either in absorption to the $3\nu_1$ spectral range or in stimulated emission to the ν_1-region.

ν_1, Σ	ν_2, Σ	ν_3, Σ	ν_4, Σ	ν_5, Π	ν_6, Π	ν_7, Π
3327.372	2273.9954	2079.306	884.766	663.2220	498.8022	222.402
CH-stretch	CN-stretch	C≡C str.	C-C-str.	HCC-bend	CCN-bend	CCC-bend

Table 1: Vibrational fundamentals of HCCCN (values given in cm^{-1})

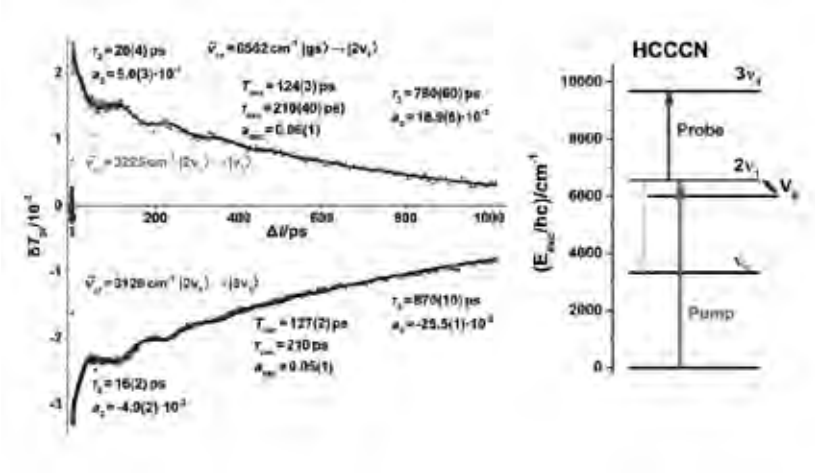

Fig.1: Time evolution of the probe signal after excitation of the $2\nu_1$-mode in HCCCN. The probe signal is obtained as absorption signal to $3\nu_1$ or as stimulated emission signal to ν_1.

The measured probe signal in absorption and stimulated emission can be fitted with a model function of the following form:

$$\delta T_{pr}(t) = a_1 + a_2 \exp\left(\frac{-t}{\tau_2}\right) + a_3\, exp\left(\frac{-t}{\tau_3}\right) +$$

$$a_{\mathrm{osc}}|a_2 + a_3| \sin\left(\frac{2\pi t}{T_{osc}} + \varphi_{\mathrm{osc}}\right) \exp\left(\frac{-t}{\tau_{osc}}\right)$$

It consists of a double exponential decay where a damped oscillation is superimposed. Nearly identical fit parameters are obtained for the absorption and stimulated emission signal. The IVR signal itself relaxes with two significantly different decay times of 15 to 25 ps and approximately 800 ps. The oscillation superimposed on the decaying IVR signal shows an oscillation period of 125 ps and a decay time of 210 ps. To investigate the IVR process for cyano-acetylene in the frequency domain the high resolution infrared spectrum has been measured with our high resolution Fourier transform spectrometer (Bruker prototype ZP2001, IFS125). The spectral width of the spectrum measured at a

sample pressure of 100 Pa is close to the calculated Doppler width of 0.0114 cm^{-1}. The IR-spectrum is dominated by the transition from the ground state to $2\nu_1$, the first overtone of the CH-stretching vibration, and by the corresponding hot band originating from the CCC-bending mode ν_7.

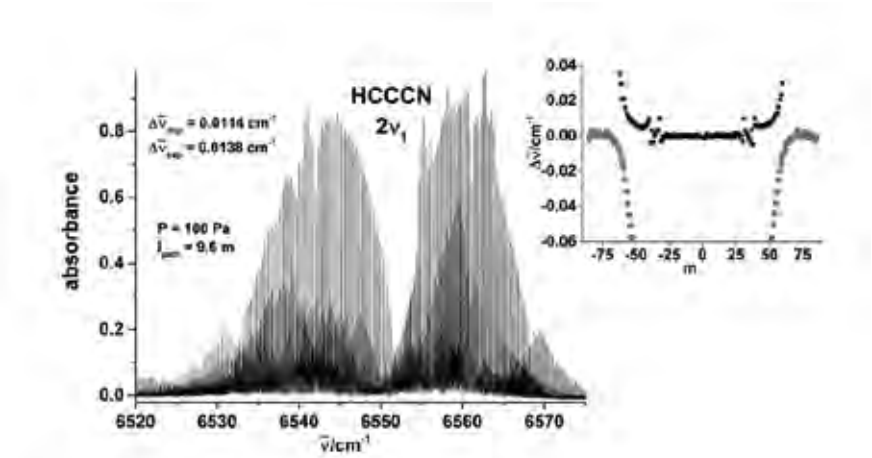

Fig. 2: High resolution IR-spectrum of HCCCN in the region of the $2\nu_1$-mode. The insert on the right shows the measured rovibrational transitions in a reduced energy scheme.

A closer inspection of the transition to the $2\nu_1$-state shows a strong perturbation around $J = 58$ and a weaker one around $J = 35$. As we are not yet able to assign the perturbing state either a two level anharmonic resonance or a Coriolis resonance could be considered in a first analysis. A significantly better fit is obtained assuming an anharmonic resonance with quite reasonable molecular parameters. Also the measured oscillations in the time dependent experiments indicate a more global resonance. The zero order states are separated by approximately 0.2 cm^{-1} and a *J*-independent Fermi coupling constant of 0.015 cm^{-1}, mainly responsible for the oscillations in the time resolved measurements is obtained from the fit. Also the relative line intensities in the region of the perturbation are well reproduced by the fitted spectroscopic parameters. Three processes contribute to the time evolution of the probe signal: the decay of the rotational coherence, the exchange dynamics between the two coupled states and the decay of the population to the background

states. The vibrational density of background states in the energy range of the $2\nu_1$ overtone is estimated to be about 100 states per cm^{-1}. The oscillation period of 125 ps would correspond to an energy separation of 0.266 cm^{-1}. At a sample pressure of 10 kPa collisional contributions to the slower decay of the population with τ_3 = 800 ps cannot be completely excluded.

References:

1. M. Quack, *Nuovo Cimento B*, **63**, 358 (1981)
2. H. R. Dübal and M. Quack, *J. Chem. Phys*. **81**, 3779 (1984)
3. M. Quack, *Annu. Rev. Phys. Chem*. **41**, 839 (1990)
4. M. Quack and J. Stohner, *J. Phys. Chem*. **97**, 12574 (1993)
5. M. Quack in '*Femtosecond Chemistry'*, J. Manz and L. Wöste (eds), 781 (Verlag Chemie, 1995)
6. M. Quack and J. Troe, *Encycl. Comput. Chem.* **4**, 2708, P. von Ragué Schleyer, N. Allinger, T. Clark, J. Gasteiger, P. A. Kollman, H. F. Schaefer, P. R. Schreiner (eds.), John Wiley (1998)
7. A. Charvat, J. Assmann, B. Abel, D. Schwarzer, K. Henning, K. Luther, and J. Troe, *Phys. Chem. Chem. Phys*. **3**, 2230 (2001).
8. C. G. Elles, M. J. Cox, F. F. Crim, *J. Chem. Phys*. **120**, 6973 (2004).
9. V. Krylov, A. Kushnarenko, E. Miloglyadov, M. Quack, G. Seyfang, *Proc. SPIE* **6460**, 64601D-1 (2007)
10. V. Krylov, A. Kushnarenko, E. Miloglyadov, M. Quack, G. Seyfang, *Ultrafast Phenomena XVI*, Springer Ser. Chem. Phys. **92**, 349 (2009)
11. W. C. Turell, W. D. Jones, A. Maki, *J. Chem. Phys*. **26**, 1544 (1957)
12. P. D. Mallison and A.Fayt, *Mol. Phys*. **32**, 473 (1976)
13. K. M. T. Yamada and R. A. Creswell, *J. Mol. Spectr*. **116**, 384 (1986)
14. F. Winther, S. Klee, G. Mellau, S. Naïm, L. Mbosei, A. Fayt, *J. Mol. Spectrosc.* **175**, 354 (1996)
15. T.Carrington, in *Handbook of High Resolution Spectroscopy*, M. Quack and F. Merkt (eds), Vol. 1, 573, (Wiley 2011)
16. J. Tennyson, *Handbook of High Resolution Spectroscopy*, M. Quack and F. Merkt (eds), Vol. 1, 551, (Wiley 2011)
17. A. G. Császár, C. Fábri, T. Szidarovszky, E. Mátyus, T. Furtenbacher G. Czakó, *Phys. Chem. Chem. Phys*. **14**, 1085 (2012)
18. S. Albert, K. Keppler Albert, H. Hollenstein, C. Manca Tanner, M. Quack, in *Handbook of High Resolution Spectroscopy*, M. Quack and F. Merkt (eds), Vol. 1, 117, (Wiley 2011)
19. M. Hippler, E.Miloglyadov, M.Quack, G. Seyfang, *in Handbook of High Resolution Spectroscopy*, M. Quack and F. Merkt (eds), Vol. 2, 1069, (Wiley 2011)

A dynamic ion-atom hybrid trap for high-resolution cold-collision studies

A. D. Dörfler[1], P. Eberle[1], H. da Silva[2], M. Raoult[2], O. Dulieu[2] and S. Willitsch[1]

[1] Department of Chemistry, University of Basel, Klingelberg-Strasse 80, 4056 Basel, Switzerland

[2] Laboratoire Aimé Cotton, CNRS, Université Paris-Sud XI, 91405 Orsay Cedex, France

E-mail: alexander.doerfler@unibas.ch

The recent progress in the combined trapping of ions and atoms has paved the way to study collisions and chemical processes in a new physical regime at extremely low energies. Such experiments promise to elucidate the quantum character of collisions and enable to accurately characterize molecular interaction potentials and to study the details of chemical reaction mechanisms with high precision [1, 2, 3]. However, to observe quantum signatures in ion-atom collisions, an improved energy resolution compared to previous experiments is required [4]. Here, we introduce a new technique to precisely control collision energies in hybrid ion-atom experiments for this purpose.

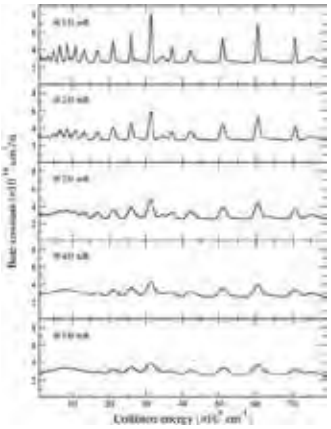

Figure 1: Theoretical rate constants for Ca^++Rb radiative association and charge transfer obtained from quantum scattering calculations, convoluted for different collision energy resolution [6]

Previously an ultracold Rb atom cloud was stationary overlapping with a Coulomb crystal of Ca^+ ions in the trap center, which resulted in a large spread of collision energies. However, theoretical calculations of the rate constants for the Ca^++Rb radiative association and charge transfer (Figure 1) obtained from quantum scattering calculations at low collision energies predict the occurrence of numerous orbital resonances. They are evidenced by marked enhancements of the reaction rate within a very small collision-energy interval [7, 8, 4, 12, 13, 14].

Their explicit positions and widths are very sensitive to the interaction potential as well as the collisional angular momentum and thus reveal important details of the scattering dynamics. The observation of scattering resonances has recently been reported in cold collisions of neutral molecules [7,8,9]. However, to the best of our knowledge they have thus far not been observed for cold ionic processes.

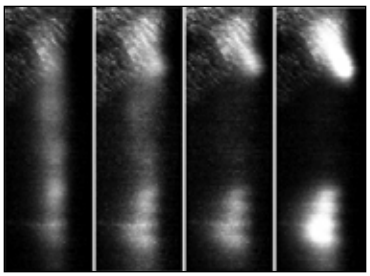

Figure 2: Images of an atom cloud during dynamic MOT operation (shuttling). This figure illustrates the effect of changing the hold time of an atom cloud in the off-center positions. From left to right: 5 ms, 10 ms, 15 ms and 25 ms hold time.

Inspired by previous experiments on moving optical molasses [5], we designed a scheme to create an ultracold atom cloud in an off-center position and use controlled radiation pressure to push it at a precise velocity through the interaction region with the cold ions. The atom cloud is then recaptured at a second off-center position on the other side of the trap center for re-use (Figure 2). This offers a new approach for controlled cold-collision experiments yielding precise energies and a high energy resolution.

Here we present a detailed characterization of the setup and first results on velocity-controlled collisions between Ca^+ ions and neutral Rb atoms in the cold regime.

Acknowledgements

This work is supported by the European Commission under the Seventh Framework Programme FP7 GA 607491 COMIQ and the University of Basel.

References

[1] Willitsch S. 2012 Int. Rev. Phys. Chem. 31

[2] Hall F. H. J. *et al* 2011 PRL 107 243202

[3] Hall F. H. J., Willitsch S. 2012 PRL 109 233202

[4] Hall F. H. J. *et al* 2013 Mol. Phys. 111 2020

[5] Wohlleben W. *et al* 2001 Eur. Phys. J. D 15237

[6] Dulieu O., Raoult M., da Silva jr H. 2015, privat communication

[7] Tacconi M. *et al* 2011 Phys. Chem. Chem. Phys. 13 19156

[8] Belyaev A. K. *et al* 2012 Phys. Rev. A 85 042716

[9] Henson A. B. *et al* 2012 Science 338 234

[10] Chefdeville S. *et al* 2013 Science 341 1094

[11] Jankunas J. *et al* 2015 J. Chem.

[12] Hall F. H. J. *et al* 2013 Mol. Phys. 111 1683 Phys. 142 164305

[13] Sayfutyarova E. R. *et al* 2013 Phys. Rev. A 87 052717

[14] da Silva jr H. *et al* 2015 New J. Phys. 17 045015

State-to-state scattering of CH4(v3) from a Ni(111) surface

M.E. van Reijzen, J. Werdecker, and R.D. Beck
Laboratoire de Chimie Physique Moléculaire (LCPM)
Ecole Polytechnique Fédérale de Lausanne (EPFL),
1015 Lausanne, Switzerland

In recent years the dissociation reaction of CH_4 on Ni(111) has been studied extensively both by quantum state resolved experiments and by first principles theory.[1-4] In these dissociation studies, it was observed that typically a large fraction of the incident methane molecules does not dissociate but scatters from the surface even if their incident energy is significantly higher than the minimum barrier height of ~0.8 eV.

Such inefficient dissociation could either be explained by a very narrow transition state, requiring a very specific deformation of the reactant, or by fast vibrational energy transfer between the incident reactant and the metal surface by electron-hole pair excitation which could compete with the dissociation reaction. Efficient vibrational energy transfer in a gas/surface collisions has been observed for NO and HCl on Au(111)[5, 6] but has never been investigated for collisions of methane with transition metal surfaces.

In order to probe the extend of vibrational energy transfer for a quantum state prepared methane molecule, $CH_4(\nu_3)$, scattered from a well defined Ni(111) surface, we have developed a state-to-state molecular beam/surface scattering experiment. This was achieved by equipping an existing molecular beam/surface science machine with state specific detection capability for scattered methane by combining a liquid helium cooled bolometric detector with infrared laser tagging. The setup allows for the preparation of the incident molecular beam in a specific rovibrational state and the state-selective detection of the scattered molecules following the collision with the metal surface.

Using this setup, we have measured rotational and vibrational state distributions of scattered CH_4 for a state prepared $CH_4(\nu_3)$ beam incident

on a Ni(111) surface. We detect both vibrationally elastic and inelastic scattering of CH_4 and quantify the probabilities for the different channels. Efficient vibrational energy transfer is observed for incident $CH_4(\nu_3)$ leading to scattered $CH_4(\nu_1)$ where ν_3 and ν_1 are the anti-symmetric and symmetric C-H stretch normal modes of CH_4, respectively. Energy transfer probabilities to other vibrational states including the vibrational ground state are currently under investigation and will be reported in this contribution.

1 R. R. Smith, D. R. Killelea, D. F. DelSesto, and A. L. Utz, Science **304**, 992 (2004).

2 R. D. Beck, P. Maroni, D. C. Papageorgopoulos, T. T. Dang, M. P. Schmid, and T. R. Rizzo, Science **302**, 98 (2003).

3 S. Nave, A. K. Tiwari, and B. Jackson, J Phys Chem A **118**, 9615 (2014).

4 R. Dâiez Muiäno and H. F. Busnengo, *Dynamics of Gas-Surface Interactions Atomic-level Understanding of Scattering Processes at Surfaces* (Springer Berlin Heidelberg, Berlin, Heidelberg, 2013).

5 R. Cooper, I. Rahinov, C. Yuan, X. M. Yang, D. J. Auerbach, and A. M. Wodtke, J Vac Sci Technol A **27**, 907 (2009).

6 Y. H. Huang, C. T. Rettner, D. J. Auerbach, and A. M. Wodtke, Science **290**, 111 (2000).

GC-MS and FTIR analyses of products from atmospheric pressure glow discharge generated in nitrogen-methane gas mixture with CO_2 addition

David Trunec[1], Lucie Töröková[1,2], Kristýna Jančíková[1,2], Simona Nicoara[2], Věra Mazánková[1], František Krčma[1], and Nigel J Mason[2]
[1]*Faculty of Chemistry, Brno University of Technology, Purkyňova 118, 612 00, Brno, Czech Republic*
[2]*Faculty of Science, Open University, Walton Hall, Milton Keynes MK7 6AA, United Kingdom*
e-mail: trunec@physics.muni.cz

This contribution extends our previous experimental studies of the chemistry of Titan's atmosphere by atmospheric glow discharge. It reports the results from the Gas Chromatography with Mass Spectrometry (GC-MS) and in situ Fourier-Transform-Infra-Red spectroscopy (FTIR) analyses of gaseous phase species produced by an atmospheric plasma glow discharge in N_2-CH_4 gas mixtures (with methane concentrations of 1%) with CO_2 addition up to 3%. The major products identified in the GC-MS spectra were: hydrogen cyanide, acetylene, acetonitrile, ethane, ethane, propene-nitrile and small amount of toluene. The same compounds were detected in the FTIR spectra and also ammonia was detected by the FTIR.

1. Introduction

Simple organic molecules play an important role in the formation of complex organics in planetary atmospheres. Titan is the largest satellite of the Saturn and its atmosphere composition is principally nitrogen with 2-6 % methane and some trace gases as nitriles (HCN, HC_3N, HC_5N, and C_2N_2) and lower molecule hydrocarbons (C_2H_2, C_2H_4, C_2H_6, C_3H_8, C_3H_4) as well as hydrogen [1]. Lightning activity is one of the most probable initiators of organic molecules formation on Titan lower atmosphere and it has been also suggested as a mechanism for triggering the prebiotic chemistry on Earth. The gliding arc configuration has been shown to be a good mimic of planetary atmospheres [2] being used to replicate physical and chemical conditions on Titan.

The present work is focused on the experimental study of gaseous products produced in the atmospheric pressure glow discharge. Gas Chromatography with Mass Spectrometry (GC-MS) and in-situ Fourier-Transform-Infra-Red

spectroscopy (FTIR) were used for analyses. In more detail the influence of the CO_2 admixture on production of the major neutral product detected HCN and on the formation of NH_3 has been studied.

2. Experiment

The experimental set-up was detail described in our previous studies [2,3]. A simplified schematic diagram of the experimental set up is presented in Figure 1. An atmospheric pressure DC glow discharge was created between two stainless steel electrodes separated by a 2 mm gap. The electrode system used the standard configuration of the gliding arc discharge, but due to the low applied power as well as low gas velocity the discharge does not move along the electrodes. The discharge was operated with an applied voltage of 400 V and discharge current in range 15-40 mA in pure nitrogen enriched by 1 % of CH_4 with admixture of CO_2 up to 3% at the total flow rate of 50 sccm. The exhaust gas was analysed in-situ by FTIR spectroscopy using IR multipath cell with total length of 3 m. For GC-MS analyses the exhaust gas was sampled using the cold trap technique as it is shown in Figure 1. The sampling time was 5 min and the efficiency was close to 100 %.

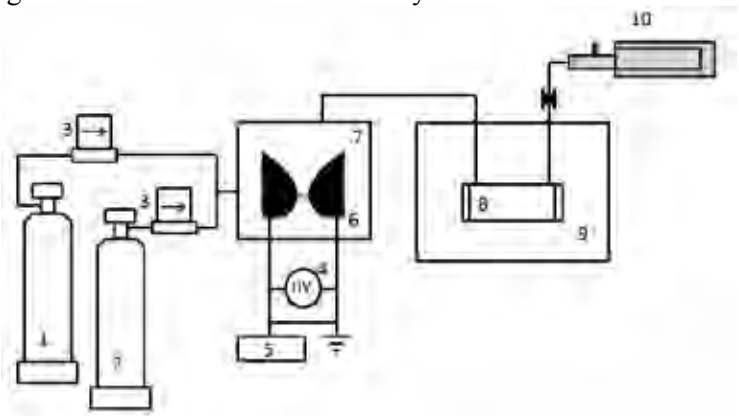

Figure 1: Experimental setup: 1- storage bottle of nitrogen, 2 - storage bottle of methane, 3 - MKS mass flow controllers, 4 - DC power supply, 5 - oscilloscope, 6 - electrode system, 7 - reactor body, 8 - IR gas cell, 9 - FTIR spectrometer, 10 - cold trap.

3. Results

A typical example of chromatogram is shown in Figure 2. All peaks have been identified using their retention time in the sequence and their mass spectra using the program MSD Chemistry with the NIST MS library. The peaks corresponding to nitrogen, methane and carbon dioxide as the original

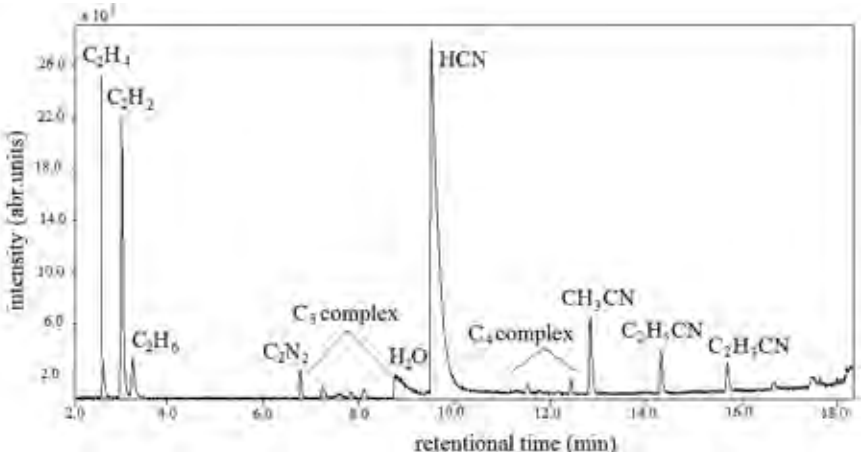

Figure 2: Chromatogram from GC-MS analysis of gas sample trapped during experiment with 98% N_2-1% CH_4-1% CO_2 mixture.

gas mixture were recorded at retention times under 2 minutes and thus they are not depicted in Figure 2. The most dominant peak corresponds to hydrogen cyanide (HCN), the second dominant peak is acetylene (C_2H_2) and the third main product is acetonitrile (CH_3CN).

A typical FTIR spectrum showing the products formed in our experiments for 98% N_2-1% CH_4-1% CO_2 gas mixture is shown in Figure 3.

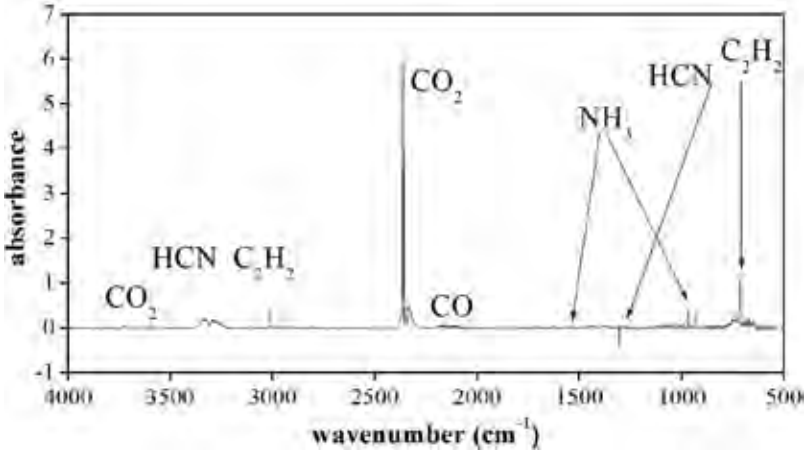

Figure 3: An example of FTIR spectrum for 98% N_2-1% CH_4-1% CO_2 gas mixture.

Similar spectra were observed for other N_2:CH_4:CO_2 ratios. HCN was found to be the most abundant product at wavenumbers of 1430 cm^{-1} and of

720 cm^{-1}. Ammonia (NH_3) was identified at 966 cm^{-1} which was surprising because ammonia was not detected in previous experimental studies. The other major products were C_2H_2 as well as carbon monoxide (CO) and water (H_2O). These products were recognized in all N_2:CH_4:CO_2 gas mixtures. The products concentrations are strongly dependent on the composition of the gas mixtures.

Figure 4 shows the quantitative analysis of HCN (1430 cm^{-1}) formed for different CO_2 amount. Influence of CO_2 addition is related to the complex kinetics of the discharge and detailed explanation of the processes associated with it should be object of further experimental work and computer simulation of the discharge kinetics.

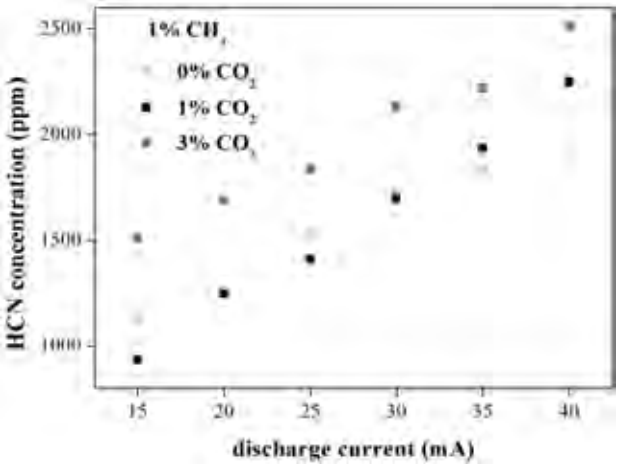

Figure 4: The dependence of hydrogen cyanide concentration on discharge current for different initial concentrations of carbon dioxide.

4. Acknowledgements

This work has been supported by project LD15011 and within the collaboration of the COST Action TD 1308.

5. References

[1] Nixon CA, Jennings DE, Bezard B et al. 2013 *Astrophys J Lett* **776** L13.
[2] Torkova L, Mazankova V, Krcma F, Mason N J and Matejcik S 2015 *EPJ Appl Phys* **71** 20806.
[3] Torokova L, Watson J, Krcma F, Mazankova V, Mason NJ, Horvath G and Matejcik S 2015 *Contrib Plasma Phys* **55** 470.

Frequency Comb Assisted Spectroscopy in 22-pole Ion Traps

Pavol Jusko, Oskar Asvany, Sandra Brünken, Alexander Stoffels and Stephan Schlemmer
I. Physikalisches Institut, Universität zu Köln, Zülpicher Straße 77, Köln, Germany

1. Instrumentation

Ion traps, due to their excellent properties, are a well known tools widely used for spectroscopy of charged particles. Since the number of particles is low (i.e. low for traditional spectroscopic methods), different forms of action spectroscopy have to be employed. Amongst many, for vibrational spectroscopy Laser Induced Reactions (LIR, [Scl02]), for electronic excitation Laser Induced Inhibition of Cluster Growth (LIICG, [Cha13]), for rotational spectroscopy two photon processes [Jus14], or LIICG [Bru14] can be used.

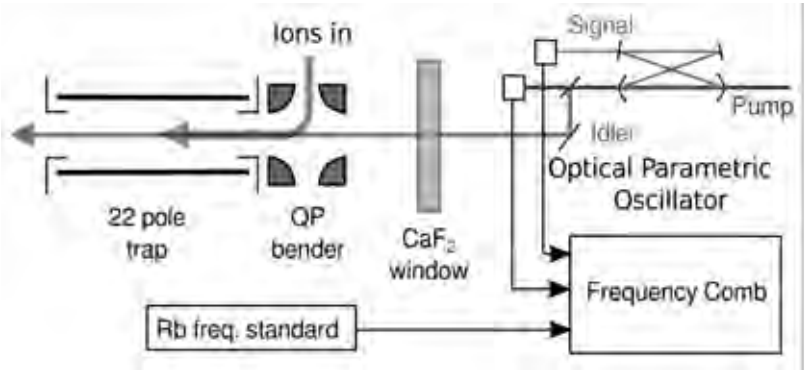

Fig. 1. Schematic drawing of the 22-pole trap setup together with the Optical Parametric Oscillator (OPO), as well as its coupling to the Frequency Comb (FC). Note, that the Signal and Pump signals are coupled to the FC system. Frequency stability is provided by a 10 MHz Rb frequency standard.

The ion trap setup used in Köln – COLTRAP – is depicted in Fig. 1. The hearth of the instrument is a 22-pole rf trap mounted on a 4 K cold head. Sources of the radiation include an Optical Parametric Oscillator (OPO) in near infrared, equipped with Frequency Comb (FC) for high accuracy

[Asv12, Asv13]. For rotational spectroscopy, rf synthesis and multiplier chains are used in order to cover frequencies from ca. 100 GHz up to >1 THz (with gaps).

2. Example 1: Spectroscopy of CD_2H^+

As a good example of system capabilities, we present preliminary measurements of ν_1 rovibrational band of CD_2H^+ ion (see Fig. 2.). So far ca. 90 transitions has been measured and assigned. Very high precision of the measurements allows us to accurately fit the ground state rotational parameters of a simple asymmetric rotor and to estimate the pure rotational transition frequencies. The predicted frequencies facilitate our search of the transitions, while scanning using GHz multiplier chains and LIICG method for pure rotational spectroscopy.

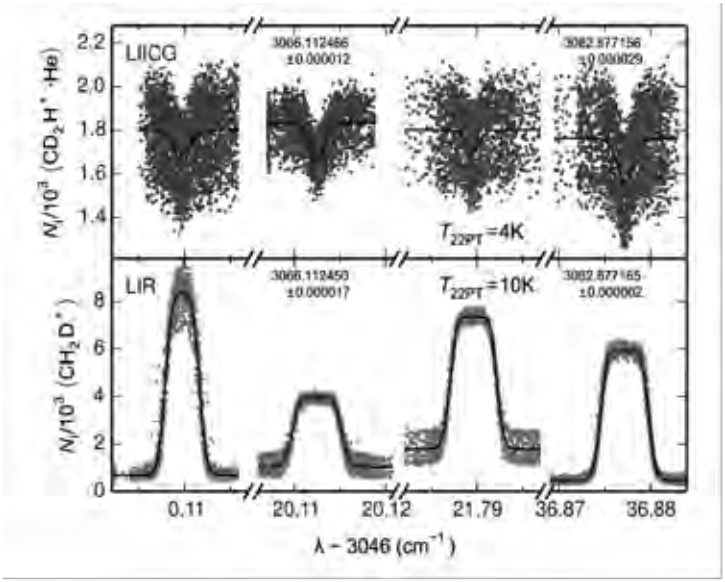

Fig. 2. Example of measured transitions of CD_2H^+ using LIICG (upper panel) and LIR (lower panel) transitions of ($0_{00} \leftarrow 1_{11}$, $1_{11} \leftarrow 0_{00}$, $2_{02} \leftarrow 1_{11}$, $2_{20} \leftarrow 1_{11}$, from left to right) at nominal temperature of 4 K (LIICG) and 10 K (LIR).

3. Example 2: Spectroscopy of H_3^+

With help of the FC system transition frequencies of H_3^+ and its 2 deuterated isotopologues has been determined with precision well below 1 MHz (see Table 1.).

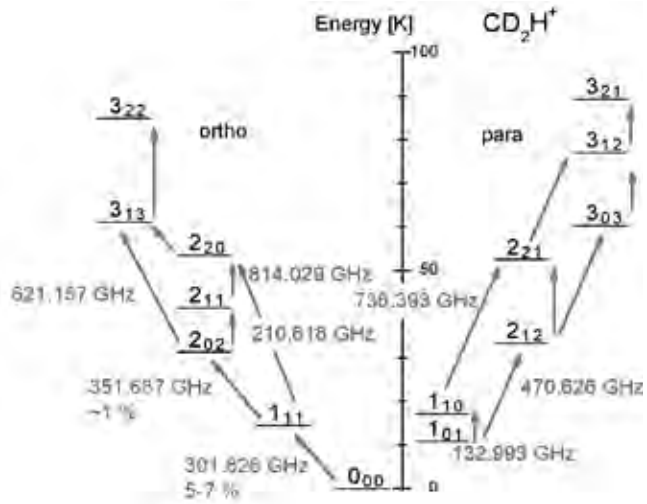

Fig. 3. Lowest CD_2H^+ energy levels according to [Rou13]. Green arrows represent data measured so far using LIICG in COLTRAP.

Even with given precision, we did not observe any discrepancies between the LIR and LIICG method. The small differences between the methods are a little sharper line profile due to smaller doppler broadening at lower temperature for LIICG and a very high signal to background ratio for the LIR.

Table 1. H_3^+ ν_2 band transitions starting from the three lowest rotational states (1,1), (1,0), (2,2). Only values acquired with LIR method are presented, due to its higher accuracy.

Transition	cm^{-1} (this work)	MHz (this work)
$R(1,1)^l$	2691.44272	80687423
R(1,0)	2725.89835	81720377
$R(1,1)^u$	2726.22001	81730020
$R(2,2)^l$	2762.06982	82804770

Acknowledgement:
P.J. acknowledge financial support from the Alexander von Humboldt Foundation. This work was also supported by the Collaborative Research Center (SFB) 956, sub-project B2, funded by the DFG.

References:

[Asv13] O. Asvany, J. Krieg, and S. Schlemmer, *Review of Scientific Instruments* 83, 093110 (2012)

[Asv13] O. Asvany, S. Brünken, L. Kluge, and S. Schlemmer, *Applied Physics B* 114, 203 (2013)

[Bru14] S. Brünken, L. Kluge, A. Stoffels, O. Asvany, and S. Schlemmer, *The Astrophysical Journal Letters* 783:L4 (2014)

[Cha13] S. Chakrabarty, M. Holz, E. K. Campbell, A. Banerjee, D. Gerlich, and J. P. Maier, *J. Phys. Chem. Lett.* 4, 4051 (2013)

[Jus14] P. Jusko, O. Asvany, A-C. Wallerstein, S. Brünken, and S. Schlemmer, *Physical Review Letters* 112, 253005 (2014)

[Rou13] E. Roueff, M. Gerin, D. C. Lis, A. Wootten, N. Marcelino, J. Cernicharo, and B. Tercero, *The Journal of Physical Chemistry A* 117, 39 (2013)

[Sch02] S. Schlemmer, E. Lescop, J. von Richthofen, D. Gerlich, and M. Smith, *J. Chem. Phys.* 117, 2068-2075 (2002)

High resolution GHz and THz (FTIR) spectroscopy and theory of parity violation and tunneling for 1,2-dithiine ($C_4H_4S_2$) as a candidate for measuring the parity violating energy differences between enantiomers of chiral molecules

S. Albert[1,2], I. Bolotova[1], Z. Chen[1], C. Fábri[1], Ľ. Horný[1], M. Quack[1], G. Seyfang[1] and D. Zindel[1]

[1]*Physical Chemistry, ETH Zurich, CH8093 Switzerland,*
[2]*Swiss Light Source, PSI Villigen, Switzerland,*

Introduction

In the framework of ordinary "electromagnetic" quantum theory the ground states of the enantiomers of chiral molecules are energetically equivalent. However, when one considers electroweak quantum chemistry and parity violation, one can predict a small "parity violating" energy difference $\Delta_{PV}E$ on the order of 100 aeV, typically, depending on the molecule, corresponding to a reaction enthalpy for stereomutation of about 10^{-11} J mol^{-1} [1,2]. While there has been considerable progress on the theory of this effect during the last decades ([1,3] and references therein), so far, this effect has never been observed experimentally. Here, we report exploratory spectroscopy and theory in view of a possible use of the chiral C_2-symmetric molecule 1,2-dithiine ($C_4H_4S_2$) for detecting molecular parity violation using a current experimental setup in our laboratory [4] following an experimental scheme proposed by us in 1986 [5].

Theory

The geometry of 1,2-dithiine was optimized at the MP2/cc-pVTZ, MP2/ccpVQZ and CCSD(T)/cc-pVTZ levels of theory. Calculated harmonic wavenumbers (in cm^{-1}, with IR intensities in km mol^{-1}) and anharmonic fundamentals of 1,2-dithiine are listed in **Table 1**. The most intense fundamental in the infrared, $\nu_7 = 630$ cm^{-1}, corresponds to an out-of-plane mode, followed by $\nu_2 = 205$ cm^{-1} (ring twist), $\nu_{17} = 1331$ cm^{-1} (C-H in-plane mode) and $\nu_{19} = 1576$ cm^{-1} (C-C asymmetric stretch). We calculated the parity violating energy difference $\Delta_{PV}E^{el}$ using our recently developed coupled cluster linear response approach [3]. We find $\Delta_{PV}E^{el}(q_e) / (hc) = 11.44 \times 10^{-12}$ cm^{-1}. The tunneling splitting in

the ground state $\Delta E_{\pm}$ is calculated using our quasiadiabatic channel reaction path Hamiltonian approach [6] to be $\Delta E_{\pm}/(hc) = 4 \times 10^{-25}$ cm^{-1} many orders of magnitude smaller than $\Delta_{PV}E$.

Mode	Sym.	$\tilde{\omega}_i$ /cm^{-1} MP2/cc-VTZ	I /(km mol^{-1})	$\tilde{\nu}_i$ /cm^{-1} MP2/cc-VTZ	approximate description
1	A	3230	8.574	3092	CH-stretches
2	A	3209	0.271	3082	CH-stretches
3	A	1576	11.094	1531	CC-stretches
4	A	1393	4.131	1361	CH in-plane bends
5	A	1182	0.110	1165	CH in-plane bends
6	A	1001	2.847	986	C_2C_3 stretch
7	A	939	0.683	921	CH out of plane bends
8	A	784	4.405	772	CH out of plane bends
9	A	746	3.746	734	CS sym. stretches
10	A	580	0.102	572	SS stretch, CH out-of plane bends
11	A	532	0.045	526	SS stretch, CH out-of plane bends
12	A	449	0.285	442	CCC in-plane bends
13	A	201	0.002	198	ring pucker
14	B	3225	5.732	3123	CH stretches
15	B	3201	0.747	3080	CH stretches
16	B	1616	7.829	1571	CC stretches
17	B	1331	14.647	1305	CH in-plane bends
18	B	1185	1.168	1167	CH in-plane bends
19	B	928	0.123	909	CH out-of-plane bends
20	B	861	2.620	850	CCC in-plane bends
21	B	711	0.998	700	CS asym. stretches
22	B	630	93.554	621	CH out-of-plane bends
23	B	316	0.076	312	CSS in-plane bends
24	B	204	12.322	205	CCC out-of plane bends

Table 1: The calculated vibrational harmonic wavenumbers $\tilde{\omega}_i$ and anharmonic fundamentals $\tilde{\nu}_I$ of 1,2-dithiine. The integrated band strengths I were calculated in the doubly harmonic approximation.

Spectroscopy

We have measured and analyzed the GHz spectrum between 68 and 108 GHz (**Figure 1,** $\Delta\nu$ = 100 kHz) using a setup modified after [7] and we have measured the IR spectrum in the range 600 - 3300 cm^{-1} with a resolution of $\Delta\nu$ = 33 MHz (self-apodized) using our highly resolving FTIR spectrometer [8,9]. We were able to perform a first rovibrational analysis of two bands, ν_7 ($\tilde{\nu}_0$ = 623.0940 cm^{-1}) consisting of *c*-type transitions **(Figure 2)** and ν_{17} ($\tilde{\nu}_0$ = 1308.8724 cm^{-1}) consisting of *a*-type transitions **(Figure 3)**.

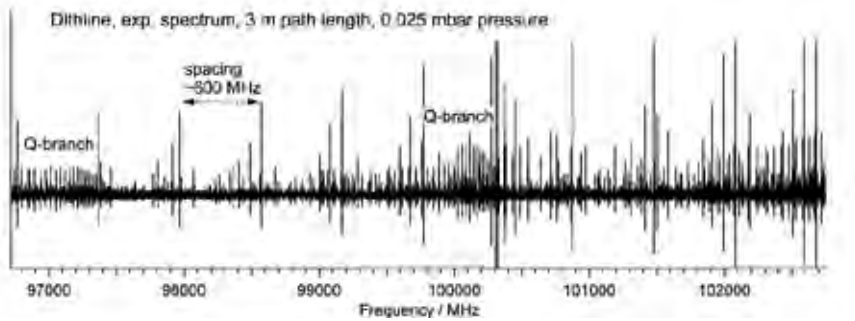

Figure. 1: Part of the rotational spectrum of 1,2-dithiine. (97-102 GHz).

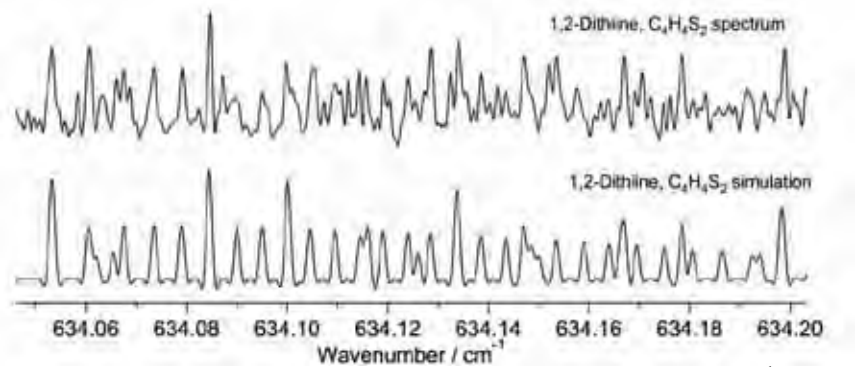

Figure 2: Part of the ν_7 fundamental of 1,2-dithiine at 634 cm^{-1} (upper trace: experimental spectrum, lower trace: simulation, p=0.5 mbar, l=3.2 mbar, T = 295 K).

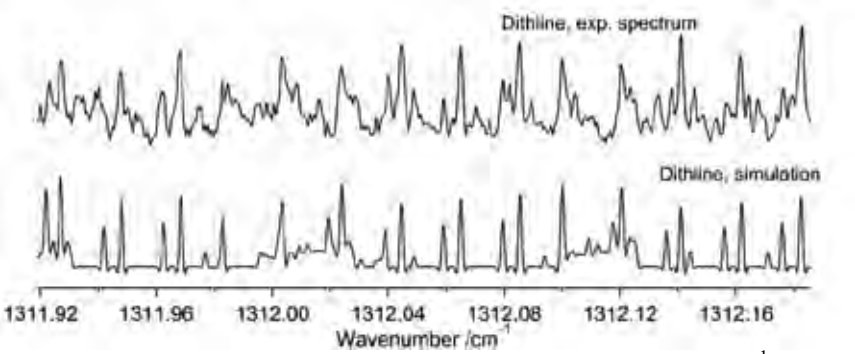

Figure 3: Part of the ν_{17} fundamental of 1,2-dithiine at 1312 cm^{-1} (upper trace: experimental spectrum, lower trace: simulation, p=0.5 mbar, l=3.2 mbar, T = 295 K, $\Delta\nu$ = 33 MHz, self-apodized).

Conclusions

Here we report the first analysis of the ν_7 and ν_{17} bands of 1,2-dithiine. Building upon the results of the work reported here, we currently continue our analyses towards higher wavenumbers. We can use our current experimental setup [4] to detect molecular parity violation in the wavenumber region above the barrier. Indeed, the relatively large value of $\Delta_{PV}E$, and the modest barrier of about 2500 cm^{-1} for stereomutation, easily overcome by IR lasers make this molecule a very good candidate for our experiments on parity violation by reaching tunneling levels with well defined parity above the barrier, similar to the case of ClOOCl, for which detailed simulations of such experiments using the "infrared route" were carried out [10].

Acknowledgements

Our work is supported financially by the Schweizerischer Nationalfonds, ETH Zürich, Paul-Scherrer-Institute and by an Advanced Grant (No 290925) of the European Research Council.

References:

[1] M. Quack, *Fundamental symmetries and symmetry violations from high resolution spectroscopy*, in *Handbook of High-Resolution Spectroscopy*, Vol. 1, (Eds. M. Quack and F Merkt), Wiley, Chichester (**2011**), *659-722*.

[2] M. Quack, *Angew. Chem.-Int. Edit. Engl.* **1989**, *28*, 571-586.

[3] L. Horný and M. Quack, *Mol. Phys*. **2015,** 113, 1768-1779.

[4] P. Dietiker, E. Miloglyadov, M. Quack, A. Schneider and G. Seyfang, in *Proceedings of the 19th Symposium on Atomic, Cluster and Surface Physics (SASP 2014), University center Obergurgl, Austria, 8th to 14th February 2014*, edited by D. Stock, R. Wester and R. Scheier (Innsbruck University Press, Innsbruck, 2014), pp. 226–229. ISBN: 978–3–902936–26–4 and *J. Chem. Phys* **2015**, 143, 000 in press.

[5] M. Quack, *Chem. Phys. Lett.* **1986** 132, 147.

[6] B. Fehrensen, D. Luckhaus, M. Quack, *Chem. Phys.* **2007**, *338*, 90.

[7] M. Suter and M. Quack, *Applied Optics* **2015**, 54, 4417.

[8] S. Albert, K. K. Albert and M. Quack, *High Resolution Fourier Transform Infrared Spectroscopy*, in *Handbook of High-Res. Spectrosc.*, Vol. 2, (Eds. M Quack and F. Merkt), Wiley, Chichester (**2011**), 965.

[9] S. Albert and M. Quack, *ChemPhysChem*. **2007**, 8, 1271-1281.

[10] R. Prentner, M. Quack, J. Stohner and M. Willeke, *J. Phys. Chem. A* **2015**, doi:10.1021/acs.jpca.5b08958.

Pinpointing mechanochemical bond rupture in single molecule force spectroscopy

Michael F. Pill, Hauke Clausen-Schaumann
Department of Applied Natural Sciences and Mechatronics, Munich University of Applied Sciences, Munich, Germany

Doreen Schütze, Julian Müller, Bernd Hartke
Institut für Physikalische Chemie, Christian-Albrechts-Universität zu Kiel, Kiel, Germany

Katharina Holz, Ulrich Lüning
Otto-Diels-Institut für Organische Chemie, Christian-Albrechts-Universität zu Kiel, Kiel, Germany

Florian Berger, Martin K. Beyer
Institut für Ionenphysik und Angewandte Physik, Leopold-Franzens-Universität Innsbruck, Innsbruck, Austria

Mechanophores usually contain a mechanically labile bond that can be broken by an external mechanical force. Single-molecule force spectroscopy (SMFS) affords the quantitative measurement and control of the applied force by atomic force microscopy (AFM), forming the basis for a quantitative description of the underlying processes. In order to uniquely identify the rupturing bond, a macrocycle can be synthesized that contains both the mechanophore and an aliphatic chain that acts as a "safety line" upon bond breaking.[1] This ring-opening mechanophore unit is linked to poly(ethylene glycol) spacers, which allow investigation by SMFS. The length increase upon rupture of the mechanophore is measured and compared with quantum chemical calculations.

[1] Schütze, D.; Holz, K.; Müller, J.; Beyer, M.K.; Lüning, U.; Hartke, B. *Angew. Chem. Int. Ed.* **2015**, *54*, 2556–2559.

The first mechanophore studied with this approach is a 1,2,3-triazole.[1] Rupture forces above 1 nN have been observed. The macrocycle opens up, and the defined length increase together with the force constant of the stretched polymer allow unambiguous assignment of the event to a single-molecule bond rupture. However, whether cycloreversion of the 1,2,3-triazole occurs, or a bond next to the triazole molecule breaks cannot be deduced from the experiment.

For cyclobutane mechanophores, mechanochemical cycloreversion is well established.[2] We synthesized two macrocycles with a cyclobutane bypassed by a poly(ethylene glycol) (PEG) chain with two different lengths. As expected, the measured length increase changed with the length of the PEG chain in the macrocycle, showing that the assignment of bond rupture within the macrocycle is valid.

This approach shows how individual covalent bonds can be mechanically manipulated, with the success of the experiment directly documented in the experimental force-distance curve.

[2] Kryger, M.J.; Munaretto, A.M.; Moore, J.S. *J. Am. Chem. Soc.* **2011**, *133*, 18992–18998.

On the excited states of N_2^+ produced in (near-) thermal charge transfer between He^+ and N_2

Thomas R. Govers
Aecono Consulting,59 rue de Prony, 75017 Paris, France

1. Update of earlier work

At (near-)thermal energies, charge transfer ("CT") between helium ions (RE = 24.587 eV) and molecular nitrogen produces emission from the C $^2\Sigma_u^+$ state of N_2^+, from the B $^2\Sigma_u^+$ state, and, at low pressures, extensive emission from one or more long-lived, initially unidentified state(s) of N_2^+[1-4]. Its lifetime was estimated to be larger than $6x10^{-7}$ s, and probably of the order of 10^{-5} s [3]. Cossart et al. were able to assign the most prominent of these emissions to the transition D' $^2\Pi_g$(v') → A $^2\Pi_u$ (v" =7,8,and 9) [5]. Using a novel discharge source and photographic recording, they carried out a rotational analysis complemented by SCF ab-initio calculations. The emitting D' $^2\Pi_g$(v') vibrational levels were tentatively labeled as v' = 0,1,2 [5]. They are located at 23.698, 23.786 and 23.870 eV above the ground state of N_2 and their formation by CT from He^+ is thus exothermic by 0.889, 0.801 and 0.717 eV, respectively.

Baltzer et al. reported a weak vibrational progression starting at about 23.7 eV in the UV photoelectron spectrum (PES) of N_2 and assigned it to a N_2^+ state labeled 2 $^2\Pi_g$ [6]. Its vibrational level v'=2 was observed at 23.881 eV, in close agreement with the value D' $^2\Pi_g$ v' =2 at 23.870 eV obtained from the analysis by Cossart et al. [5]. The levels v' = 0 and 1 were not clearly seen in the PES. The difference between the corresponding energies listed by Baltzer et al. as 23.755 and 23.809 eV, and those determined by Cossart et al. for D' $^2\Pi_g$ v' =0 and 1, is probably not significant. One thus concludes that the state labeled 2 $^2\Pi_g$ by Baltzer et al. [6] and the one earlier called D' $^2\Pi_g$ by Cossart et al. [5] are one and the same electronic state of N_2^+. The vibrational numbering adopted is consistent between the two publications.

The potential curve computed for the D' state has a broad, irregular well which supports close-lying vibrational levels with initial spacings of the order of 85 meV [5-7]. From an energetics point of view it can be populated by (near-)thermal He^+/N_2 charge transfer up to the level v'=10

located by Baltzer et al. at 24.541 eV [6] and by Yencha et al. at 24.548 eV [7]. In the spectra of refs. [1,3,4], however, only emission from the vibrational levels v'=0 and v'=1 can be clearly identified on the basis of the bandhead wavelengths determined by Cossart et al. [5], the most prominent emissions being those corresponding to the transitions from D' (v'=0) to A (v"=7 and 9) and from D' (v'=1) to A (v"= 8 and 9). Sekiya et al. also identify the transitions from v'=2 to v"= 7 and 8 [4], but overlap with v'=0 to v"=6 and 7 renders this attribution less certain. Higher vibrational levels could not be identified in any of the spectra reported in references [1,3,4]. The D' state is thus seen to be populated in a very narrow range of vibrational levels, just as in the case of the C $^2\Sigma_u^+$ state where (near-)thermal He^+/N_2 CT populates only the levels v'=3 and 4, even though CT into the lower vibrational levels would be exothermic by only a fraction of an eV [1-3]. In the case of CT into the D' $^2\Pi_g$ state, the populated vibrational levels are off-resonance by between 0.7 and 0.9 eV.

A propensity for a rather narrow range of product states can be rationalised as resulting from curve-crossings between vibronic diabates, where only a limited number of crossings will effectively lead to CT, namely those where the system "hesitates" between diabatic and adiabatic behaviour, resulting in a rather narrow range of product levels [8].

2. Implications

The main configuration of the D' $^2\Pi_g$ state differs from that of the A $^2\Pi_u$ state by two spin-orbitals [5]. Its transition strength thus relies on intensity borrowing by configuration interaction, which is consistent with the long lifetime cited above. In the absence of collisional quenching, the D' levels resulting from charge transfer between He^+ and N_2 will emit to the vibrational levels of the A state concentrated around v"=7,8 and 9. These in turn radiate to the N_2^+ electronic ground state, an emission system known as the Meinel bands. Transitions from high vibrational levels of the A state, ranging from v"=5 to 17, were identified by observing the emission from beams of N_2^+ ions; their lifetime was evaluated at about 6 x 10^{-6} s [9]. A detailed analysis was carried out by Maier and Holland, for both $^{28}N_2^+$ and $^{30}N_2^+$ [10]. Their paper lists vibrational branching ratios, those pertaining to transitions from A $^2\Pi_u$ (v"=7,8,9) to $X^2\Sigma_g^+$(v) being as follows for $^{28}N_2^+$:

	$X^2\Sigma_g^+(v)$							
	0	1	2	3	4	5	6	7 and more
$A\ ^2\Pi_u$ (v")								
7	0.0031	0.0397	0.1945	0.3972	0.2698	0.0097	0.0577	0.0284
8	0.0010	0.0156	0.0964	0.2893	0.3774	0.1428	0.0017	0.0756
9	0.0003	0.0059	0.0441	0.1709	0.3485	0.3022	0.0528	0.0784
Equal 7;8;9	0.0015	0.0204	0.1117	0.2858	0.3319	0.1516	0.0374	0.0598

Vibrational branching ratios for A→X emission

It is apparent that He^+/N_2 charge transfer into the D' $^2\Pi_g$ state, followed by D'→A and A→X emission will, in the absence of collisional quenching, lead to the production of vibrationally excited $N_2^+(X)$ on a timescale of the order of 10^{-5} s. More than half of this N_2^+ is produced in the levels v = 3 and 4 of the electronic ground state, and hardly any in the level v = 0. A lower limit to the reaction rate for this production can be evaluated from simultaneous optical and mass spectrometric experiments as outlined in ref. [2]. The C $^2\Sigma_u^+$ v' = 3 and 4 levels populated by thermal He^+/N_2 charge transfer decay either by emission to ground state N_2^+, or by predissociation into ground state $N^+ + N$. The competition between the two decay modes varies considerably depending on the N_2 isotope [11]: $k(C,N^+)/k(C,N_2^+) = 10.6$ for $^{28}N_2$ and = 1.09 for $^{30}N_2$ [2] when summed over v'= 3 and 4. If all of the N^+ and N_2^+ was produced via the C state, the ratio $k(\text{total } N^+)/k(\text{total } N_2^+)$ would show the same isotope effect. In fact, the latter ratio varies less than that for the C state, which imposes alternate reaction channels as indicated in the table below.

Rate constants for $He^+ + N_2 \rightarrow He + N_2^+$ or $He + N + N^+$ as specified / 10^{-9} cm^3/sec

	Lower limit on k(other N^+)							
	Total CT	Total N_2^+	Total N^+	N_2^+ from C	N^+ from C	Total C	Other N_2^+	Other N^+
$^{28}N_2$	1.20	0.51	0.69	0.065	0.69	0.75	0.45	0.00
$^{30}N_2$	1.20	0.79	0.41	0.34	0.37	0.71	0.45	0.04

	No isotope effect on N^+/N_2^+ ratio from other than C state							
	Total CT	Total N_2^+	Total N^+	N_2^+ from C	N^+ from C	Total C	Other N_2^+	Other N^+
$^{28}N_2$	1.20	0.51	0.69	0.059	0.62	0.68	0.45	0.069
$^{30}N_2$	1.20	0.79	0.41	0.31	0.34	0.64	0.48	0.073

The top of this table shows the lower limits to alternate channels obtained by imposing these to have rate constants that are zero or positive. The lower part assumes that the alternate channels do not show an isotope effect in the N^+/N_2^+ production ratio. In both cases one finds that at least

88% of the $^{28}N_2^+$results from charge transfer into states other than the C state, the rate for production of these alternate channels representing at least 0.45 x 10^{-9} cm^3/s. Of this, at most 0.02 x 10^{-9} cm^3/s represents CT into the B $^2\Sigma_u^+$ state, followed by emission to the electronic ground state [3]. Unless yet other, unidentified, N_2^+ states are formed, CT into the D' $^2\Pi_g$ state, followed by D'→A and A→X emission is thus found to produce vibrationally excited N_2^+(X) at a rate of more than 0.43 x 10^{-9} cm^3/s. As CT between $N_2^+$and Ar [12,8] and also between N_2^+ and Kr [13] depends very strongly on the vibrational excitation of the parent ion, SIFT experiments, e.g., should be able to use these as monitor reactions to verify the high vibrational excitation of N_2^+ produced by He^+/N_2 CT.

We note that the ratio of the rate for C $^2\Sigma_u^+$ (v') state predissociation to that for C→X emission was determined in ref.[11] using calculated "vertical' excitation and emission probabilities. Photoelectron photoion coincidence measurements on an instrument such as DELICIOUSIII [14] should be able to verify the underlying assumptions by determining this ratio directly, as a function of vibrational level and isotopic substitution.

4. References

[1] R.F. Holland and W.B. Maier II, J. Chem. Phys. 55 (1971) 1299-1313
[2] T.R. Govers, F.C. Fehsenfeld, D.L. Albritton, P.G. Fournier, and J. Fournier, Chem. Phys. Letters 26 (1974) 134-137
[3] T. R. Govers, M. Gérard, G. Mauclaire, and R. Marx, Chem. Phys. 23 (1977) 411-427
[4] H. Sekiya, M. Tsuji, and Y. Nishimura, J. Chem. Phys. 87 (1987) 325-330
[5] D. Cossart, C. Cossart-Magos, G. Gandara, and J.M. Robbe, J. Molec. Spec. 109 (1985) 166-185
[6] P. Baltzer, M. Larsson, L. Karsson, B. Wannberg, and M. Carlsson Göthe, Phys. Rev. A, 46 (1992) 5545-5553
[7] A. J. Yencha, K. Ellis, and G. C. King, J. Electron Spectrosc. Relat. Phenom. 195 (2014) 160-173
[8] T. R. Govers, P.M. Guyon, T. Baer, K. Cole,H. Fröhlich, and M. Lavollée; Chem. Phys. 87 (1984) 373-387
[9] C.A. van de Runstraat, T. R. Govers,W.B. Maier II, and R.F. Holland, Chem. Phys Letters, 18 (1973) 549-552
[10] W.B. Maier II and R.F. Holland, J.Chem. Phys. 59 (1973 4501-4534
[11] T.R. Govers, C.A. van de Runstraat, and F.J. de Heer, Chem. Phys. 9 (1975) 285-299
[12] W. Lindinger, F. Howorka, P. Lukac, S. Kuhn, H. Villinger, E. Alge, and H. Ramler, Phys. Rev.A 23 (1981) 2319-2326; D. Smith and N.G. Adams, ibid. 23 (1981) 2327-2330
[13] S. Kato, J.A. de Gouw, C.-D. Lin, V. M. Bierbaum, and S. R. Leone, J. Chem. Phys. 105 (1996) 5455-5466
[14] G. A. Garcia, B. K. Cunha de Miranda, M. Tia, S. Daly, and L. Nahon; Rev. Sci. Instruments (2013) 053112 1-11; Erratum ibid. 84 (2013) 069902 1

Hydrogen Abstraction Reactions in Ion Trap – from N^+ to NH_4^+ at Low Temperatures

Štěpán Roučka, Serhiy Rednyk, Artem Kovalenko, Thuy Dung Tran, Radek Plašil, Juraj Glosík
Department of Surface and Plasma Science, Faculty of Mathematics and Physics, Charles University in Prague, Czech Republic

1. Introduction

It is understood that the main pathway to gas-phase formation of ammonia in the interstellar medium is a sequence of hydrogen abstraction reactions followed by dissociative recombination (Herbst & Klemperer 1973). In particular, the following reactions lead to formation of NH_4^+ (ammonium) from N^+ (endothermicities and activation energy were taken from (Rist *et al.* 2013) and (Zymak *et al.* 2013)):

$$N^+ + H_2 \rightarrow NH^+ + H, \qquad E_A = 16 \text{ meV} \qquad (1)$$

$$NH^+ + H_2 \rightarrow NH_2^+ + H, \qquad \Delta H = -1.9 \text{ eV} \qquad (2)$$

$$NH_2^+ + H_2 \rightarrow NH_3^+ + H, \qquad \Delta H = -1.1 \text{ eV} \qquad (3)$$

$$NH_3^+ + H_2 \rightarrow NH_4^+ + H. \qquad \Delta H = -1.0 \text{ eV} \qquad (4)$$

Ammonia is then a possible product of dissociative recombination of NH_4^+. Although the actual branching ratio for NH_3 production from $NH_4^+ + e^-$ recombination is not known, the experiments of Adams *et al.* (1991) indicates that it is the dominant channel. Alternatively, the sequence may start with H_2^+ transfer reaction

$$H_3^+ + N \rightarrow NH_2^+ + H. \qquad \Delta H = -1.1 \text{ eV} \qquad (5)$$

The experimental work of Scott *et al.* (1997) suggests that reactions (5) and (1) are of comparable importance in initiating the reaction chain.

The subject of the present work is experimental study of the sequence of reactions (1)–(4) at cryogenic temperatures with emphasis on reactions (2) and (3) which have not been studied in detail before. The rate limiting processes are reactions (1) and (4), therefore, a considerable effort has been dedicated to studying these reactions at low temperatures in previous works. In particular, a recent ion trap experiment (Zymak *et al.* 2013) studied the rate coefficient of reaction (1) as a function of kinetic temperature, H_2 nuclear spin state, and N^+ fine structure state. Previous work concerning this reaction is also summarized by Zymak *et al.* (2013).

It was found that this reaction has activation energy of approximately 16 meV, but it is not known, whether it is due to genuine endothermicity. Our laboratory is currently attempting to answer this question by studying the reverse reaction (Plasil *et al.* 2015). The measured rate coefficients of the forward and reverse processes are shown in Fig. 1.

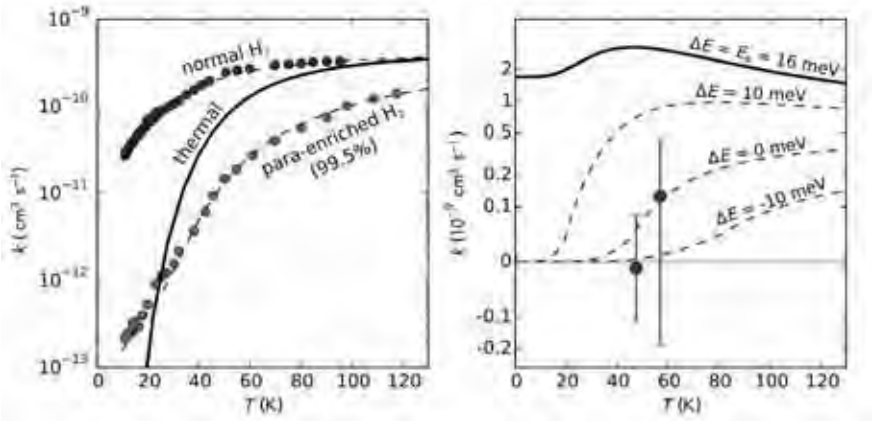

Figure 1: Left panel – temperature dependence of rate coefficient of reaction (1) with normal and para-enriched H_2 measured by Zymak *et al.* (2013). The solid line indicates the rate coefficient calculated for H_2 in thermodynamic equilibrium. Right panel – rate coefficient of the reverse reaction ($NH^+ + H \rightarrow N^+ + H_2$). The lines indicate rate coefficients calculated using principle of microreversibility, assuming different endoergicities, ΔE, of reaction (1). Preliminary analysis of the experimental data (points) indicates that a reaction barrier may contribute to the observed activation energy.

Reactions (2) and (3) have been systematically studied only at room temperature by means of selected ion flow tube (Adams *et al.* 1980), ion cyclotron resonance (Kim *et al.* 1975), and flowing afterglow (Fehsenfeld *et al.* 1967). The only low temperature values have been measured in ion trap experiment by Gerlich (1993). Additionally, $NH^+ + H$ can also react by proton transfer

$$NH^+ + H_2 \rightarrow N + H_3^+, \qquad \Delta H = -1.0 \text{ eV} \qquad (6)$$

which has only been studied by Adams *et al.* (1980) at room temperature. Reaction (4) is hindered by a barrier but its rate coefficient is increasing towards low temperatures due to tunnelling. This reaction has been studied experimentally and theoretically at temperatures between 10 K and 300 K as summarized by Herbst *et al.* (1991).

2. Experimental

The experiments were carried by means of a linear radiofrequency 22-pole trap (Gerlich 1992). N^+ ions were produced by electron bombardment of N_2, while H_2 was leaked directly into the trap. The ions were cooled by approximately 100 collisions with He buffer gas in the trap before colliding with H_2. Reaction products were analysed by a quadrupole mass spectrometer. For details, see e.g. (Zymak et al. 2013).

3. Results

The present results were obtained by injecting N^+ ions into the trap and observing the whole reaction chain (1)–(4) and (6), which leads to conversion of majority of ions to NH_4^+ as shown in Fig. 2. Small amount of H_3^+ is also produced by reaction (6) and we assume that it is then converted to N_2H^+ by reaction with N_2 from the ion source.

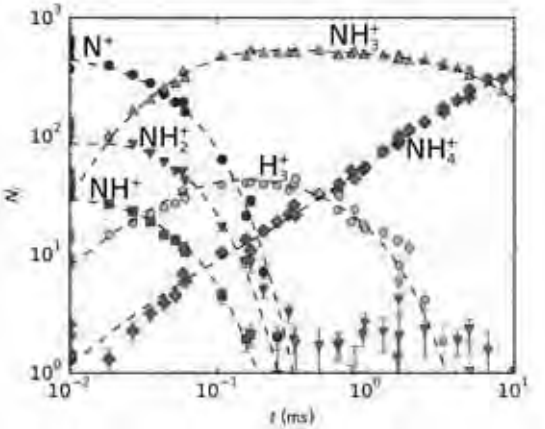

Figure 2: Time evolution of numbers of trapped ions (points) fitted by a kinetic model (lines) measured at trap temperature 12.5 K and H_2 number density 3.3×10^{11} cm^{-3}.

This experimental procedure allows us to obtain rate coefficients of all involved reactions by fitting a model of chemical kinetics. As suggested by Gerlich (1993), our model also takes into account the different reactivity of excited NH_3^+ produced by reaction (3). The measured rate coefficients of reactions (2), (3), and (4) are presented in Fig. 3.

The large values of rate coefficients of reactions (2) and (3) confirm that there are no significant reaction barriers in their path. Nevertheless, the reaction efficiency (relative to Langevin rate coefficient) is not 100 %.

Measuring the temperature dependence of rate coefficients in detail, together with investigating the branching ratio between reaction (2) and (6) will reveal more information.

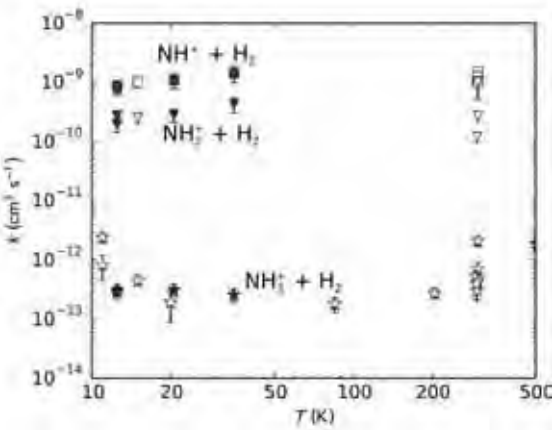

Figure 3: Rate coefficients of reactions (2), (3), and (4) indicated by squares, triangles, and stars, respectively. The present data are shown as blue symbols. The data indicated by open symbols were obtained by (Gerlich 1993, Adams et al. 1980, Kim et al. 1975, Fehsenfeld et al. 1967, Barlow and Dunn 1987)

Acknowledgment We thank the Chemnitz University and the Deutsche Forschungsgemeinschaft for lending us the 22-pole instrument. We thank Dieter Gerlich for fruitful discussions. This work was partly supported by GACR (P209/12/0233, 14-14715P, 208/10/1281) and GAUK 572214.

References

Adams, N. G. *et al. J. Chem. Phys.* **72,** 288–297 (1980).
Adams, N. G. *et al. J. Chem. Phys.* **94,** 4852–4857 (1991).
Barlow, S. E. & Dunn, G. H. *Int. J. Mass Spec. Ion Proc.* **80,** 227 (1987).
Fehsenfeld, F. C. *et al. J. Chem. Phys.* **46,** 2802–2808 (1967).
Gerlich, D. & Horning, S. *Chem. Rev.* **92,** 1509–1539 (1992).
Gerlich, D. *J. Chem. Soc., Faraday Trans.* **89,** 2199–2208 (1993).
Herbst, E. *et al. J. Chem. Phys.* **94,** 7842–7849 (1991).
Herbst, E. & Klemperer, W. *Astrophys. J.* **185,** 505–534 (1973).
Rist, C. *et al. J. Phys. Chem. A* **117,** 9800–9806 (2013).
Scott, G. B. I. *et al. MNRAS* **290,** 636–638 (1997).
Zymak, I. *et al. Astrophys. J.* **768,** 86 (2013).

Stable O_4H^+ and O_4D^+ in Helium Nanodroplets

M. Renzler[1], L. Kranabetter[1], E. Barwa, P. Scheier[1] and A. M. Ellis[2]

[1]Institute for Ion Physics and Applied Physics, University of Innsbruck,
Technikerstraße 25, 6020 Innsbruck, Austria
[2]Department of Chemistry, University of Leicester,
University Road, LE1 7RH Leicester, United Kingdom

Recent studies [1],[2] of O_4H^+ suggested the molecule as a tracer for oxygen in the interstellar medium. Those studies used *ab initio* calculations to propose the spectroscopic fingerprint of the molecule which should be produced via the exothermic ($19.4\,\frac{kcal}{mol}$) collision reaction:

$$H_3^+ + O_4 \quad \rightarrow \quad O_4H^+ + H_2 \tag{1}$$

We used helium nanodroplets created by means of supersonic jet expansion and exposed them to H_2 and O_2 environments to confirm these results. The doped nanodroplets were subsequently ionized by electron impact ($70\,eV$ electrons). The reaction products which are formed in this very cold ($0.37\,K$) matrix are analyzed by means of a time of flight mass spectrometer. The present results were obtained using only D_2 since this facilitates to rule out contributions from ions such as H_2O^+, which might originate from the ionization of trace amounts of H_2O in the vacuum chamber. The experimental data agree with the recent calculations [1] in the way that it suggests that O_4H^+ and O_4D^+ are particularly stable ions. Preliminary results are displayed in figure 1, clearly showing the stable nature of O_4D^+.

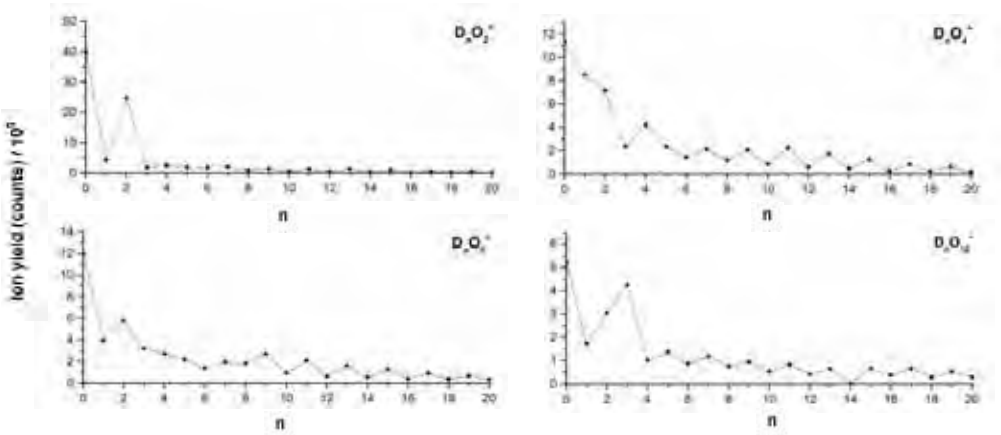

Figure 1: Size distribution of $D_nO_m^+$ clusters

Acknowledgement:
This work was supported by the Austrian Science Fund (FWF projects P23657, P24443 and I978).

References:

[1] F.G.D. Xavier et al. J. Chem. Phys., 141:081101, 2014.

[2] F.G.D. Xavier and R. Hernandez-Lamoneda. Phys. Chem. Chem. Phys., 17:16023, 2015.

Influence of Hydrocarbon Adducts on the Absorption Behaviour of Sodium Iodide Clusters

Nina K. Bersenkowitsch, Christian van der Linde, Martin K. Beyer
Universität Innsbruck, Institut für Ionen- und Angewandte Physik

1. Introduction

Marine aerosols [1] consist of a variety of components and play an important role in a variety of atmospheric processes, such as backscattering of solar radiation via clustered sea salt particles [2]. In the present study, sodium iodide clusters [3] with their simple isotope pattern serve as model systems for laboratory studies. Their interaction with hydrocarbon adducts is investigated with an FT-ICR Mass Spectrometer [4] and an Optical Parametric Oscillator (OPO). Absorption spectra are recorded via photodissociation and the photochemical reaction products are examined.

2. Setup

The setup of the experiments is shown in Figure 1.

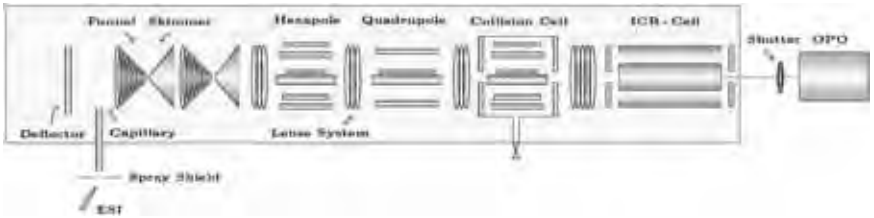

Figure 1. Schematic setup of the FT-ICR instrument. The OPO beam is introduced through a fused silica viewport.

Ions are produced with Electrospray Ionization (ESI). They are guided through a Fourier Transform- Ion Cyclotron Resonance Mass Spectrometer (FT-ICR MS). An Optical Parametric Oscillator (OPO, tuneable from 225-2600nm) is coupled into the ICR-Cell, which irradiates the ions. The irradiation time is controlled via a shutter. Via the photodissociation products, absorption spectra are obtained.

3. Results

The absorption spectrum of $(NaI)_5Na^+$ is illustrated in Figure 2.

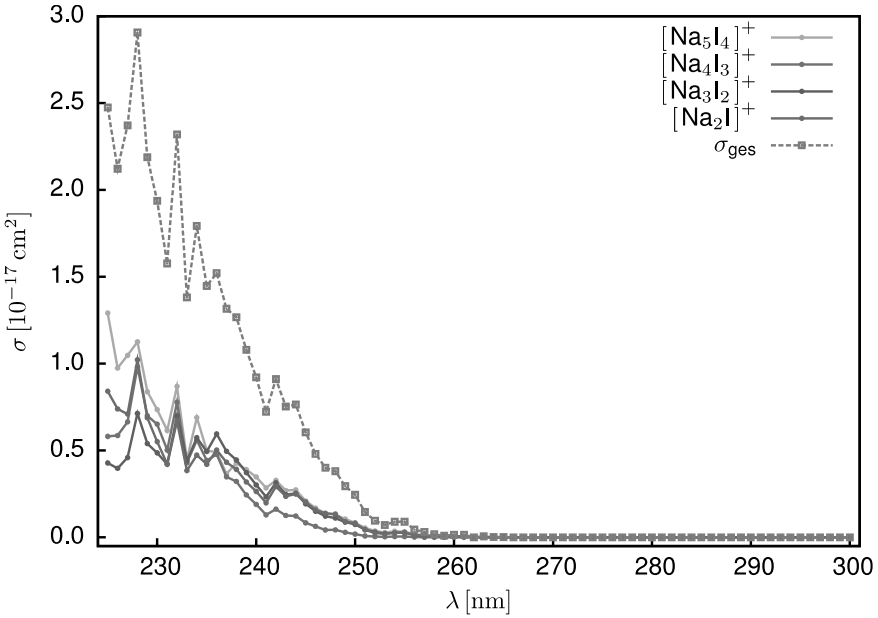

Figure 2. Absorption spectrum from 225-300nm of $(NaI)_5Na^+$ with contributions from individual fragmentation channels.

Evaporation of one NaI represents the main fragmentation channel, but the preference is not very pronounced. The cluster starts to absorb at wavelengths <260nm with an absorption maximum below 225 nm.
Camphor ($C_{10}H_{16}O$) clusters to $[Na_6I_5]^+$ and is preferably evaporated with $(NaI)_x$. Interesting is that the absorption maximum of Camphor in the gas phase lies at 290nm, but the local maximum of the Camphor absorption in the $[Na_6I_5(C_{10}H_{16}O)]^+$ complex is blueshifted by about 12 nm (see Figure 3).

Other hydrocarbons added to the sodium iodide cluster are various Bromoalcanoic Acids and Formic Acid. In contrast to Camphor, which adsorbs moleculary on the cluster, the deprotonated acid substitutes an I^- ion in the $[Na_6I_5]^+$ cluster. In these cases, the sodium iodide cluster makes spectroscopy of the bound deprotonated acid possible, since evaporation of weakly bound $(NaI)_x$ units is initiated by photon absorption.

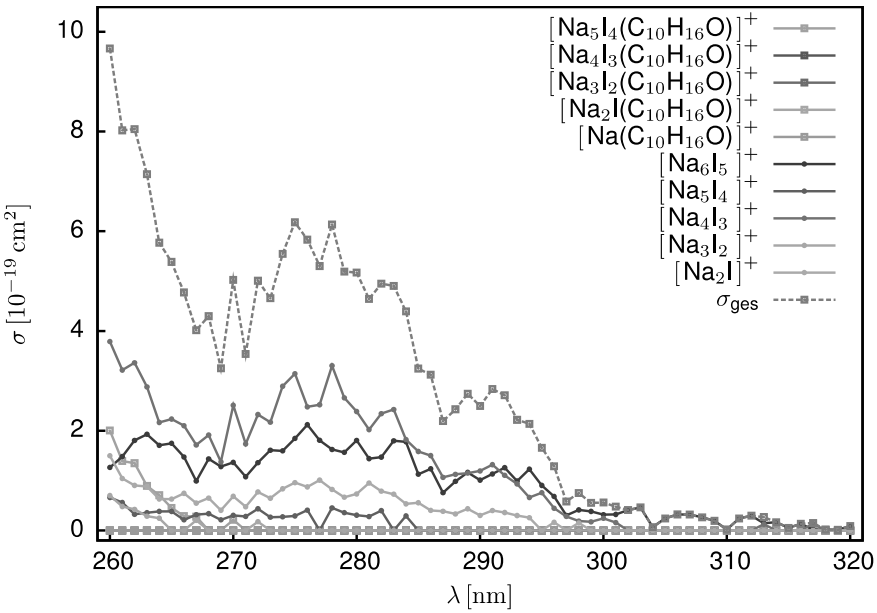

Figure 3. Absorption spectrum from 260-320nm of $[Na_6I_5(C_{10}H_{16}O)]^+$ with contributions from individual fragmentation channels

References

1. O'Dowd, C. D. & Leeuw, G. de. Marine aerosol production: a review of the current knowledge. *Philosophical transactions. Series A, Mathematical, physical, and engineering sciences* **365,** 1753–1774 (2007).

2. Finlayson-Pitts, B. J. & Pitts, J. N. *Chemistry of the upper and lower atmosphere. Theory, experiments, and applications* (Academic Press, San Diego, 2000).

3. Aguado, A. Ayuela, A. López, J. M. & Alonso, J. A. Ab initio calculations of structures and stabilities of (NaI)nNa+ and (CsI)nCs+ cluster ions. *Phys. Rev. B* **58,** 9972–9979 (1998).

4. Marshall, AG (Marshall, AG), Hendrickson, CL (Hendrickson, CL) & Jackson, GS (Jackson, GS). Fourier transform ion cyclotron resonance mass spectrometry: A primer. *Mass Spectrometry Reviews (17),* 1–35 (1998).

Classical simulations of decorated fullerene clusters

Alexander Kaiser, Stefan Ralser, Paul Scheier, Michael Probst
Institut für Ionenphysik und Angewandte Physik, Universität Innsbruck, Technikerstraße 25, A-6020 Innsbruck, Austria

In recent years neutral, cationic, and anionic fullerene complexes decorated with methane, ethane, carbon dioxide, or water have been simulated in our group. Global energy minima are generally very hard to find for fullerenes with many adsorbate molecules and DFT theory is too expensive to sample a sufficiently large configuration space. Classical force fields can help to identify particularly stable structures and can also give insight into the dynamics of adsorbed molecules depending on the temperature. With parameters from literature and an evenly distributed charge of +1 on the carbon atoms of the fullerene we could, for example, find an appealing symmetric structure for twelve CO_2 molecules adsorbed on C_{60} as depicted in Figure 1. The Mulliken charge distribution is shown color-coded and was obtained in a subsequent DFT calculation.

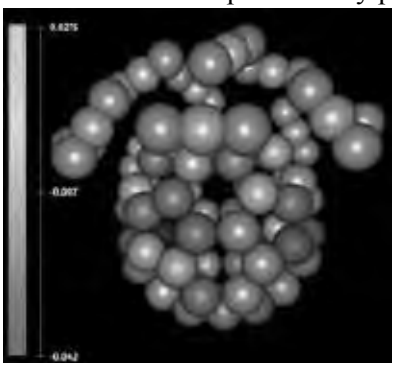

Figure 1. Mulliken charges (colorcoded) of $C_{60}(CO_2)_{12}^{+}$

In this contribution we discuss the merits and limitations of classical simulations and global optimizations with force fields for these clusters. The force field itself, the global optimization procedure and for polar molecules also the charge distribution play important roles. With custom-made force fields based on dispersion corrected DFT energies, and by discarding the Lennard-Jones 12-6 dogma, classical simulations can achieve more than expected without tuning parameters to match experimental results. The latest progress and results in simulations of $C_{60}(CO_2)_n^{+,0,-}$ and $(C_{60})_m(H_2O)_n^{+,0,-}$ are discussed as well.

Observation of the Efimov state of the helium trimer

Maksim Kunitski, Stefan Zeller, Jörg Voigtsberger, Anton Kalinin,
Lothar Ph. H. Schmidt, Markus Schöffler, Achim Czasch,
Robert E. Grisenti, Till Jahnke and Reinhard Dörner
Institut für Kernphysik, Goethe-Universität Frankfurt am Main,
Max-von-Laue-Straße 1, 60438 Frankfurt/M, Germany

Wieland Schöllkopf
Department of Molecular Physics, Fritz-Haber-Institut, Faradayweg 4-6,
14195 Berlin, Germany

Dörte Blume
Department of Physics and Astronomy, Washington State University,
Pullman, WA 99164-2814, USA

In 1970 Vitali Efimov predicted remarkable counterintuitive behaviour of a three-body system made up of identical bosons. Namely, a *weakening* of pair interaction in such a system brings about in the limit appearance of *infinite* number of bound states of a huge spatial extent [1]. The helium trimer has been predicted to be a molecular system having an excited state of this Efimov character under natural conditions without artificial tuning of the attraction between particles by an external field. Though many theoretical works predict the existence of this state in the helium trimer, it has not been observed experimentally so far. Main reasons for that are the tiny binding energy and a huge spatial extent that makes it fragile for preparation and elusive for detection.

Here we report experimental observation of the Efimov state of $^4He_3$ by means of Coulomb explosion imaging of mass-selected clusters [2]. Helium trimers were prepared under supersonic expansion of the gaseous helium through a 5 μm nozzle. The clusters were selected from the molecular beam by means of matter wave diffraction [3]. Each atom of a trimer was singly ionized by a strong ultrashort laser field resulting in Coulomb explosion of the cluster. The momenta, the ions acquired during Coulomb explosion, were measured by COLTRIMS. These momenta were utilized for reconstruction of the initial spatial geometry of the neutral trimer at the instant of ionization using Newton's equation of motion.

Structures of the excited Efimov state of the $^4He_3$ (Figure 1A) are about eight times larger than those of the ground state (Figure 1B), which is in accordance with theory. Whereas the ground state corresponds to an almost randomly distributed cloud of particles [4], the excited Efimov state is dominated by configurations in which two atoms are close to each other and the third one further away.

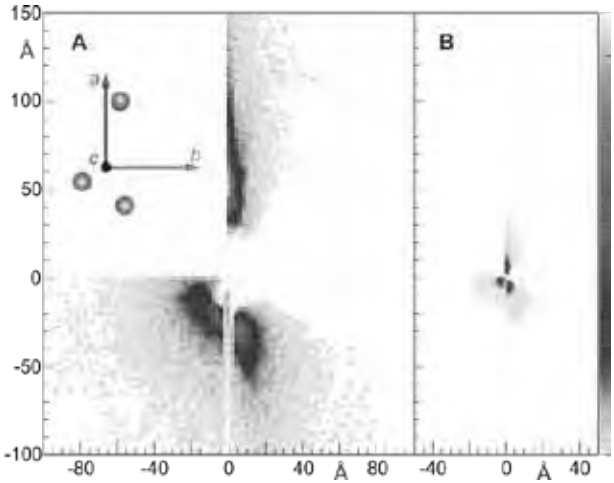

Figure 1. Structures of the helium trimer: A – excited state, experimental, B – ground state, theoretical. Three helium atoms of each trimer are plotted in the principal axis frame *abc*.

References

[1] V. Efimov, *Phys. Lett. B* **33**, 563-564, 1970
[2] M. Kunitski et al, *Science* **348**, 551-555, 2015
[3] W. Schöllkopf, J. P. Toennies, *Science* **266**, 1345-1348, 1994
[4] J. Voigtsberger et al, *Nat. Comm.* **5**, 5765:1-6, 2014

Imaging Molecular Beam Scattering from Surfaces

Dan J. Hardning[1,2], J. Neugebohren[1,2], D.J. Auerbach[1,2]
T.N. Kitsopoulos[1,2,3,4] and A.M. Wodtke[1,2]

[1]*Max Planck Institute für Biophysikalisches Chemie, Göttingen, Germany*
[2]*Institute für Physikalisches Chemie, Georg August Universität Göttingen, Germany*
[3] *Department of Chemistry University of Crete, Greece*
[4] *Institute of Electronic Structure and Laser, FORTH Crete, Greece*

In this work we will be presenting a new apparatus Ref. 1 for studying state to state molecular scattering from surfaces using ion imaging and its variants slicing and velocity mapping. Imaging surface scattering has been reported previously Ref. 2,3 however adaptation by the surface dynamics community was limited because of inherent difficulties in those experimental approaches. In this work we present a novel experimental methodology that circumvents many of the previous shortcomings, and essentially borrows from the imaging methods Ref. 4 well established in the gas phase molecular beam experiments. Our initial results to be presented here involve scattering of NO(v=0,J) and N2(v=0, J) molecules from Au(111), where we study the translational to rotational energy transfer, through facile velocity measurements obtained from imaging state selected products using REMPI. For the case of Au (111) the experimental temperature range was limited from 20 to 700 oC. The influence of molecular overlayers on the Au(111) surface on the translational energy transfer to the scattered products is addressed and characterized.

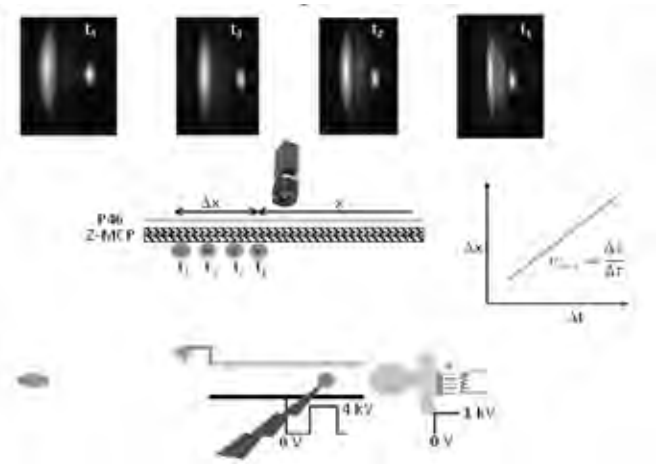

Figure: Schematic of the experiment

References

[1] Dan J. Harding, J. Neugebohren, D. J. Auerbach, T. N. Kitsopoulos, and A.M. Wodtke J. Phys. Chem. A, in press (2015).
[2] D. Corr and D.C. Jacobs, Rev. Sci, Instrum. **63**, 1969 (1992).
[3] J. R. Roscioli, D. J. Bell, D. J. Nelson and D. J. Nesbitt, Phys. Chem. Chem. Phys. **14**, 4070 (2012).
[4] Ed. B. J. Whitaker Imaging in Molecular Dynamics (Cambridge University Press, Cambridge 2003).

Photofragmentation of $C_{60}^{+}He_n$ Complexes

M. Kuhn, J. Postler, S. Ralser, M. Renzler, M. Simpson, S. Spieler, R. Wester and P. Scheier
Department of Ion Physics and Applied Physics, University of Innsbruck,
Technikerstraße 25, 6020 Innsbruck, Austria

presenting Author: martin.kuhn@uibk.ac.at

Based on the measurements of Campell, Gerlich, Holz and Maier1, who confirmed C60 + as the carrier of two diffuse interstellar bands by photofragmentation, we confirmed these results and extended the measurements to C60Hen + (2<n<100). In our case we use, instead of a radio frequency ion trap, helium nanodroplets to form the C60He complexes2. We excite the helium covered fullerenes after ionisation with a narrow linewidth tuneable ring laser (fig.1). This results in fragmentation of He near the respective resonance frequencies (fig.2) which is measured as a signal loss of the corresponding ion via mass spectrometry utilizing a high-resolution reflectron time-of flight instrument.
We also measured a frequency dependence (~0.7Å / He) for different cluster sizes (fig.3). Ongoing measurements reveal a different frequency behaviour of the second shell (Hen>32). Neglecting power broadening we can perform fast scans through large frequency ranges searching for unknown resonances of fullerene containing ionic complexes that might be of relevance in the interstellar medium.

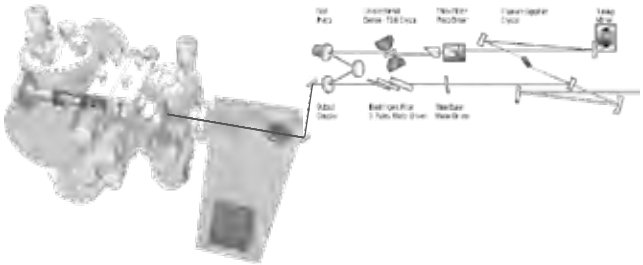

Figure 1: Experimental Setu

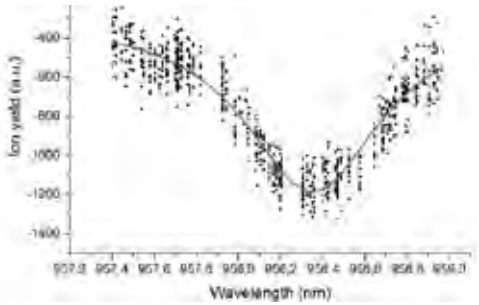

Figure 2: $C_{60}^{+}He_6$ depletion

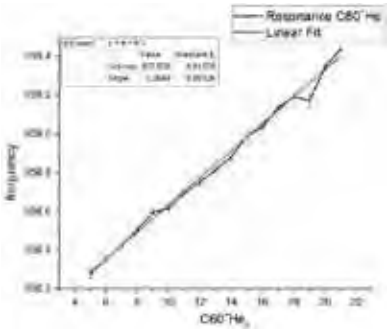

Figure 3: $C_{60}^{+}He_n$ resonances

This work was supported by the Austrian Science Fund (FWF projects P26635 and I978)

References:

[1] E. K. Campbell, M. Holz, D. Gerlich & J. P. Maier (2015): Laboratory confirmation of C60+ as the carrier of two diffuse interstellar bands. Nature 523, p322-323. doi:10.1038/nature14566

[2] L. An der Lan, P. Bartl, C. Leidlmair, H. Schöbel, R. Jochum, S. Denifl, T. D. Märk, A.M. Ellis & P. Scheier (2011): The Submersion of Sodium Clusters in Helium Nanodroplets: Identification of the Surface → Interior Transition. *J. Chem. Phys.* 135, 044309.
doi: 10.1063/1.3610388

A new global potential energy surface for the FHF^- anion

Yann Cornaton
Center for Theoretical and Computational Chemistry
Institut for kjemi, Universitetet i Tromsø, Norway

Roberto Marquardt
Laboratoire de Chimie Quantique
Institut de Chimie UMR 7177 CNRS/Université de Strasbourg
1, rue Blaise Pascal - BP 296/R8 - 67008 Strasbourg cedex - France
roberto.marquardt@unistra.fr

The biluoride anion (FHF^-) is a prototype example of a three-center four-electron bond [1]. The true nature of the chemical bonding in this system is yet still subject to controversy. It is still considered as the strongest known example of hydrogen-bonding [2]. Its size makes of it an excellent playground to develop accurate analytical representations of potential energy surfaces (PES). A large number exist today of experimental and theoretical work on this system. For brevity, we focus here on a recent theoretical work by Seebald *et al.* [3], on the scattering work of Wenthold and Squires [2], as well as on the spectroscopic work of Kawaguchi and Hirota [4, 5].

Good PES that are global are capable of describing to a fairly good degree of accuracy, the infrared spectrum pertaining to small amplitude displacements of the nuclei from their equilibrium position, as well as the behaviour of the motion of the nuclei when they undergo very large displacements from the equilibrium position, which lead either to isomerization, bond rupture and bond formation, including the dissociation of the species described by the PES. The PES of the FHF^- anion is challenging, because its linear equilibrium configuration and the rather low dissociation energy leading to $HF + F^-$ [2]. Of all PES developed so far, only the PES from ref. [3] achieves the spectroscopic accuracy given by the experimental results. That PES is, however, not

global, as will be shown below. It cannot be used for dynamical calculations involving the formation of the anion.

In the present contribution a new analytical representation is developed that matches experimental results both from the low energy spectroscopic regime, as well as from the high energy regime limit of bond dissociation. It is set up as a simple sum of three two-body interaction terms, which involve, however, a sophisticate mix of switching functions. Details of the formula will be exposed in the contribution.

$$v_{2b}(r) = V_e\left(w(r)\left[y(r)\,[y(r)\,w(r) - 2\,Z]\right]\right) \quad (1)$$

where

$$w(r) = \exp\left(-B(r)\frac{(r-r_e)^3}{r^2}\right) \quad (2)$$

$$y(r) = \exp\left(-A(r)\,(r-r_e)\right) \quad (3)$$

Key ingredients of the formula are two-body interaction potentials that describe covalent interaction energies: $V_{cov} = V_{2b}(r_1) + V_{2b}(r_2) + V_{2b}(r_F)$. The individual functions V_{2b} have the form

The quantities $A(r)$ and $B(r)$ are themselves also functions of r, which leads to a more flexible and hence improved description of the anharmonicity of the potential.

The parameter Z defined in Eq. (1) may vary between 1 and 0. In the first limit, describes a Morse-like potential [6], in the second, the potential is completely repulsive. Quite amazingly, the energy points can be well represented with the choice Z=1 for the HF potentials and Z=0 for the FF potential; i.e. the model can be based on simple attractive potentials describing HF bonds, , and repulsive potentials .

Energy points were calculated at the CCSD(T) level of theory within the MOLPRO package and the cc-pVQZ-F12 basis set. The quality of this basis set is high, nevertheless counterpoise corrections were considered to account for remaining basis set superposition errors. Adjustment to the *ab initio* calculated energy points was carried out with a modified version

of the Levenberg-Marquardt algorithm [7], in which additional non-linear constraints among adjustable parameters can be incorporated.

In addition to the covalent potential we also consider electrostatic interaction terms that include charge-dipole, charge induced, dipole induced and a dispersion term. Expressions for these terms were adapted from [8]. The relative weight of the covalent and electrostatic terms can be an indicator of the covalent or electrostatic nature of the bond.

The figure below presents a one dimensional section of the potential along one HF bond length; the second bond is kept fixed at its equilibrium value of 114 pm, which is 0.1% larger than the experimentally estimated value [5]. In this figure we compare the three potential energy surfaces: the potential from ref. [3], a potential function based on the covalent part of the present model only and named for brevity, and the full potential from this work including the covalent and electrostatic parts. The potential was obtained from an independent fit of the covalent part of the potential while the electrostatic part was removed. The *ab initio* points are indicated on the figure by the ∗ symbol.

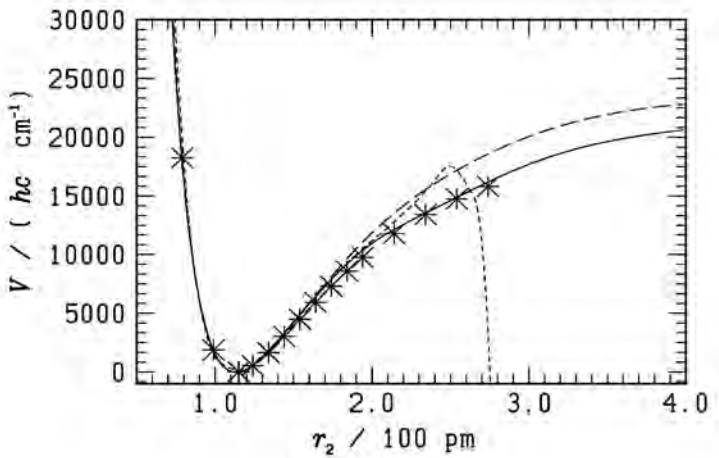

One dimensional sections of the PES in the linear F-H-F configuration along the H-F(2) bond length coordinate; continuous and long dashed lines: present work ; short dashed line from ref. [3]; ∗ CCSD(T)-F12 data from the present work.

All three model potentials behave well around the equilibrium. Upon dissociation, however, the purely covalent model potential is much too stiff, while the potential from ref. [3] succeeds well to describe the behavior of the ab initio energy points up to 200 pm, but generates an unphysical hole for longer HF bonds. The joint electrostatic and covalent model yields the expected behavior with an asymptote at approximately 23 200 $hc\text{cm}^{-1}$ for this section, where the other HF bond is kept fixed at 115 pm. The bond rupture energy is 15 690 $hc\text{cm}^{-1}$ on the potential surface, when the other HF bond is allowed to relax to its equilibrium value of 91.71 pm for the isolated HF molecule. Inclusion of zero point energies yields the reaction enthalpy 185 kJmol^{-1}, which differs from the experimental value by 1 kJmol^{-1} .

While the graphical representation gives evidence for the global character of the PES, its accuracy in terms of the reproducibility of vibrational term will be discussed in this contribution. The theoretical term values from the present model potential agree with the values reported from experimental work within 1 to 1.5 cm^{-1}, which is the targeted accuracy for a global analytical representation. Our study shows that the accuracy of the present data requires: (i) to adjust the combined covalent and electrostatic model potential to the ab initio data set, in particular to capture correctly the bending mode number 2; (ii) to use the counter poise correction to eliminate residual BSSE, in particular to describe the asymmetric stretching mode number 3.

References

[1] W. Kutzelnigg. *Einfürung in die Theoretische Chmie; Band 2: Die chemische Bindung*. Verlag Chmie, Weinheim, Germany, (1978).
[2] P. G. Wenthold and R. R. Squires, jpc, **99**, 2002–2005 (1995).
[3] P. Sebald, A. Bargholz, R. Oswald, C. Stein, and P. Botschwina, J. Phys. Chem. A, **117**, 9695–9703 (2013).
[4] K. Kawaguchi and E. Hirota, J. Chem. Phys., **84**, 2953–2960 (1986).
[5] K. Kawaguchi and E. Hirota, J. Chem. Phys., **87**, 6838–6841 (1987).
[6] Y. Cornaton, B. M. Krishna, and R. Marquardt, Mol. Phys., **111**, 2263–2282 (2013).
[7] R. Marquardt, J. Math. Chem., **50**, 577–587 (2012).
[8] A. J. Stone. *The theory of intermolecular forces*. Clarendon Press, Oxford, (2002).

Contributed Papers
Posters

Synchrotron-based THz Spectroscopy at the Swiss Light Source

S. Albert[1,2], S. Bauerecker[3], I. Bolotova[1], Ph. Lerch[2], M. Quack[1] and A. Wokaun[4]
[1]Physical Chemistry, ETH Zurich, Switzerland, [2]SwissLight Source, PSI Villigen, Switzerland, [3]Institute for Physical Chemistry, TU Braunschweig, D-38106, Germany, [4]Energy Research Department, Paul-Scherrer-Institute, CH-5232 Villigen, Switzerland.

Introduction

One of the great challenges of modern high resolution spectroscopy is to find devices which cover the "THz gap" between 0.7 and 5 THz (23 - 166 cm^{-1}). Synchrotron sources in combination with interferometers can be used in this frequency range and are able to close the THz gap [1].

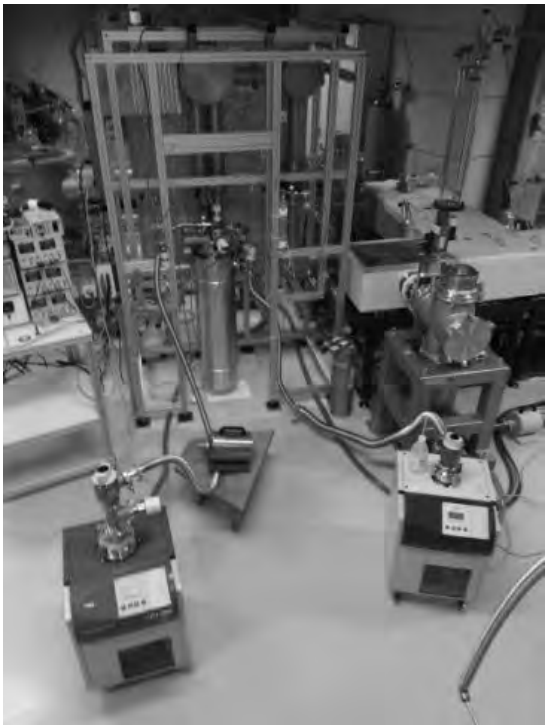

Figure 1: FTIR setup of the eleven chamber Bruker IFS 125 at the Swiss Light Source, including the collisional cooling cell [1,2,10].

FTIR / THz Setup

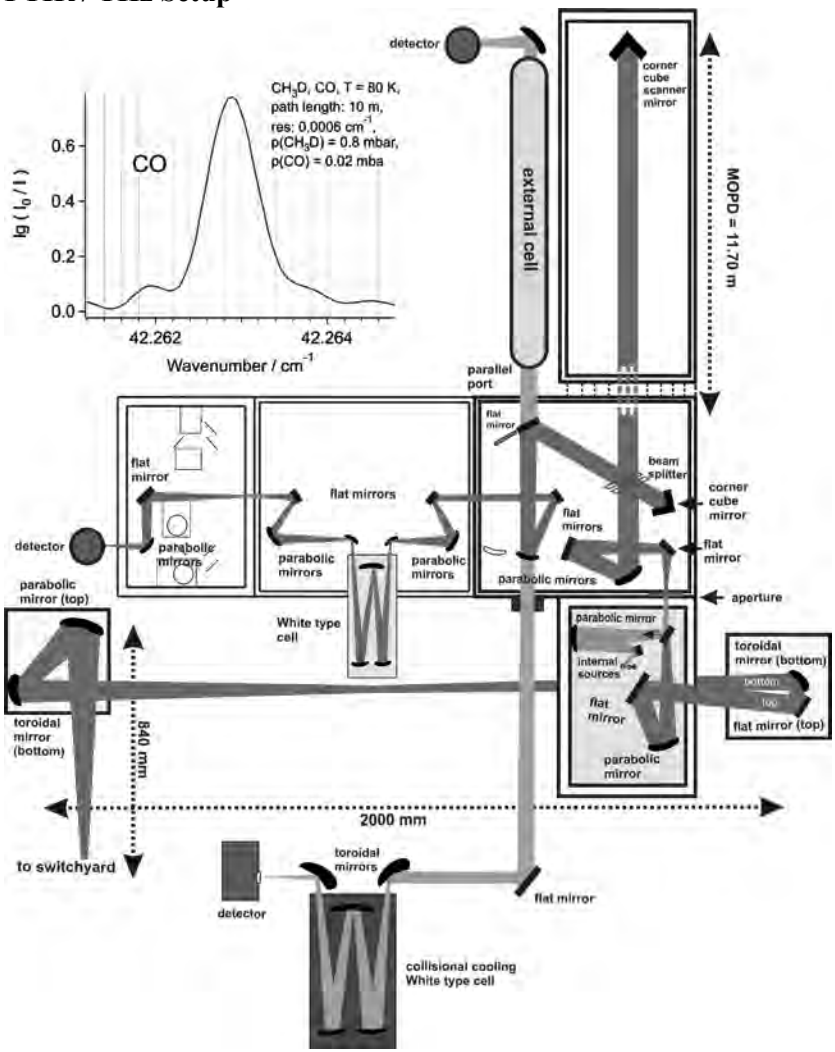

Figure 2: Optical layout of the FTIR setup of the eleven chamber Bruker IFS 125 at the Swiss Light Source and a measured CO line with an effective resolution of 0.0006 cm-1 (20 MHz).

We have extended our high resolution FTIR setup at the Swiss Light Source (**Figures 1** and **2**) described in Refs. [1-7] with a collisional cooling multireflection cell [10] which makes it possible to record spectra

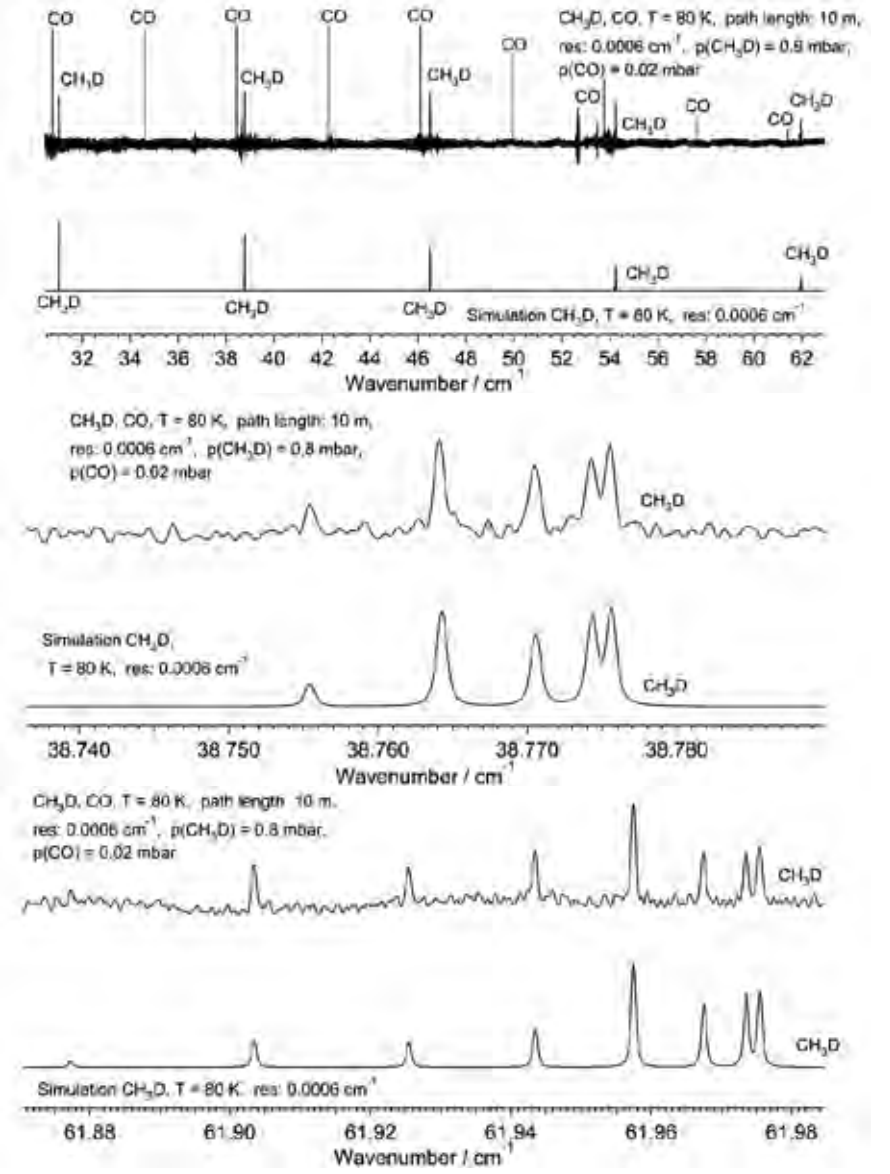

Figure 3: Rotational THz spectrum of a mixture of CO and CH_3D. The upper trace is the experimental spectrum and the lower trace the simulation. The lower panels are enlargements of parts of the spectrum.

at present from about 850 GHz (28 cm^{-1}) towards higher frequencies. Due to the high brightness of the synchrotron radiation, the signal-to-noise ratio is effectively 20 to 50 times better than that obtained using conventional thermal sources in the spectral region below 4 THz. The instrumental bandwidth is on the order of 17 MHz, which makes it possible to measure rotational spectra at high resolution. Using the collisional cooling method, we are able to measure rotationally resolved spectra at temperatures as low as 80 K or even at 10 K and below.

Spectra

We have measured spectra of the deuterated methanes and we present here analyses of the rotational spectra of the mono deuterated methane (CH_3D, **Figure 3**) measured at 80 K from 0.7 to 3 THz. The deuterated methanes have a small dipole moment which has been the subject of a long controversy resolved in [8,9] (see also discussion in [6]). The CO has been used to determine the rotational temperature of 80 K in situ.

Acknowledgements

Our work is supported financially by the Schweizerischer Nationalfonds, ETH Zürich, Paul-Scherrer-Institute and by an Advanced Grant (No 290925) of the European Research Council.

References

[1] S. Albert and M. Quack, Trendbericht: Physikalische Chemie 2013, *Nachrichten aus der Chemie* **2014**, 62, 313.
[2] S. Albert, K. Keppler , Ph. Lerch, M. Quack, A. Wokaun, *J. Mol. Spectrosc.* **2015**, **315**, 92-101.
[3] S. Albert, Ph. Lerch, R. Prentner, M. Quack, *Angew. Chem. Int. Ed.* **2013**, 52, 346-349.
[4] S. Albert, Ph. Lerch and M. Quack. *ChemPhysChem* **2013**, 14, 3204.
[5] S. Albert, K.K. Albert, Ph. Lerch, M. Quack, *Faraday Discussions* **2011**, 150, 71-99.
[6] S. Albert, K.K. Albert, M. Quack, *Fourier transform infrared spectroscopy*, in Handbook of High-Resolution. Spectroscopy, Vol. 2, (Eds. M. Quack and F. Merkt), Wiley, Chichester 2011, 965-1019.
[7] S. Albert and M. Quack, *ChemPhysChem.* **2007**, 8, 1271-1281.
[8] R. Signorell, R. Marquardt, M. Quack, M. A. Suhm,, Mol. Phys. **1996**, 89, 297-313,
[9] H. Hollenstein, R. R. Marquardt, M. Quack, M. A. Suhm, *J. Chem. Phys.* **1994**, 101, 3588-3602.
[10] S. Albert, S. Bauerecker, M. Quack and A. Steinlin, *Mol. Phys.* **2007**, 105, 541–558.

GHz and synchrotron-based THz spectroscopy of mono deuterated oxirane (*c*-CH_2OCHD)

S. Albert[1,2], Z. Chen[1], Ph. Lerch[2], K. Keppler[1], M. Quack[1] V. Schurig[3] and O. Trapp[4]

[1]Physical Chemistry, ETH Zurich, Switzerland, [2]Swiss Light Source, PSI Villigen, Switzerland, [3]University Tübingen, Germany, [4]University Heidelberg, Germany

Introduction

Deuterated molecules have been detected in several interstellar objects [1]. Surprisingly, the D/H ratio for some of the interstellar molecules is much higher than the average galactic value. Oxirane (*c*-CH_2OCH_2) has been detected in interstellar spectra (Sgr B2N) [2] and thus *c*-CH_2OCHD is an interesting candidate because it is chiral [3,4] and thus may become the first chiral molecule to be detected in interstellar space [5]. We report here a combined GHz and THz analysis of the rotational spectrum of mono deuterated oxirane. It is a small cyclic molecule like the main species oxirane (also called ethylene oxide, *c*-CH_2OCH_2). It is an isomer of acetaldehyde (CH_3CHO) which lies more than 1eV lower in energy [6]. Oxirane´s rotational spectrum in the ground state has been measured and analysed in the MW [7], in the submm [6] ranges using the FASSST system [8], and recently using synchrotron-based THz spectroscopy [9]. The rovibrationally resolved infrared spectum of oxirane has also been analysed in the range 600 - 3500 cm^{-1} [10]. The spectrum of mono deuterated oxirane has been analysed in the microwave region [11] up to 70 GHz. Recently calculated rotational constants of *c*-CH_2OCH_2 have been provided [12].

Experimental

c-CH_2OCHD has been synthesized as described in [5]. We have measured *c*-CH_2OCHD between 65 and 117~GHz using our GHz spectrometer described slightly modified compared to [13]. It consists of a microwave synthesizer working in the range 250 kHz to 20 GHz with a frequency resolution of 0.001 Hz and a long-term stability frequency accuracy of $\Delta\nu/\nu = 10^{-11}$. The signal is frequency multiplied by a factor of 6 leading to an operation in the frequency range of 67 to 118 GHz. All transitions were collected using the frequency modulation technique (second harmonic lock-in detection) with a modulation frequency of 50 kHz. We have measured the THz spectra of *c*-CH_2OCHD with our FTIR

setup at the Swiss Light Source [14,15]. This FTIR spectrometer currently has the highest resolution and is unique among related FTIR spectrometers worldwide. The spectra have been taken within a pressure range of 0.01 to 0.5 mbar.

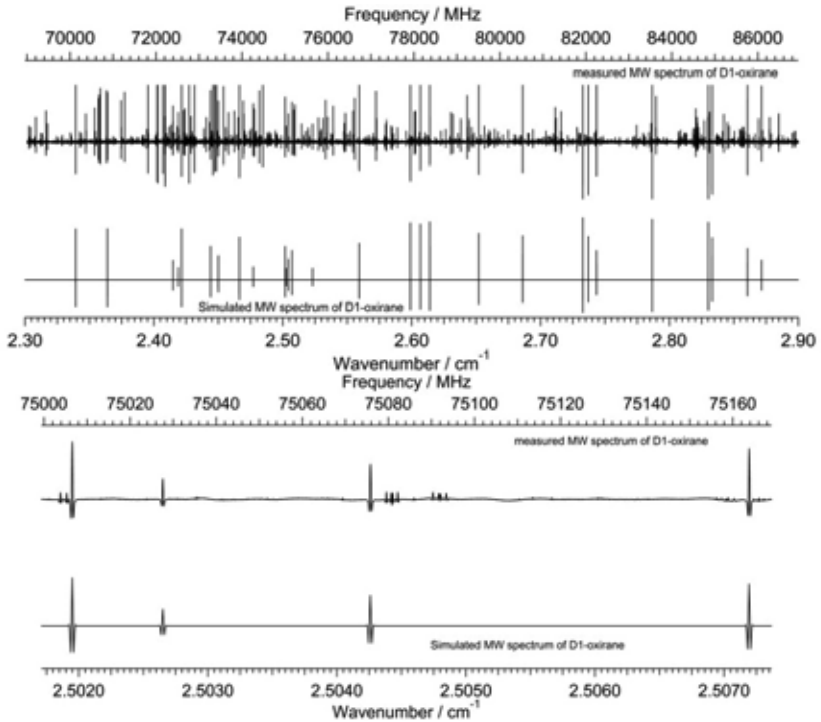

Figure 1: Rotational MW spectrum of *c*-CH_2OCHD. The upper traces show the experimental spectrum and the lower traces show the simulation (T_{rot} = 295 K). The lower panel is an enlargement of part of the spectrum.

Analysis of the spectra

The assignment of the spectra analysed here was performed up to J = 72 with the assistance of Loomis-Wood-type assignment programs. The rovibrational analysis of the spectra of the molecules described here was conducted using Watson's A-reduced effective Hamiltonian, including up to sextic centrifugal distortion constants using the Wang program [16]. Simulations performed using these constants reproduce the observed spectra fairly well, as can be seen in **Figures 1** and **2**. The measured linewidths (FWHM) are on the order of 0.0006-0.0008 cm^{-1}.

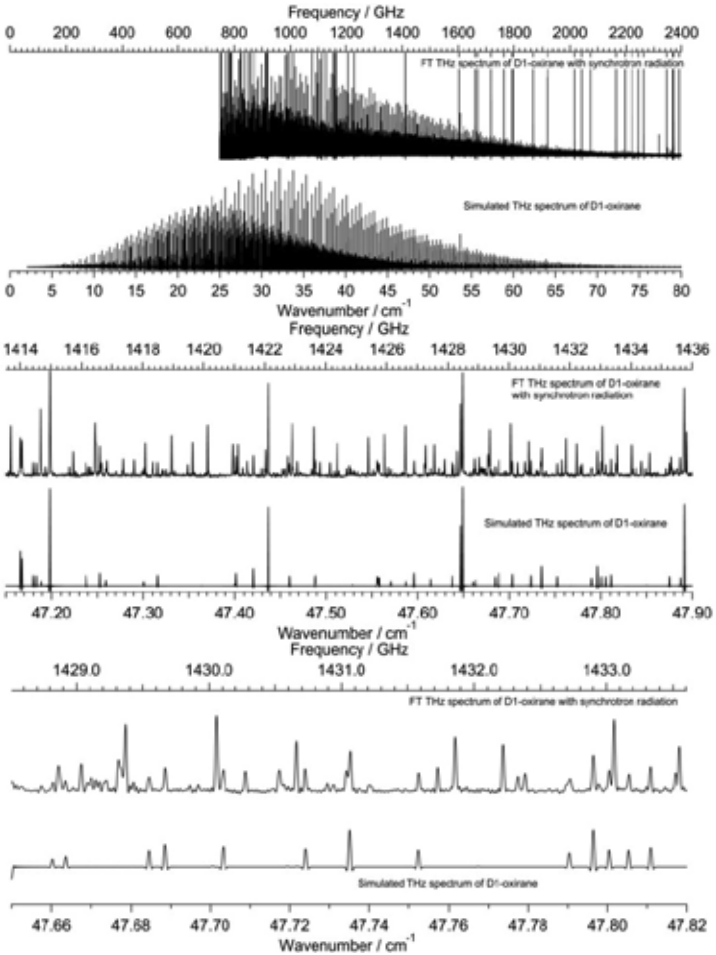

Figure 2: Rotational THz spectrum of *c*-CH_2OCHD. The upper traces show the experimental spectrum and the lower traces show the simulation (T=295 K, p=0.8 mbar, l=10 m). The lower panel is an enlargement. Strong extra lines arise from CH_2Cl_2.

Conclusion

Synchrotron-based THz spectroscopy now makes it possible to record the entire rotational spectrum of interstellar molecules. Using the simulations at different rotational temperatures we can predict the specific spectral regions in which a possible interstellar search for the chiral *c*-CH_2OCHD might be successful based on the accurate rotational parameters. As seen in **Figure 2** we recommend the range between 0.9 and 1.1 THz for *c*-CH_2OCHD search in interstellar objects with T_{rot} = 295 K for example.

Acknowledgements
Our work is supported financially by the Schweizerischer Nationalfonds, ETH Zürich, Paul-Scherrer-Institute and by an Advanced Grant (No 290925) of the European Research Council.

References

[1] C. Ceccarelli. *Planetary and Space Science* **2002**, 50,1267–1273.
[2] J. E. Dickens, W. M. Irvine, M. Ohishi, M. Ikeda, S Ishikawa, A. Nummelin, and A. Hjalmarson, *ApJ*, **1997**, 489, 753.
[3] M. Quack, *Angew. Chem. Intl. Ed. (Engl.)* **2002**, 41(24), 4618.
[4] M. Quack, *Fundamental symmetries and symmetry violations from high resolution spectroscopy*, in Handbook of High-Resolution Spectroscopy, Vol. 1, (Eds. M Quack and F Merkt), Wiley, Chichester **2011**, 659-722. M. Quack, J. Stohner, and M. Willeke, *Annu. Rev. Phys. Chem.* **2008**, 59, 741-769.
[5] K.K. Albert, S. Albert, M. Quack, J. Stohner, O. Trapp and V. Schurig, *19th Colloqium on High Res. Mol. Spectrosc.*, Salamanca, Spain, September 11th–13th, 2005, Paper H15 (and to be published).
[6] L. Pan, S. Albert, K.V.L.N. Sastry, E. Herbst, and F.C. De Lucia, *ApJ*, **1998,** 499, 517–519.
[7] J. G. L Cunningham, A.W. Boyd, R.J. Myers, W.D. Gwinn, and W. I. Le Van, *J. Chem. Phys*. **1951**, 19, 676.
[8] D.T. Petkie, T.M. Goyette, R. Bettens, S.P. Belov, S. Albert, P. Helminger and F.C. De Lucia, *Rev. Sci. Instrum.* **1997** 68, 1675–1683.
[9]C. Medcraft, C. D. Thompson, E.G. Robertson, D. R. T. Appadoo and D. McNaughton, *ApJ* **2012,** 753, 18.
[10] Flaud, J.-M., Lafferty, W. J., Kwabia Tchana, F., Perrin, A., and Landsheere, X. *J. Mol. Spectrosc.* **2012**, 271, 38.
[11] C. Hirose, *Bull. Chem. Soc. Jap.* **1974**, 47, 1311-1318.
[12] C. Puzzarini, M. Biczysko, J. Bloino and V. Barone, *ApJ* **2014,** 785 107.
[13] M. Suter and M. Quack, *Applied Optics* **2015** , 54, 4417.
[14] S. Albert, Ph. Lerch, R. Prentner, M. Quack, *Angew. Chem. Int. Ed.* **2013**, 52, 346-349, S. Albert, Ph. Lerch and M. Quack. *ChemPhysChem* **2013**, 14, 3204-3208, S. Albert, K.K. Albert, Ph. Lerch, M. Quack, *Faraday Discussions* **2011**, 150, 71-99.
[15] S. Albert, K.K. Albert, M. Quack, *Fourier transform infrared spectroscopy*, in Handbook of High-Res. Spectroscopy, Vol. 2, (Eds. M. Quack and F. Merkt), Wiley, Chichester **2011**, 965-1019.
[16] D. Luckhaus and M. Quack, *Mol. Phys*. **1989**,68, 745.

THz Spectroscopy of cyano-oxirane (*c*-C_2H_3OCN) and methyl oxirane (*c*-$C_2H_3OCH_3$) with synchrotron light

S. Albert[1,2], Ph. Lerch[2], K. Keppler[1], M. Quack[1]
[1]*Physical Chemistry, ETH Zurich, Switzerland,*
[2]*SwissLight Source, PSI Villigen, Switzerland,*
[3]*University Heidelberg, Germany*

Introduction

Chiral precursor molecules of evolution like oxirane carbonitrile [1,2] and other chiral molecules like methyl oxirane and mono deuterated oxirane [3] are of interest for laboratory spectroscopy in relation to molecular parity violation [4-6] and to possible astrophysical observation [2] of these molecules.

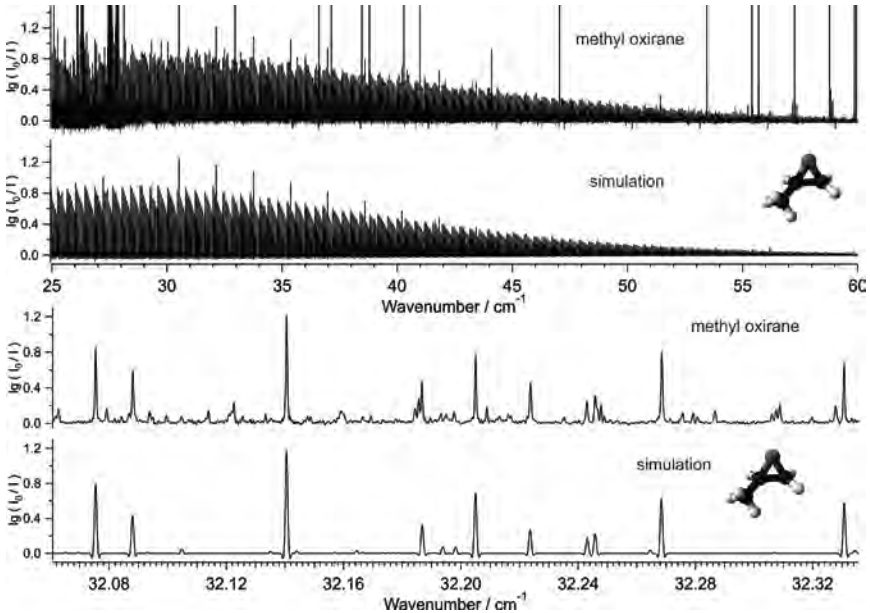

Figure 1: Rotational THz spectrum of methyl oxirane. The upper traces show the experimental spectrum and the lower traces show the simulation. The lower panel is an enlargement (p=0.9 mbar, l=10 m, instrumental bandwidth = 17 MHz).

As a chiral molecule, the heterocyclic molecule *c*-C_2H_3OCN (cyano oxirane or in systematic nomenclature oxirane carbonitrile) is also of potential interest when relating biomolecular evolution and molecular parity violation [4-6]. Using our high resolution FTIR setup [7,8] at the Swiss Light Source, we have measured the rotational spectra of oxirane carbonitrile and methyl oxirane with a resolution of 18 MHz in the range 1 to 2 THz at room temperature. Oxirane carbonitriles have been suggested as a prebiotic precursor molecule [1]. Both microwave [2] and Millimeter wave spectra [9] have been previously recorded, and their analysis has provided useful ground state rotational parameters. This molecule has also been the subject of so far unsuccessful searches in interstellar space [10]. Methyl oxirane is another classical chiral molecule and it has also not yet been found in the interstellar space. Its spectrum has been analysed in the MW region up to 60 GHz [11,12].

Analysis

The assignment of the spectra analyzed here was performed with the assistance of Loomis-Wood-type assignment programs. The rovibrational analysis of the spectra of the molecules described here was conducted using Watson's A-reduced effective Hamiltonian, including up to sextic centrifugal distortion constants. Oxirane carbonitrile has been analysed up to J=95 and methyl oxirane up to J = 70. Simulations performed using these constants reproduce the observed spectra fairly well, as can be seen in **Figures 1** and **3.**

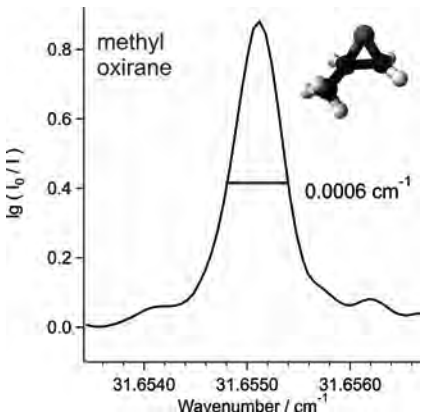

Figure 2: A selected methyl oxirane line (on the order of 0.0006 cm^{-1} FWHM, p=0.9 mbar, l=10 m, instrumental bandwidth = 17 MHz).

As **Figures 1** and **3** show, the rotational lines become very weak around 2 THz if the rotational spectra are measured at 295 K. The measured spectral line width FWHM is in the order of 0.0006 - 0.0008 cm^{-1} as is shown in **Figure 2**.

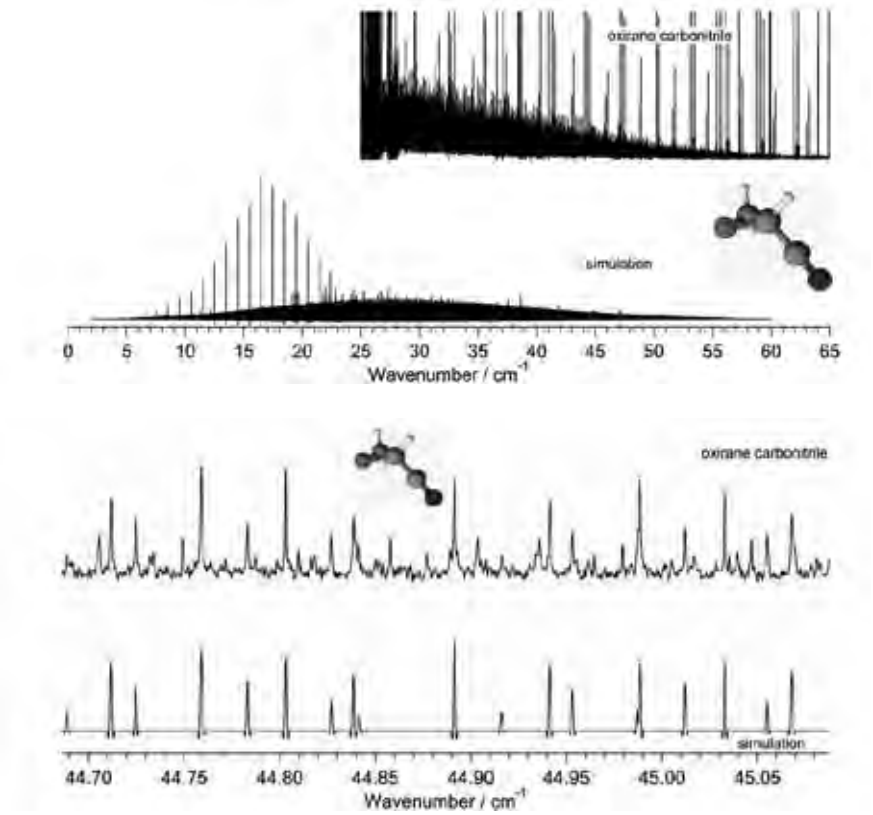

Figure 3: Rotational THz spectrum of oxirane carbonitrile. The upper traces show the experimental spectrum and the lower traces show the simulation. The lower two sets of panels are enlargements (p=0.6 mbar, l=10 m, instrumental bandwidth = 17 MHz).

Conclusion

Synchrotron-based THz spectroscopy now makes it possible to record the rotational spectrum of potential interstellar molecules at high frequency. Using the simulations at different rotational temperature, we can predict spectral regions in which a possible interstellar search might be successful for oxirane carbonitrile. The range around15 cm^{-1} is predicted

to be favourable for the search in interstellar objects with temperatures of 295 K and lower wavenumbers with lower temperatures.

Acknowledgements
Our work is supported financially by the Schweizerischer Nationalfonds, ETH Zürich, Paul-Scherrer-Institute and by an Advanced Grant (No 290925) of the European Research Council.

References

[1] A. Eschenmoser and E. Loewenthal, *Chem. Soc. Rev.* **1992**, 21(1), 1.
[2] F. Müller and A. Bauder, *J. Mol. Spectrosc.* **1996**, 179(1), 61.
[3] S. Albert, Z. Chen, Ph. Lerch, K. Keppler, M. Quack, V. Schurig and O. Trapp, paper at SASP 2016.
[4] M. Quack, *Angew. Chem. Intl. Ed. (Engl.)* **2002**, 41(24), 4618.
[5] R. Berger, M. Quack and G.S. Tschumper, *Helv. Chim. Acta* **2000**, 83(8), 1919.
[6] M. Quack, *Fundamental symmetries and symmetry violations from high resolution spectroscopy*, in Handbook of High-Resolution Spectroscopy, Vol. 1, (Eds. M Quack and F Merkt), Wiley, Chichester **2011**, 659-722, M. Quack, J. Stohner, and M. Willeke, *Annu. Rev. Phys. Chem.* **2008**, 59, 741-769.
[7] S. Albert, Ph. Lerch, R. Prentner, M. Quack, *Angew. Chem. Int. Ed.* **2013**, 52, 346- 349, S. Albert, Ph. Lerch and M. Quack. *ChemPhysChem* **2013**, 14, 3204-3208, S. Albert, K.K. Albert, Ph. Lerch, M. Quack, *Faraday Discussions* **2011**, 150, 71-99.
[8] S. Albert, K.K. Albert, M. Quack, *Fourier transform infrared spectroscopy*, in Handbook of High-Res. Spectroscopy, Vol. 2, (Eds. M. Quack and F. Merkt), Wiley, Chichester **2011**, 965-1019.
[9] M. Behnke, I. Medvedev, M. Winnewisser, F. C. De Lucia and E. Herbst, *ApJ. Suppl. Series* **2004**, 152, 97.
[10] J.E. Dickens, W.M. Irvine, M. Ohishi, G. Arrhenius, S. Pitsch, A. Bauder, F. Muller, and A. Eschenmoser, *Origins of Life and Evolution in the Biosphere* **1996**, 26(2*)*, 97.
[11] J. D. Swalen, D. R. Herschbach, *J. Chem. Phys.* **1957** 27(1), 100, D. R. Herschbach, J. D. Swalen, *J. Chem. Phys.* **1958**, 29, 761.
[12] M. Imachi, R.L. Kuczkowski, *J. Mol. Struct.* **1983**, 96, 55-60.

Tunneling dynamics of aniline studied by synchrotron-based high resolution THz spectroscopy

S. Albert[1,2], Ph. Lerch[2], and M. Quack[1]
[1]*Physical Chemistry, ETH Zurich, Switzerland,*
[2]*SwissLight Source, PSI Villigen, Switzerland,*

Introduction

A better understanding of the quantum dynamical behavior of functional groups like the amino (NH_2) group in organic molecules is essential for a profound understanding of the kinetic properties of biomolecular systems.

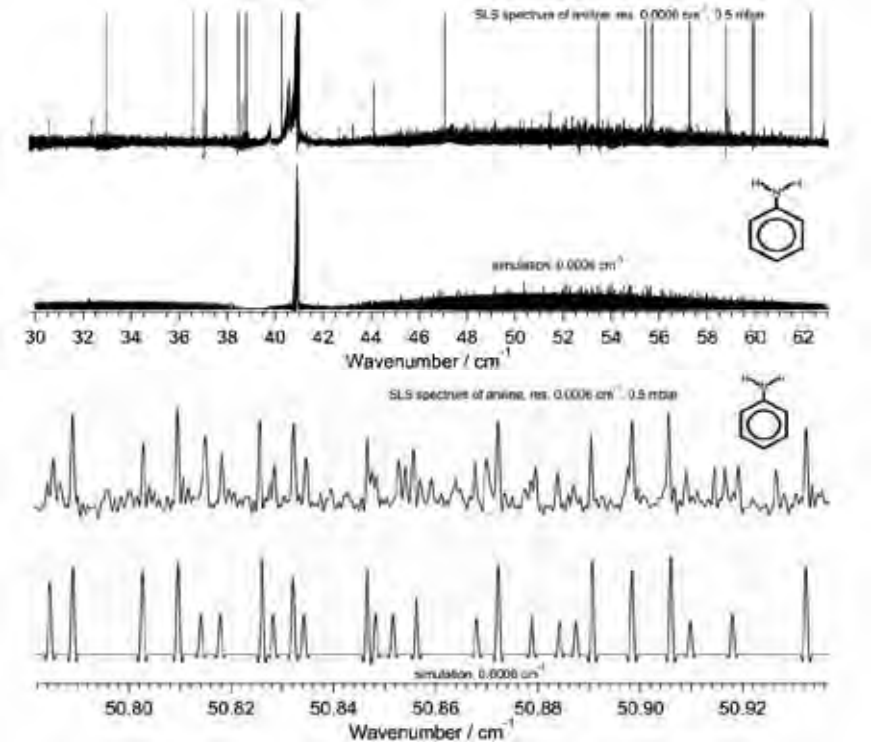

Figure 1: THz spectrum of the aniline band between the inversion levels in the vibrational ground state. The upper trace is the experimental spectrum and the lower trace the simulation. The lower panel is an enlargement of part of the spectrum (p=0.75mbar, T=295 K, l=10 m, instrumental bandwidth=17 MHz).

In particular, tunneling processes which are generally neglected in classical biomolecular dynamics modeling are in fact quite important and

deserve study [1-3]. For that reason we have investigated the tunneling dynamics of aniline ($C_6H_5NH_2$) [4] as a prototypical molecule containing the amino group attached to an aromatic framework using high resolution ($\Delta\nu$ = 17 MHz) FTIR (THz) spectroscopy with synchrotron radiation [5-7]. We were able to detect tunneling processes for aniline in the spectral range from 1 to 30 THz (33-1000 cm^{-1}). The inversion tunneling dynamics of aniline were analysed decades ago using low resolution single vibronic level UV flourescence spectra [8] leading to a first determination of the inversion barrier of about 450 cm^{-1}. These dynamics have been an important topic since that time [4] and are investigated here at very high resolution "quantum state resoved" but without hyperfine structure.

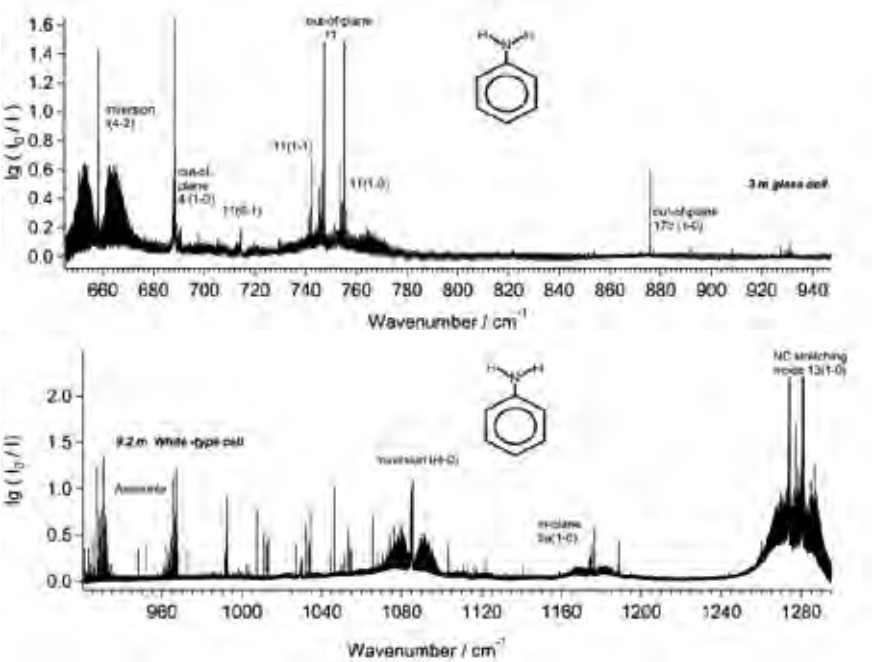

Figure 2: The FTIR spectrum of aniline between 600 and 1300 cm^{-1}. The hotbands within the inversion polyad are visible (p=0.9 mbar, l=3 m, and p= 0.1 mbar, l=9.2 m in a White cell, T=295 K).

Inversion polyad

We have measured and analysed the inversion tunneling level of aniline at 40.95031 cm^{-1} and various excited tunneling levels as shown in **Figures 1** and **2**. The term value diagram is shown in **Figure 3**. Numerous interactions have been detected at higher energy. We have

identified two bands, a I_3-I_2 hot band at 275.9 cm-1 and a second band shifted by 1 cm^{-1} compared to the band between the two inversion tunneling levels of the first excited inversion state which might be due to torsional tunneling splitting.

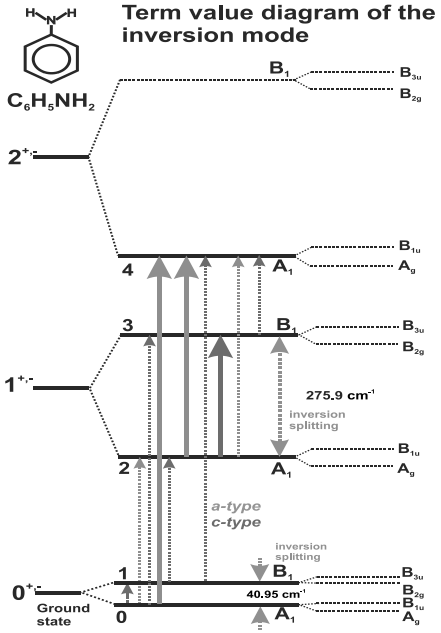

Figure 3: Term value diagram of the inversion mode of aniline

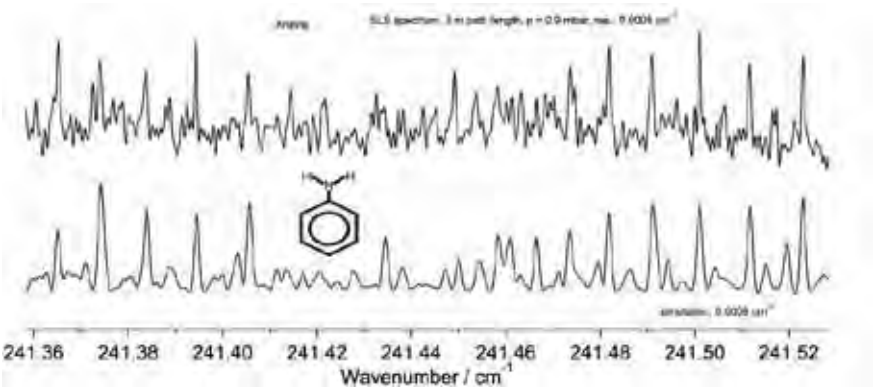

Figure 4: FIR SLS spectrum of the aniline torsional subbands. The upper trace is the experimental spectrum and the lower trace the simulation. This shows part of the lower torsional subband (p=0.9mbar, T=295 K, l=3 m).

Torsional levels

In addition, we have identified the two torsional components rovibrationally resolved including the inversion splitting in the torsional fundamental of aniline and have detected two bands within each inversion-torsional component. A comparison of the experimental spectrum and a simulation is shown in **Figure 4**. Our results lead to an inversion splitting of 28.33 cm^{-1}, identifying the torsional motion as inhibiting mode. The torsional tunneling is not yet resolved, predicted to be on the order of 0.00003 cm^{-1} [2], although two other bands have been identified, currently assigned as torsional hot bands.

Acknowledgements

Our work is supported financially by the Schweizerischer Nationalfonds, ETH Zürich, Paul-Scherrer-Institute and by an Advanced Grant (No 290925) of the European Research Council.

References

[1] M. Quack, *Fundamental symmetries and symmetry violations from high resolution spectroscopy*, in Handbook of High-Resolution Spectroscopy, Vol. 1, (Eds. M. Quack and F. Merkt), Wiley, Chichester **2011**, 659-722.

[2] B. Fehrensen, D. Luckhaus and M. Quack, *Z. Phys. Chem.* **1999**, 209, 1-19, B. Fehrensen, D. Luckhaus and M. Quack, *Chem. Phys.* **2007**, 338, 90-105.

[3] S. Albert, Ph. Lerch, R. Prentner, M. Quack, *Angew. Chem. Int. Ed.* **2013**, 52, 346-349.

[4] M. Hippler, E. Miloglyadov, M. Quack, G. Seyfang, *Mass and Isotope Selective Infrared Spectroscopy,* in Handbook of High-Resolution Spectroscopy, Vol. 2 (Eds.: M. Quack, F. Merkt), Wiley, Chichester; New York, **2011**, pp. 1069-1118.

[5] S. Albert, K.K. Albert, M. Quack, *Fourier transform infrared spectroscopy*, in Handbook of High-Resolution Spectroscopy, Vol. 2, (Eds. M. Quack and F. Merkt), Wiley, Chichester 2011, 965-1019.

[6] S. Albert, K.K. Albert, Ph. Lerch, M. Quack, *Faraday Discussions* **2011**, 150, 71-99.

[7] S. Albert, Ph. Lerch and M. Quack. *ChemPhysChem* **2013**, 14, 3204-3208.

[8] M. Quack and M. Stockburger, *J. Mol. Spectrosc.* **1972**, 43, 87-116.

Synchrotron-based THz and FTIR spectroscopy of collisionally cooled NF_3

I. Bolotova[1], O. Ulenikov[1,6], S. Albert[1,2], S. Bauerecker[3], Ph. Lerch[2], M. Quack[1], T. Peter[4] and A. Wokaun[5]

[1]Physical Chemistry, ETH Zurich, Switzerland, [2]SwissLight Source, PSI Villigen, Switzerland, [3]Institute for Physical Chemistry, TU Braunschweig, Germany, [4]Institute of Atmospheric and Climate Science, ETH Zurich, Switzerland, [5]Energy Research Department, PSI Villigen, Switzerland, [6]Tomsk Polytechnic University, General Physics Department, Tomsk, Russia.

1. Introduction

Nitrogen trifluoride (NF_3) is an interesting molecular prototype for intramolecular dynamics including inversion [1] and it is an industrial gas used for plasma etching of semiconductors, the cleaning of chambers in the production of liquid crystal displays and in thin film solar cells. It is known to be an atmospheric pollutant and greenhouse gas, recently included in the second Kyoto protocol.

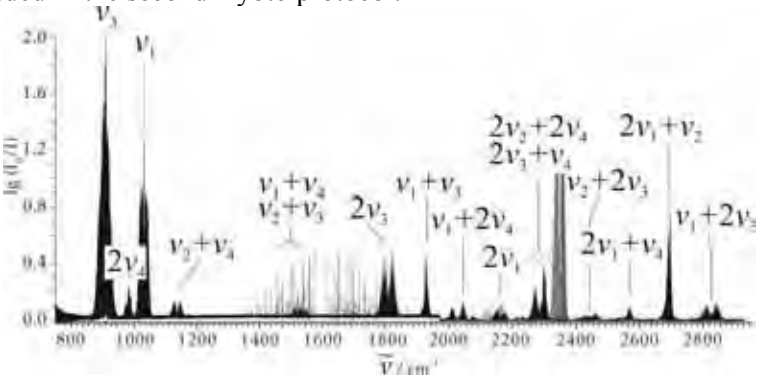

***Figure 1**. Survey of the high resolution FTIR spectrum of NF_3 measured with the Zurich collisional cooling FTIR setup. The range 800-2000 cm^{-1} was measured with a resolution of 0.001 cm^{-1}, path length l=7.5m, pressure p=0.02mbar at temperature T=80K; 2000-3000 cm^{-1}range was measured with a resolution (defined as nominal instrumental bandwidth, FWHM [10]) of 0.0017 cm^{-1}, l=7.5m and p=1mbar (total pressure with buffer gas He) at T=120K.*

Several studies of NF_3 spectra were performed in the microwave [3,8] as well as in the infrared region between 500 and 2000 cm^{-1} [2-10]. In the present study the spectra of nitrogen trifluoride have been measured with the Zurich Bruker prototype spectrometer (ZP 2001) [11,12] and the SLS THz /FTIR setup (2009 prototype) [13,14] in the range 20-2000 cm^{-1} at a temperature of 110 K using a collisional cooling cell [15] designed with White cell multipath reflection optics.

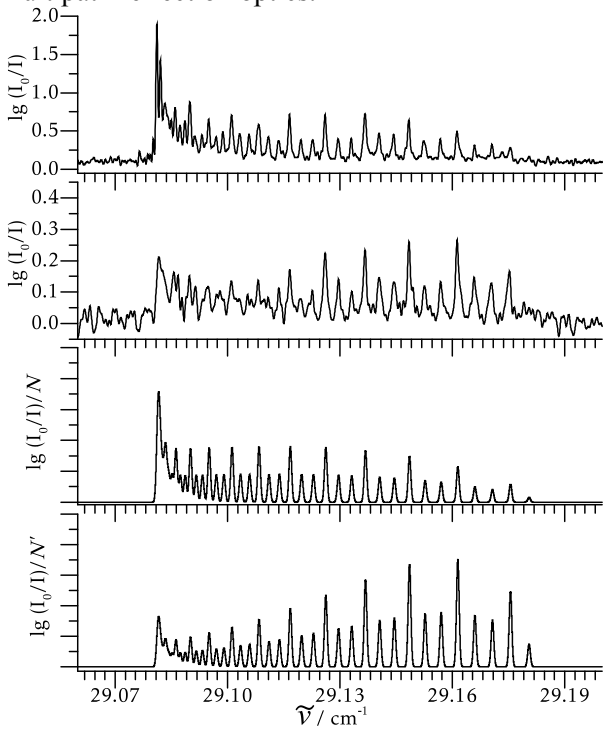

***Figure 2**. High resolution far infrared spectrum of NF_3 measured at the Swiss Light Source at 293K (**I** - p=2.2mbar, l=10m with resolution 0.0008 cm^{-1}). **II** – at T=100K using the collisional cooling cell (p=3.5mbar, l=10m with resolution 0.0008 cm^{-1}). The spectra **III** and **IV** illustrate simulations at T=293K and at T=100K correspondingly using arbitrary normalisations N and N'.*

Spectra

Figure 1 shows an overview of the fundamentals and the combination bands of NF_3 analysed by us. Rovibrational transitions were assigned to 14 different vibrational bands and were used then in the fitting procedure. We reinvestigated the bands $2\nu_4$, ν_1, $\nu_2+\nu_4$, $\nu_1+\nu_4$, $2\nu_3$ and $\nu_1+\nu_3$, which

have been studied before, and we have analysed the $2\nu_1$, $\nu_1+\nu_2+\nu_4$, $\nu_1+2\nu_4$, $2\nu_3+\nu_4$, $\nu_2+2\nu_3$, $\nu_1+\nu_2+\nu_3$, $2\nu_1+\nu_2$, $\nu_1+2\nu_3$ bands for the first time and present here preliminary results of our work. An effective Hamiltonian defined in [16] was used in the analysis, using also the program of [17] for the ground state. **Figure 2** shows a part of the THz spectrum of NF_3. The spectra have been taken at 293K (***I***) and at 110K (***II***). One recognizes the influence of the different rotational temperatures. In addition, the nuclear spin statistics is visible. The simulations are based on the adjusted spectroscopic constants listed in **Table 1**.

Parameter	Ref.[6]	Ref.[8]	this work
	1	2	3
B	0.35628234(15)	0.3562822451(21)	0.3562823158(23)
C			0.19499250
$D_J/10^{-6}$	0.487350(7)	0.4873325(27)	0.4873331(55)
$D_{JK}/10^{-6}$	-0.759642(13)	-0.759652(8)	-0.759654(6)
$D_K/10^{-6}$			0.34343
$H_J/10^{-12}$	0.6275(32)	0.61352(106)	0.6113(234)
$H_{JK}/10^{-11}$	-0.33353(157)	-0.33509(76)	-0.3353(38)
$H_{KJ}/10^{-11}$	0.5027(24)	0.48580(206)	0.4858(57)
$H_K/10^{-11}$			-0.10335
$L_J/10^{-16}$			-0.0(34)
$L_{JJK}/10^{-16}$	0.0	0.38(4)	0.1(24)
$L_{JK}/10^{-16}$		-0.96(10)	-0.37(65)
$L_{JKK}/10^{-16}$		0.74(12)	0.38(42)
$h_3^0/10^{-12}$		0.177(24)	0.170(98)
$h_3^J/10^{-17}$		-0.213(136)	
N_{data}		252	2276

Table 1. *Spectroscopic Parameters of the ground vibrational state of NF_3 (in cm^{-1}). The 2024 far infrared transitions were combined with 252 transitions obtained from the submillimetre-wave spectrum of NF_3 [8] yielding the set of ground state parameters presented in the last column. Uncertainties are quoted as 1σ in parentheses of the last digits given. Parameters quoted without uncertainties were held fixed at the values of [7].*

Conclusion

We measured and analysed the rotationally resolved THz and IR spectra in the temperature range 110K to 293K relevant for the Earth's atmosphere. Based on our high resolution measurements and analyses we can provide precise frequency and also intensity values for a qualitative and quantitative determination of NF_3 in the Earth's atmosphere.

Acknowledgements
Our work is supported financially by the Schweizerischer Nationalfonds, ETH Zürich, Paul-Scherrer-Institute and by an Advanced Grant of the European Research Council (grant No. 290925).

References
[1] S. Albert, K. Keppler Albert, H. Hollenstein, C. Manca-Tanner, and M. Quack, *Fundamentals of Rotation-Vibration Spectra*, Vol. 1, p. 117 in Handbook of High Resolution Spectroscopy M. Quack and F. Merkt eds., Wiley Chichester 2011.
[2] R. J. L. Popplewell, F. N. Masri and H. W. Tompson, Spect. Act. **23A** 2797 (1967).
[3] W. Höhe, U. Häring, W. A. Kreiner, H. Essig, and A. Ruoff, Can. J. Phys. **72** 1051 (1994).
[4] K. Akkard, N. Ben Sari-Zizi, B. Bakri, J. Demaison, H. Bürger, and E.B. MKadmi, J. Mol. Spectrosc. **218** 36 (2003).
[5] H. Najib, N. Ben Sari-Zizi, J. Demaison, B. Bakri, J.-M. Colmont, and E.B. MKadmi, J. Mol. Spectrosc. **220** 214 (2003).
[6] J. Breidung, L. Constantin, J. Demaison, L. Margulès, and W. Thiel, Mol. Phys. **101**, 1113 (2003).
[7] N. Ben Sari-Zizi, H. Najib, J. Demaison, B. Bakri, J.M. Colmont, and H. Bürger, J. Mol. Spectrosc. **228** 511 (2004).
[8] G. Cazzoli, and C. Puzzarini, J. Mol. Spectrosc. **239** 59 (2006).
[9] N. Ben Sari-Zizi and H. Najib, J. Mol. Spectrosc. **240** 210 (2006).
[10] S. Hmimou, H. Msahal and H. Najib, Mol. Phys. **108** 787 (2010).
[11] S. Albert, K.K. Albert, M. Quack, *Fourier transform infrared spectroscopy*, Vol. 2, p. 965 in Handbook of High Resolution Spectroscopy M. Quack and F. Merkt eds., Wiley Chichester 2011.
[12] S. Albert and M. Quack, ChemPhysChem. **8** 1271 (2007).
[13] S. Albert, K. Keppler , Ph. Lerch, M. Quack, A. Wokaun, J. Mol. Spectrosc. **315** 92 (2015).
[14] S. Albert, K.K. Albert, Ph. Lerch, M. Quack, Faraday Discussions **150** 71 (2011).
[15] S. Albert, S. Bauerecker, M. Quack, A. Steinlin, Mol. Phys. **105** 541 (2007).
[16] O. Ulenikov, A. Malikova, S. Alanko, M. Koivusaari, and R. Anttila, J. Mol. Spectrosc. **179** 175 (1996).
[17] H. M. Pickett, J. Mol. Spectrosc. **148** 371 (1991).

High resolution analysis of the FTIR spectra and quantum dynamics of CHF_3

I. Bolotova[1], O. Ulenikov[1,2], E. Bekhtereva[1,2], S. Albert[1,3], S. Bauerecker[1,4], H. Hollenstein[1], and M. Quack[1]

[1]*Physical Chemistry, ETH-Zürich, CH-8093, Zürich, Switzerland;* [2]*Tomsk Polytechnic University, General Physics Department, 634050, Tomsk, Russia;* [3]*Swiss Light Source, PSI, CH-5232, Villigen, Switzerland;* [4]*Institute for Physical Chemistry, TU Braunschweig, D-38106, Germany.*

1. Introduction

Fluoroform (CHF_3) is a prototype molecule for the study of intramolecular energy flow [1-4]. Despite a long history [2-20] its rotationally resolved infrared spectrum is poorly understood due to numerous strong interactions. We report the infrared spectrum of fluoroform molecule from the Terahertz (Far infrared) region (about 1THz or 30 cm^{-1}) up to about 3000 cm^{-1} in the temperature range 100 K to 300 K. The spectra were recorded and analysed in the region of the ν_3 fundamental (700.0989 cm^{-1}), the ν_2, ν_5, $\nu_3+\nu_6$ polyad (1200 cm^{-1} range), the $\nu_4/2\nu_3$ dyad (1400 cm^{-1}) and the $2\nu_4$ (A_1, E bands around 2700 cm^{-1}) dyad at high resolution (about 0.001 cm^{-1} instrumental bandwidth FWHM). An overview spectrum is shown on Fig. 1.

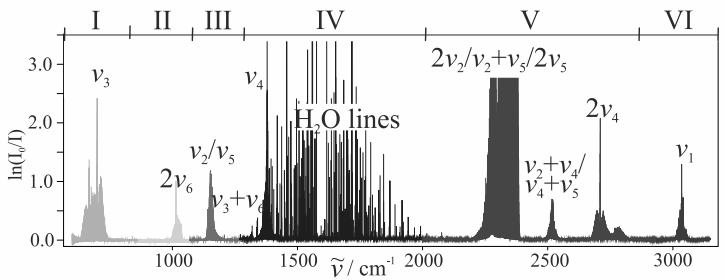

Figure 1. Survey of the high resolution FTIR spectrum of CHF_3 measured with the Bruker IFS 120 HR Zürich Prototype. I: resolution 0.001 cm^{-1}, path length l=3.2m, pressure p=0.3mbar, temperature T=293K; II: resolution 0.001 cm^{-1}, l=10.0m, p=0.25mbar, T=115K; III: resolution 0.001 cm^{-1}, l=3.2m, p=0.1mbar, T=293K; IV: resolution 0.0018 cm^{-1}, l=16.0m, p=0.5mbar, T=293K; V: resolution 0.0011 cm^{-1}, l=16.0m, p=0.5mbar, T=293K; VI: resolution 0.0017 cm^{-1}, l=19.2m, p=1.0mbar, T=110K.

2. Ground state

For the analysis the ground state the rotational constants were obtained from the far-infrared spectra of CHF_3 (see Fig. 2), which we measured at the Swiss Light Source (SLS) with the Bruker ETH-SLS 2009 prototype spectrometer (resolution defined here as nominal unapodized instrumental bandwidth FWHM 0.00053 cm^{-1} resulting from d_{MOPD} = 11.7 m) [1]. The analysis yields a set of parameters, presented in Table 1. The far infrared data we obtained were combined with the microwave [9] and the sub-millimeter wave [10] data in a joint fit.

Parameter	Ref.[9]	Ref.[10]	Ref.[14]	this work
	1	2	3	4
B	0.3452011705(28)	0.3452011656(66)	0.3452011705(28)	0.3452009580(1)
C			0.1892550(15)	0.189255
$\Delta_J/10^{-6}$	0.3784291(60)	0.3784224(36)	0.3784291(60)	0.3782997(55)
$\Delta_{JK}/10^{-6}$	-0.604300(17)	-0.604339(16)	-0.604300(17)	-0.6042685(2)
$\Delta_K/10^{-6}$			0.2779(26)	0.2779
$H_J/10^{-12}$	0.6680(26)	0.6694(8)	0.6680(26)	0.640681(54)
$H_{JK}/10^{-11}$	-0.27589(77)	-0.28679(33)	-0.27589(77)	-0.27523(18)
$H_{KJ}/10^{-11}$	0.3608(20)	0.3793(9)	0.3608(20)	0.35859(33)
$H_K/10^{-11}$			-0.1428	-0.1428
$L_J/10^{-17}$	-0.186(79)	-0.2231(53)		
$L_{JJK}/10^{-16}$		0.1652(26)		
$L_{JK}/10^{-15}$		-0.39(1)		
$L_{JKK}/10^{-15}$		0.37(1)		
$h_3/10^{-12}$		0.099031(15)	0.100890(97)	
$h_3^J/10^{-17}$		-0.685(17)	-0.167(31)	
N_{data}	274	253		274+253+3310

Table 1. Spectroscopic parameters of the ground vibrational state of CHF_3 (in cm^{-1}). The parameters have quoted uncertainties as 1σ in parentheses, in units of the last digits. Parameters given without uncertainties were fixed at the values of [13, 19].

3. The FTIR spectrum of fluoroform

The vibrational states of CHF_3 are listed in Table 2 up to about 3000 cm^{-1} in part as preliminary result. Columns 1 and 2 represent the harmonic wavenumbers ω and the fundamental wavenumbers $\tilde{\nu}$ calculated here *ab initio* at MP2/cc-pVTZ level [21]. In Columns 4 and 5 the experimental values are summarized. About 1430 transitions with J^{max} = 66 and K^{max} = 65 have been assigned to ν_3 vibrational band (700.0989 cm^{-1}). The $2\nu_3$-ν_3 "hot" band located in this region has also been analysed at highest resolution J^{max} = 43 and K^{max} = 15. Parameters

obtained in the fitting procedure reproduce the initial experimental information with the root mean square deviation $d_{rms} \approx 0.00029$ cm^{-1}.

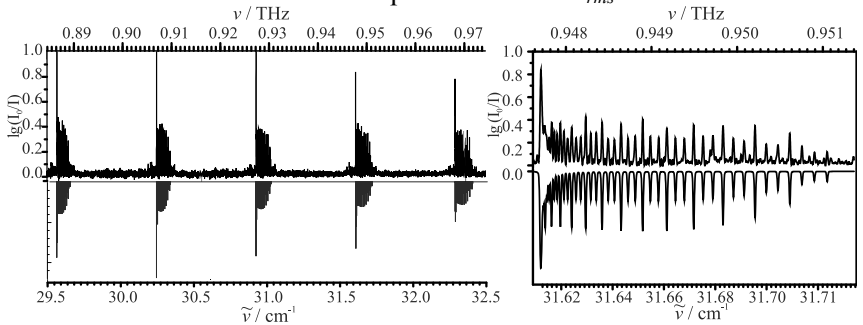

Figure 2. Left panel: part of the high resolution far-infrared rotational spectrum of CHF_3 measured with the synchrotron source at the Swiss Light Source at room temperature (resolution 0.0008 cm^{-1}, l=10 m, p=1.4mbar, upper trace) compared to the simulated spectrum (lower trace). Right panel: Detail of the high resolution far-infrared rotational spectrum of CHF_3 for the series of lines with J=45.

The strongly interacting fundamentals v_2 and v_5 correspond to the symmetric CF_3 stretching and degenerate FCF bending vibrations, coupled by a Coriolis interaction. Resonance interactions of anharmonic and Coriolis type between these fundamentals and the v_3+v_6 combination make the analysis difficult. At the first stage a spectrum of collisionally cooled CHF_3 has been analysed (J^{max} = 24). As a result, about 4000 transitions were assigned to the bands of the polyad with $J^{max} = K^{max} = 66$ for v_2 (1141.4568 cm^{-1}), $J^{max} = K^{max} = 55$ for v_5 (1157.3351 cm^{-1}) and $J^{max} = K^{max} = 71$ for v_3+v_6 (1208.7713 cm^{-1}). Strong resonance interactions between the states have been taken into account providing the anharmonic interaction constants between v_3+v_6 and v_5 (F_0 = 22.560(34) cm^{-1}). On the basis of our analysis, the parameters of the effective Hamiltonian were obtained, which reproduce the initial experimental information with an accuracy close to experimental uncertainties with a d_{rms} =0.00022 cm^{-1}. The FTIR spectrum of CHF_3 was also recorded and re-analysed in the region of v_4 fundamental band, for which about 4500 ro-vibrational transitions with $J^{max} = K^{max} = 60$ were assigned. The Coriolis type interaction between v_4 and very weak $2v_3$ bands was taken into account by using also our data for $2v_3$-v_3. The $2v_4$ band of fluoroform, located between 2650 and 2850 cm^{-1} was previously investigated at lower resolution [2, 18]. The level is known to be involved in Fermi resonance with the stretching fundamental v_1, which is an

essential doorway to intramolecular vibrational redistribution [1-4,8, 20]. The high resolution FTIR spectrum of CHF_3 has been measured at room temperature with the Bruker 125 HR Zürich Prototype spectrometer using a White type multireflection cell with optical path length of 19.2 meters. As a result of the analysis, transitions up to $J^{max} = 30$ have been assigned for the symmetric component A_1 of $2v_4$ band, and $J^{max} = 60$ for the $2v_4$ (E) band. The new analysis results in a set of effective Hamiltonian parameters, which reproduce the experimental data with accuracy close to the experimental uncertainties. The analysis of further interacting levels is in progress.

State	$\omega_{harm.}$ cm^{-1}	$\tilde{\nu}_{calc.}$ cm^{-1}	$\tilde{\nu}_{MCTDH}$ cm^{-1}	$\tilde{\nu}_{exp.}$ cm^{-1}	$\tilde{\nu}_{exp.}$ cm^{-1}	
	this work	this work	Ref. [11]	this work	Literature	[Ref.]
	1	2	3	4	5	
ν_6 (E)	516.510	510.756	507.01		507.82208	[12]
ν_3 (A_1)	713.491	705.841	703.73	700.09898(85)	700.098	[13]
$2\nu_6$ (E)	1033.020	1021.159	1014.63		1014.5415	[14]
$2\nu_6$ (E)	1033.020	1021.161	1015.53		1015.9530	[14]
ν_2 (A_1)	1168.172	1151.128	1157.82	1141.456816(33)	1141.4577	[15]
ν_5 (E)	1202.185	1173.738	1175.80	1170.705247(51)	1158.342	[15]
$\nu_3 + \nu_6$ (E)	1230.001	1218.679	1211.62	1195.400413(21)	1207.763	[15]
ν_4 (E)	1430.558	1397.513	1396.23	1377.8472422(91)	1377.845	[16]
$2\nu_3$ (A_1)	1426.982	1410.980	1406.26	1399.3972(38)		
$\nu_2 + \nu_6$ (E)	1684.682	1659.820	1522.80		1647.5	[17]
$\nu_5 + \nu_6$ (A_1)	1718.695	1680.035	1660.60		1657.5	[17]
$\nu_5 + \nu_6$ (E)	1718.695	1680.313	1660.60			
$\nu_2 + \nu_3$ (A_1)	1881.663	1855.002	1857.18		1839.8	[17]
$\nu_5 + \nu_3$ (E)	1915.676	1872.896	1874.60		1851.9	[17]
$\nu_4 + \nu_6$ (A_1)	1947.068	1906.816	1886.02			
$\nu_4 + \nu_6$ (E)	1947.068	1906.825	1894.89			
$\nu_3 + \nu_4$ (E)	2144.049	2101.245	2090.95		2077	[17]
$2\nu_2$ (A_1)	2336.344	2297.514	2305.85		2281.1	[17]
$\nu_2 + \nu_5$ (E)	2370.357	2318.519	2326.15			
$2\nu_5$ (A_1)	2404.369	2333.023			2316.3	[17]
$2\nu_5$ (E)	2404.369	2340.668				
$\nu_2 + \nu_4$ (E)	2598.730	2548.232				
$\nu_2 + \nu_4$ (E)	2598.730	2548.234				
$\nu_4 + \nu_5$ (A_1)	2632.743	2563.237				
$\nu_4 + \nu_5$ (E)	2632.743	2569.251				
$2\nu_4$ (A_1)	2861.116	2759.441		2710.209984(11)	2710.2094	[18]
$2\nu_4$ (E)	2861.116	2795.005		2754.799178(93)	2754.7981	[18]
ν_1 (A_1)	3209.810	3091.158				
$\nu_1 + 2\nu_4$ (E)					5959.443	[3]

Table 2. Vibrational term values with respect to the ground state for some selected states of CHF_3 (in cm^{-1}), preliminary (theory from [21]).

References

[1] a) S. Albert, K. Keppler Albert, H. Hollenstein, C. Manca-Tanner, and M. Quack Fundamentals of Rotation-Vibration Spectra, Vol. 1, p. 117; b) S. Albert, K. Keppler Albert, and M. Quack High-Resolution Fourier Transform Infrared Spectroscopy, Vol. 2, p. 965; c) M. Quack Fundamental Symmetries and Symmetry Violations from High-Resolution Spectroscopy, Vol. 1, p. 659 in Handbook of High Resolution Spectroscopy, M. Quack and F. Merkt eds., Wiley Chichester 2011.
[2] H. R. Dübal, and M. Quack, Chem. Phys. Lett. **80** 439 (1981).
[3] H. R. Dübal , and M. Quack, J. Chem. Phys. **81** 3779 (1984).
[4] R. Marquardt, M. Quack, J. Stohner and E. Sutcliffe, J. Chem. Soc., Far. Tr. **82** 1173 (1986).
[5] J. Segall, R. N. Zare, H. R. Dübal , M. Lewerenz, and M. Quack, J. Chem. Phys. **86** 634 (1986).
[6] A. Amrein, M. Quack, and U. Schmitt, Mol. Phys. **60** 237 (1987).
[7] A. Amrein, M. Quack, and U. Schmitt, J. Phys. Chem. **92** 5455 (1988).
[8] M. Quack, Annu. Rev. Phys. Chem. **41** 839 (1990).
[9] R. Bocquet, D. Boucher, W. Chen, D. Papousek, G. Wlodarczak, and J. Demaison, J. Mol. Spectrosc. **163** 291 (1994).
[10] G. Cazzoli, L. Cludi, G. Cotti, L. Dore, C. Esposti, M. Bellini, and P. Denatale, J. Mol. Spectrosc. **163** 521 (1994).
[11] L. J. Doriol, F. Gatti, C. Iung, and H.-D. Meyer, J. Chem. Phys. **129** 224109 (2008).
[12] A. Ceausu-Velcescu, J. Cosélou, J. Demaison, G. Graner, G. Duxbury, and H. Bürger, J. Mol. Spectrosc. **220** 291 (2003).
[13] K. M. Smith, G. Duxbury, D. A. Newnham, and J. Ballard, J. Mol. Spectrosc. **212** 6 (2002).
[14] A. Ceausu-Velcescu, H. Bürger, and G. Graner, J. Mol. Spectrosc. **220** 298 (2003).
[15] J. P. Champion, and G. Graner, Mol. Phys. **58** 475 (1986).
[16] S. Sofue, K. Kawaguchi, E. Hirota, and T. Fujiyama, Bull. Chem. Soc. Jpn. **54** 897 (1981).
[17] N. J. Fyke, P. Lockett, J. K. Thompson, and M. P. Wilt, J. Mol. Spectrosc. **58** 87 (1975).
[18] A. S. Pine, and J. M. Pliva, J. Mol. Spectrosc. **130** 431 (1988).
[19] G. Klatt, A Willets, N. C. Handy, R. Tarroni, and P. Palmieri, J. Mol. Spectrosc. **176** 64 (1996).
[20] M. Quack *Molecules in motion*, Chimia **55** 753 (2001).
[21] I. Bolotova, L. Horny, and M. Quack, *in preparation*.

Vibrational energy pooling in multilayer CO on NaCl studied with nanosecond time resolution using a superconducting nanowire single photon detector

Li Chen, Dirk Schwarzer, Alec M. Wodtke
Max Planck Institute for Biophysical Chemistry, Göttingen, Germany

The dynamics of vibrational energy pooling[1, 2] in multilayer CO (ca. 1300 layers) on NaCl(100) is studied in both time and frequency domain, using laser induced fluorescence (LIF) spectroscopy measured with new emerging superconducting nanowire single photon detectors (SNSPDs)[3, 4]. Due to the fast time response of SNSPD, the vibrational pooling dynamics in solid CO was time resolved for the first time.

In frequency domain, as shown in Figure 1, upon overtone (v=0→2) excitation with a 6 ns laser pulse, infrared emission is detected in the range 1700 to 5200 cm^{-1} covering one-quantum (Δv=-1), two-quanta (Δv= -2), and three-quanta (Δv= -3) emission lines of CO. The emission originates from states up to v=29 implying efficient vibrational energy pooling within a few microsecond after the laser pulse.

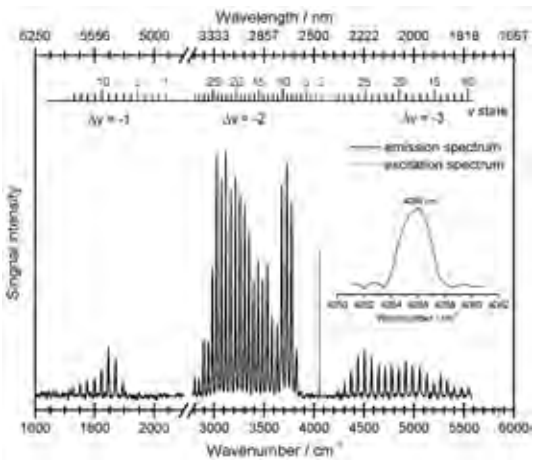

Figure 1 Emission spectrum of multilayer CO (ca. 1300 layers) on NaCl(100) at T_s= 12 K upon v=0→2 overtone excitation.

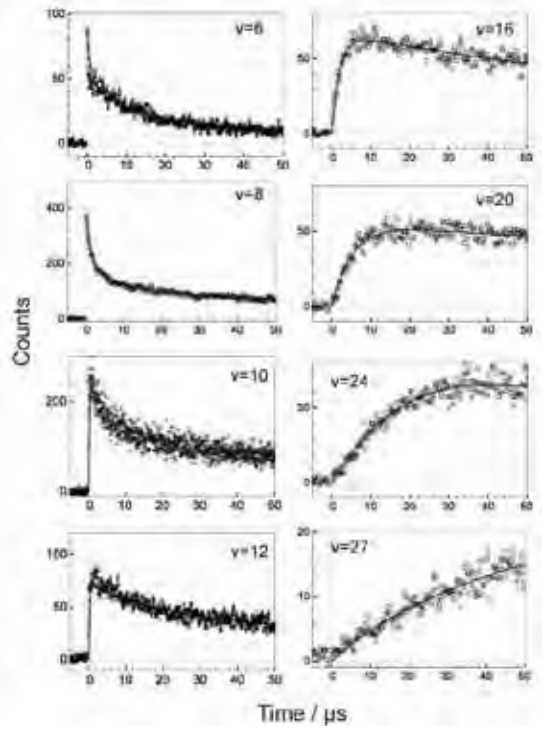

Figure 2 The vibrational state dependent fluorescence time profile.

In time domain, for the v=1 and v=2 states, the emissions decay within about 1μs; while for the higher vibrational states, the signals are characterized by a fast rise followed by a multi-exponential decay on a millisecond timescale. With increasing vibrational quantum number the rise time increases from 0.2 μs for v=10 to 50 μs for v=27, as shown in Figure 2. Kinetic modelling of the experimental data provides detailed information about the rate constants involved in the vibrational energy pooling process.

References

[1] H. C. Chang, and G. E. Ewing, J Phys Chem-Us **94** (1990).
[2] S. A. Corcelli, and J. C. Tully, J Chem Phys **116** (2002).
[3] B. Baek *et al.*, Appl Phys Lett **98** (2011).
[4] F. Marsili *et al.*, Nano Lett **12** (2012).

Helium droplet assisted preparation and spectroscopy of alkali-alkaline earth diatomics

Johann Pototschnig, Florian Lackner, and Wolfgang E. Ernst
Institute of Experimental Physics, Graz University of Technology, Petersgasse 16, A-8010 Graz, Austria

The unique experimental conditions provided by helium nanodroplets (He_N)[1] are utilized to form diatomic molecules from one alkali (Ak) and one alkaline earth (Ake) atom, both heliophobic dopants that reside on the droplet surface. Ak-Ake molecules have attracted considerable attention as candidates for the formation of ultracold molecules with a magnetic and an electronic dipole moment. In order to explore this interesting group of molecules, we recently recorded laser excitation spectra of LiCa [2], RbSr [3,4], and RbCa [5] on helium droplets. Our own quantum chemistry calculations allowed the assignment of the electronic band systems in the wavenumber range between 11,500 and 23,000 cm^{-1}[2,4-6].
In our studies we found that the permanent electric dipole moment points in different directions for certain electronically excited states, and changes the sign in some cases as a function of bond length. We summarize our results, give causes for the measured trends in terms of molecular orbital theory and extrapolate the tendencies to other combinations of AK and Ake – elements [7].

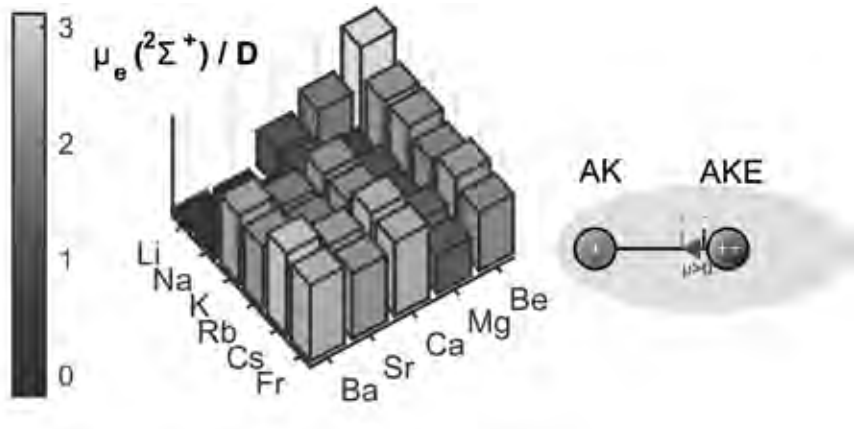

[1] C. Callegari and W. E. Ernst, in: *Handbook of High Resolution Spectroscopy*, Eds. F. Merkt and M. Quack, 1st Edition, Vol. 3, 1551-1594 (2011).

[2] Günter Krois, Johann V. Pototschnig, Florian Lackner, and Wolfgang E. Ernst, Spectroscopy of cold LiCa formed on helium nanodroplets, J. Phys. Chem. A **117** (50), 13719–13731 (2013), http://dx.doi.org/10.1021/jp407818k .

[3] Florian Lackner, Günter Krois, Thomas Buchsteiner, Johann V. Pototschnig, and Wolfgang E. Ernst, Helium Droplet Assisted Preparation of Cold RbSr Molecules, Phys. Rev. Lett. **113**, 153001-1-5 (2014), http://dx.doi.org/10.1103/PhysRevLett.113.153001 .

[4] Günter Krois, Florian Lackner, Johann V. Pototschnig, Thomas Buchsteiner, and Wolfgang E. Ernst, Characterization of RbSr Molecules: A Spectral Analysis on Helium Droplets, PCCP **16**, 22373-22381 (2014), http://dx.doi.org/10.1039/C4CP03135K .

[5] Johann Valentin Pototschnig, Günter Krois, Florian Lackner, Wolfgang E. Ernst, Investigation of the RbCa Molecule: Experiment and Theory, J. Mol. Spectrosc. **310**, 126-134 (2015) (special issue in honor of Marilyn Jacox), http://dx.doi.org/10.1016/j.jms.2015.01.006

[6] Johann V. Pototschnig, Günter Krois, Florian Lackner, and Wolfgang E. Ernst, Ab initio study of the RbSr electronic structure: Potential energy curves, transition dipole moments and permanent electric dipole moments, J. Chem. Phys. **141**, 234309-1-10 (2014) , http://dx.doi.org/10.1063/1.4903791 .

[7] Johann V. Pototschnig, Andreas W. Hauser, and Wolfgang E. Ernst, Electric Dipole Moments and Chemical Bonding of Diatomic Alkali - Alkaline Earth Molecules, submitted to PCCP (2015).

Pure beams of free radicals for radical-surface chemistry

Felicity E Gossan, Stephen D Price

University College London

The chemistry of free radicals is critical to media as varied as interstellar clouds, etching plasmas and planetary atmospheres. To date, the lack of a general source generating solely a specific free radical has led to a lack of information pertaining to the kinetics and chemistry of these ubiquitous species with surfaces.[1] Indeed, the paucity of data available to quantify the interaction of free radicals with surfaces has limited our understanding in this important field. This poster presents the work currently being undertaken at UCL to develop an apparatus that produces a pure beam of free radicals to conduct radical-surface experiments.

The experimental techniques employed to produce fluxes of radicals for surface studies usually rely upon the dissociation of a molecule *via* a discharge, a method that produces the radical of interest amongst a wealth of other species such as ions, electrons and un-dissociated molecules.[2] When studying radical-surface interactions, current standard surface-science methods cannot generally selectively probe the interaction of individual radicals with a substrate, instead monitoring all reactions occurring on the surface (e.g XPS, RAIRS). Indeed, the presence of a significant number of species in addition to the radical of interest leads to convoluted datasets that cannot be interpreted easily. This poster presents the development of a pure source of free radicals that provides a generic method for producing a flux of radicals that consists overwhelmingly of one species.

The pure radical beam is generated *via* negative ion photo-detachment (NIP). Well established techniques are used to generate a mass selected anion beam, which is photoionized yielding neutral molecules. As described above, the apparatus is used to study radical-surface chemistry. To allow us to investigate radical-surface reactions, the radical beam is coupled to an ultrahigh vacuum chamber where a substrate is irradiated by the neutral flux. Various surface science techniques are used to investigate the chemistry that may occur at the radical-surface interface including: reflection absorption infra-red spectroscopy (RAIRS), temperature programmed desorption (TPD), auger electron spectroscopy (AES) and X-ray photoelectron spectroscopy (XPS). In combination, these powerful surface science techniques are used to interrogate the species adsorbed on the target.

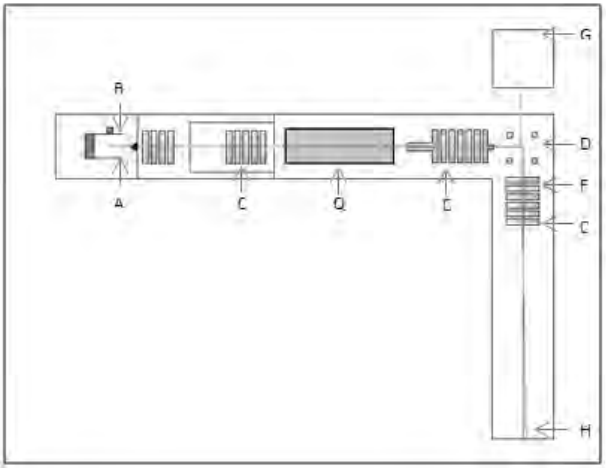

Figure 1 Schematic of the radical source. A = electron gun, B = Free jet expansion, C = Focussing ion optics, D = Quadrupole bending lens, E = Channeltron, F = Decelerator, G = 520nm Laser, H = Radical beam, Q = Wien filter

We will use the apparatus that is being built to study the chemistry that may be occurring between gas phase radicals and molecular ices (e.g. CN on water ice) accreted onto the dust grains found within the dense molecular clouds of the interstellar medium (ISM). It is known that radicals are present in these dusty, dark clouds however the precise molecular mechanisms that occur between the surface of dust grains and gas phase radicals is unknown.[3] Studying these reactions will provide kinetic data that will further our understanding of the chemistry occurring in interstellar space.[4] This poster presents the results of the initial experiments performed during the commissioning of this apparatus.

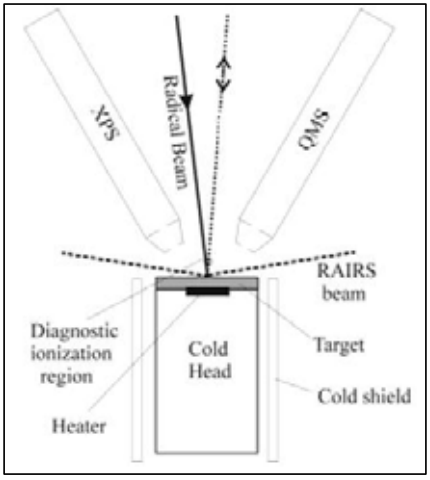

Figure 2 Schematic of target

[1] J. A. Stillahn, K. J. Trevino, E. R. Fisher, in *Annual Review of Analytical Chemistry, Vol. 1*, Annual Reviews, Palo Alto, **2008**, pp. 261-291.
[2] K. Ikejiri, H. Ohoyama, Y. Nagamachi, T. Teramoto, T. Kasai, *Chemical Physics Letters* **2003**, *379*, 255-260.
[3] A. Sternberg, A. Dalgarno, S. Lepp, *Astrophysical Journal* **1987**, *320*, 676-682; P. Theule, F. Duvernay, G. Danger, F. Borget, J. B. Bossa, V. Vinogradoff, F. Mispelaer, T. Chiavassa, *Advances in Space Research* **2013**, *52*, 1567-1579.
[4] H. Feuchtgruber, F. P. Helmich, E. F. van Dishoeck, C. M. Wright, *Astrophysical Journal* **2000**, *535*, L111-L114.

Towards hybrid trapping of cold molecules and cold molecular ions

D. Haas, C. von Planta, D. Zhang, S. Willitsch
Department of Chemistry, University of Basel, Klingelbergstrasse 80, 4056 Basel, Switzerland

S. Y. T. van de Meerakker,
Radboud University Nijmegen, Institute for Molecules and Materials, Heijendaalseweg 135, 6525 AJ Nijmegen, The Netherlands

1. Introduction

Hybrid systems of cold atoms and ions have been studied intensively in recent years. The simultaneous trapping of atoms with ions has opened up new possibilities for the investigation of interactions between the two species and has greatly contributed to the understanding of collisional and chemical processes at low temperatures [1].

Here, we report on the development of an advanced hybrid trapping technique which aims at trapping neutral molecules and molecular ions simultaneously. A translationally cold package of neutral molecules is produced by means of Stark deceleration. This deceleration technique exploits the Stark effect experienced by polar molecules in switched inhomogeneous electric fields, thereby producing a molecular package at translational temperatures $T_{trans} > 1$ mK [2]. During the last deceleration stage, the molecular package is loaded into a magnetic trap [5], which is incorporated into an RF ion trap. With this set-up, the superposition of cold neutral molecules with molecular ions allows for quantum-state selective investigations of elastic, inelastic and reactive collisions at low translational energies $E_{coll} < 30$ mK. Initial experiments will focus on OH + Ca^+, OH + N_2^+ and OH + H_2O^+ as collision systems.

2. Experimental Setup

A supersonic molecular beam of OH radicals seeded in Krypton is generated by electric arc dissociation of H_2O vapour. After having passed the skimmer, the OH cloud enters a 123 stage Stark decelerator. Besides acting as a magnetic trap for OH, a pair of 1.4 T NeFeB permanent

magnets is used as final deceleration stage by applying HV directly onto the magnets.

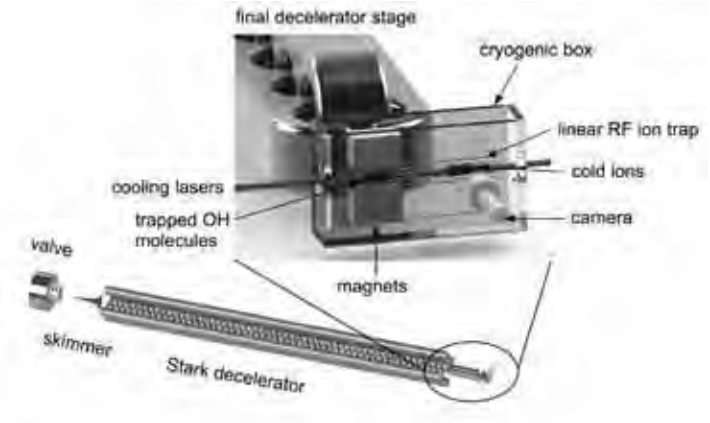

Figure1: Schematic for an ion-molecule hybrid trap setup consisting of a Stark decelerator coupled to a magnetic trap encompassing a cryogenic ion trap.

The ion trap has been realised in the form of a thin wire RF ion trap, which has proven to provide a very versatile and robust trapping environment, especially in the case of limited space [3]. Here, the small spatial extent of the wires allows for a reduced vertical separation (3mm) between the magnets, which provides sufficient trap depth. The OH cloud can be overlapped with the Coulomb crystal by sliding the bar magnets from the loading region towards the interaction region. In order to prolong the trapping lifetime, the hybrid setup is surrounded by a cryogenic shield.

3. Coupling the Stark decelerator to a magnetic trap

The translationally cold OH radicals leaving the Stark decelerator are in the $J = 3/2$, $m_J = \pm 3/2$, f states, where J denotes the total angular momentum quantum number, m_J the corresponding space-fixed projection quantum number and f designates the parity label. As Stark deceleration provides OH molecules at relatively low densities ($\approx 10^7$-10^8 molecules cm^{-3}) [2,5], it is crucial to minimise the loss during the loading procedure. Successful loading depends on minimising the volumetric mismatch between the decelerator and the trap. During stretches of free flight, the molecular package starts expanding in both, longitudinal and

transversal directions. Therefore, designing the trap such that it can be placed close to the decelerator helps to prevent loss. Using the magnets as last stage allows for faster initial loading, since the final deceleration step occurs right at the trap centre [4,5,6]. The four wires serve to introduce further degrees of freedom in shaping the stopping fields. The depth of the magnetic trap has been calculated to be $D_{trap} \approx 0.14$ cm^{-1} (14.3 m/s) using analytic expressions for the B-field. Only molecules in the low field seeking $J = 3/2$, $m_J = +3/2$, f Zeeman states can be confined magnetically. [6,7] As this comprises only 50 % of the decelerated ensemble, it is of great importance to optimise the trap-loading procedure to obtain high loading efficiencies. Here, the loading efficiency is defined as the ratio between the number of trapped molecules and the number of molecules in the ensemble leaving the decelerator.

4. Monte Carlo trajectory simulations and optimisation

As the loading efficiency is a complicated function of the phase angle, the potentials and the trap geometry, it is almost impossible to optimise the design manually. Instead, we report on the usage of the NOMAD direct search algorithm package to optimise the loading efficiency determined by realistic Monte Carlo Trajectory simulations. [8] The trajectory simulations start with the generation of a molecular ensemble, which is then propagated through the experimental setup taking into account all geometric obstacles. The molecular package is decelerated from 450 m/s to 39 m/s at the end of the decelerator, before coming close to a standstill at the trap centre. After the optimisation ≈ 53% of the molecules were found to match the phase-space acceptance of the magnetic trap. This amounts to ≈ 27 % loading efficiency, taking into account only molecules in the $J = 3/2$, $m_J = +3/2$, f Zeeman states. Based on the trajectory simulations, a temperature of ≈ 42 mK for the trap ensemble is estimated. The greatest loss of molecules during the loading procedure is caused by the reflection of slower molecules from the stopping fields. Compared to manually determined loading efficiencies, the optimised geometry results in a loading efficiency improved by a factor of ≈ 2.

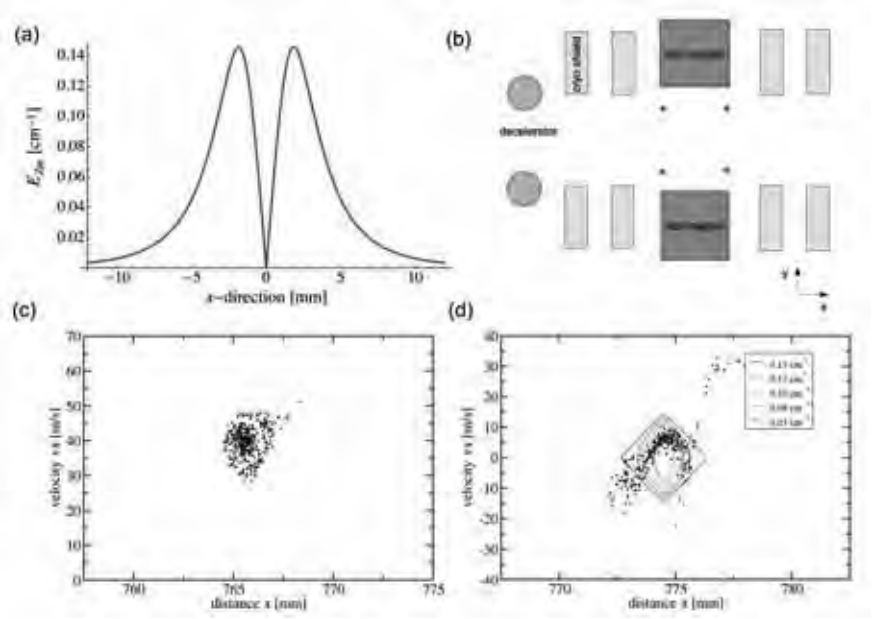

Figure2: (a) Zeeman energy E_{ZM} for the polar molecule along the longitudinal x-direction of the trap. (b) Schematic cross section of the trapping region illustrating the optimisation parameters. (c) Monte Carlo phase space distribution after the decelerator. (d) OH phase space distribution at the trap centre, where the contour lines indicate the acceptance of the trap.

1. S. Willitsch, *Ion-atom hybrid systems*, **2014**, arXiv:1401.1699v1 [physics.atom-ph].
2. S.Y.T. van de Meerakker, H.L. Bethlem, N. Vanhaecke, G. Meijer*, Chem. Rev.*, **2012**, *112*, 4828.
3. T. Ray, S. Jyothi, N. Bhargava Ram, S.A. Rangwala*, Appl. Phys. B*, **2014**, *114*, 267.
4. B. Stuhl, *Ultracold Molecules for the Masses*, Thesis, University of Colorado, **2012**.
5. B.C. Sawyer, B.L. Lev, E.R. Hudson, B.K. Stuhl, M. Lara, J.L. Bohn, J. Ye, *Phys. Rev. Lett.*, **2007**, *98*, 253002.
6. B.K. Stuhl, M. Yeo, M.T. Hummon, J. Ye, *Molec. Phys.*, **2013**, *111*, 1798.
7. J.L. Bohn, G. Quéméner, Molec. Phys., **2013**, *111*, 1931.
8. M.A. Abramson, C. Audet, G. Couture, J.E. Dennis, Jr., S. Le Digabel, C. Tribes, *The NOMAD project*, https://www.gerad.ca/nomad/

Using Ion Imaging to Probe Scattering and Reactions at Surfaces

Dan J. Harding[1], J. Neugebohren[1], H. W. Hahn[1], Daniel J. Auerbach[1], T.N. Kitsopoulos[1,2], Alec M. Wodtke[1]

[1]*Institute for Physical Chemistry, Georg-August University of Göttingen, 37077 Göttingen, Germany and Max Planck Institute for Biophysical Chemistry, 37077 Göttingen, Germany*

[2]*Department of Chemistry, University of Crete, 71003 Heraklion, Greece and Institute of Electronic Structure and Laser, Foundation for Research and technology-Hellas, 71003 Heraklion, Greece*

Abstract

We present a new implementation of ion imaging for the study of surface scattering processes. The technique uses a combination of spatial ion imaging with laser slicing and delayed pulsed extraction.

The scattering velocities of interest are parallel to the imaging plane, allowing speed and angular distributions to be extracted from a single image. We illustrate the possibilities provided by the method to investigate both direct and trapping-desorption scattering, and to the probe the kinetics of reactions occurring on the surface. The image shows the spatial separation of CO2 formed by the Eley-Rideal and Langmuir-Hinshelwood reaction channels in the oxidation of CO on oxygen covered Pt(111).

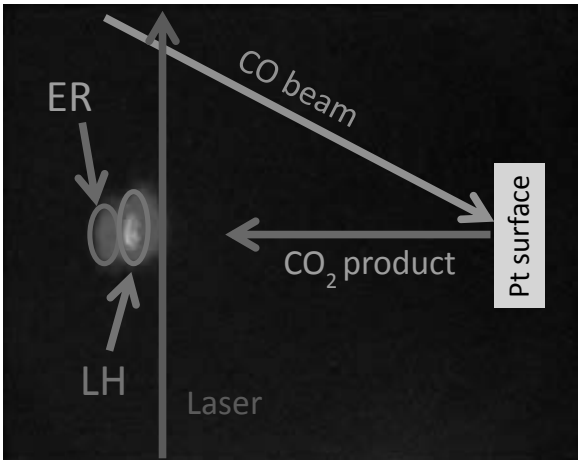

Photodissociation of ionized Leucine Enkephalin

Andreas Herburger, Christian van der Linde, Martin K. Beyer
Universität Innsbruck, Institut für Ionenphysik und Angewandte Physik

1. Introduction

Spectroscopy of peptides has been and remains a field of interest in chemical physics.[1] Sequencing and analysis of the fragments has been achieved by laser induced dissociation.[2] Particular interest has been given to the mechanisms of dissociation and the role of the mobile proton inducing the location of fragmentation.[3] However, the wavelength dependence of the fragmentation cross section deserves a closer look. Here the pentapeptide Leucine Enkephalin (YGGFL) is ionized by electrospray ionization and irradiated at wavelengths from 225-300 nm. Fragmentation patterns and photodissociation cross sections are investigated.

2. Experimental

Experiments were performed on a BRUKER APEX Qe Fourier Transform Ion Cyclotron Resonance Mass Spectrometer (FTICR-MS) with a 9.4 T superconducting magnet and an electrospray source (Fig. 1). The beam of an EKSPLA NT342B 20 Hz optical parametric oscillator tuneable wavelength laser system is guided into the ICR-cell via two CaF_2 right angle prisms. Laser irradiation times are controlled by a triggered diaphragm shutter. Leucine Enkephalin is dissolved at a concentration of 100 µM/l in 1:1 H_2O/Methanol (*v*/*v*). 0.5% acetic acid is added to the mixture.

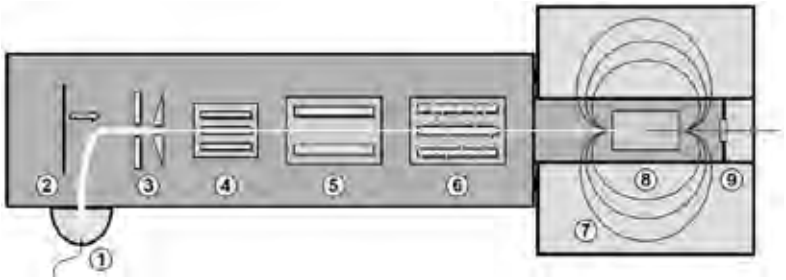

Figure 1: *Schematic view of FT-ICR MS: 1) Electrospray Source, 2) Repeller, 3) Electrostatic Lenses and Funnel, 4) Hexapole, 5) Quadrupole Mass Filter, 6) Collision Cell, 7) 9.4 T Superconducting Magnet, 8) ICR Cell, 9) Window for Laser Irradiation.*

3. Results and Discussion

Fig. 2 shows the fragmentation pattern of protonated Leucine Enkephalin at 225 nm and 1 sec irradiation time. Fragments are labelled by Roepstorff and Fohlman nomenclature.[4] If the charge sits on the N-terminal fragment, it is labelled as either a, b or c depending on the position of the backbone rupture. If it is retained on the C-terminal part, fragments are labelled as either x, y or z. Indices indicate the number of amino acid residues retained in the fragment. Full sequencing of the peptide has been achieved for all types but z-fragments (z_4 has not been detected).

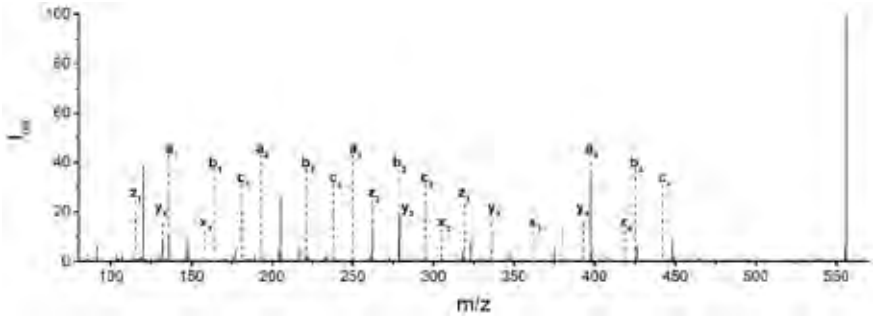

***Figure 2**: Laser induced dissociation mass spectrum of protonated Leucine Enkephalin. Intense but not labelled fragments are: 91 Da – Phenylalanine (F) aromatic side chain ion, 120 Da – F iminium ion, 147 Da – internal F ion, 205 Da – internal GlycineF ion*

Fragmentation cross sections have been observed by irradiating YGGFL at wavenumbers from 44444 to 33333 cm^{-1} (225-300 nm, $\Delta\upsilon$=150 cm^{-1}) for 1 sec (Fig. 3). 44444 cm^{-1} is the upper range of our OPO and there is no fragmentation at wavenumbers lower than 35000 cm^{-1}. Cross sections for single-photon processes are calculated by the formula

$$\sigma = -\log\left(\frac{I_0}{\sum_{i=0}^{n} I_i}\right)\frac{hcA}{\lambda pE}$$

with the intensities of the reactant ion I_0 and the n product ions I_i (i=1-n), the Planck Constant h, the speed of light c, the pulse energy E per area A, the number of pulses p and the wavelength λ.

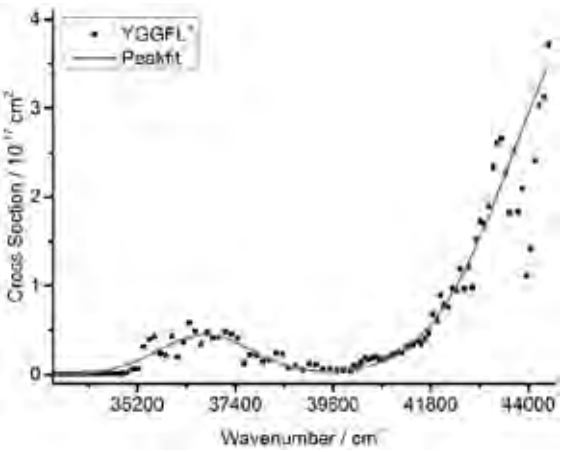

***Figure 3**: Fragmentation cross section of protonated Leucine Enkephalin. There is a high maximum outside of OPO range (>4×10^{-17} cm^2) and a smaller one at 36500 cm^{-1} (~0.5×10^{-17} cm^2). They are fitted by two Gaussians (solid line).*

References

1. Burke, N. L. Redwine, J. G. Dean, J. C. McLuckey, S. A. & Zwier, T. S. UV and IR spectroscopy of cold protonated leucine enkephalin. *International Journal of Mass Spectrometry* **378,** 196–205 (2015).
2. Tabarin, T. Antoine, R. Broyer, M. & Dugourd, P. Specific photodissociation of peptides with multi-stage mass spectrometry. *Rapid communications in mass spectrometry : RCM* **19,** 2883–2892 (2005).
3. Wysocki, V. H. Tsaprailis, G. Smith, L. L. & Breci, L. A. Mobile and localized protons: a framework for understanding peptide dissociation. *Journal of Mass Spectrometry,* 1399–1406 (2000).
4. Roepstorff, P. & Fohlman, J. Proposal for a common nomenclature for sequence ions in mass spectra of peptides. *Biomedical mass spectrometry* **11,** 601 (1984).

Oxygen atom reactivity on amorphous, porous interstellar dust grain analogues.

Helen Kimber and Stephen D Price
Department of Chemistry*, 20 Gordon Street,* University College London*, WC1H 0AJ*

Cornelia Jäger
Institute of Solid State Physics, Fredrich Schiller University Jena, Helmholtzweg 3, D-07745 Jena, Germany

The interstellar medium (ISM) is home to a rich array of chemistry. For a typical interstellar molecule approximately 80% of the abundance of that species can usually be accounted for by gas-phase kinetics with the other 20% generated *via* surface reactions on dust grains. When interplanetary dust, and particles suspected to have interstellar origin, are analysed, it is clear they are porous, amorphous silicates or carbonaceous material (Fig 1a).

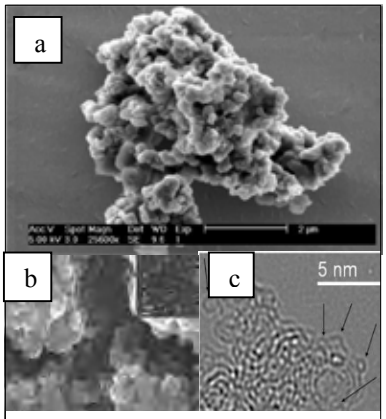

Figure 1a An interplanetary dust grain, 1b Silicate dust grain produced in Jena, 1c Carbonaceous dust grains produced in Jena. [3]

Oxygen atoms are the third most abundant species, after hydrogen and helium, in the interstellar medium and so O atom reactivity on interstellar dust grain analogues has attracted much attention in recent years. For example, O atoms have been shown to have high diffusion coefficients on interstellar dust grain analogues at temperatures as low as 6 K.[1] Furthermore, reaction barriers of O atoms, on these surfaces, have been shown to be sufficiently low for significant oxidation of astrophysically relevant molecules to take

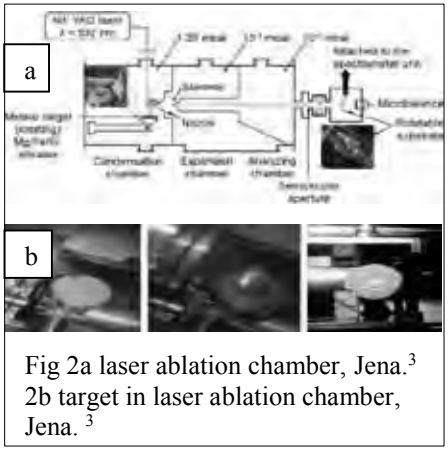

Fig 2a laser ablation chamber, Jena.[3] 2b target in laser ablation chamber, Jena. [3]

place on cold dust grains.[2,3] Up until now all these studies of O atom reactivity have been performed on ordered silicates, graphite and ices on silicates or graphite.

Amorphous, porous dust grains have been prepared using laser ablation at the Fredrich Schiller University, Jena (see Fig 2).[3,4] The apparatus for generating dust grains produces a beam of silicaceous or carbonaceous material (by laser ablation) which is deposited onto a graphite surface. The grain sizes can be controlled by varying the deposition time of the beam. A shorter deposition time leads to smaller grains. The carbonaceous grains were produced using a ^{13}C target for the laser. Changing the gaseous environment in which the carbonaceous grains are formed, changes the chemical structure of the grains. In a pure He environment fullerene type structures form, whilst in a mixed He/H_2 environment open hydrogenated fullerenes form. The silicates' chemical composition was also varied. However, this was performed by varying the ablation target. Specifically, grains were produced using a pure magnesium silicate target and a mixed target of iron and magnesium silicates. Typical silicate and carbonaceous grain morphologies can be seen in Fig 1b and 1c.

Recently H_2 formation from H atoms has been studied on dust grains similar to those generated above using the FORMOLISM apparatus at the University Cergy Pontoise. Using REMPI the rotational temperature of H_2 ejected from the surface can be probed. It was found that H_2 molecules formed on, and ejected from, a crystalline silicate had a cold ($T_{rot} \approx 120$ K) rotational energy distribution, whilst molecules formed on amorphous silicate films, had a rotational temperature of about 310 K. The authors

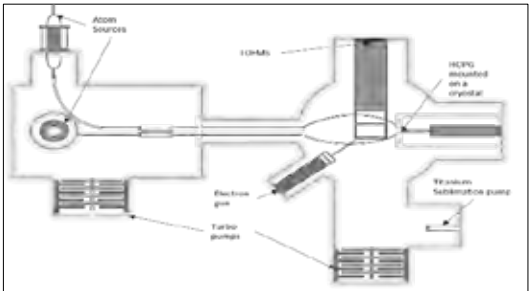

Fig 3 UHV experimental apparatus at UCL

suggest the difference in rotational temperature may be due to flatter grains hindering the "cartwheel" rotational modtion of the nascent H_2.[5] This study clearly indicates that grain morphology can affect reactions on interstellar dust grains.

The interstellar dust grain analogues made in Jena will be taken to UCL and inserted into a UHV chamber designed to probe the surface reactivity of O atoms, Fig 3. The diffusion coefficient of O atoms will be evaluated through the reaction of O atoms with molecular oxygen. [1] Rate coefficients for the reactivity of the ^{13}C dust grains with atomic oxygen will be measured and modelled. The results from these experiments will be reported in this poster.

References

1. E. Congiu, M. Minissale, S. Baouche, H. Chaabouni, A. Moudens, S. Cazaux, G. Manico, V. Pirronello and F. Dulieu, *Faraday Discuss.*, 2014, **168**, 151-166.
2. H. J. Kimber, C. P. Ennis and S. D. Price, *Faraday Discuss.*, 2014, **168**, 167-184.
3. T. Sabri, L. Gavilan, C. Jaeger, J. L. Lemaire, G. Vidali, H. Mutschke and T. Henning, *Astrophysical Journal*, 2014, **780**.
4. F. Huisken, C. Jaeger, H. Mutschke and T. Henning, *Diamond and Related Materials*, 2009, **18**, 392-395.
5. L. Gavilan, J. L. Lemaire, G. Vidali, T. Sabri and C. Jaeger, *Astrophysical Journal*, 2014, **781**.

Synthesis and derivative resolution of halogenated enantiomers

Stole Manov, Vanessa Galati, Manuela Meister, Manuel Mazenauer,
Benjamin Spenger and Jürgen Stohner*
Zurich University of Applied Sciences (ZHAW)
Institute for Chemistry and Biotechnology (ICBT)
Einsiedlerstrasse 31, CH-8820 Wädenswil
Email: juergen.stohner@zhaw.ch

Introduction

Small chiral halomethanes are of great importance as prototype molecules for the determination of the absolute configuration with new direct methods [1-3], the study of frequency dependent chiroptical properties [4], and photo-electric circular dichroism [5] because they are very well suited for high-quality *ab initio* calculation. The determination of the absolute configuration with new methods like coulomb explosion with COLTRIMS gained considerable interest [1-3]. While other methods need the enantiomers in crystalline form (X-ray structure analysis) and additional calculations (e.g. VCD), the analysis following Pitzer et al. [1] (see also [2,3]) determines the absolute configuration directly. Our main goal is to obtain small enantiopure prototype molecules such as halomethanes (CHBrClF, CHBrFI, CDBrFI, etc) and small rings (halooxiranes) in relatively large quantities for the applications described above.

Synthesis

The most common way to obtain an enantiopure component is to start from enantiopure reagents. For example, both enantiomers of 2-iodobutane were synthesised by converting (S)-(+)- and (R)-(-)-2-butanol into an intermediate which then reacts with phosphor triiodide to the respective 2-iodobutane (Scheme 1) [6].

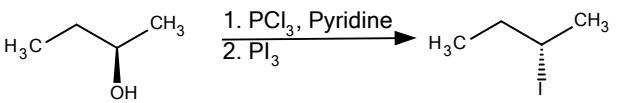

Scheme 1: Synthesis of (S)-(+)-2-iodobutane from (R)-(-)-2-butanol [6].

VCD spectra of the enantiomers were measured (Fig. 1, top) where blue full line represents the (R)-(-)- and red dashed line the (S)-(+)-enantiomer.

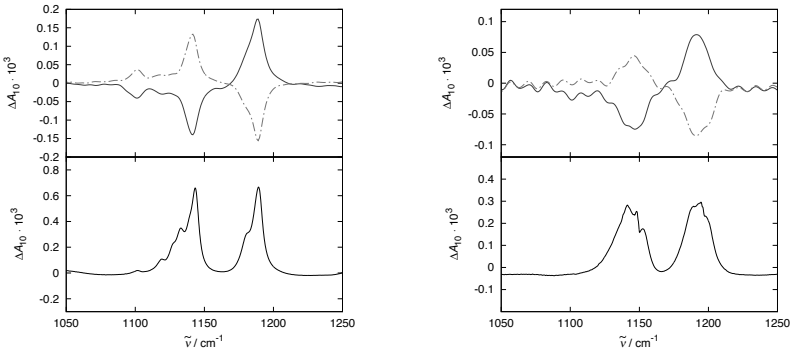

Figure 1: VCD measurement (top) of (R)-(-)-2-iodobutane, continuous blue line, and (S)-(+)-2-iodobutane, dashed red line, (top) and the IR-spectrum of (R)-(-)-2-iodobutane (bottom). The left graphic is the measurement in gas phase and the right one in solution (CCl4).

As expected, the signals are mirror-images and the absolute configuration has been verified with the aid of *ab initio* calculations.
A frequently used route to synthesise small halomethanes started out from chlorotrifluoroethene [7,8], which has a low boiling point and its commercial availability is very limited. We used 1,2-dichloro-1,2-difluoro ethylene [9], which is easier to handle (higher boiling point) and readily available. However, as the availability of those starting materials becomes more and more difficult, a new method was developed which is based on diethylmalonate [9]. This compound offers the advantage to obtain a whole family of chiral halogenated acetic acids with high purity and yield (Scheme 2).

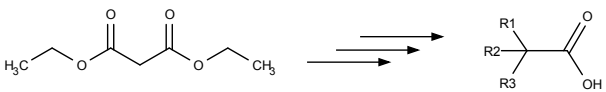

Scheme 2: Illustration of the possibility to produce chiral and achiral halogenated acetic acid from diethylmalonate [9] in several steps. Currently, R1-R3 can be any combination of Br, Cl, F, D and H.

Resolution

For many substances it is difficult even impossible, to synthesise them from enantiopure starting material. Thus, various methods were developed to

separate enantiomers. In our team we used diastereomeric resolution [10], fractional crystallisation [11] and enantioselective gas-chromatography [12] intended to separate large quantities of small enantiomers on a gr-scale. For all three methods an enantiopure partner reagent is needed. For the diastereomeric resolution the racemic substance has to have a functional group, so that it can be derivatised. Most common are carboxyl-groups which then react with chiral amines or alcohols to the corresponding amides (Scheme 3) or esters.

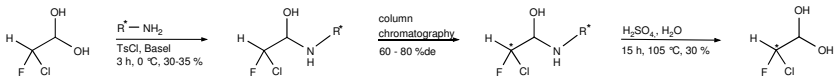

Scheme 3: Reaction of the racemic halogen acetic acid with an enantiopure reagent and the separation via column chromatography [10].

The resulting diastereomers were separated with medium pressure liquid chromatography on a non-chiral column. Another separation method creates a diastereomeric salt from a carboxylic acid with an enantiopure amine. The salt of racemic bromochlorofluoroacetic acid was obtained with strychnine according to Doyle [13] and afterwards separated with fractional crystallization in a methanol/water mixture (Scheme 4).

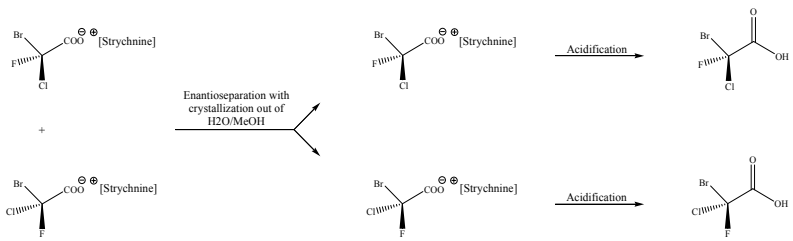

Scheme 4: Salt formation followed by a fractional crystallisation. The acid was recovered with acidification of the salt [11,13].

The acid can be used to decarboxylate to the bromochlorofluoromethane. Lastly, enantioselective gas-chromatography was used to separate and collect bromofluoroiodomethane and similar compounds with a preparative chiral column which was coated with a newly synthesised cyclodextrin derivative ([12], and patent pending). In contrast to analytical separation, no chiral stationary phases were available to a preparative separation of our target compounds. A self-devised fraction collector condensates the enan-

tiomers into two traps in an automated procedure. The enantiomers were separated and collected serial on the preparative chiral GC-column, as only a few mg halomethane could be injected on the column.

Outlook

Our universal synthesis schemes will be used to obtain halogenated molecules like fluoroxirane [14] or methanes which can even be isotopically chiral with deuterium and hydrogen. It is clear that enantioseparation does not work for isotopically chiral molecules, therefore more sophisticated synthetic routes have to be devised. The fractional crystallisation and enantioselective gas-chromatography proved to be the best way to synthesise or collect the bromochlorofluoromethane and similar compounds with high enantiomeric excess in large quantities.

References

[1] M. Pitzer, M. Kunitski, A. S. Johnson, T. Jahnke, H. Sann, F. Sturm, L. P. H. Schmidt, H. Schmidt-Böcking, R. Dörner, J. Stohner, J. Kiedrowski, M. Regglin S. Marquardt, A. Schiesser, R. Berger, M. S. Schöffler. *Science*, 341:1096, **2013**.

[2] P. Herwig, K. Zawatzky, M. Grieser, O. Heber, B. Jordon-Thaden, C. Krantz, O. Novotny, R. Repnow, V. Schurig, D. Schwalm, Z. Vager, A. Wolf, O. Trapp, H. Kreckel, *Science* 342:1084, **2013**.

[3] K. Zawatzky, P. Herwig, M. Grieser, O. Heber, B. Jordon-Thaden, C. Krantz, O. Novotny, R. Repnow, V. Schurig, D. Schwalm, Z. Vager, A. Wolf, H. Kreckel, O. Trapp, *Chemistry-A European J.* 20:555, **2014**.

[4] K. B. Wiberg, Y. Wang, S. M. Wilson, P. H. Vaccaro, W. L. Jorgensen, T. D. Crawford, M. L. Abrams, J. R. Cheeseman, M. Luderer, Mark, *J. Phys. Chem. A* 112:2415, **2008**

[5] C. Lux, M. Wollenhaupt, C. Sarpe, T. Baumert, *ChemPhysChem* 16:115, **2015**.

[6] D. G. Goodwin, H. R. Hudson. *J. Chem. Soc. B: Phys. Organics*, 1333, **1968**.

[7] A. C. Beil. *Dissertation ETH Nr. 11744*, **1996**.

[8] R. N. Haszeldine. *J. Chem. Soc. (Resumed)*, 4259, **1952**.

[9] M. Mazenauer, Master's Thesis, *ZHAW*, **2015**.

[10] S. Manov, Bachelor's Thesis, *ZHAW*, **2014**.

[11] V. Galati, Bachelor's Thesis, *ZHAW*, **2015**.

[12] B. Spenger, Master's Thesis, *ZHAW*, **2013**.

[13] T. R. Doyle. *Dissertation*, Polytechnic University, **1989**.

[14] J. Pochert. *Dissertation ETH Nr. 12601*, **1998**.

Determination of oxygen atom wall recombination probability in Ar – O_2 afterglow

Věra Mazánková, David Trunec, František Krčma
Faculty of Chemistry, Brno University of Technology, Purkyňova 118, Brno, 612 00, Czech Republic

The reaction kinetics in argon – oxygen flowing afterglow (post-discharge) was studied using NO titration and optical emission spectroscopy. The $O(^3P)$ atom concentration was determined by NO titration at different places along the flow tube. The optical emission spectra were also measured along the flow tube. A zero-dimensional kinetic model for the reactions in the afterglow was developed. This model allows to calculate the time dependencies of particle concentrations. The wall recombination probability for $O(^3P)$ atoms $\gamma_O = (1.60 \pm 0.01) \times 10^{-3}$ and wall deactivation probability for $O_2(b\ ^1\Sigma_g^+)$ molecules $\gamma_{O2(b)} = (1.56 \pm 0.03) \times 10^{-3}$ were determined from the fit of model results to experimental data.

1. Introduction

Afterglow systems containing oxygen have a wide range of applications in different fields due to the presence of reactive oxygen species (oxygen atoms and excited metastable oxygen molecules). For example, Ar – O_2 afterglows were used for surface treatment, sterilization and thin film deposition. The afterglows of Ar – O_2 plasmas have been studied experimentally or theoretically by numerous groups.

The present work is focused on the experimental study of an argon - oxygen flowing afterglow with the aim to determine the wall reaction probabilities for $O(^3P)$ atoms and $O_2(b\ ^1\Sigma_g^+)$ molecules. The concentration of atomic oxygen was determined by NO titration along the flow tube. Also the spectra of atmospheric band of molecular oxygen were recorded along the flow tube and the intensity of this band was determined. A kinetic model was developed in order to explain the experimental results. The fit of calculated concentrations to experimental data allows to determine the wall recombination probability for oxygen atoms and the wall deactivation probability for $O_2(b\ ^1\Sigma_g^+)$ excited molecules.

2. Experimental set-up

The flowing configuration of argon DC discharge with oxygen admixture was used for this experimental study. The experimental set-up was

already used for our previous studies of argon afterglow with nitrogen admixture [1] and nitrogen afterglow with mercury vapour admixture [2]. A simplified schematic drawing of the experimental set-up is given in Figure 1.

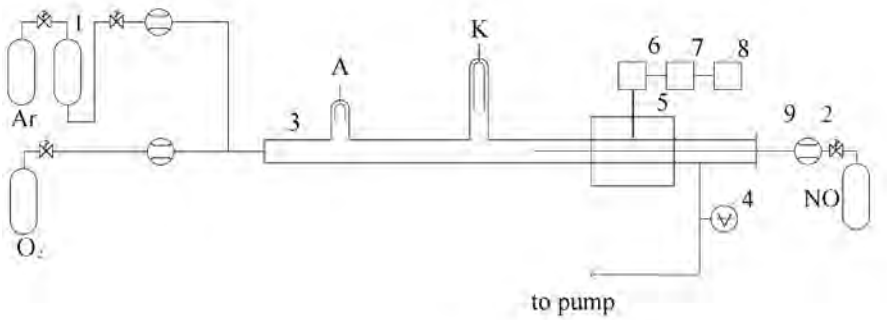

Fig. 1 Scheme of the experimental setup. 1 - catalyzer Oxiclear; 2 - mass flow controllers; 3 - quartz discharge tube; 4 - capacitance gauge; 5 - quartz optical fibre; 6 - monochromator Jobin Yvon Triax 550; 7 - CCD; 8 - PC; 9 - movable Pyrex titration capillary tube.

The active discharge was created in a quartz discharge tube with the inner diameter of 12 mm at the constant total gas pressure of 1000 Pa and the discharge power of 90 W. Hollow molybdenum electrodes were placed in the side arms (at the interelectrode distance of 120 mm) of the main discharge tube. The argon flow of 1400 sccm and oxygen flow of 10 sccm were automatically controlled by the Bronkhorst mass flow controllers and mixed together. The input gas temperature was 300 K.
The moveable capillary tube for NO titration was made of Pyrex and it was immersed upstream from the discharge into the quartz tube at its axis. Its external diameter was 2 mm, the inner diameter was 0.5 mm and the length was 400 mm. The flow analysis was performed in the same way as in previous study on argon metastable quenching [1]. The optical spectra were measured by Jobin Yvon monochromator TRIAX 550 with 1200 gr/mm grating and with CCD detector. The emitted light was led to the entrance slit of the monochromator by the multimode quartz optical fibre movable along the discharge tube.

3. Results

A zero-dimensional kinetic model for the argon – oxygen afterglow was developed. The following particles were considered in the kinetic model - electrons, Ar^+, Ar_2^+, O_2^+, O^+ and O^- ions, excited (metastable) argon

species $Ar^*(^3P_2)$ and Ar_2^*, oxygen atoms in ground state $O(^3P)$ and in excited states $O(^1D)$ and $O(3p\ ^3P)$, electronically excited states of molecular oxygen $O_2(a\ ^1\Delta_g)$, $O_2(b\ ^1\Sigma_g^+)$ and ozone O_3.

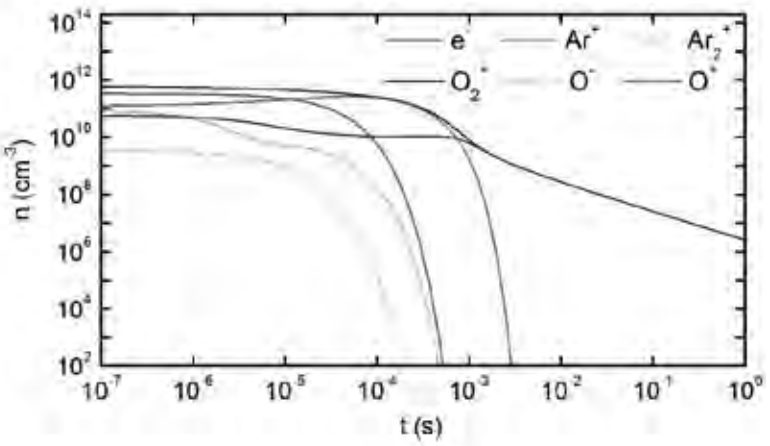

Fig. 2 The calculated time dependence of electron and ion concentrations in the afterglow.

The Figure 2 shows the time dependence of electron and ion concentrations. During the first hundred μs, the Ar^+ ions are converted to Ar_2^+ molecular ions, however both these ions react with oxygen in charge transfer reactions producing O^+ and O_2^+ ions. So, after the first millisecond all positive ions are converted to O_2^+ ions.
Also O^- negative ions are destroyed very quickly by recombination with O_2^+ ions and by collisions with $O_2(a)$ molecules and again after the first millisecond the concentration of O^- ions is negligibly small. Thus, after the first millisecond only electrons and ions O_2^+ are the remaining charged particles, which recombine mutually and their concentrations further decrease. The Figure 3 shows the time dependence of neutral particle concentrations. The Ar^* metastables produced in the discharge are converted to excimer Ar_2^* molecules, both Ar^* and Ar_2^* react with molecular oxygen producing atomic oxygen in ground or excited state. After the first millisecond, the concentrations of argon excited species are negligibly small. So after the first millisecond the remaining neutral particles with significant concentrations in afterglow are atomic oxygen in ground state O(P), metastable molecular oxygen states $O_2(a)$ and $O_2(b)$ and ozone together with argon and molecular oxygen in ground states.

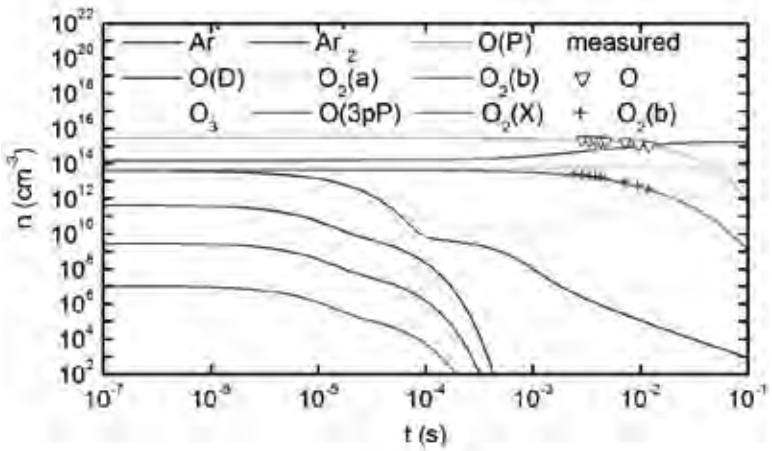

Fig. 3 The calculated time dependence of neutral particle concentrations in the afterglow. The points are experimental results: triangles - O(P) atom concentration determined by NO titration; crosses - atmospheric A-band intensities.

Wall recombination probability for O(P) atoms γ_O and wall deactivation probability for O_2(b) molecules $\gamma_{O2(b)}$ were considered as free parameters in the kinetic model. The least squares method was used to fit the calculated results to the experimental data. The values $\gamma_O = (1.60 \pm 0.01) \times 10^{-3}$ and $\gamma_{O2(b)} = (1.56 \pm 0.03) \times 10^{-3}$ were obtained from this method for quartz tube walls. The obtained value for γ_O is in good agreement with values obtained by other authors for Pyrex and $T = 300$ K, i.e. $(2 \pm 0.5) \times 10^{-3}$ [3]. The obtained value for $\gamma_{O2(b)}$ is lower than the value 2×10^{-2} used by other authors for Pyrex.

4. Acknowledgements

The present work has been supported by the project LD15010 and within the collaboration of the COST Action CM 1401.

5. References

[1] Mazankova V, Trunec D and Krcma F 2013 *J. Chem. Phys.* **139** 164311.
[2] Mazankova V, Trunec D and Krcma F 2014 *J. Chem. Phys.* **141** 154307.
[3] Macko P, Veis P and Cernogora G S 2004 *Plasma Sources Sci. Technol.* **13** 251.

Towards Cold Chemistry on a Multi-functional Ion Trap Chip

A. Mokhberi, and S. Willitsch
Department of Chemistry, University of Basel, Klingelbergstrasse 80, 4056 Basel, Switzerland

R. Schmied
Department of Physics, University of Basel, Klingelbergstrasse 82, 4056 Basel, Switzerland

Chip-based trapping techniques present novel possibilities for precise experiments with cold, quantum-state controlled particles with potential applications in mass spectrometry, chemistry, quantum information science, and spectroscopy [1-7]. We have designed and characterized a multi-functional monolithic miniaturized device for shuttling and manipulation of sympathetically cooled molecular ions [8-9] using accurately shaped electric fields above the surface of the chip. The chip consists of quadrupolar and octupolar surface-electrode RF traps featuring a few experimental sites that are connected via two optimized junction structures as shown in Fig 1.

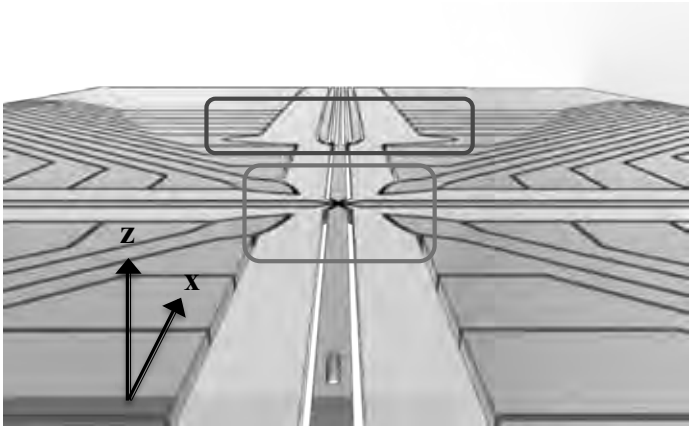

Fig 1) The structure of the multi-functional ion trap chip.

The experiment aims to shuttle translationally cold N_2^+, CaH^+, and CaO^+ with laser-cooled $^{40}Ca^+$ ions in the milikelvin range. However, our design based on a mass-independent normalized optimization presents a universal surface pattern structure applicable to any other mass as well as trapping parameters.

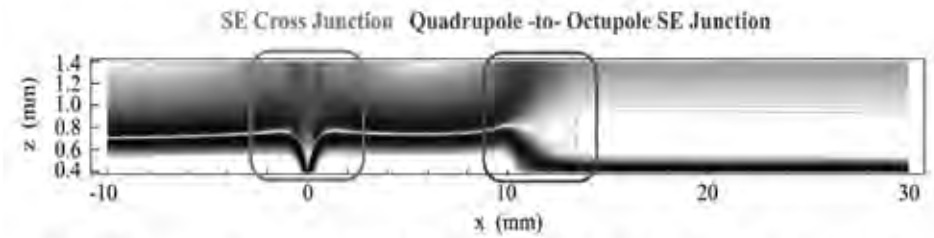

Fig 2) Calculated trapping pseudopotential for $^{40}Ca^+$ (h ≈700 μm) in the plane perpendicular to the chip intersecting the center of the junctions.

This compact, flexible technology will progressively impact on experiments with hybrid quantum systems [10-11] as well as highly integrated experiments with molecular ions combining various tasks such as chemistry and spectroscopy, which have thus far been in the domain of costly and complex guided-ion beam machines [12].

References

[1] J. Chiaverini, et al., Quantum Inf. Q Comput. **5**, 419 (2005)
[2] S. A. Meek, H. Conrad, and G. Meijer, Science **324**, 1699 (2009)
[3] M. D. Hughes, et al., Contemp. Phys. **52**, 505-529 (2011) and R. C. Sterling, et al., Nat. Commun. **5**, 3637 (2013)
[4] D. T. C. Allcock, et al., New J. Phys. **12**, 053026 (2010)
[5] R. Schmied, et al., Phys. Rev. Lett.**102**, 233002 (2009)
[6] J. M. Amini, et al., New J. Phys. **12**, 033031 (2010).
[7] A. Mokhberi and S. Willitsch, Phys. Rev. A **90**,023402 (2014)
[8] S. Willitsch. Int. Rev. Phys. Chem., **31**,175(2012)
[9] A. Mokhberi and S. Willitsch, New J. Phys. **17,** 045008 (2015)
[10] S. Willitsch, et al., Phys. Rev. Lett. **100**, 043203 (2008)
[11] F. H. J. Hall and S. Willitsch, Phys. Rev. Lett. **109**, 233202 (2012)
[12] D. Gerlich, in *Advances in Chemical Physics*, Vol. **82,** edited by C.-Y. Ng and M. Baer (Wiley, New York, 1992)

Conformationally and state controlled chemistry

D. Rösch, H. Gao, S. Willitsch
Department of Chemistry, University of Basel, 4056 Basel, Switzerland

Y.-P. Chang, J. Küpper
Center of Free-Eelctron Laser Science, DESY, 22607 Hamburg, Germany, Department of Physics, University of Hamburg, 22761 Hamburg, Germany

1. Introduction

Many molecules have multiple conformations (rotational isomers), which can exhibit different reactivites, opening up perspectives to manipulate chemical reactions by selecting specific molecular conformations [1]. However, a detailed understanding of the role of conformations in gas-phase chemical reactions still has to be established.

2. Conformer specific reaction rates of the 3-Aminophenol + Ca^+ reaction

In a recent experiment we studied the reactive collisions between conformationally selected 3-aminophenol and a Coulomb crystal of laser-cooled Ca^+ ions [2,3]. This reaction was chosen as a model system. 3-aminophenol exhibits two different conformations (cis and trans) with different permanent dipole moments. Their interaction with external inhomogeneous electric fields enables the two conformers to be spatially separated in a molecular beam passing through an electrostatic deflector [4]. Coulomb-crystals of spatially localized Ca^+ ions stored in an ion trap [5] provide a suitable stationary target for the conformer-selected molecular beams enabling the study of conformer-specific reactive collisions with extremely high sensitivities down to the level of single reaction events.
By tilting the molecular beam machine mechanically with respect to the ion trap, conformationally pure components of the molecular beam have been overlapped with the ion trap. The progress of the reaction was

monitored by imaging the laser-induced fluorescence of unreacted ions. The observed rate constant for cis-3-aminophenol is a factor of 2 larger than the one measured for the trans-3-aminophenol. These results agree well with the results from adiabatic capture theory calculations [6], indicating that the dynamics of the Ca^+ - cis/trans-3-aminophenol reaction are mainly controlled by conformer-specific differences in the long-range ion molecule interaction potential

3. A new ion trap for radial ion extraction into a time of flight mass spectrometer

We built a new apparatus dedicated to study reactions between ions and conformationally selected neutral molecules. To be able to analyze the masses of the ionic products with good resolution we designed a new ion trap that allows us to eject the ions from the trap radially into a time of flight mass spectrometer. The ion trap is a linear Paul trap with additional meshes for ion extraction and additional acceleration electrodes to focus the ions onto a multichannel plate detector.

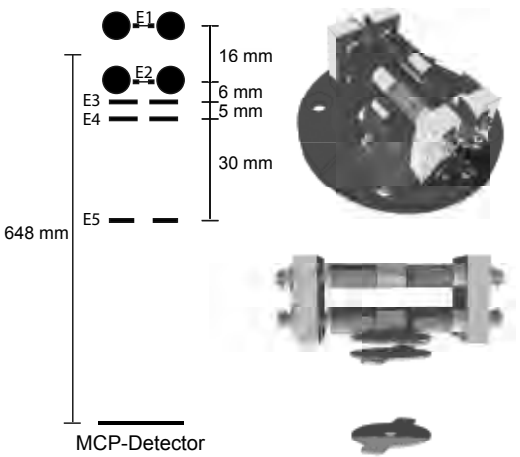

4. Outlook on future developments

In future experiments we want to study conformationally resolved organic ion-neutral and neutral-neutral reactions. The ion-neutral reactions will be studied on the apparatus with the new TOF ion trap. For the study of neutral-neutral reactions we are building a crossed molecular beam setup with a velocity map imaging time of flight mass spectrometer. One of the first reactions that we want to investigate is the Diels-Alder reaction:

Diels-Alder reactions are pericyclic reactions between a diene and a dienophile forming a cyclic product in a stereo- and regioselective reaction. The diene in our case will be 2,3-dibromobutadiene. This molecule has two different conformations and should only undergo Diels Alder reactions in its s-cis conformation. This molecule will be reacted with suitable ionic and neutral collision partners.

6. References

[1] F. Filsinger, U. Erlekam, G. von Helden, J. Küpper, and G. Meijer, *Phys. Rev. Lett.* **100**, 133003 (2008)
[2] Y.-P. Chang, K. Długołęcki, J. Küpper, D. Rösch, D. Wild and S. Willitsch, *Science* **342**, 98 (2013)
[3] D. Rösch, S. Willitsch, Y.-P. Chang and J. Küpper, *JCP* **140**, 124202 (2014)
[4] F. Filsinger, J. Küpper, G. Meijer, J. L. Hansen, J. Maurer, J. H. Nielsen, L. Holmegaard, and H.Stapelfeldt, *Angew. Chem. Int. Ed.* **48**, 6900 (2009).
[5] S. Willitsch, *Int. Rev. Phys. Chem.* **31**, 175 (2012)
[6] D. C. Clary, *J. Chem. Soc. Faraday Trans.* **88**, 901 (1992)
[7] J. H. Nielsen, P. Simensen, C. Z. Bisgaard, H. Stapelfeldt, F. Filsinger, B. Friedrich, G. Meijer and J. Küpper *Phys. Chem. Chem. Phys.,* **13**, 18971 (2011)

Mathematical compensation of multi-modulation artefacts in medium resolution gas-phase spectra using Fourier transform infrared spectroscopy

Mathias Schilling and Jürgen Stohner*
Zurich University of Applied Sciences (ZHAW)
Institute for Chemistry and Biotechnology (ICBT)
Einsiedlerstrasse 31, CH-8820 Wädenswil
Email: juergen.stohner@zhaw.ch

Introduction

Fourier transform infrared spectroscopy (FT-IR) is widely used to record rovibrational spectra of molecules in gas-phase and to assign the corresponding transitions [1]. In analytical applications, medium resolution is often sufficient. For spectrometers with medium resolution, multi-modulation artefacts can arise due to reflections at an integral multiple of the energy of associated absorption signals (fundamental, overtones and combination bands) with smaller intensities [2-12, 14]. These artefacts were observed in the past for CO and CO_2 in the gas-phase [2]. We report here nice cases for HCl and CH_4, where the artefacts extend over a much broader spectral range and therefore overlap with overtone and combination bands, thus perturbing the line shapes and intensities. A reduction or full elimination of those artefacts should be strived for. Several methods for their reduction (technical as well as computational) were proposed [2-4], but those methods led to an intensity loss and/or to a rise of the noise level. In contrast, we devised a scheme to strongly reduce or even eliminate those artefacts numerically and propose device-oriented modifications for a fully computerised compensation.

Mathematical description of double-modulation artefacts

The equation for the intensity, $I(x)$, of a detected interferogram with a part of it undergoing a second modulation due to inter-reflections depends on the offset of the moving mirror x, the wavenumber $\tilde{\nu}$, the transmissivity of reflection effects τ_{R} and true absorption mechanisms τ_{A}. Therefore, two interferograms are detected in superposition, one single-modulated (s) with the quantity $\tau_{\mathrm{R,s}}$ and a double-modulated (d) with the quantity $\tau_{\mathrm{R,d}}$ respectively and can be written as follows:

$$
\begin{aligned}
I(x) &= I_{\mathrm{s}}(x) + I_{\mathrm{d}}(x) \\
&= \frac{1}{2} I_0[(1+\cos(2\pi\tilde{\nu}x))\tau_{\mathrm{A}}\tau_{\mathrm{R,s}} + (1+\cos(2\pi\tilde{\nu}2x))\tau_{\mathrm{A}}\tau_{\mathrm{R,d}}],
\end{aligned}
\tag{1}
$$

with $0 \leq \tau_{\mathrm{A}}\tau_{\mathrm{R}} < 1$ [13].

Compensation

The aim of our compensation scheme is to eliminate or reduce the contribution $I_{\mathrm{d}}(x)$ caused by double-modulation to obtain the compensated interferogram $I_{\mathrm{c}}(x)$

$$
\begin{aligned}
& \underline{n=0} \\
I_{\mathrm{c}}(x) = \quad & (-1)^0 \frac{1}{2} I_0(1+\cos(2\pi\tilde{\nu}2^0 x))\tau_{\mathrm{A}}\tau_{\mathrm{R,s}}\gamma_0 && \text{(2.a)} \\
+ \; & (-1)^0 \frac{1}{2} I_0(1+\cos(2\pi\tilde{\nu}2^1 x))\tau_{\mathrm{A}}\tau_{\mathrm{R,d}}\gamma_0 && \text{(2.b)} \\
& \underline{n=1} \\
+ \; & (-1)^1 \frac{1}{2} I_0(1+\cos(2\pi\tilde{\nu}2^1 x))\tau_{\mathrm{A}}\tau_{\mathrm{R,s}}\gamma_1 && \text{(2.c)} \\
+ \; & (-1)^1 \frac{1}{2} I_0(1+\cos(2\pi\tilde{\nu}2^2 x))\tau_{\mathrm{A}}\tau_{\mathrm{R,d}}\gamma_1 && \text{(2.d)} \\
& \underline{n=2} \\
+ \; & (-1)^2 \frac{1}{2} I_0(1+\cos(2\pi\tilde{\nu}2^2 x))\tau_{\mathrm{A}}\tau_{\mathrm{R,s}}\gamma_2 && \text{(2.e)} \\
+ \; & (-1)^2 \frac{1}{2} I_0(1+\cos(2\pi\tilde{\nu}2^3 x))\tau_{\mathrm{A}}\tau_{\mathrm{R,d}}\gamma_2 && \text{(2.f)} \\
& \vdots
\end{aligned}
$$

with a compensation coefficient $\gamma_n = \left(\tau_{\mathrm{R,d}}/\tau_{\mathrm{R,s}}\right)^n$. For a compensation of order $n = 1$ the terms (2.b) and (2.c) cancel. New artefacts are generated with a negative contribution (2.d) at double the frequency. Since $\tau_{\mathrm{R,s}} > \tau_{\mathrm{R,d}}$, the intensities of the newly produced artefacts are smaller, $\left(\tau_{\mathrm{R,d}}/\tau_{\mathrm{R,s}}\right)^n << 1$, with respect to the original artefacts. Further compensations of higher order can be applied to any degree $n_{\max}$.

Equation (2) can be simplified to

$$I_{\mathrm{c}}(x) = \sum_{n=0}^{m} (-1)^n \frac{1}{2} I_0 \Big[\big(1 + \cos(2\pi 2^n \tilde{\nu} x)\big) \tau_{\mathrm{A}} \tau_{\mathrm{R,s}} + \big(1 + \cos(2\pi 2^{n+1} \tilde{\nu} x)\big) \tau_{\mathrm{A}} \tau_{\mathrm{R,d}} \Big] \gamma_n . \tag{3}$$

With every iteration, the artefact intensity is lowered by a power of n and also change sign. Due to alias overlap, the newly produced artefacts can be folded into the spectrum, their intensities are much lower, therefore, the corresponding perturbations can be neglected. Eq. (3) can also be used to compensate for k^{th}-order modulations by substitution of 2^n and 2^{n+1} with k^n and k^{n+1}, respectively.

Results

It could be shown that using Eq. (3) leads to a very good compensation of the double-modulation artefacts without loss of spectral information nor raise of the noise level. This was be verified by measurements of CH_4 in the gas-phase (see fig. 1).

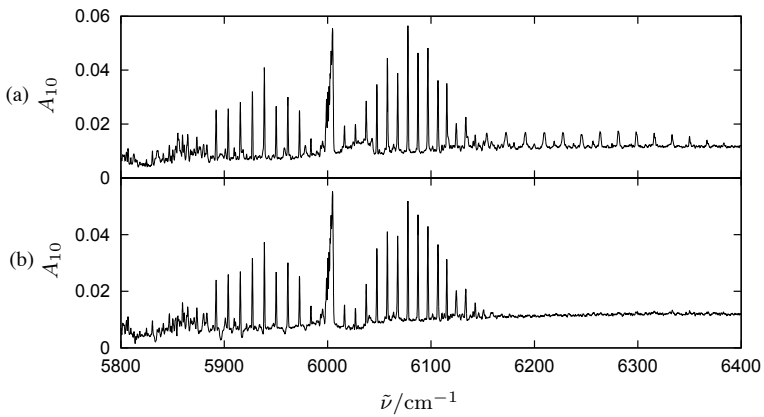

Figure 1: (a) First overtone of CH_4 ($5800 - 6150\mathrm{cm}^{-1}$) and double-modulation artefacts (because of overlap with spectral signals only visible between 6150 and 6400 cm^{-1}. (b) Single compensation using Eq. (3) with $\gamma = 0.0045$.

Intensities of fundamentals slightly increased and those of overtones slightly decreased. With allocating a too high value of γ, one tends to over-com-

pensate the artefacts. Using no other techniques, an "ideal" coefficient γ has to be determined for each experiment in an iterative scheme.

Outlook

By measuring the reflection interferogram, the coefficient γ can be calculated using the ratio of the intensity difference between the main interferogram and the reflection interferogram. Such a reflection interferogram could be detected by introducing parabolic mirrors with holes parallel to the focused and collimated beam in combination with secondary detectors at the positions (C), where the reflection intensity seems to be the highest (see fig. 2). The intensity of that interferogram must be corrected by the illuminated areas (by the reflected light) of the parabolic mirror and the diameter of the holes respectively, and by the gain of the secondary detectors in relation to the main detector. This would offer a complete automation of this compensation method.

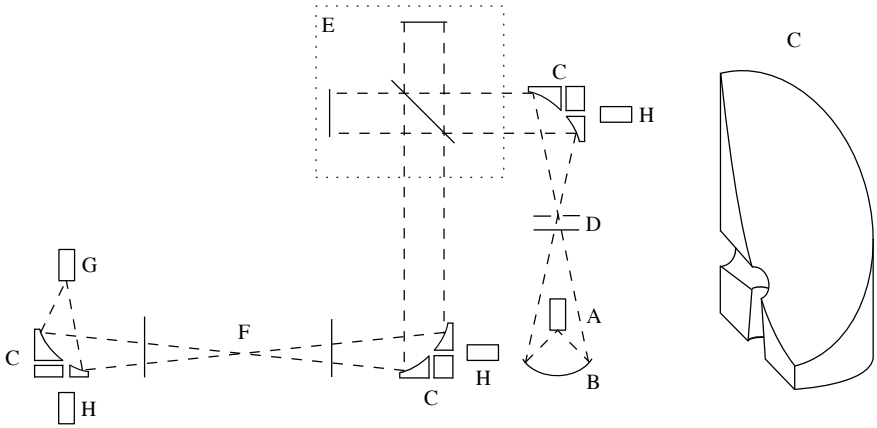

Figure 2: Left: Proposed modifications for a FT-IR spectrometer containing a source (A), reflection optics (B, C), filters and apertures (D), the interferometer (E), the sample compartment (F), the main detector (G) and secondary detectors (H). Right: Cross section of such a parabolic mirror (C) having two conic holes, one parallel to the focused and one parallel to the collimated beam, for measuring the reflection interferogram and preventing further reflections towards the interferometer [14].

Acknowledgement

Our work was supported financially by grant ASF-2014 from the ZHAW.

References

[1] M. Quack, F. Merkt, *Handbook of High-Resolution Spectroscopy*, vol. 1 & 2. Wiley, **2011**.

[2] T. J. Johnson, R. L. Sams, T. A. Blake, S. W. Sharpe, P. M. Chu. *Applied Optics*, 41(15):2831, **2002**.

[3] L. Lin. *Stray Radiation in Optical System*, 1331:179, **1990**.

[4] Application Note # 12, Bruker Optics, **2009**.

[5] J. R. Birch, F. J. J. Clarke. *Spectroscopy Europe*, 4(7):16, **1995**.

[6] J. R. Birch, F. J. J. Clarke. *Analytica Chimica Acta*, 380:369, **1999**.

[7] F. J. J. Clarke, J. A. Larkin. *Infrared Physics*, 25(1):359, **1985**.

[8] J. M. Chalmers. *Handbook of Vibrational Spectroscopy*, p. 2327. Wiley, **2002**.

[9] G. Guelachvili. *Spectrometric Techniques*, vol. II. Academic Press, **1981**.

[10] R. C. M. Learner, A. P. Thorne, J. W. Brault. *Applied Optics*, 35(16):2947, **1996**.

[11] B. Saggin, L. Comolli, V. Formisano. *Applied Optics*, 46(22):5248, **2007**.

[12] M. Schilling, Bachelor's Thesis, *ZHAW*, **2013**. (unpublished)

[13] J. Chamberlain, *The Principles of Interferometric Spectroscopy*. Wiley, **1979**.

[14] M. Schilling, Master's Thesis, *ZHAW*, in preparation, and to be published.

Reaction control with electrons – pick your mechanism

Jan Hendrik Bredehöft, Petra Swiderek
Institute for Applied and Physical Chemistry
University of Bremen, Germany

…

Interactions of electrons and molecules are part of a great number of processes in nature as well as in technological applications. They vary in scope from repairing nano-structures by Focussed Electron Beam Induced Deposition (FEBID) all the way up to interstellar chemistry induced by the interaction of high-energy ionizing radiation with cosmic dustgrains.

We study the reaction mechanisms involved in these processes by Thermal Desorption Spectroscopy of very thin films of condensed matter that have been irradiated by a defined number of electrons with specific energy. By carefully looking at the energy- and dose-dependence of products and by-products it is possible to work out reaction kinetics and elucidate reaction mechanisms.

Electron-molecule interactions can come in a variety of different "flavours" depending on the electron energy and nature of the molecule. The two most important primary steps for further chemical reactions are bond dissociation by either electron-attachement (yielding an anion), or by electron impact ionization (yielding a cation). These highly reactive intermediates will then go on to form more stable compounds with neighbouring molecules.

By controlling the electron energy it is possible to selectively trigger a specific reaction channel thus selecting one reaction mechanism out of possibly several. By controlling the electron dose, the formation of by-products can be suppressed allowing for even further control over the chemical reactions taking place.

In recent years we have studied a number of systems that utilize electron radiation to attach electron-rich species like ammonia (NH_3) or water to electron-rich double bonds. This kind of reaction is very hard to do in classical solution-based chemistry since it requires specialized catalysts and high pressures and temperatures to overcome electrostatic repulsion between reaction partners. By ionizing one reaction partner, the interaction turns from repulsive to attractive, enabling the reaction to proceed without catalysts and even at cryogenic temperatures. In addition many of these reactions can be tuned to be atom-efficient, meaning that all atoms of both reaction partners end up in the product.

The addition of ammonia and primary and secondary amines to ethylene (C_2H_2) and to carbon monoxide (CO) is presented as is the addition of water to ethylene, yielding ethanol.

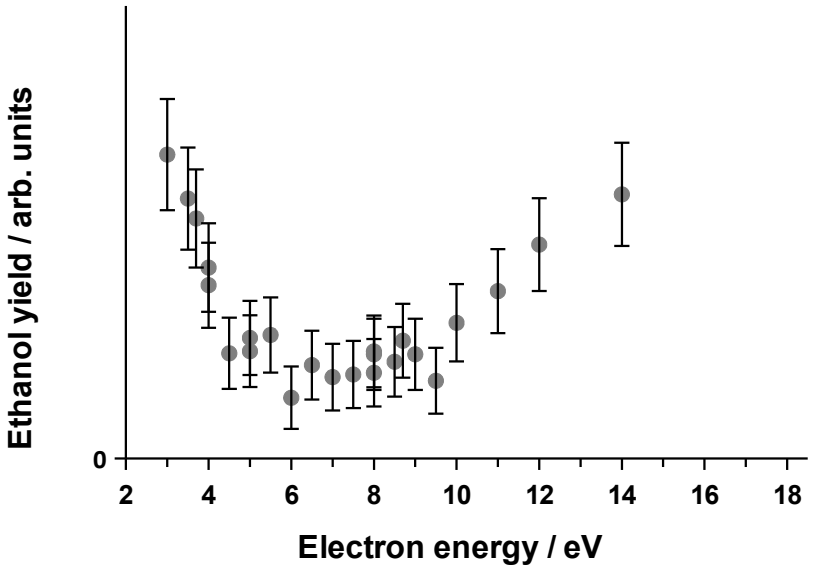

In all cases the reaction mechanisms could be clarified and in some cases different reaction pathways with different by-products are available depending on electron energy and dose. These results show that understanding electron-induced chemistry and reaction pathways will not only help in understanding natural processes but can also help in designing better and more efficient technological applications.

Authors Index